babcock & wilcox nuclear energy
• 13024 ballantyne corporate place, suite 500 • charlotte, nc 28277 usa
• phone 704.626.4800 • fax 704.625.4801 • www.babcock.com

August 31, 2010

BW-JAH-2010-223

U.S. Nuclear Regulatory Commission
ATTN: Document Control Desk
One White Flint North
11555 Rockville Pike
Rockville, MD 20852-2738

Babcock & Wilcox Nuclear Energy, Inc.
Docket Number-PROJ0776
Project Number-776

Subject: B&W mPower™ Reactor Core Nuclear Design Codes and Methods Qualification Topical Report

On April 28, 2009, the Babcock & Wilcox Company (B&W) notified the U.S. Nuclear Regulatory Commission (NRC) of its intent to submit an application for the Design Certification of the B&W mPower™ reactor in accordance with the process defined in 10 CFR Part 52.

As part of the continuing design process for the B&W mPower reactor, B&W has prepared the enclosed "Core Nuclear Design Codes and Methods Qualification" Topical Report. As described in this report, the underlying core physics qualification analyses were performed with the Studsvik Scandpower Core Management System code suite consisting of the two-dimensional lattice physics and cross-section generation code *CASMO-5*, the cross-section processing and functionalization code *CMS-LINK*, and the three-dimensional core simulator code *SIMULATE-3*. B&W is seeking NRC approval for the use of these codes and nuclear computational methodology for performing future design calculations for the B&W mPower reactor core.

The report does not contain any proprietary information.

Questions concerning this submittal may be directed to T. J. Kim at 434-382-9791 (email: tjkim@babcock.com) or to Jeff Halfinger at 434-316-7507 (email: jahalfinger@babcock.com).

We look forward to working with the NRC staff on this important part of our design process and will support meetings with the NRC staff to discuss this submittal as necessary.

Jeffrey A. Halfinger
VP, mPower Development
B&W NE

Robert E. McLaughlin
Director, Quality Assurance
B&W NE

T. J. Kim
Licensing Director
B&W NE

JHA/jlr

cc: Joelle L. Starefos, NRC, TWFN 9-F-27
Stewart L. Magruder, Jr., NRC, TWFN 9-F-27

Add: J. Starefos, S. Magruder > TO ERIDS

T007
NRR

R003-03-002106

Core Nuclear Design Codes and Methods Qualification

Topical Report

DOCUMENT #: R003-03-002106	REVISION: 000

TITLE: Core Nuclear Design Codes and Methods Qualification

SIGNATURES

	Printed Name	Signature	Date
Prepared By:	Gary W. Neeley	Gary W. Neeley	8/31/2010
Prepared By:	Dominic Napolitano	Dominic Napolitano	8/31/10
Prepared By:	Madalina A. Erighin	Madalina Erighin	08-31-2010
Reviewed By:	Hassan A. Hassan	H. Hassan	8/31/2010
Reviewed By:	Dudley A. Raine	Dudley A. Raine, III	8/31/2010
Reviewed By:	Billy E. Bingham	Billy E. Bingham	8/31/2010
Approved By:	Michael T. Childerson		8/31/2010

Acknowledgments

The authors wish to thank their colleagues at B&W for their time, energy, patience, and help in providing the valuable assistance that made this topical report possible. Special thanks must be given to David Dean, Scott Vanevenhoven, and Arthur DiGiovine of Studsvik for their assistance with this project and providing technical information on ***CASMO-5/SIMULATE-3***. The authors are especially appreciative of the efforts and immeasurable hard work of Mr. Shane Stimpson in making this document possible.

Executive Summary

The nuclear computational methodology that will be used in performing nuclear design calculations for the B&W mPower™ reactor core has been qualified by making comparisons between computed and measured: (1) Criticality conditions and localized pin power distributions of various heterogeneous cold, clean, critical configurations; and (2) Critical boron concentrations, local and core-wide power distributions, temperature coefficients, and boron and control rod worths for various TMI-1 Cycles 1 and 2 reactor core operating and burnup states. The core physics qualification analysis was performed with the StudsvikScandpower Core Management System (CMS) code suite consisting of the two-dimensional lattice physics and cross-section generation code ***CASMO-5***, the cross-section processing and functionalization code ***CMS-LINK***, and the three-dimensional core simulator ***SIMULATE-3***. The CMS code suite is an industry standard, state of the art computer code package for comprehensive neutronic simulation of light water reactors. The primary applications of the CMS code package are fuel bundle design (e.g., enrichment zoning and burnable poison design), incore fuel management and loading pattern optimization, evaluation of fuel cycle energy, and various fuel and core licensing calculations (e.g., reactivity coefficients and shutdown margin).

The core physics qualification analysis performed for the 40 cold, critical experiments included: (1) 17 critical experiments with UO_2 fuel conducted at the B&W Lynchburg Research Center (LRC) as part of the Physics Verification Program; (2) 17 critical experiments containing UO_2-Gd_2O_3 bearing assemblies performed at LRC as part of the Urania-Gadolinia Critical Experiment Benchmark Program; and (3) six UO_2-PuO_2 (2 wt%) critical experiments carried out in the Plutonium Recycle Critical Facility at the Pacific Northwest National Laboratory. The eigenvalues and local pin power distributions within a fuel assembly calculated using ***CASMO-5/SIMULATE-3*** were compared to the measured results from the critical experiments to determine the accuracy of the computational methodology. The overall comparisons between calculated and measured data are in very good agreement. The standard deviations between the calculated and measured eigenvalues and pin powers are:

Eigenvalues

- ✓ σ_T = 0.00202 for the UO_2 Cold, Clean Critical Experiments
- ✓ σ_T = 0.00056 for the UO_2-Gd_2O_3 Cold, Clean Critical Experiments
- ✓ σ_T = 0.00155 for the UO_2-PuO_2 Cold, Clean Critical Experiments

Pin Powers

- ✓ σ_T = 0.01615 for the UO_2 Cold, Clean Critical Experiments
- ✓ σ_T = 0.01736 for the UO_2-Gd_2O_3 Cold, Clean Critical Experiments
- ✓ σ_T = 0.03361 for the UO_2-PuO_2 Cold, Clean Critical Experiments

The nuclear computational methodology was also verified by making comparisons between computed and measured critical boron concentrations, local and core-wide power distributions, temperature coefficients, and boron and control rod worths using data from TMI-1 Cycles 1 and 2. With respect to the TMI-1 Cycles 1 and 2 power distributions, 1160 relative power distribution (RPD) data points were used in the comparative analysis of the RPD for Cycles 1 and 2. These data points were obtained from RPD maps of 40 core follow state points. In general, there was very good agreement between predicted and measured cycle critical boron concentrations, temperature coefficients, boron and control rod worths, and relative power distributions and axial power shapes. Specifically, the standard deviations for the relative power distributions for TMI-1 Cycles 1 and 2 are:

- ✓ σ_T = 0.03589 for TMI-1 Cycle 1
- ✓ σ_T = 0.03326 for TMI-1 Cycle 2
- ✓ σ_T = 0.03453 for Combined TMI-1 Cycles 1 and 2

The results from the comparative analysis performed in this Topical demonstrate that the ***CASMO-5/SIMULATE-3*** methods and model used for nuclear reactor core calculations can

accurately predict criticality conditions for various heterogeneous configurations, local and core-wide power distributions, temperature coefficients, boron and control rod worths, etc. for various core operating and burnup states. The scope of the nuclear methodology qualification analysis was designed to encompass a wide range of geometric and material configurations to adequately represent the core physics embodied by the B&W mPower reactor core design concept.

Table of Contents

List of Tables:

List of Figures:

Acronyms

BOL	Beginning of Life
BPR	Non-Integral Burnable Poison Rod (Al_2O_3-B_4C)
CMS	Core Management System
CRA	Control Rod Assembly
Cycle 1	Three Mile Island Unit 1 Cycle 1
Cycle 2	Three Mile Island Unit 1 Cycle 2
Cycles 1 & 2	Three Mile Island Unit 1 Cycles 1 & 2
EOL	End of Life
FBPR	Integrated Fuel Burnable Poison Rod
IFBA	Westinghouse Integrated Fuel Burnable Absorber (Zirconium Diboride Coated Pellets)
JAERI	Japan Atomic Energy Research Institute
LRC	B&W Lynchburg Research Center
MCNP	Monte Carlo N-Particle code
MOL	Middle of Life
PNNL	Pacific Northwest National Laboratory
PRCF	Plutonium Recycle Critical Facility
RPD	Relative Radial Power Distribution
SPND	Self-Powered Neutron Detector
TMI-1	Three Mile Island Unit 1

1.0 Introduction

This report documents the codes and nuclear computational methodology that will be used in performing nuclear design calculations for the B&W mPower™ reactor core. The core physics qualification analysis was performed with the StudsvikScandpower Core Management System (CMS) using operating data for Cycles 1 and 2 of Three Mile Island (TMI) Unit 1 [Reference 1] and cold, clean, critical experiment data from the following: (1) The Physics Verification Program [Reference 2 and 3] performed at the Babcock & Wilcox (B&W) Lynchburg Research Center (LRC); (2) The Urania-Gadolina Critical Experiment Benchmarks [Reference 4] conducted at the LRC; and (3) The Plutonium Recycle Critical Facility (PRCF) at the Pacific Northwest National Laboratory (PNNL) [Reference 5].

The CMS code suite is an industry standard computer code package for comprehensive neutronic simulation of light water reactors. The primary applications of the CMS code package are fuel bundle design (e.g., enrichment zoning and burnable poison design), incore fuel management and loading pattern optimization, evaluation of fuel cycle energy, various fuel and core licensing calculations (e.g., reactivity coefficients and shutdown margin). The CMS package consists of the two-dimensional transport code ***CASMO-5*** [Reference 6] used to generate homogenized cross-section data and heterogeneous pin-by-pin form functions, which are subsequently used in the two-group three-dimensional nodal diffusion code ***SIMULATE-3*** [Reference 8] for whole core coupled neutronic-thermal-hydraulic analysis. Macroscopic cross sections generated by ***CASMO-5*** are processed into a binary library format accessible to ***SIMULATE-3*** by the auxiliary utility processing and functionalization code ***CMS-LINK*** [Reference 7].

1.1 CMS Code Suite Description

1.1.1 CASMO-5

CASMO-5 is a multi-group two-dimensional transport theory code for burnup calculations on boiling water reactor (BWR) and pressurized water reactor (PWR) assemblies or pin cells [Reference 6]. ***CASMO-5*** is the newest generation of the ***CASMO*** lattice code, and has many improvements over its predecessor, ***CASMO-4***. Some of the high-level physics enhancements that have been added to ***CASMO-5*** include:

- ✓ Quadratic gadolinia depletion model allowing for larger depletion step sizes without compromising accuracy.
- ✓ More exact scattering kernel for resonance upscattering.
- ✓ An energy release model that explicitly computes the isotopic energy yields as lattice compositions evolve, maintaining the physical dependence on fuel exposure, gadolinia, and boron concentrations, MOX composition, and void fractions.
- ✓ Addition of the ENDF/B-VII Cross-Section Library. This extensive update from the previous ***CASMO*** library improves accuracy and enhances resonance treatments including an updated 18-group gamma library for gamma-sensitive in-core detector modeling and gamma energy deposition calculations. Cross-section data is available for over 400 nuclides and materials including more than 200 explicitly defined fission products, 45 heavy nuclides, and an expanded array of detailed depletion chains.

CASMO-5 has been rigorously benchmarked by the code vendor (StudsvikScandpower) against measured critical experiments, post-irradiation benchmarks, and continuous-energy Monte Carlo calculations, including: (1) B&W Series 1810 and 1484, DIMPLE, and KRITZ-4 criticals; (2) MCNP (BOL and ***MCODE*** depletions) for pin-cells and whole assemblies; and (3) JAERI nuclide benchmarks. These tests have demonstrated excellent agreement with no significant bias versus the number of gadolinia pins, number of Ag-In-Cd rods, boron concentration, geometry, or presence of reflector/baffle. The overall

accuracy of ***CASMO-5*** and its associated ENDF/B-VII neutron data library have been repeatedly validated, ensuring reliably accurate results regardless of core type, fuel type, or operating strategy.

CASMO-5 handles a geometry consisting of cylindrical fuel rods of varying composition in a square pitch array with allowance for fuel rods loaded with gadolinium, erbium, integral fuel burnable absorber (IFBA) pellets, burnable absorber rods, cluster control rods, incore instrument channels, water gaps, and cruciform control rods in the regions separating fuel assemblies. Reflector/baffle calculations can also be performed with ***CASMO-5***. ***CASMO-5*** incorporates the direct microscopic depletion of burnable absorbers such as gadolinia and erbium into the main calculation and a fully heterogeneous model is used for the two-dimensional transport calculation.

The two-dimensional transport solution methodology used by ***CASMO-5*** is based upon the Method of Characteristics and can be performed in a number of different energy group structures. The macroscopic group cross-sections for ***CASMO-5*** are prepared for the micro-group calculations. The nuclear data library of 586 energy groups covering a range from 0 to 20 MeV are an integral part of the code system and macroscopic cross-sections are directly calculated from the densities, geometries, etc., provided in the user's input.

The effective cross-sections in the resonance energy region for resonance absorbers are calculated using an equivalence theorem that relates tabulated effective resonance integrals for each resonance absorber in each resonance group to the particular heterogeneous problem. The equivalence expression is derived from rational approximations for the fuel self-collision probability. The resonance integrals obtained from the equivalence theorem are used to calculate effective absorption and fission cross-sections. The "shadowing" effect between different pins is taken into account through the use of Dancoff factors that are calculated internally by ***CASMO-5***.

The resonance region, the energy region where data is explicitly shielded in ***CASMO-5***, is defined to lie between 10 eV and 9118 eV. Absorption above 9118 eV is assumed to be unshielded. The 1 eV resonance in ^{240}Pu and other low energy resonances in plutonium and other nuclides are adequately covered by the concentration of thermal groups around these resonances and are consequently excluded from the special resonance treatment.

The cross-sections thus prepared are used in a series of collision probability micro-group calculations to obtain detailed neutron energy spectra in the 586 energy groups used for the energy condensation of the cross-sections. The micro-group calculations are quite fast and are repeated for each type of pin in the assembly, such that individual spectra are obtained for each pin type, e.g., pins containing fuel of different enrichment. To provide micro-group spectra for condensation of an absorber pin cell, a micro-group calculation is performed for the absorber rod surrounded by coolant and a buffer region representing the surrounding fuel pins. The same procedure is used to determine micro-group spectra for water holes within the assembly. The generated cross-section data constitutes the input to the heterogeneous, two-dimensional characteristics based transport calculation, normally performed in 19 or 35 energy groups, which gives the eigenvalue and the associated flux distribution.

Isotopic depletion as a function of burnup is calculated for each fuel pin and for each region containing a burnable absorber. Ten radial rings are typically used for the depletion of gadolinia within a pellet. The burnup calculation is performed using a predictor-corrector approach. For each burnup step, the depletion is calculated twice, first using the spectra at the start of the step, and then after a new spectrum calculation, using the spectra at the end of the step. Average number densities from these two calculations are then used as starting values for the next burnup step.

Reflector data, including data for homogenized baffle/water are accurately generated by a two-dimensional calculation modeling one segment plus the reflector on one side.

CASMO-5 contains an automated case matrix capability for generating data suitable for the downstream three-dimensional nodal code, ***SIMULATE-3***. ***CASMO-5*** also contains a module that calculates prompt and delayed gamma sources and solves the 18 group, two-dimensional gamma transport problem such that the gamma detector response may be calculated.

CASMO-5 can accommodate symmetric fuel assemblies using half, quadrant, or octant symmetry as well as fully non-symmetric fuel bundles. Absorber rods or water holes covering 1x1, 2x2, 3x3, or 4x4 pin cell positions are allowed within the assembly. Thermal expansion of dimensions and densities is performed automatically. ***CASMO-5*** employs a simple user oriented input with default values available for many input quantities and nuclear data are automatically read from the library which is an integral part of the ***CASMO-5*** code package. Input and number densities may be saved on a restart file at each burnup step to be used in subsequent calculations.

The ***CASMO-5*** output is designed to be flexible and generates edits for the eigenvalue, the power distribution, reaction rates and few-group parameters for use in core calculations. The output also contains flux discontinuity factors for assembly interfaces and reflector regions. These discontinuity factors can be used by ***SIMULATE-3*** in two or multi-group diffusion theory in order to preserve net currents calculated by the ***CASMO-5*** multigroup transport solution. Figure 1-1 summarizes the ***CASMO-5*** program computational flow.

Figure 1-1: CASMO-5 Program Computational Flow

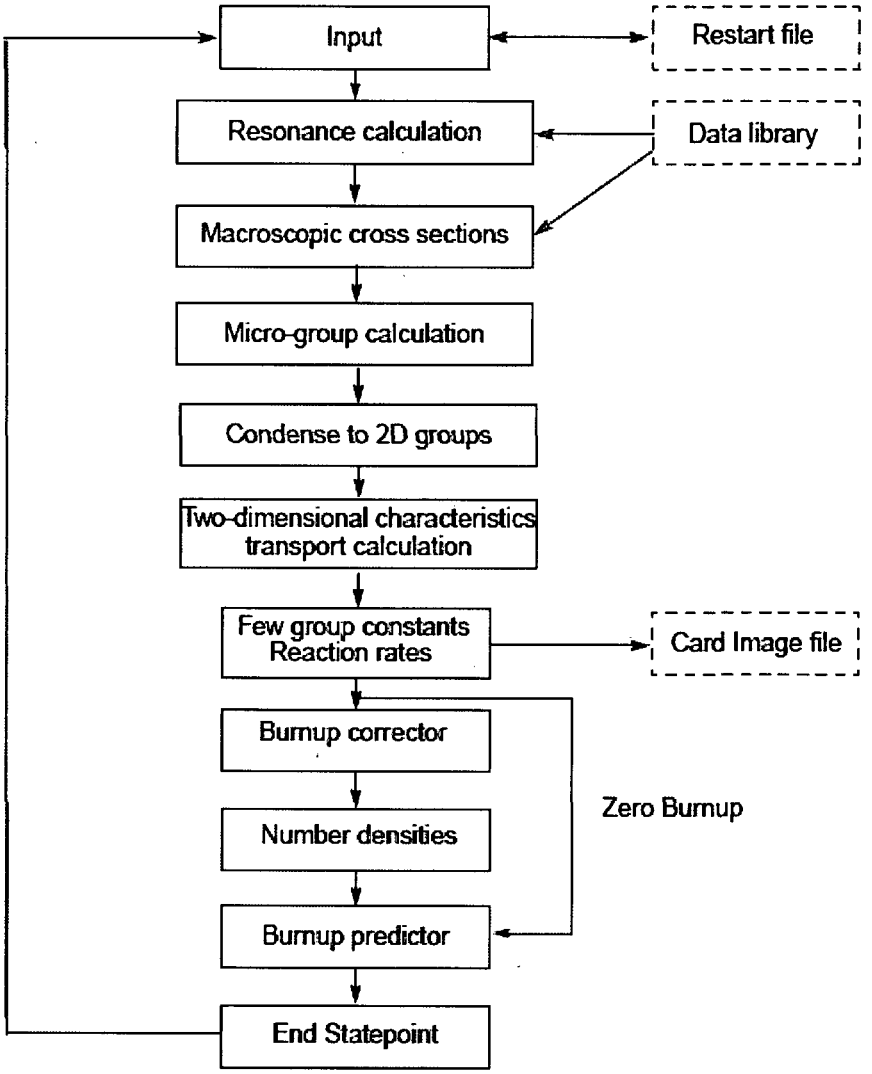

1.1.2 CMS-LINK

CMS-LINK is a linking code that processes ***CASMO-5*** Card Image files into a binary formatted nuclear data library for use by ***SIMULATE-3*** [Reference 7]. The code collects the two-group macroscopic cross-sections, two-group discontinuity factors, fission product data, detector data, pin power reconstruction data, kinetics data, isotopic data, and spontaneous fission data from the ***CASMO-5*** Card Image files and creates a binary library for ***SIMULATE-3***. ***CMS-LINK*** is capable of processing data for: (1) standard hot

and cold PWR segments with and without burnable poison; (2) pulled and reinserted burnable poison for PWR segments; (3) standard cold and hot BWR segments; (4) standard cold and hot PWR and BWR reflector segments; and (5) scoping libraries.

The data functional dependencies (case matrices) that depend on the reactor type are predefined in the code. The library functionalization used for the macroscopic cross-sections is used for the fission product data and discontinuity factors as well. The pin library that includes pin peaking, kinetics, isotopic and detector data is written for each fuel segment by default. The one-dimensional tables of these parameters are determined by the program. The output of the code is a summary of card image file content, segments present in the library both before and after the execution of the code, the case matrix functionalization, and tables of k_{inf}.

1.1.3 SIMULATE-3

SIMULATE-3 is a three-dimensional, two-group, steady-state reactor core simulator that performs incore fuel management studies, core design calculations, and calculation of safety parameters [Reference 8]. ***SIMULATE-3*** employs an advanced nodal expansion method (***QPANDA*** model [Reference 8]) to solve the two-group neutron diffusion theory representation of the reactor core without requiring normalization to fine-mesh calculations or to measured data. ***SIMULATE-3*** provides for thermal-hydraulic feedback, modeling of equilibrium or time-dependent xenon and samarium, and isotopic depletion. In addition, it allows for the generation of pin-by-pin power distributions using a pin power reconstruction technique.

The ***SIMULATE-3*** solution methodology involves subdividing the spatial domain of the reactor into a set of rectangular parallelepiped nodes, with each node typically representing a full assembly or a quarter assembly in the radial plane and a 15-30 cm axial region of an assembly. The three-dimensional diffusion equation is integrated over the volume of each node to obtain the neutron balance equation. Determination of the nodal averaged scalar fluxes requires the intra-nodal flux distributions in both the

fast and thermal groups that are derived by integrating the three-dimensional diffusion equation over two of the three directions of a node to obtain a transverse-integrated one-dimensional diffusion equation. Using a fifth-degree polynomial representation for the transverse-integrated flux distribution within a node and a quadratic polynomial representation for the net leakage so that the transverse leakage shape preserves the average transverse leakage in each of the neighboring nodes, then an iterative solution to the nodal balance equation is performed until the nodal coupling coefficients and node-averaged fluxes are converged.

The ***SIMULATE-3*** nodal code allows octant-, quadrant-, half-, and full-core geometries. In quarter- and half-core cases, reflective or rotational boundary conditions are permitted on the core interior boundaries. ***SIMULATE-3*** explicitly models the radial and axial reflectors, and conventional albedo conditions are not required at the core periphery. The diffusion equation does, however, require a boundary condition at the outer surface of the reflector. Either zero flux or zero incoming flux boundary conditions can be used, and the sensitivity of the solution to the boundary condition is extremely small if the reflector region is comparable in size to a fuel assembly. ***SIMULATE-3*** allows rotationally symmetric and reflective boundary conditions. In addition, special studies are permitted with infinite geometry boundary conditions: opposite face periodic, rotationally symmetric, and reflective.

In ***SIMULATE-3***, the reactor power, coolant density, and fuel temperature distributions are intimately coupled. ***SIMULATE-3*** performs a coupled neutronics/thermal-hydraulics iteration to find these distributions. At any point during the iterative process, the reactor power distribution can be considered known, and the coupled problem is reduced temporarily to a problem of determining the coolant density and fuel temperature distributions for a fixed power distribution. The thermal-hydraulic model used in ***SIMULATE-3*** for PWRs is a simple heat balance model that assumes that: (1) the coolant inlet flow and temperature distributions are known; (2) coolant flow is in parallel channels, cross flow is ignored, and the core exit water condition remains

subcooled; (3) the power produced by fuel rods within a node is also deposited in the coolant in that node; and (4) the pressure drop across the core is assumed to be negligible, and all water properties are evaluated at a single pressure. These assumptions imply that the coolant enthalpy distribution can be calculated by a simple heat balance of the enthalpy at the inlet of a node, the heat generated within the node, and the enthalpy at the outlet of a node. The node-average density is calculated by evaluating the state properties of water at the average of the node inlet and outlet enthalpies. The state calculation is based on interpolation of data from ASME Steam Tables or direct ASME Steam Table evaluation. The average temperature of the fuel pellets in any given node is calculated from a polynomial fit to nodal power density relative to core the averaged power density at 100% of rated power and the moderator temperature. As a result, the fuel temperature coefficients may be different for each fuel segment type in the core.

2.0 Cold Clean Critical Experiments

The predicted and measured results from numerous critical experiments were analyzed to determine the accuracy of the ***CASMO-5/SIMULATE-3*** computational methodology. Detailed models were used to calculate the local pin power distribution within a fuel assembly. The cold, critical experiments included: (a) 17 critical experiments with UO_2 fuel; (b) 17 critical experiments containing UO_2-Gd_2O_3 bearing assemblies; and (c) six UO_2-PuO_2 (2 wt%) critical experiments. The UO_2 experiments were conducted at LRC, as part of the Physics Verification Program, and the UO_2-Gd_2O_3 experiments were conducted at the same facility as part of the Urania-Gadolinia Critical Experiment Benchmark Program. The UO_2-PuO_2 (2 wt%) critical experiments were performed in the Plutonium Recycle Critical Facility at PNNL.

2.1 Critical Experiments at the B&W Critical Experiment Laboratory Facility

The UO_2 critical experiments from the Physics Verification Program provided local power distribution data covering all possible fuel assembly configurations at beginning-of-life (BOL) conditions. These critical assembly measurements were completed during the early 1970s. The fuel rods, control rods, and lumped burnable poison (LBP) rods (Pyrex) used in these critical experiments are typical of those used in B&W designed power reactors and provide a database sufficient to determine the accuracy of the ***CASMO-5/SIMULATE-3*** computational model at BOL conditions.

The critical experiments from the Urania-Gadolinia Critical Experiment Benchmark Study that were selected were a subset of the DOE Extended-Burnup Program performed by B&W in 1984. As part of this program, a nuclear model for calculated UO_2-Gd_2O_3 was developed and critical experiments were conducted to provide BOL data for benchmarking the model. Specifically, in the core studies, UO_2-Gd_2O_3 fuel rods (either solid or annular), control rods, void tubes, and water holes were spaced in selected patterns in an otherwise uniform, clean lattice to study their effects on reactivity and power distribution. Appendix A contains a full description of the facilities, experimental procedures and detailed information on the critical experimental configurations performed at both LRC and PNNL.

2.1.1 Core Loadings Used for Comparisons

2.1.1.1 B&W Physics Verification Program Core Loadings

The basic critical assembly, designated as Core XI, used to provide data for the comparative analyses performed as discussed in this report is shown in Figure 2-1.

Figure 2-1: Cross-Sectional Layout of the Experimental Core

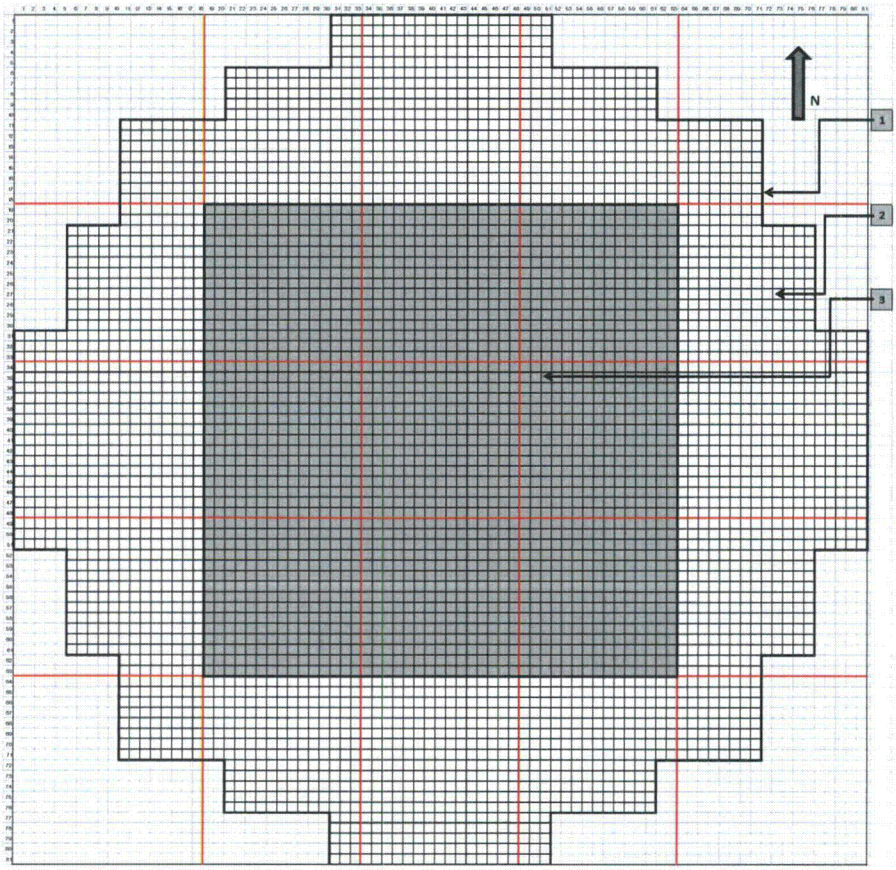

1 – Core boundary
2 – Driver region
3 – Fuel assembly (load specific)
Assembly (modeled) boundary

As indicated in this figure, the center portion of Core XI is divided into nine fuel assemblies equal in size to the standard B&W Mark B fuel assembly. The lattice layout and composition of the different subassemblies that are part of the Core XI critical experiments are shown in Figure 2-2.

Figure 2-2: Subassembly Loadings Within Core XI

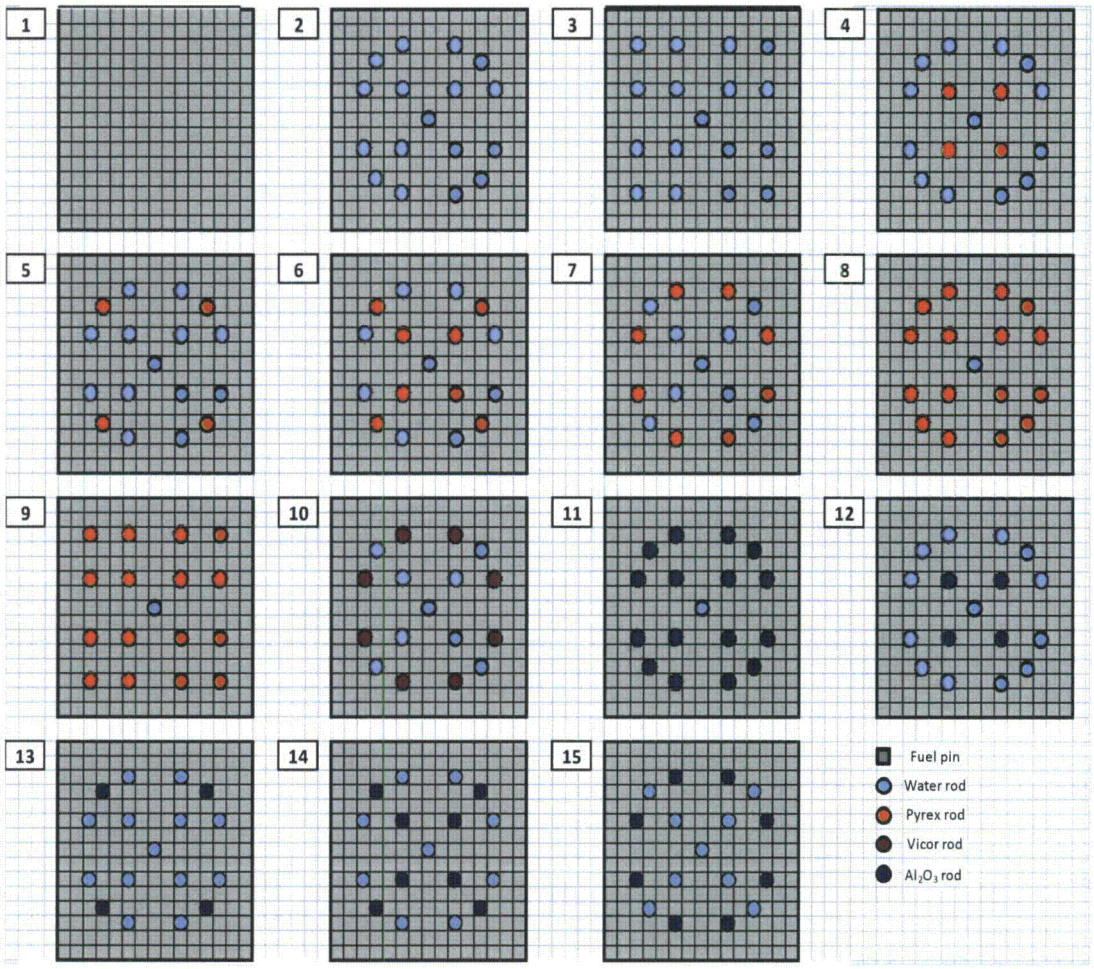

The lattice configurations, attributes, and measured critical boron concentrations for the 17 UO_2 critical assemblies selected for analysis are summarized in Table 2-1.

Table 2-1: Lattice Identifications of the UO_2 Critical Experiments and Critical Boron Concentrations

Core	Loading	Number of Fuel Rods	Number of Water Filled Rod Positions	Number of Pyrex Rods	Number of Ag-In-Cd Rods	Number of Al_2O_3 Rods	Number of Void Tubes	Moderator Boron Conc. Producing Critical Conc. when Mod. Height = 145 cm (ppm)
XI	1	4961	0	0	0	0	0	1506.543
XI	2	4808	153	0	0	0	0	1330.065
XI	3	4808	153	0	0	0	0	1333.056
XI	4	4808	117	36	0	0	0	1179.51
XI	5	4808	117	36	0	0	0	1177.516
XI	6	4808	81	72	0	0	0	1030.95
XI	7	4808	81	72	0	0	0	1027.959
XI	8	4808	9	144	0	0	0	791.658
XI	9	4808	9	144	0	0	0	776.702
XI	10	4808	81	0	72	0	0	1241.327
XI	11	4808	9	0	0	144	0	1379.917
XI	12	4808	117	0	0	36	0	1344.023
XI	13	4808	117	0	0	36	0	1344.023
XI	14	4808	81	0	0	72	0	1358.979
XI	15	4808	81	0	0	72	0	1357.982
XI	16	4691	270	0	0	0	0	1154.584
XI	17	4457	504	0	0	0	0	918.283

2.1.1.2 Urania-Gadolinia Critical Experiment Benchmark Program Core Loadings

A total of 23 cores were assembled in the Urania-Gadolinia Critical Experiment Benchmark Program. In 22 of the 23 cores studied, UO_2-Gd_2O_3, B_4C rods, void tubes and water holes were spaced on selected patterns in an otherwise uniform clean lattice in order to study their effect on reactivity, power distribution and incore detector signal. In essence, these cores simulate a full PWR checkerboard loading of assemblies containing UO_2-Gd_2O_3 fuel rods. To provide generic data germane to all domestic PWR designs, each core loading was a variation of two basic configurations, namely:

- B&W Configurations with:
  - 15x15 Fuel Rods per Assembly Using 2.46 wt% Enriched Fuel: and
  - 15x15 Fuel Rods per Assembly Using 2.46 and 4.02 wt% Enriched Fuel
- Combustion Engineering Configuration with 16x16 fuel configuration

Representative core loadings of B&W configurations are shown in Figure 2-3.

Figure 2-3: B&W Urania-Gadolinia Critical Experiment Benchmark Program Representative Core Loadings

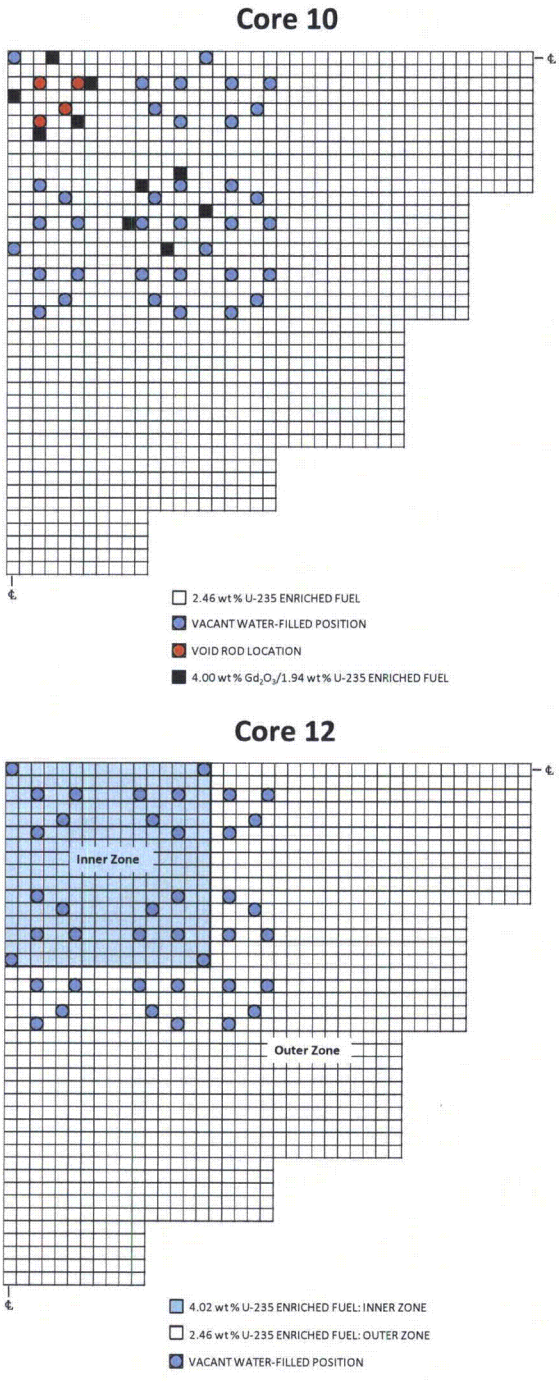

Core 13

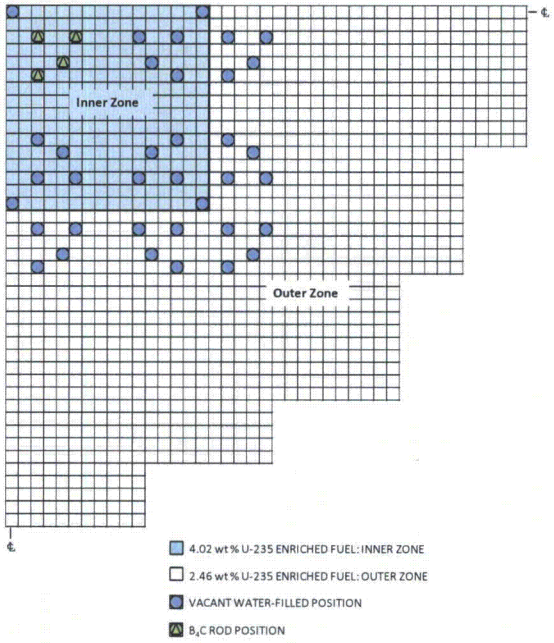

Core 14

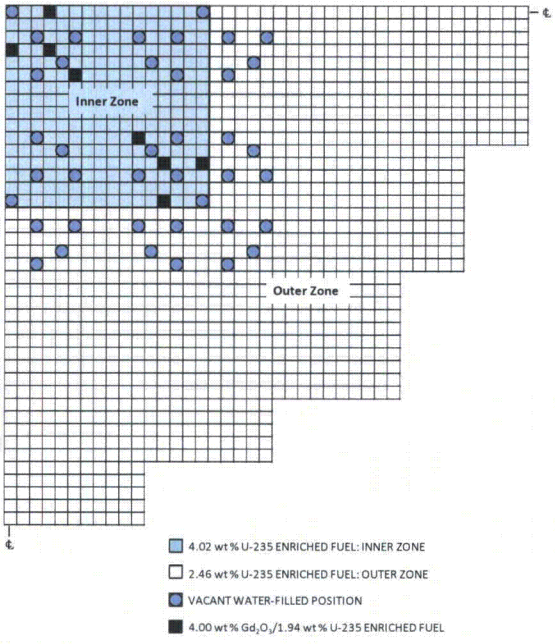

The lattice configurations, attributes, and measured critical boron concentrations for the 17 UO_2–Gd_2O_3 critical experiments selected for analysis are summarized in Table 2-2.

Table 2-2: B&W Urania-Gadolinia Critical Experiment Benchmark Program Cores Evaluated

Core	Description	No. of 2.46 wt% Rods	No. of 4.02 wt% Rods	No. of Gd Rods	No. of B_4C Rods	No. of Ag-In-Cd	No. of Void Rods	No. of Water Holes	Soluble Boron Conc, ppm
1	15x15, 0 Gd Pin Configuration	4808	0	0	0	0	0	153	1337.9
2	15x15, 0 Gd Pin Configuration, Ag-In-Cd in Center	4808	0	0	0	16	0	137	1250
3	15x15, 8 Gd Pin Configuration, Checkerboard, 1/4 Gd	4788	0	20	0	0	0	153	1239.3
4	15x15, 8 Gd Pin Configuration, Checkerboard, 1/4 Gd	4788	0	20	0	16	0	137	1171.7
5	15x15, 12 Gd Pin Configuration, Checkerboard, 1/4 Gd	4780	0	28	0	0	0	153	1208
5A	15x15, 12 Gd Pin Configuration, Checkerboard, 1/4 Gd	4776	0	32	0	0	0	153	1191.3
5B	15x15, 12 Gd Pin Configuration, Checkerboard, 1/4 Gd	4780	0	28	0	0	0	153	1207.1
6	15x15, 12 Gd Pin Configuration, Checkerboard, 1/4 Gd	4780	0	28	0	16	0	137	1155.8
6A	15x15, 12 Gd Pin Configuration, Checkerboard, 1/4 Gd	4776	0	32	0	16	0	137	1135.6
7	15x15, 12 Gd Pin Configuration, Checkerboard, 1/4 Gd	4780	0	28 Annular	0	0	0	153	1208.8
8	15x15, 12 Gd Pin Configuration, Checkerboard, 1/4 Gd	4772	0	36	0	0	0	153	1170.7
9	15x15, 12 Gd Pin Configuration, Checkerboard, 1/4 Gd	4772	0	36	0	16	0	137	1130.5
10	15x15, 12 Gd Pin Configuration, Checkerboard, 1/4 Gd	4772	0	36	0	0	16	137	1177.1
12	15x15, 0 Gd Pin Configuration	3920	888	0	0	0	0	153	1899.3
13	15x15, 0 Gd Pin Configuration, B4C in Center Assembly	3920	888	0	16	0	0	137	1635.4
14	15x15, 0 Gd Pin Configuration, 1/4 Gd Loading in Diagonals	3920	860	28	0	0	0	153	1653.8
15	15x15, 12 Gd Pin Configuration, 1/4 Gd Loading in Diagonals,	3920	860	28	16	0	0	137	1479.7
16	15x15, 16 Gd Pin Configuration, 1/4 Gd Loading in Diagonals	3920	860	36	0	0	0	153	1579.4
17	15x15, 16 Gd Pin Configuration, 1/4 Gd Loading in Diagonals,	3920	860	36	16	0	0	137	1432.1

2.2 Description of Critical Experiments at the Plutonium Recycle Critical Facility (PRCF)

A series of twelve lattice experiments were performed at PNNL to provide benchmark neutronics data for use in assessing the accuracy of neutronics analysis methods for slightly enriched uranium lattices and for mixed oxide (UO_2-PuO_2) lattices. Specifically, the twelve experiments consisted of six core configurations containing UO_2 enriched to 2.15 wt% ^{235}U and six core arrangements containing UO_2-PuO_2 (2 wt%). The lattice pitches were selected to provide configurations that were under-moderated, near optimum moderation, or over-moderated, and that had approximately the same water-to-fuel volume ratio for both fuel types in each degree of moderation. However, since UO_2 critical experiments had previously been analyzed as part of the B&W Physics Verification Program, only the six UO_2-PuO_2 (2 wt%) core configurations were analyzed to provide rods-in and rods-out local power distribution data that simulated an extreme core burnup condition. This was done to obtain the uncertainty in the ***CASMO-5/SIMULATE-3*** calculational model under end-of-life (EOL) fuel burnup conditions.

2.2.1 Core Loadings

The six UO_2-PuO_2 (2 wt%) critical experiments selected for analysis consisted of core configurations with three lattices of different fuel rod pitches, specifically 0.7-inch, 0.87-inch, and 0.99-inch. Two experiments were performed for each type of lattice, one with borated water as the moderator and one with unborated water. Loading maps of the three borated cores are shown below, in Figure 2-4. Detailed loading maps of each of the six experiments modeled are provided in Appendix A, Figure A-35 through Figure A-37. All cores were loaded to be as nearly cylindrical as possible within the constraints of keeping the control/fuel follower rods inside the core boundary. The heavy line on each map denotes the actual boundary of the core loading.

Figure 2-4: Borated MOX Critical Loadings

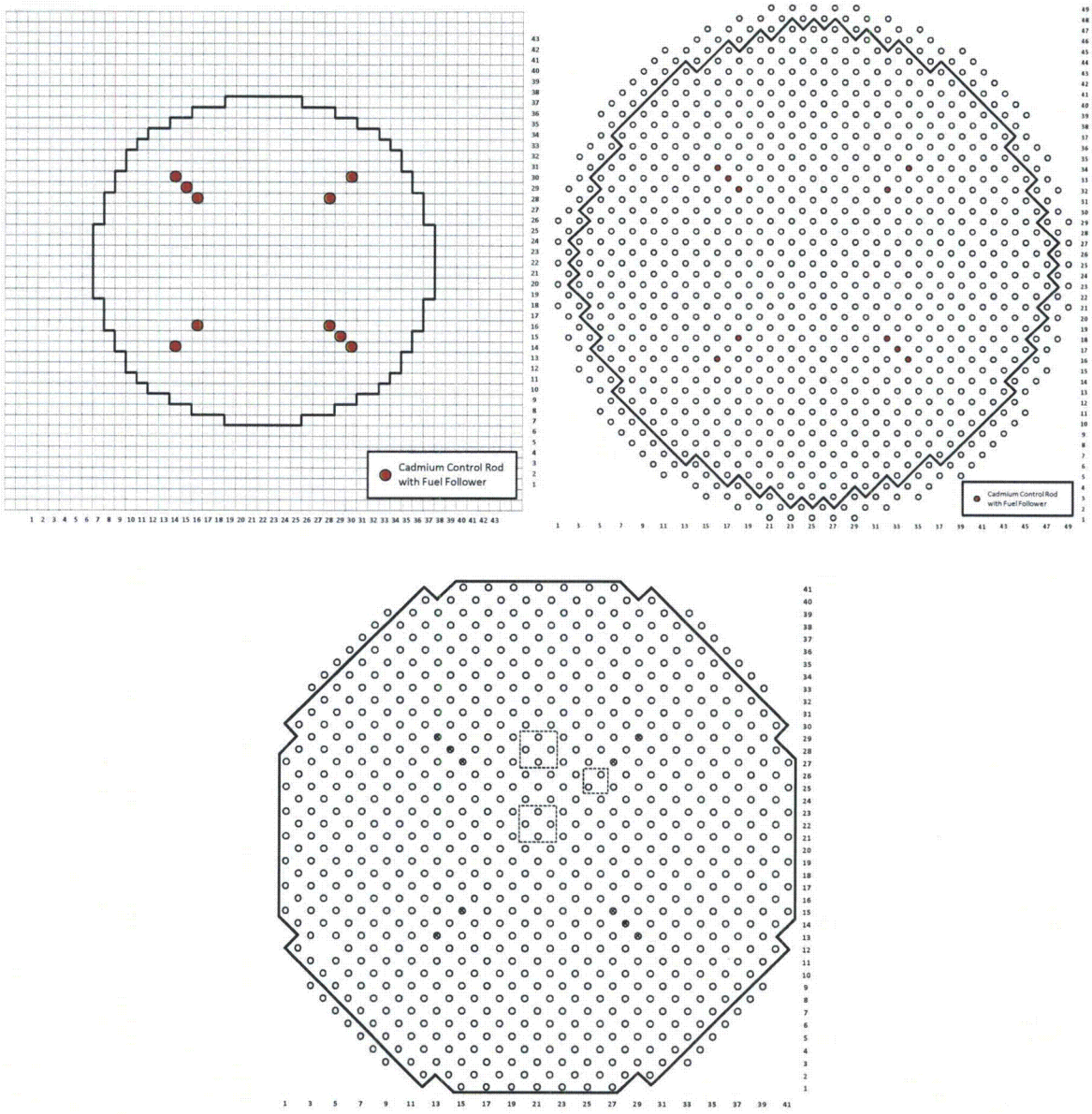

2.3 Determination of Measured to Calculated Data Accuracy

The combination of critical assembly power distribution data from the Physics Verification Program and the Urania-Gadolinia Critical Experiment Benchmark Program provides an overall data base sufficient to determine the accuracy of the ***CASMO-5/SIMULATE-3*** calculational model at both BOL and EOL conditions. However, to make the required comparisons between the measured and calculated data, the measurement uncertainty for the pin powers must be

established. To that end, eight sets of symmetric fuel pins from a representative core loading in the Physics Verification Program were analyzed to determine the uncertainty on the measured pin power value.

The uncertainty associated with the measured values results from random errors introduced by counting statistics and geometry and fuel homogeneity. The component of the error introduced into the measured values by counting statistics was estimated to be about 1.0%. However, the total measurement uncertainty is based on the standard and average deviations of the eight sets of data from their average values. Each set consisted of four fuel pins with measured axial powers at 27 axial locations. The average value of each set of four symmetric points was determined, and the deviation from the average was used for the analysis. A total of 850 data points were used with a variance of 0.000149. On a percentage basis, the total measurement uncertainty for the critical experiments is 1.11%. A detailed discussion of this analysis is given in References 2 and 3 .

The standard deviation associated with the comparisons of measured to calculated data is the combined total uncertainty, σ_t, which is defined as the square root of the sum of the squares of the measurement and calculation uncertainties, σ_m and σ_c, respectively:

$$\sigma_T = \sqrt{\sigma_m^2 + \sigma_c^2}$$

Therefore, the use of total standard deviation σ_T would conservatively represent the accuracy of the ***CASMO-5/SIMULATE-3*** calculational model and its ability to predict the eigenvalues and power distribution of very heterogeneous geometry configurations.

2.4 Calculated Versus Measured Results

This section describes the calculated values used as a basis for the evaluation of the computational methodology using the CMS code suite ***CASMO-5/CMS-LINK/SIMULATE-3***. Comparisons are made between calculated and measured parameters for the cold clean critical experiments from: (1) the B&W Physics Verification Program; (2) the Urania-Gadolinia Critical

Experiment Benchmark Program; and (3) the UO_2-PuO_2 critical experiments from the Plutonium Recycle Critical Facility.

2.4.1 B&W Physics Verification Program UO_2 Critical Experiments

The 17 candidate loadings described previously were modeled for computational methodology evaluation. Although sufficient information for the 17 loadings was available for the critical eigenvalue comparative analysis, only nine loadings were adequate for the pin power comparisons. More specifically, Reference 2 does not list pin powers for Loadings 1, 10 and 12 – 15. Data for Loadings 16 and 17 are available only for pins 0 to E22 (horizontal axis of the core, from center to right edge, 23 pins), which is not sufficient for proper normalization of data; hence, any comparison between ***SIMULATE-3*** calculated and experimentally measured data becomes inconsistent. As a result, only Loadings 2 through 9 and 11 from Reference 2 were used in the pin power comparative analysis.

2.4.1.1 Computational Model

The candidate core loadings described previously were modeled for computational methodology evaluation. Specifically, cross-sections and discontinuity factors for interior zone fuel lattice types (segments), one exterior zone lattice, and one reflector configuration were computed with ***CASMO-5***. The ***CASMO-5*** lattice segments were created based on the 15x15 fuel assembly layout in the interior zone of the cores using eighth-core lattice symmetry.

The S3C default case matrix was selected in ***CASMO-5/CMS-LINK*** to parameterize the lattice cross-sections and associated reactor physics data. Since the constraints of the S3C case matrix and the default ***CMS-LINK*** processing requires fuel depletion at arbitrary hot full power conditions, a limited depletion of 20 MWd/kg was performed, but only a "cold" library was generated and all critical experiments were performed at zero exposure and are thus clean.

All benchmark calculations were performed with ***SIMULATE-3*** in two-dimensional mode using an applied axial buckling of 0.00037 cm^{-2} as an input parameter. This value was obtained from an analysis of the benchmark experiments with MCNP and reported in Reference 9. In order to preserve the 15x15 pin lattice model for all assemblies, the outer driver region was modeled as twelve 15x15 assemblies, plus four "1/4 assemblies", in the corners. This results in a total of 2925 fuel rods in the driver, whereas, in reality, there were 2936 rods in this outer region (as shown in Figure 2-1). The corner assemblies were modeled as 1/4 fuel and 3/4 reflector. The 3x3 inner region was modeled in detail. Figure 2-5 shows the layout of the modeled cores.

Figure 2-5: Cross-Sectional Layout of the B&W Physics Verification Program UO_2 Critical Experiments Model

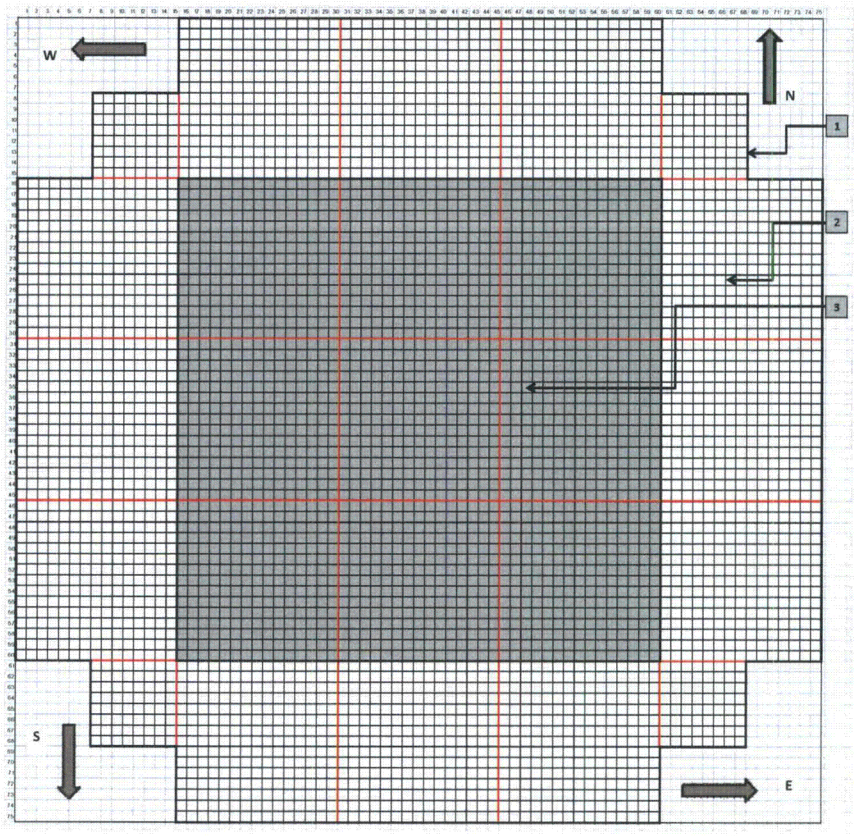

1 – Core boundary **2** – Driver region **3** – Fuel assembly (load specific)

Assembly (modeled) boundary

2.4.1.2 Eigenvalue Comparisons

2.4.1.2.1 *Biases and Uncertainties in the Critical Eigenvalue Calculation*

Modeling-Induced Biases

The above mentioned approximation made in the model for the outer driver region introduces a bias in the calculations. This bias was evaluated by increasing the fuel density of the driver pins from 10.24 g/cm^3 to 10.26 g/cm^3 to account for the total actual mass of the fuel in the driver. A sensitivity study performed with ***SIMULATE-3*** to assess the difference in k_{eff} yielded by this increase in fuel density showed an increase in k_{eff} of 0.0001 (1.00224 for 10.26 g/cm^3 versus 1.00214 for 10.24 g/cm^3).

Boron Concentration Uncertainties

The measured cold critical eigenvalue reported in References 2 and 3 for all experiments is 1.0007, with an experimental uncertainty of ±3 ppm in the soluble boron concentration. A sensitivity study performed with ***SIMULATE-3*** for Loading 1 to account for a ±3 ppm uncertainty in boron concentration showed a variation in k_{eff} of ±0.00041.

Overall Uncertainties in Eigenvalue Calculations

Table 2-3 summarizes the uncertainties introduced in the calculation of the critical eigenvalue by the various idealizations made in modeling of the experimental cores.

Table 2-3: Estimated Biases and Uncertainties in the Critical Eigenvalue Calculation

	Parameter	Biases and Uncertainties			
1	Fuel length	None	Length (cm)	153.4	145.0
			$k_{eff} = k_1$	k_1	k_1
2	"Cold" temperature[1]	+0.00017	Temp (°C)	20	25
			$k_{eff} = k_2$	k_2	$k_2 + 0.00017$
3	Buckling	+0.00268	Buckling (cm^{-2})	4.41×10^{-4}	3.7×10^{-4}
			$k_{eff} = k_3$	k_3	$k_3 + 0.00268$
4	Boron concentration (PPM)[2]	+0.0006	B Conc. (PPM)	1511	1506.54255
			$k_{eff} = k_4$	k_4	$k_4 + 0.0006$
5	Boron concentration uncertainty[3]	±0.00041	B Conc. (PPM)	1511 + 3 PPM	1511 –3 PPM
			$k_{eff} = k_5$	k_5 +0.00041	$k_5 - 0.00041$
6	Modeling	+0.0001	Pellet ρ (g/cc)	10.24	10.26
			$k_{eff} = k_6$	k_6	$k_6 + 0.0001$

Notes: 1. The higher Δk, obtained for the core with lowest boration (Loading 9), was considered.
2. From differences between References 2 and 3 definition of ppm and SIMULATE-3 methodology.
3. From ±3 ppm assumed boron concentration uncertainty.

It can be concluded that none of the biases introduced in the benchmark models by the various assumptions made ("cold" temperature definition, boron concentration, number of pins modeled in the driver region, buckling) significantly affect k_{eff}, with the exception of buckling. The level of significance for reactivity effects arising from the idealizations employed to produce the benchmark models was taken to be ± 0.0045 Δk, to cover for all uncertainties and biases listed in Table 2-3. The resulting benchmark-model critical eigenvalue for all of these cases is then: 1.0007 ± 0.0045.

2.4.1.2.2 *Calculated Versus Measured Critical Eigenvalues*

Table 2-4 summarizes the cold critical k_{eff} calculated with ***SIMULATE-3*** for all 17 critical experiments. Comparisons are presented between three data sets: ***SIMULATE-3***, the Physics Verification Program (as reported in References 2 and 3) the

MCNP benchmark described in Reference 9. As mentioned in Reference 9, the three-dimensional models produce a k_{eff} approximately 0.002 lower than the two-dimensional models. However, Reference 9 considers this difference to be insignificant.

Overall, the ***SIMULATE-3*** data was in very good agreement with both the ***MCNP***–calculated value of k_{eff} (corrected to include Los Alamos uncertainties and three-dimensional versus two-dimensional biases) and B&W value of k_{eff} inferred from boron concentration measurements. The highest differences were recorded for Loadings 8 and 9 (0.00431 and 0.00422 respectively), which had the lowest boron concentrations and the highest number of Pyrex rods. The standard deviation of all eigenvalues was 0.0020 for ***SIMULATE-3/B&W*** and 0.0009 for ***SIMULATE-3/MCNP.*** This type of behavior was encountered in other benchmark studies for the same loadings [Reference 9].

These results indicate that the ***CASMO-5/SIMULATE-3*** methods and model used for the calculation can accurately predict the criticality condition and power distribution of the various heterogeneous configurations presented.

Table 2-4: Calculated Versus Measured Eigenvalues

#	SIMULATE-3 Benchmark[1]	B&W Tests[2]	MCNP[3] Corrected Benchmark[4]	(SIMULATE-3/B&W)		(SIMULATE-3/MCNP)
				Abs. Diff.	Within estimated?	Abs. Diff.
1	1.0021	1.0007	1.0003	0.00142	YES	0.0018
2	1.0030	1.0007	1.0030	0.00226	YES	0.0000
3	1.0029	1.0007	1.0008	0.00224	YES	0.0021
4	1.0017	1.0007	1.0018	0.00102	YES	0.0001
5	1.0014	1.0007	1.0012	0.00073	YES	0.0002
6	1.0005	1.0007	1.0016	0.00025	YES	0.0011
7	1.0001	1.0007	1.0010	0.00058	YES	0.0009
8	0.9964	1.0007	1.0001	0.00431	YES	0.0037
9	0.9965	1.0007	1.0006	0.00422	YES	0.0041
10	1.0019	1.0007	1.0020	0.00115	YES	0.0002
11	1.0029	1.0007	1.0022	0.00221	YES	0.0007
12	1.0027	1.0007	1.0008	0.00197	YES	0.0019
13	1.0027	1.0007	0.9999	0.00199	YES	0.0028
14	1.0023	1.0007	1.0010	0.00160	YES	0.0013
15	1.0024	1.0007	1.0010	0.00166	YES	0.0014
16	1.0019	1.0007	1.0028	0.00121	YES	0.0009
17	1.0006	1.0007	0.9998	0.00012	YES	0.0008
AVG	1.0013	1.0007	1.0012			
STD DEV	0.0020	0.0000	0.0009			

Notes:
1. CASMO-5/SIMULATE-3, using two dimensional lattice physics and the ENDF/B-VII.0 based 586 group cross-section library.
2. Boron concentration measurements, determined by titration against a standard KOH solution.
3. MCNP, using continuous-energy ENDF/B-VI cross-section libraries.
4. Corrected to include the uncertainties listed in Table 20, Reference 9, and the 0.002 bias between two-dimensional and three-dimensional models (per Reference 9).

2.4.1.2.3 *Pin Power Comparisons*

Pin powers for Loadings 2 through 9 and 11 were calculated with ***SIMULATE-3*** and compared to the B&W Physics Verification Program (References 2 and 3) measured data. Figure 2-6 and Figure 2-7 summarize the result of the comparative analysis for loadings 2 and 3; the results for the other loadings can be seen in Appendix A, Figure A-38 through Figure A-46. All experimentally measured data was renormalized to a quarter-core lattice for comparison with the calculated result.

Figure 2-6: Pin Powers Comparison for Loading 2

MEA	0.000	1.071	0.993	0.96	0.99	0.993	0.948	0.951
CAL	0.000	1.079	1.028	1.00	0.99	0.995	0.963	0.942
DIF	0.000	0.008	0.035	0.03	0.00	0.002	0.015	-0.009
		1.033	1.040	1.00	1.01	1.062	0.993	0.970
		1.052	1.072	1.02	1.01	1.046	0.984	0.946
		0.019	0.032	0.01	0.00	-0.016	-0.009	-0.024
			0.000	1.08	1.08	0.000	1.035	0.930
			0.000	1.08	1.07	0.000	1.033	0.952
			0.000	0.00	-	0.000	-0.002	0.022
				1.05	1.10	1.096	0.999	0.894
				1.05	1.09	1.071	0.989	0.943
				-	-	-0.025	-0.010	0.049
					0.00	1.073	0.974	0.942
					0.00	1.051	0.962	0.939
					0.00	-0.022	-0.012	-0.003
						0.982	0.941	0.939
						0.982	0.940	0.919
						0.000	-0.001	-0.020
							0.939	0.919
							0.922	0.909
							-0.017	-0.010
								0.890
								0.900
								0.010

MAX DIFF	0.049
ST DEV	0.019

UO

Wate

Pyre

Vico

Al2O

Figure 2-7: Pin Powers Comparison for Loading 3

The average difference between the measured and calculated pin powers was less than 1%, with maximums in the low 3 – 4%, range prior to consideration of the uncertainties listed in Tables 4 through 12 in References 2 and 3. When those uncertainties are taken into account, better agreement is obtained.

2.4.2 UO_2–Gd_2O_3 Experiments from the Urania-Gadolinia Critical Benchmark Program

As discussed previously, a total of 23 cores were assembled in the Urania-Gadolinia Critical Experiment Benchmark Program. In 22 of the 23 cores, UO_2-Gd_2O_3, B_4C rods, void tubes and water holes were spaced on selected patterns in an otherwise uniform

clean lattice to study their effect on reactivity, power distribution, and incore detector signal. Seventeen of the cores (15x15 B&W type lattice) were selected for evaluation with ***CASMO-5/SIMULATE-3.*** The configurations of these cores are summarized in Table 2-2. The measured pin power distributions for Cores 1, 5, 12 and 14 were compared to the ***CASMO-5/SIMULATE-3*** pin power reconstruction calculations.

2.4.2.1 Computational Model

Cross-sections and discontinuity factors for fifteen interior zone fuel lattice types (segments), one exterior zone lattice, and one reflector configuration were computed with ***CASMO-5***. These cases are shown in Table 2-5. ***CASMO-5*** lattice segments were created based on the 15x15 fuel assembly layout in the interior zone of the cores. In most cases, this required eighth-core lattice symmetry, but in some cases adjacent lattices contained two or four gadolinia rods along the fuel assembly centerline, which necessitated using quarter-core lattice symmetry. In addition, since the Ag-In-Cd and B_4C rods were placed in the water holes (guide tube locations) of the central assembly, this was modeled as control rod insertion ('ROD') in ***CASMO-5, CMS-LINK*** and ***SIMULATE-3***.

Table 2-5: CASMO-5 Calculation Summary for Urania-Gadolinia Critical Experiments

Case	Symmetry	w/o ^{235}U	No. Gd Rods	Control Rod	CR Type	Water Holes	Core	Zone
1	⅛	2.46	0	in/out	AIC	17	1 and 2	Interior
2	⅛	2.46	0	-	-	-	1 and 2	Exterior
3	⅛	2.46	8	in/out	AIC	17	3 and 4	Interior
4	¼	2.46	2	-	-	17	3 and 4	Interior
5	⅛	2.46	12	in/out	AIC	17	5 and 6	Interior
6	¼	2.46	2	-	-	17	5 and 6	Interior
7	⅛	2.46	12	in/out	AIC	17	5A and 6A	Interior
8	¼	2.46	4	-	-	17	5A and 6A	Interior
9	⅛	2.46	12 annular	-	-	17	7	Interior
10	¼	2.46	2 annular	-	-	17	7	Interior
11	⅛	2.46	16	in/out	VOID	17	8, 9 and 10	Interior
12	⅛	4.02	0	in/out	B4C	17	12 and 13	Interior
13	¼	2.46/4.02	0	-	-	17	12 and 13	Interior
14	⅛	4.02	12	in/out	B4C	17	14 and 15	Interior
15	¼	2.46/4.02	2	-	-	17	14 and 15	Interior
16	⅛	4.02	16	in/out	B4C	17	16 and 17	Interior
17	¼	2.46	-	-	-	-	All	Reflector

The S3C default case matrix and data functionalization was selected in ***CASMO-5/CMS-LINK*** to parameterize the lattice cross-sections and associated reactor physics data. Given the constraints of the S3C case matrix and the default ***CMS-LINK*** processing, depletion was required for cross-section processing even for cold clean critical experiments. Thus a limited depletion at arbitrary hot full power conditions was performed, but only a "cold" library was generated. However, all critical experiments were modeled in ***SIMULATE-3*** at zero exposure and are thus clean. ***CMS-LINK*** was used to process the ***CASMO-5*** card image files into a cross-section library. The cross-sections and other data were ultimately represented as a function of instantaneous reactor operational parameters such as exposure, moderator temperature, soluble boron, and control rod presence.

All cores were modeled in ***SIMULATE-3*** in a two-dimensional mode with an axial buckling factor. The value of the applied axial buckling factor was 0.05334 in^{-2} and is

based on B&W measurements provided in Reference 4. A 5x5 fuel assembly representation of the core was created with four nodes per assembly. This representation captured the 3x3 interior zone in detail, but approximated the exterior driver zone and core-reflector boundary. However the edge details of the driver zone were unimportant to the computation of central assembly pin powers. Also the core loading was approximately correct, so the eigenvalues should be accurate.

2.4.2.2 Eigenvalue Comparisons

2.4.2.2.1 *Uncertainties in the Critical Eigenvalue Calculation*

Reference 4 indicates that the soluble boron given in Table 2-6 of this report is that for critical (k=1.0) when the moderator height is at 145 cm and the temperature is at 77 °F. Uncertainty in moderator boron was reported to be on average ± 1 ppm for the Urania-Gadolinia experiments. Based on this and the uncertainty in the physical parameters of the 2.46 wt % enriched fuel rods such as density and enrichment, an evaluation was made of experimental uncertainties on the critical eigenvalues. Also the impact of modeling fewer rods due to core periphery and use of axial buckling on critical eigenvalue was made. Table 2-6 summarizes the evaluation of experimental uncertainties in the calculation of the critical eigenvalue by the various uncertainties in physical parameters and idealizations (axial buckling and core geometry approximation) made in modeling of the experimental cores.

The principal physical parameters that introduce uncertainty are the fuel density, fuel enrichment temperature and boron concentration. The standard deviation on the critical eigenvalue for these physical parameters is ± 0.00070. This implies the benchmark critical eigenvalues are 1.00000 ± 0.00070 (0.99930 to 1.00070). Note the ***SIMULATE-3*** Core 1 eigenvalue is within this range.

The bias introduced by the model approximation in the core periphery and the resultant 11 fewer rods than the actual loading was found to be 0.00008 Δk. This is

small but should be added to the results of Table 2-7. The uncertainty introduced by assuming an axial buckling was found to be 0.00114 Δk. Note Reference 4 does not give a measured axial buckling. The axial buckling assumed in these evaluations is inferred from earlier measurements given in References 2 and 3.

Table 2-6: Estimated Uncertainties in the Critical Eigenvalue Calculation

	Parameter	Uncertainty/bias	Average	High	ΔK
1	Fuel Density	± 0.04 g/cc	10.24	10.28	
			0.99939	1.00006	+0.00067
2	Fuel Enrichment	± 0.002 wt %	2.459	2.461	
			0.99939	0.99952	+0.00013
3	Temperature	± 1 F	77	78	
			0.99939	0.99940	+0.00001
4	Buckling Bias	± 0.00031 cm^{-2}	$4.41x10^{-4}$	$4.1x10^{-4a}$	
			0.99939	1.00053	+0.00114
5	Boron Conc.	± 1 ppm	1138	1139	
			0.99939	0.99923	-0.00016
6	Modeling Bias	-11 rods	1925	1936	
			0.99939	0.99947[b]	+0.00008

Notes: [a] Studsvik recommended value based on 150 cm active fuel zone.
[b] Computed from eigenvalue due to the addition of one quadrant of 52 fuel rods scaled down to 11 additional rods

2.4.2.2.2 *Calculated Versus Measured Critical Eigenvalues*

The Urania-Gadolinia core eigenvalues are summarized in Table 2-7. The average k_{eff} is 0.99811 ± 0.00056. These eigenvalues are consistent, i.e. no apparent trends, over the range of experimental variables.

Table 2-7: Urania-Gadolinia Core Eigenvalues

Core	k_{eff}	Soluble Boron (ppm)	No. of Gd Rods	No. of B_4C Rods	No. of Ag-In-Cd Rods	No. of Void Rods	No. of Water Holes
1	0.99939	1338	0	0	0	0	153
2	0.99808	1250	0	0	16	0	137
3	0.99875	1239	20	0	0	0	153
4	0.99854	1172	20	0	16	0	137
5	0.99782	1208	28	0	0	0	153
6	0.9974	1156	32	0	0	0	153
5A	0.99804	1191	28	0	0	0	153
6A	0.99757	1136	28	0	16	0	137
5B	0.99796	1207	32	0	16	0	137
7	0.99782	1209	28 Annular	0	0	0	153
8	0.99779	1171	36	0	0	0	153
9	0.99716	1131	36	0	16	0	137
10	0.99771	1177	36	0	0	16	137
12	0.9988	1899	0	0	0	0	153
13	0.99897	1635	0	16	0	0	137
14	0.99824	1654	28	0	0	0	153
15	0.99815	1480	28	16	0	0	137
16	0.99808	1579	36	0	0	0	153
17	0.99785	1432	36	16	0	0	137

Average	0.998112
ST DEV	0.000562

2.4.2.3 Pin Power Comparisons

Comparisons of calculated to measured central assembly pin powers are shown in Figure 2-8 and Figure 2-9 for Cores 5 and 14, respectively. Data comparisons for Cores 1, 5 12 and 14 are shown in Appendix A, Figure A-48 and Figure A-51. The standard deviation on pin powers for Cores 1 and 12, i.e., no gadolinia rods, is 0.014 (1.4%) which indicates very good agreement with measurements. The standard deviation for Cores 5 and 14 are 0.008 (0.8%) and 0.012 (1.2%), respectively, which is also very good agreement.

Figure 2-8: Core 5 Central Assembly Pin Powers Calculated to Measured

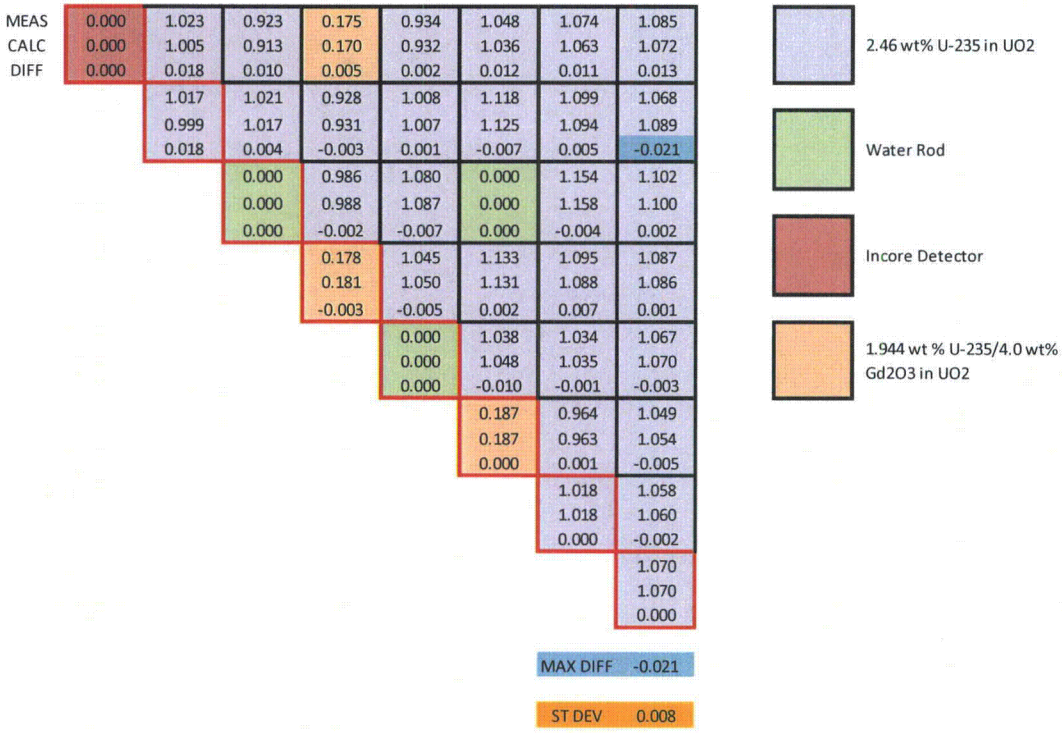

Figure 2-9: Core 14 Central Assembly Pin Powers Calculated to Measured

2.4.3 UO_2-PuO_2 Critical Experiments from the Plutonium Recycle Critical Facility

As discussed previously, six mixed oxide (UO_2-PuO_2) core configurations were selected from the Critical Experiment Benchmarks for the Plutonium Recycle Program and were analyzed to provide rods-in and rods-out local power distribution data that simulated an extreme core burnup condition. The six cases encompass three different lattice pitches providing simulated under-moderated, near optimum moderation, and over-moderated configurations. For each type of lattice, two experiments were conducted, one with unborated water and one with borated water as moderator. Table 2-8 below summarizes the general characteristics of the critical experiments evaluated with ***CASMO-5.***

Table 2-8: CASMO-5 Calculation Summary for the UO2-PuO2 Critical Experiments

Loading	Pitch (in)	Pitch (cm)	Water/Fuel Ratio	# of Rods at Critical	Boron Concentration (ppm)	Excess Reactivity (cents)	Boron Sensitivity (cents/ppm)
CORE-1	0.7	1.778	1.195	469	1.7 ± 0.1	5.1	–
CORE-2				761	680.9 ± 2	1.8	2.8
CORE-3	0.87	2.2098	2.527	195	0.9 ± 0.2	6.8	–
CORE-4				761	1090.4 ± 2	6.5	2.1
CORE-5	0.99	2.5146	3.641	160	1.6 ± 0.1	22.3	–
CORE-6				689	767.2 ± 2	3.8	5.1

2.4.3.1 Computational Model

The benchmark calculations were performed employing ***CASMO-5***, with each experiment fully and explicitly modeled. Some discontinuities occur at the top and the bottom of the core, with the most notable being that the MOX fuel rods had a blanket of UO_2 powder at one end. However, the experiments were modeled in 2D; therefore the axial inhomogeneities were ignored.

Each core configuration was considered as one two-dimensional lattice (one "fuel assembly"), with an axial buckling (cm^{-2}) applied and calculated as the average of the two values reported in Reference 5. The assembly pitch, for each experiment, was taken to be equal to the diameter of the core. The specific conditions at criticality

were input parameters in each ***CASMO-5*** input file: fuel and moderator temperature (equal values, for cold critical conditions), boron concentration and plutonium isotopic distribution at the time of each experiment (^{238}Pu, ^{239}Pu, ^{240}Pu, ^{241}Pu, ^{242}Pu and ^{241}Am). Since the isotopic distribution of plutonium, given in Reference 5 and listed in Figure A-35, was accurate as of approximately ten years prior to the experiments (a date denoted as "analysis date", in Reference 5), the plutonium vector was back-decayed to the "separation date" and then each isotope decayed to the actual date of each experiment. It should be noted that only the isotopic concentrations of ^{241}Pu (which has a short half-life of 14.4 years) and ^{241}Am, its daughter, changed noticeably from the distribution listed in Figure A-35 and from case to case (the six experiments were conducted over one year).

2.4.3.2 Eigenvalue/k-infinity Comparisons

Since the calculations were performed employing only ***CASMO-5***, the k-infinity for each model was compared to the eigenvalues computed from the fully reflected excess reactivity (cents) and the effective delayed neutron fraction (β) values listed in Reference 5 for each experiment. The effective β was the same for all experiments, 3.45×10^{-3}.

2.4.3.2.1 *Uncertainties in the k-infinity Calculation*

Fuel Pin Modeling-Induced Biases

The MOX fuel comprises irregular PuO_2 particles with an effective "mean diameter" of about 25 microns. PuO_2 and UO_2 particles were blended in a mixture and compacted in the cladding tube by vibration. Since PuO_2 exists in the fuel as finite size particles, the fuel is heterogeneous in composition, rather than homogeneous. The reactivity change relative to homogeneous fuel comes from the shielding effects of ^{239}Pu fission, ^{239}Pu capture and ^{240}Pu capture. Typical eigenvalue calculations for the MOX lattices would produce higher k-infinity values, because the fuel is assumed to be homogeneous.

Several sensitivity studies were performed with ***CASMO-5*** in order to assess the differences in k-infinity yielded by each modeling approach used. Three different approaches were employed: 1) concentric shells of heterogeneous PuO_2 and UO_2 layers, 2) concentric shells of homogeneous MOX fuel, and 3) fuel modeled with the straight-forward approach (homogeneous fuel, no concentric shells). The maximum Δk bias was found to be 0.00104, between approaches 1) and 3).

Plutonium Isotopic Composition and Concentration

The plutonium isotopes in the plutonium oxide are specified in the experiment documentation as of an "analysis date" (1965), eleven years prior to the experiments and three years after the "separation date". For ***CASMO-5*** use, the isotopic distribution of the plutonium vector was recalculated by back-decaying the isotopes to the separation date (1962) and then recalculating the isotopic distribution for each experiment, using the actual experiment date. The ^{238}Pu isotope was not included in the plutonium isotopic composition. A sensitivity study showed the impact of this approximation on k-infinity to be a negligible 0.00002 Δk.

Boron Concentration Uncertainties

The measurement uncertainty reported for all experiments with borated water is ±2 ppm. Reference 5 also lists the Boron sensitivity in cents permitting the reactivity worth of 2 ppm to be calculated. The calculated maximum uncertainty in k-infinity is 0.000704 Δk.

Buckling Uncertainties

Neutron flux measurements taken at two locations during each of experiment were fit to two "axial traverse fits". The two buckling values inferred from the cosine fits are very close, but not identical. ***CASMO-5*** calculations used an average of the two values. Sensitivity studies performed to assess the bias introduced by the buckling approximation showed a maximum Δk difference of 0.000349.

Overall Uncertainties in k-infinity Calculations

Table 2-9, below, summarizes the uncertainties introduced in the calculation of k-infinity by the various idealizations made in modeling of the experimental cores.

Table 2-9: Estimated Biases and Uncertainties in the k-infinity Calculations

Parameter	Biases and Uncertainties			
Base case	–	k_{inf} 1.001618	Buckling 9.0912×10^{4}	^{238}Pu 0 wt%
Heterogeneity of the fuel (concentric layers model)	+ 0.00104	Base case $k_{inf} = k_1$	Homogeneous $k_1 + 0.000828$	Heterogeneous $k_1 + 0.001038$
Buckling	± 0.000349	Buckling (cm^{-2}) $k_{inf} = k_1$	8.9929×10^{4} $k_1 + 0.000349$	9.1733×10^{4} $k_1 - 0.000287$
Pu isotopic composition and concentration (wt%)	+ 0.00002	^{238}Pu = 0.00897 wt% $k_{inf} = k_2$	Homogeneous, no ^{238}Pu $k_2 + 0.00002$	Heterogeneous, no ^{238}Pu $k_2 + 0.00002$
Boron concentration uncertainty	± 0.000297	B Conc. (ppm) $k_{inf} = k_3$	1090.4 + 2 ppm $k_3 + 0.000295$	1090.4 –2 ppm $k_3 - 0.000297$

Calculated Versus Measured Multiplication Factors

Table 2-10 summarizes the k-infinity calculated with ***CASMO-5*** for all 6 experimental configurations presented in Table 2-8. Comparisons are presented between three data sets: 1) k-infinity calculated using ***CASMO-5***, 2) k-effective calculated from the experimental data in Reference 5, and 3) MCNP-5 values (based on three-dimensional models that include additional axial details).

Table 2-10: Calculated Versus Measured Eigenvalues

Core #	CASMO-5 Benchmark[1]	MOX Experiments[2]	MCNP-5 Benchmark[3]	Delta (CASMO-5/MOX Experiments)		CASMO-5/ MCNP-5
				Abs. Diff.	Within acceptable limits?	Abs. Diff.
1	1.00168	1.00018	1.00163	0.0015	YES	0.0001
2	1.00121	1.00006	1.00227	0.0011	YES	0.0011
3	1.00555	1.00023	1.00153	0.0053	YES	0.004
4	1.00322	1.00023	1.00427	0.0030	YES	0.001
5	1.00350	1.00077	1.00242	0.0027	YES	0.0011
6	1.00356	1.00013	1.00301	0.0034	YES	0.0006
Average differences				0.0029		0.0013

Notes: 1. CASMO-5 version 1.07.00, using two dimensional lattice physics and the ENDF/B-VII.0 based 586 group cross-section library 'e7r0.125.586.bin'.

2. Values determined from the fully reflected excess reactivity reported in Reference 5.

3. k_{inf} results for the MCNP-5 heterogeneous model, as reported in Table V, Reference 9. These values were chosen for the comparison, rather than the homogeneous MCNP-5 results, since the heterogeneous model is considered closer to reality.

Overall, the value of k-infinity calculated using ***CASMO-5*** was in very good agreement with both the ***MCNP*** k_{eff} and the k_{eff} inferred from experimental data (excess reactivity and β-effective). For all but one computer run, the eigenvalue differences were well within the estimated uncertainties. The highest bias was recorded for CORE 3, which is consistent with other recent publications (R. D. Mosteller).

2.4.3.3 Pin Power Comparisons

The pin powers are insensitive to the benchmark assumptions that affect k_{eff}. Two representative pin power comparisons using the ***CASMO-5*** calculations and experimentally measured data are presented in Figure 2-10 and Figure 2-11. The full set of results is available in Appendix A, Figure A-52 through Figure A-57. Data from Reference 5, including the uncertainties, was used in the analysis for all the loadings. All experimentally measured data was normalized to a "normalization pin". ***CASMO-5*** calculated data was post-processed the same way, by re-normalizing it to the same normalization pin used in Reference 5, to facilitate a proper comparison. Measurement uncertainties are included in the comparisons.

The calculated data was overall in good agreement with the results of the experiments. The average difference on pin powers was less than 2%, with maximums, in general, in the vicinity of 3 – 4%.

It should also be mentioned that pin power data was not available for all locations, but rather for a limited number of pins. A reduced number of tallies always makes comparisons less accurate, since the normalization is done to a smaller number of data points. The relative pin powers calculated by ***CASMO-5*** are normalized to 1/4 lattice (the result are the same as for a normalization to the full lattice). In order to properly compare the data, the measured values should have been first re-normalized to a quarter lattice, provided that data for all fuel locations were available.

Figure 2-10: Pin Powers Comparison for CORE 1

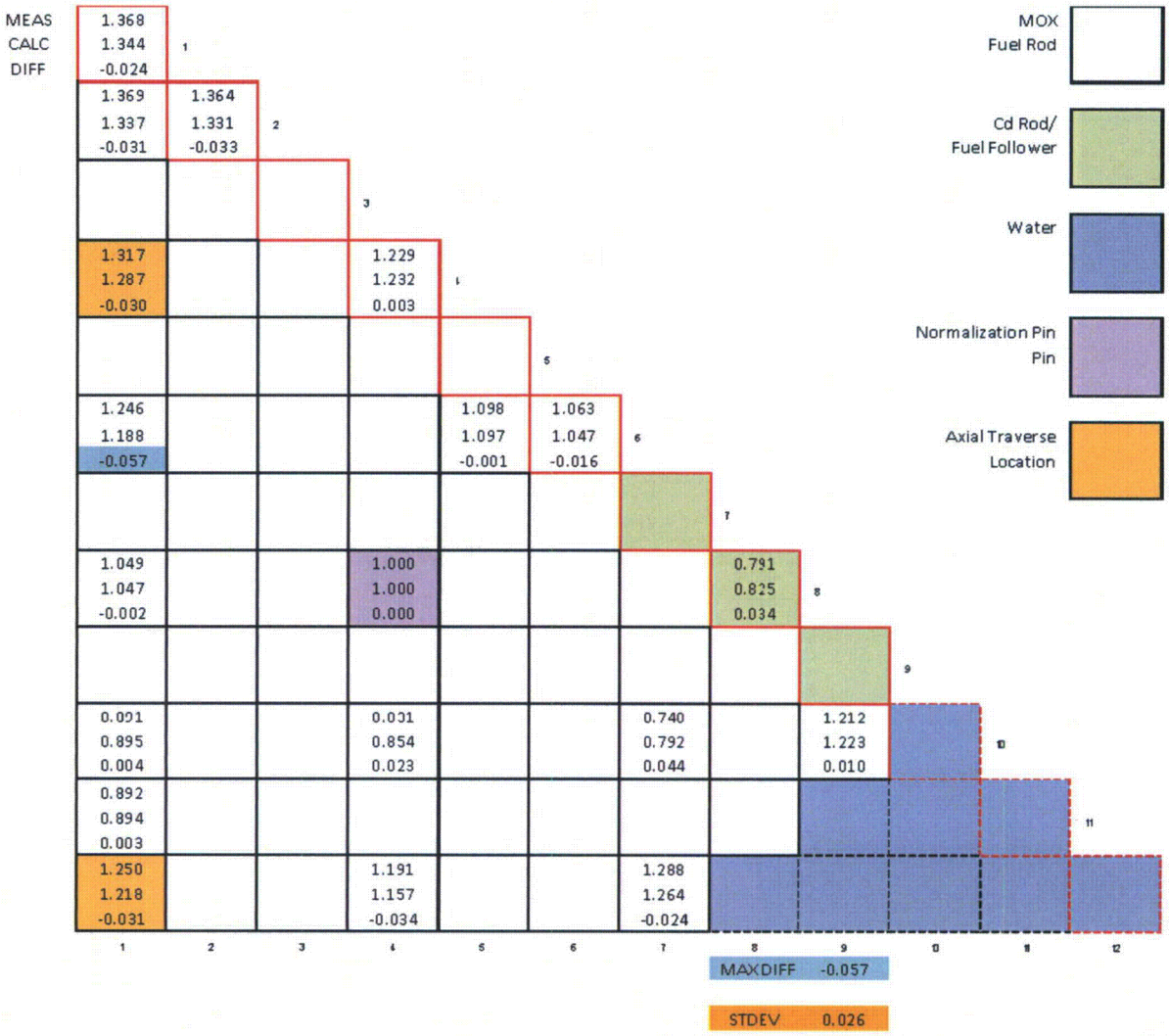

Figure 2-11: Pin Powers Comparison for CORE 2

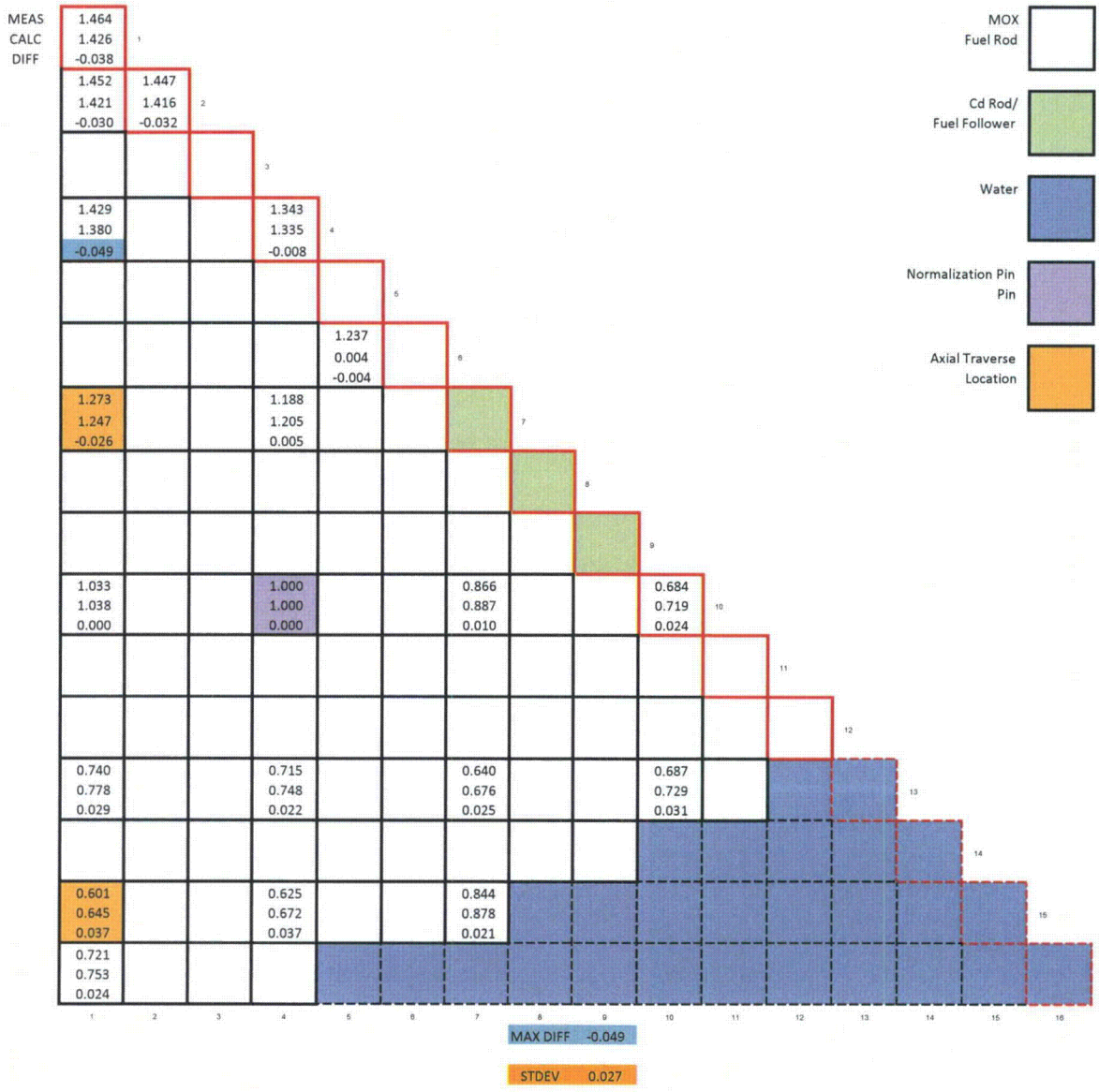

3.0 Three Mile Island Unit 1 Cycles 1 and 2 Hot Zero Power Startup and Core Follow

Predicted and measured results from Three Mile Island Unit 1 (TMI-1) Cycles 1 and 2 hot zero power startup and core cycle operation were analyzed to determine the accuracy of the ***CASMO-5/SIMULATE-3*** computational methodology. Detailed models were used to calculate: (1) hot zero power critical boron, control rod worths, and reactivity coefficients, and (2) core follow eigenvalues, critical boron, and assembly radial and axial power distributions.

3.1 Brief Description of TMI-1 Cycles 1 and 2

TMI-1 is two-loop PWR with a design thermal power of 2535 MW and a nominal operating pressure of 2185 psi. Each reactor coolant loop contains a vertical once-through straight-tube-and-shell steam generator and two coolant pumps. One loop includes a pressurizer. The reactor core consists of 177 mechanically identical fuel assemblies, each comprising a 15x15 lattice containing 208 fuel rods, 16 control/safety rod guide tubes, and one instrument tube, and arranged in a pattern that approximates a right circular cylinder. Reactivity is controlled by 61 full-length Ag-In-Cd control rod assemblies and soluble boron shim. Eight partial-length Ag-In-Cd control rods are used to control the axial power distribution.

3.1.1 Fuel Assembly Data

TMI-1 utilizes the B&W Mark B 15x15 fuel assembly design. Each fuel assembly contains 208 fuel rods on a 0.568-inch pitch consisting of uranium dioxide pellets contained in cold-worked Zircaloy-4 cladding tubes. The cladding is 0.430-inch outer diameter and 0.0265-inch thick. The pellets are 0.370-inch diameter and 0.7-inch long. The initial pressure in the gap between the pellet and the cladding is 350 psi. The active fuel length is 144 inches.

Each fuel assembly is fitted with an instrumentation tube at the center and with 16 guide tubes to accommodate the control rods. There are 61 full length control rod assemblies and eight part-length control rod assemblies. There are eight spacer grids

per assembly (six in the active fuel length) and the assembly-to-assembly pitch spacing is 8.587 inches. Additional information on the fuel assemblies is in Appendix C along with the specifications for the lumped burnable poison and control rods

3.1.2 TMI-1 Cycle 1 Core Loading and Control Rod Configuration

The core loading for TMI-1 Cycle 1 is shown in Figure 3-1. The interior of the core comprises 56 2.06 wt% ^{235}U fuel assemblies and 61 2.75 wt% ^{235}U fuel assemblies arranged in a checkerboard pattern. All of the 2.75 wt% ^{235}U assemblies except the center assembly were loaded with 1.09, 1.26, or 1.43 wt% B_4C LBP assemblies. The periphery of the core contained 60 3.05 wt% ^{235}U fuel assemblies, eight of which contained 1.26 wt% B_4C LBP assemblies. The control rod bank configuration for Cycle 1 is displayed in Figure 3-2 and Figure 3-3.

Figure 3-1: TMI-1 Cycle 1 Quarter-Core Loading Pattern

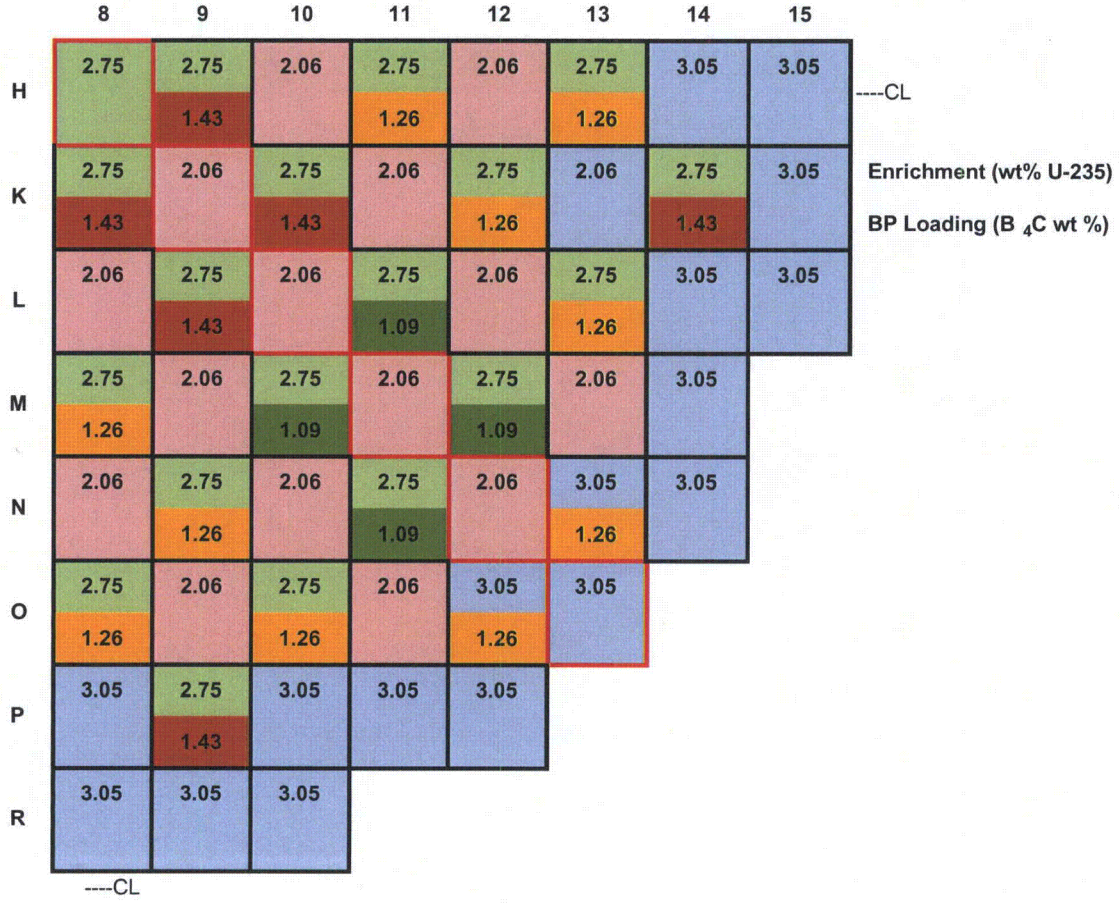

Batch	1	2	3	
BP	2.06	2.75	3.05	
0	56	1	52	
1.09		16		
1.26		24	8	
1.43		20		
	56	61	60	177

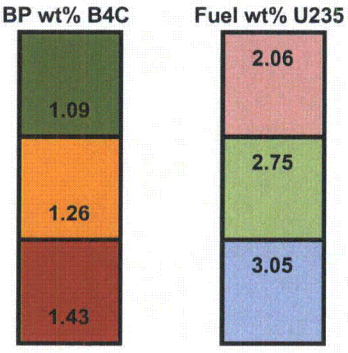

Figure 3-2: TMI-1 Cycle 1 Control Rod Group Configuration 0-250 EFPDs

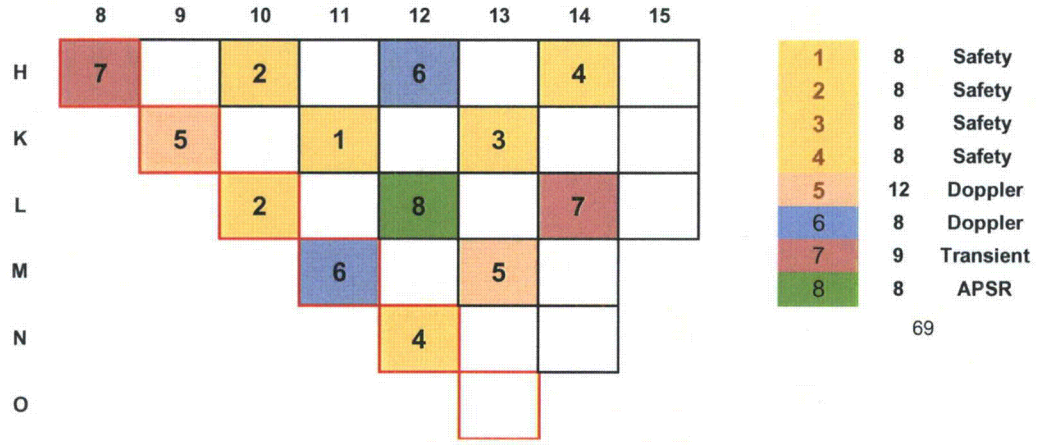

Figure 3-3: TMI-1 Cycle 1 Control Rod Group Configuration 250-466 EFPDs

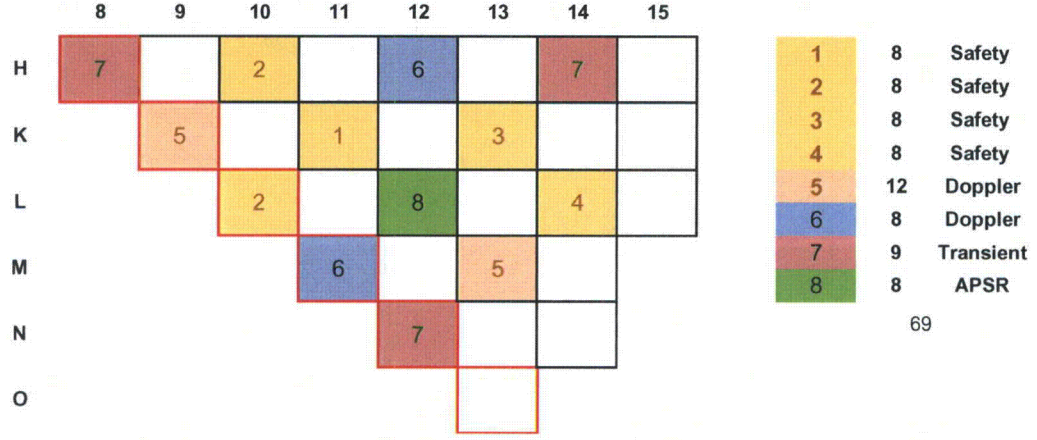

3.1.3 TMI-1 Cycle 2 Core Loading and Control Rod Configuration

The core loading for TMI-1, Cycle 2 is shown in Figure 3-4. The interior of the core comprises the 61 2.75 wt% ^{235}U fuel and 60 3.05 wt% ^{235}U fuel assemblies shuffled from Cycle 1 to Cycle 2 (the LBPs were removed from these assemblies). The periphery of the core was loaded with 56 2.64 wt% ^{235}U fresh fuel assemblies. No fuel assemblies within the core contained any LBPs. Figure 3-5 displays the control rod bank configuration for Cycle 2.

Figure 3-4: TMI-1 Cycle 2 Quarter-Core Loading Pattern

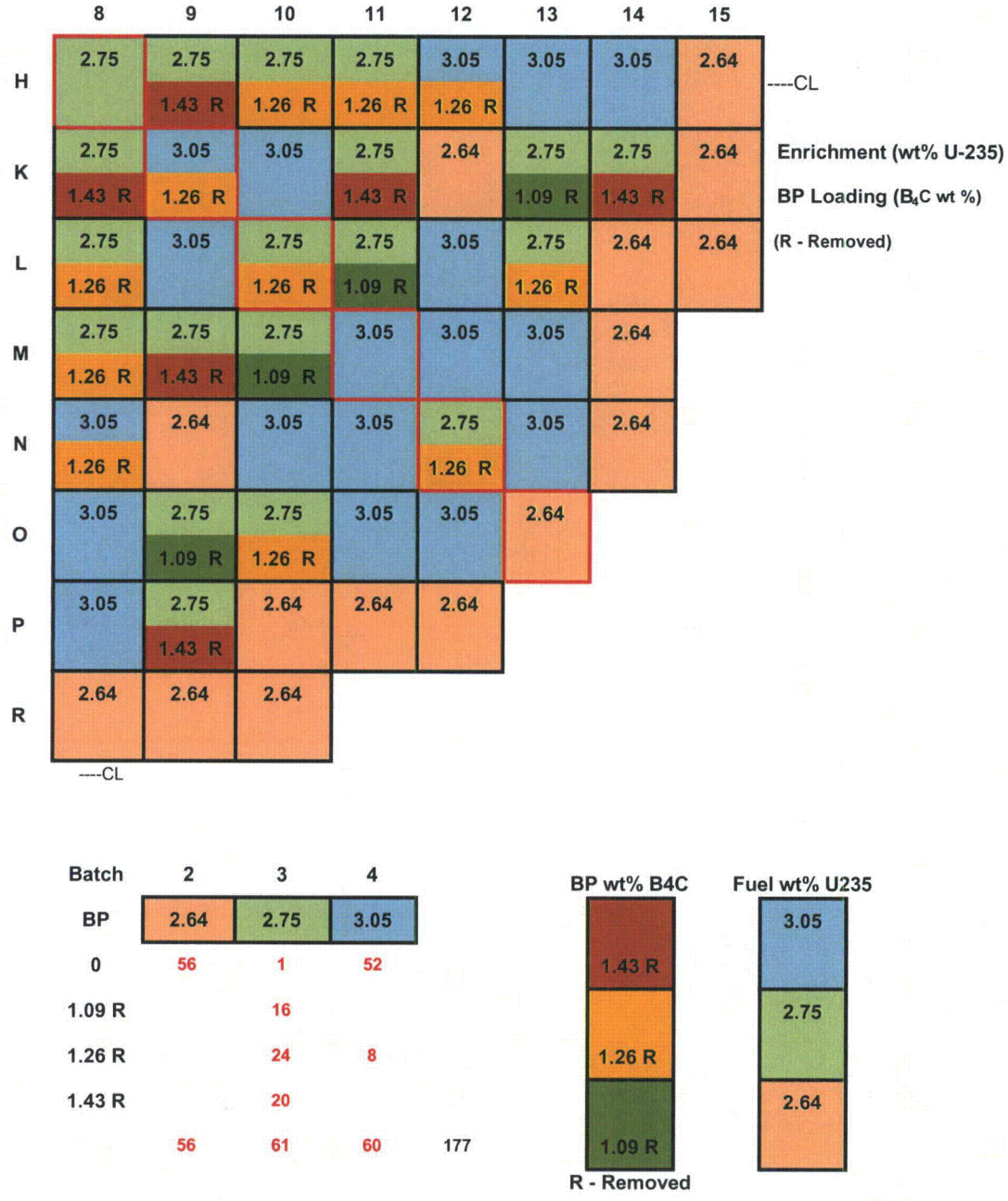

Figure 3-5: TMI-1 Cycle 2 Control Rod Group Configuration

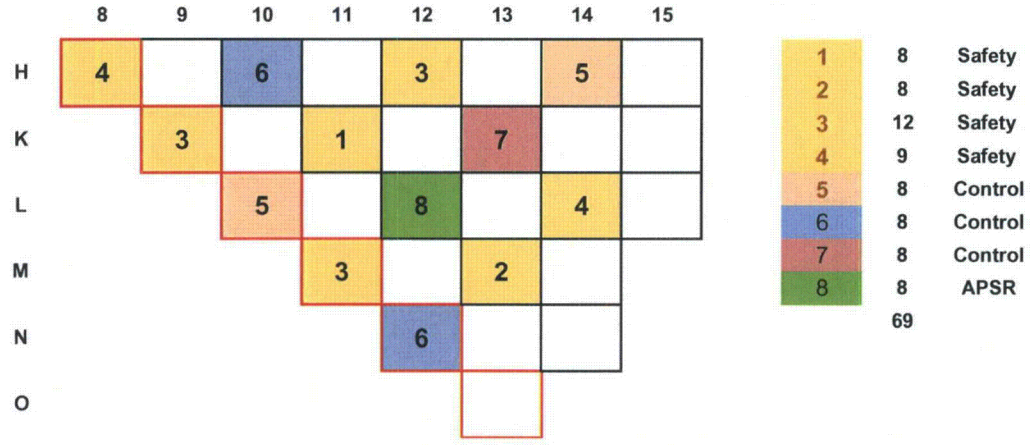

3.1.4 TMI-1 Operational Data

The TMI-1 Cycles 1 and 2 reactor cores were operated at a steady-state heat release level of 2535 MW(th), which was removed by a nominal coolant mass flow rate of about 140 Mlbm/hr. The coolant entered the reactor vessel at 554 °F and exited the reactor vessel at 601 °F, with an average coolant temperature of 579.7 °F. The average coolant velocity in the core was approximately 16.77 ft/sec.

The basic reactor operational characteristics for TMI-1 Cycles 1 and 2 are summarized in Table 3-1 and the reactor coolant temperature as a function of power level is shown in Figure 3-6. The reactor operating inputs for the TMI-1 Cycles 1 and 2 core analyses come primarily from Reference 1. Cycle specific operating data, i.e. loading pattern, power level, soluble boron letdown, rod insertion etc., are provided in Sections 3.1.5 and 0 for Cycles 1 and 2, respectively.

Table 3-1: TMI-1 Full Power Operating Characteristics

Operating Parameter	Value
Reactor Power (MW)	2535
Number of Fuel Assemblies	177
Average Fuel Temperature (F)	1280
Average Moderator Temperature (F)	579.7
Core Flow (Mlbm/hr)	140
Average Specific Power (MW/MTU)	30.866
Core Power Density (kW/l)	82.311
Ave Soluble Boron (ppm)	700

Figure 3-6: Reactor Coolant Temperature as a Function of Power Level

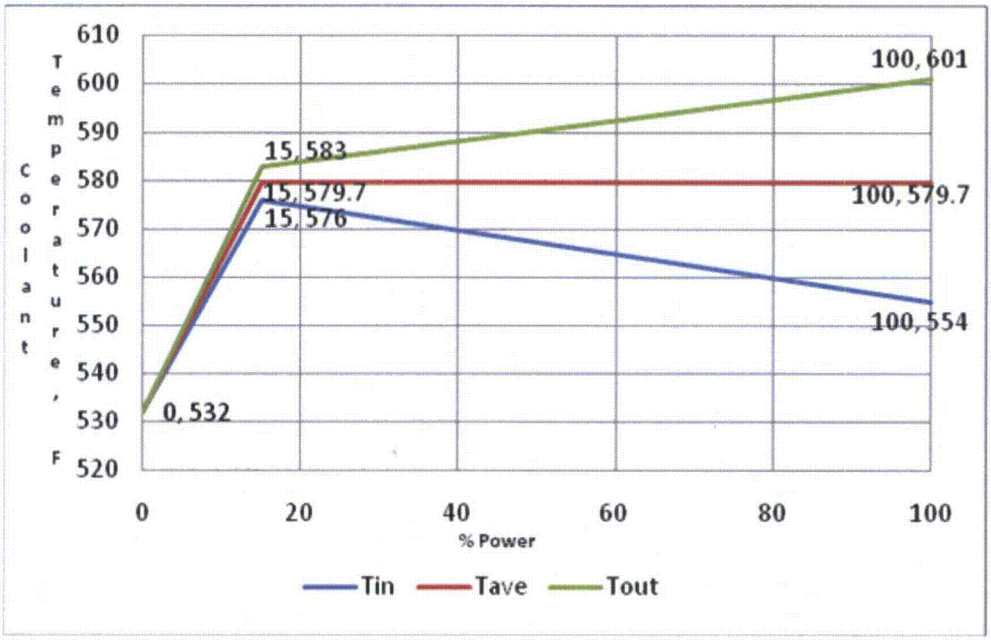

3.1.5 TMI-1 Cycle 1 Operational Data

The operational data for TMI-1 Cycle 1, including power level, soluble boron, and control rod Group 6, 7, and 8 positions are shown in Table 3-2. The design lifetime for Cycle 1 was 466 EFPD. A single interchange of the designated transient control rod group (Group 7) was scheduled at 250 EFPD. Actual plant operation was 467 EFPD with the control rod interchange being implemented at 256 EFPD.

Table 3-2: TMI-1 Cycle 1 Core Operational Data*

Core Exposure (MWd/MTU)	Power Level (%)	Soluble Boron (ppm)	Group 6 (% Withdrawn)	Group 7 (% Withdrawn)	Group 8 (% Withdrawn)
0	60	1179	73	6	20
500	86.5	1131	83	16	15
1000	96.5	1098	89	15	12
1500	99	1077	90	15	16
2000	94.5	1104	88	14	16
2500	96.5	1056	89	15	16
3000	96	1039	88	13	10
3500	100	980	89	13	9
4000	99.5	950	90	12	10
4500	97.5	933	88	12	9
5000	100	900	92	13	8
5500	99.5	864	91	13	9
6000	99.5	822	92	13	9
6500	94.5	796	89	13	10
7000	100	733	93	15	10
7500	90	717	89	13	11
8000	94	674	90	12	10
8500	100	603	93	14	8
9000	97	556	92	13	9
9500	100	512	93	13	8
10000	99	463	92	12	8
10500	100	418	92	13	9
11000	94.5	391	90	12	10
11500	98	329	92	13	9
12000	99.5	276	93	14	10
12500	97.5	246	93	15	10
13000	97	221	94	28	11
13500	100	255	100	85	21
14000	100	212	100	86	24
14406	100	212	100	86	24

* Data at each indicated Core Exposure are averages to the subsequent exposure point

3.1.6 TMI-1 Cycle 2 Operational Data

The operational data for TMI-1 Cycle 2, including the power level, soluble boron, and control rod Group 6, 7, and 8 positions are shown in Table 3-3.

Table 3-3: TMI-1 Cycle 2 Core Follow Data*

Core Exposure (MWd/MTU)	Power Level (%)	Soluble Boron (ppm)	Group 6 (% Withdrawn)	Group 7 (% Withdrawn)	Group 8 (% Withdrawn)
0	93	850	81	8	22
500	100	763	80	6	19
1000	99	720	81	7	19
1500	100	674	82	7	17
2000	91	640	75	6	19
2500	95.5	590	79	6	18
3000	100	532	81	6	19
3500	100	478	83	7	18
4000	96.5	434	79	6	18
4500	99	400	83	8	18
5000	100	321	84	8	17
5500	100	276	84	7	17
6000	100	232	84	9	15
6500	99	189	83	7	15
7000	100	115	85	8	16
7500	100	115	85	8	15
7940	100	115	85	8	15

* Data at each indicated Core Exposure are averages to the subsequent exposure point

3.2 TMI Measured Data Analysis

3.2.1 Introduction

The analytical performance of ***CASMO-5/SIMULATE-3*** in the prediction of assembly power distributions for TMI-1 Cycles 1 and 2 was determined by comparison of "measured" assembly power to calculated assembly power. However, "measured" assembly power was inferred from SPND signals that are proportional to the neutron flux at the SPND location. These signals were converted to "measured" power by multiplying by power to signal ratios determined by analytical techniques, i.e., ***CASMO-5/SIMULATE-3***. The measured powers at the fixed SPND locations were processed to compute assembly power. The details of these computations are given in subsequent paragraphs. An approach similar to what is outlined in this report could be used in future core follow benchmarking of the B&W mPower reactor.

The axial measured power shapes and radial power distributions were analyzed using an Excel spreadsheet that mimics, in a simplified way, the processing performed by a nuclear application system used in an operating reactor. It was possible to use an Excel spreadsheet because the measured signals from TMI-1 Cycles 1 and 2 reported in Reference 1 were already corrected for the following effects:

1) instrument-independent Rhodium signal from SPND
2) detector leakage
3) detector depletion

However, additional signal adjustment was made to account for the power tilt experienced in the core during the cycle because the comparisons were made in a symmetrical eighth-core configuration. The tilt correction factors used were very simple compared to what is typically done in commercial nuclear software applications. In addition, substitutions of some SPND signals from symmetrical ICDA locations within the core were necessary for suspect SPNDs.

A signal to power conversion factor for each SPND location in the core was calculated using the ***CASMO-5/SIMULATE-3*** computer package. The Rhodium SPNDs were explicitly modeled in the three-dimensional TMI-1 calculation. The reaction rate resulting from the thermal flux absorption in the Rhodium SPNDs was directly proportional to the measured nano-amp signal obtained from the incore system in the plant.

3.2.2 Processing the SPND Signals and the SIMULATE Core Follow Data

The signal data reported in Reference 1 were given in nano-amps at seven axial SPND locations for each of the 52 assemblies containing ICDAs. These data were provided at various state points in both Cycles 1 and 2. Figure 3-7 presents the layout of the core, indicating ICDA locations. This arrangement allows for an eighth-core representation to be constructed, essentially providing enough data to predict the behavior of the whole core.

A detailed core follow ***SIMULATE-3*** calculation was performed for both cycles. The output files were post processed for the calculated signals and corresponding nodal powers.

Figure 3-8 provides a representation of how each assembly was axially divided into twenty-one nodes to fully encompass each SPND (4.75 inches in length) within a node. In this figure, only the active part of the fuel is shown, versus the full modeling of the core, which includes the upper and lower reflectors. The seven SPNDs in each ICDA were located 10.29, 30.86, 51.42, 72.00, 92.57, 113.14, and 133.71 inches from the bottom, corresponding to the 2^{nd}, 5^{th}, 8^{th}, 11^{th}, 14^{th}, 17^{th}, and 20^{th} nodes, respectively. All of the data was processed in ***EXCEL***. Details of these calculations are shown in Appendix C.

3.2.3 Formulation of the Signal-to-Power Ratios

To convert the measured signals to measured powers, a signal-to-power ratio was determined from the calculated power density in the node and calculated signals that are proportional to the reaction rates within the Rhodium. The equation below demonstrates this factor, which was the basis of the power conversion:

$$\text{Conversion Factor for each SPND} = \left(\frac{Power_{calculated}}{Reaction\ Rate_{calculated}}\right)$$

where $Power_{calculated}$ is the power density within the node, and $Reaction\ Rate_{calculated}$ is the absorption rate of the thermal flux by the Rhodium SPND.

The conversion factors were then used as a multiplier to convert the measured signals to powers; these powers were further processed to obtain normalized axial power shapes and normalized radial power distributions.

Figure 3-7: Core Cross-Section with ICDAs (Highlighted)

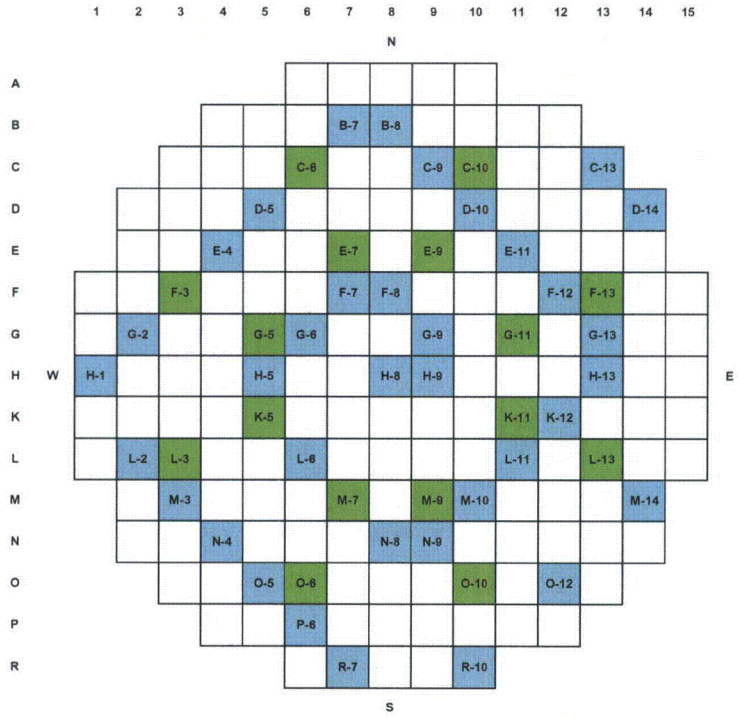

Figure 3-8: SPND/Nodal Representation

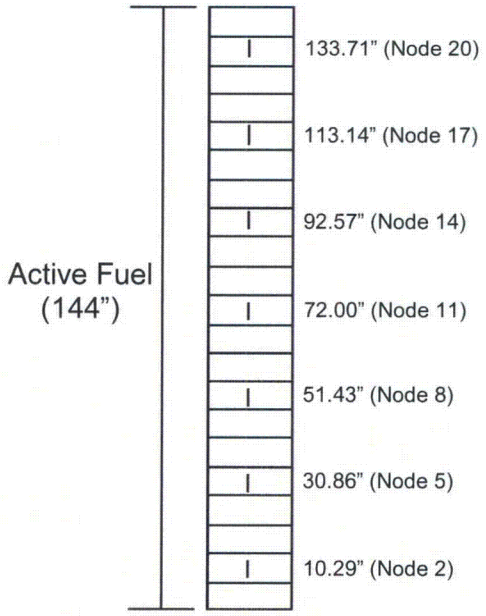

3.3 TMI-1 Calculated Versus Measured Results

The hot zero power (HZP) startup tests and core follow data for TMI-1 Cycles 1 and 2 were modeled and compared to the measured results in Reference 1. The startup tests included all rods out (ARO) critical boron, boron worth, temperature coefficients, and rod worths. The core follow data included the radial and axial power distribution for various points in the core during Cycles 1 and 2.

3.3.1 Computational Model

Cross-sections and discontinuity factors for eight fuel lattice types (segments) and four reflector configurations were computed with ***CASMO-5***. The cross-sections and discontinuity factors are parameterized over the reactor operating space, i.e., temperature, soluble boron, control rod presence, etc., with and without removal burnable poison rods using the ***CASMO-5*** S3C card. Since TMI-1 Cycle 1 had burnable poison rods that were removed in Cycle 2, the generalized removable burnable poison model was utilized for Cycle 2.

Due to the symmetry in the B&W 15x15 lattice, only an octant representation of the lattice is required. Three specific pins were modeled in the lattice, namely (1) fuel, (2) instrument tubes, and (3) guide tubes. The guide tubes were either empty or contained a control rod or a burnable poison rod. The control rods were modeled in ***CASMO-5*** using the following designations "CRD" for the full length control rod with a 0.392 inch diameter absorber clad in steel; "CR1" for the part length axial power shaping rod (APSR) with a 0.375 inch diameter absorber clad with steel; and "CR2" for the empty steel cladding above either absorber zone. Fuel assemblies with burnable poison rods were modeled with those rods in the 16 guide tube locations. The instrument tube was modeled as empty in the current analysis. Three different B_4C loadings were specified for the 2.75 wt% ^{235}U fuel assemblies and one loading was specified for the 3.05 wt% ^{235}U fuel assemblies. The burnable poisons rods were removed and the guide tube was modeled as empty or containing control rods for the Cycle 2 fuel assemblies.

CMS-LINK was used to process the ***CASMO-5*** card image files into a cross-section library usable by ***SIMULATE-3***. ***CMS-LINK*** collects (1) the two-group macroscopic cross-section, (2) the two-group discontinuity factors, (3) the pin power reconstruction data, and (4) the fission product data. The cross-sections and other data are ultimately represented as a function of instantaneous reactor operational parameters such as exposure (EXP), moderator temperature (TMO), soluble boron (BOR), and control rod presence (CRD), as well as the weighted effects of the history of certain conditions such as moderator temperature history (HTM), fuel temperature history (HTF), boron history (HBO) and control rod history (HCR). The eight ***CASMO-5*** fuel segments previously identified were processed, and four pulled burnable poison rod fuel segments were created using the generalized removable burnable poison model for use in Cycle 2. Additionally, three reflector segments were created, one radial reflector segment as well as a top and a bottom reflector segment.

A ***SIMULATE-3*** quarter-core model was constructed from the design input and the ***CMS-LINK*** library. The model was validated against HZP startup testing results and core follow data from Cycles 1 and 2.

3.3.2 Comparative Analysis for the TMI-1 Cycles 1 and 2

3.3.2.1 Hot Zero Power Critical Boron, Rod Worths, and Reactivity Coefficients

TMI-1, Cycles 1 and 2 HZP startup tests were modeled and compared to the measured results given in Reference 1. The startup tests included ARO critical boron, boron worth, temperature coefficients, and rod worths. Table 3-4 shows ARO critical boron and boron worth results. The Cycle 1 results are in excellent agreement and validate the model uranium loadings, burnable poison loadings, and core configuration. The Cycle 2 results also validate the Cycle 1 to Cycle 2 shuffle, burnable poison rod removal and fresh fuel additions.

Table 3-4: TMI-1, Cycles 1 and 2 HZP Critical Boron and Boron Worth

	Cycle 1		Cycle 2	
Parameter	**Measured**	**Calculated**	**Measured**	**Calculated**
ARO Critical Boron, ppm	1615	1609	1384	1355
Boron Worth, pcm/ppm	-10.6	-10.1	-9.7	-9.95

The isothermal temperature coefficients (ITC) at HZP for Cycles 1 and 2 are summarized in Table 3-5 and Table 3-6, respectively. For Cycle 1, the calculated ITCs are in good agreement with or without control rod group insertion. For Cycle 2, the calculated ITC is in good agreement, but a little more positive than measured. It is important to note that all the control banks were reconfigured in Cycle 2.

Table 3-5: TMI-1, Cycle 1 HZP Isothermal Temperature Coefficients

Boron Conc. (ppm)	Control Bank Positions (% wd)	Measured (pcm/°F)	Calculated (pcm/°F)
1601	Groups 1-6 (100) 7 (78) 8 (100)	4.49	4.2
1461	Groups 1-5 (100) 6 (78) 7 (0) 8 (2)	3.04	2.19
1269	Groups 1-3 (100) 4 (95) 5-7 (0) 8 (27)	-5.27	-5.83
1245	Groups 1-3 (100) 4 (50) 5-7 (0) 8 (27)	-6.04	-6.18

Table 3-6: TMI-1, Cycle 2 HZP Isothermal Temperature Coefficients

Boron Conc. (ppm)	Control Bank Positions (% wd)	Measured (pcm/°F)	Calculated (pcm/°F)
1375	Groups 1-7 (100) 8 (0)	0.94	1.33
1154	Groups 1-4 (100) 5-8 (0)	-5.3	-5.27

The Cycles 1 and 2 integral control rod group worths for Groups 5, 6, 7 and 8 (APSR) are summarized in Table 3-7. For Cycle 1, there is very good agreement in the worths of Groups 5 and 7, good agreement in the worth of Group 8, but poor agreement in the worth of Group 6. However, the worth of Group 6 is somewhat suspect. Because there are fewer rods in Group 6 than in either Groups 5 or 7, it is not credible that it could contain greater worth. In the case of Cycle 2, all the control banks were reconfigured. The worth of Groups 5 and 7 are in good agreement, but again Group 6 had poor agreement even though completely different rods were measured.

Table 3-7: TMI-1, Cycles 1 and 2 HZP Control Rod Group Worths

	Cycle 1		Cycle 2	
Control Bank Positions (% wd)	Measured (pcm)	Calculated (pcm)	Measured (pcm)	Calculated (pcm)
Group 5	1030	1009	680	574
Group 6	1250	894	1060	747
Group 7	1100	1027	772	770
Group 8	390 @ 27.5 % wd 178 @ 0 % wd	352@ 32 % wd 118@ 0 % wd	---	---

Table 3-8 shows the Cycles 1 and 2 beginning of cycle hot full power reactivity coefficients. In general, there is good agreement, with the calculated values more negative than the measured values.

Table 3-8: TMI-1, Cycles 1 and 2 HFP Reactivity Coefficients

		Core Power, %	Boron (ppm)	Temperature (pcm/°F)	Power Doppler (pcm/%)	Moderator (pcm/°F)	Doppler (pcm/°F)
Cycle 1	Measured	100	1090	-3.29	-11.4	-2.22	-1.07
	Calculated	100	1090	-4.86	-13.01	-3.36	-1.5
Cycle 2	Measured	100	820	-12.6	-11.7	-11.1	--
	Calculated	100	820	-13.4	-14.1	-11.9	--

3.3.2.2 Core Follow Eigenvalues and Critical Boron

TMI-1, Cycles 1 and 2 core follow calculations were performed with the critical boron, power level and control rod group insertion data reported in Reference 1. In the case of Cycle 1, except for the first two exposure points, the core operated close to 100 % power with control rod Groups 1-5 completely withdrawn, control rod Group 6 approximately 90% withdrawn and Groups 7 and 8 withdrawn to approximately 15% and 10%, respectively.

Figure 3-9 shows the Cycle 1 calculated critical boron letdown and the measured boron letdown at the specified control rod group insertions. The calculated critical boron is on average 27 ppm lower than the measured values reported in Reference 1.

In the case of the Cycle 2 core follow, except for the first exposure point, the core operated close to 100 % power with control rod Groups 1-5 completely withdrawn, control rod Group 6 approximately 80% withdrawn and control rod Groups 7 and 8 withdrawn to approximately 8 and 20%, respectively.

Figure 3-10 shows the Cycle 2 calculated critical boron letdown and the measured boron letdown at the specified control rod group insertions. The calculated critical boron is on average 95 ppm lower than the measured.

Figure 3-9: TMI-1, Cycle 1 Critical Boron versus Core Burnup

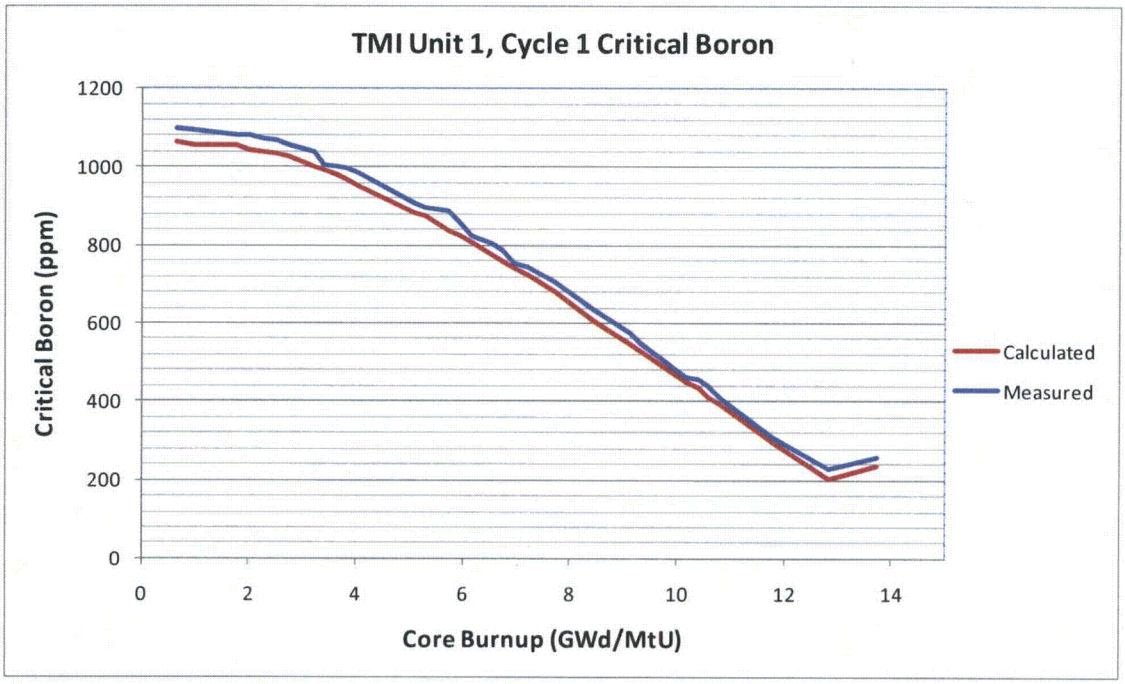

Figure 3-10: TMI-1, Cycle 2 Critical Boron versus Core Burnup

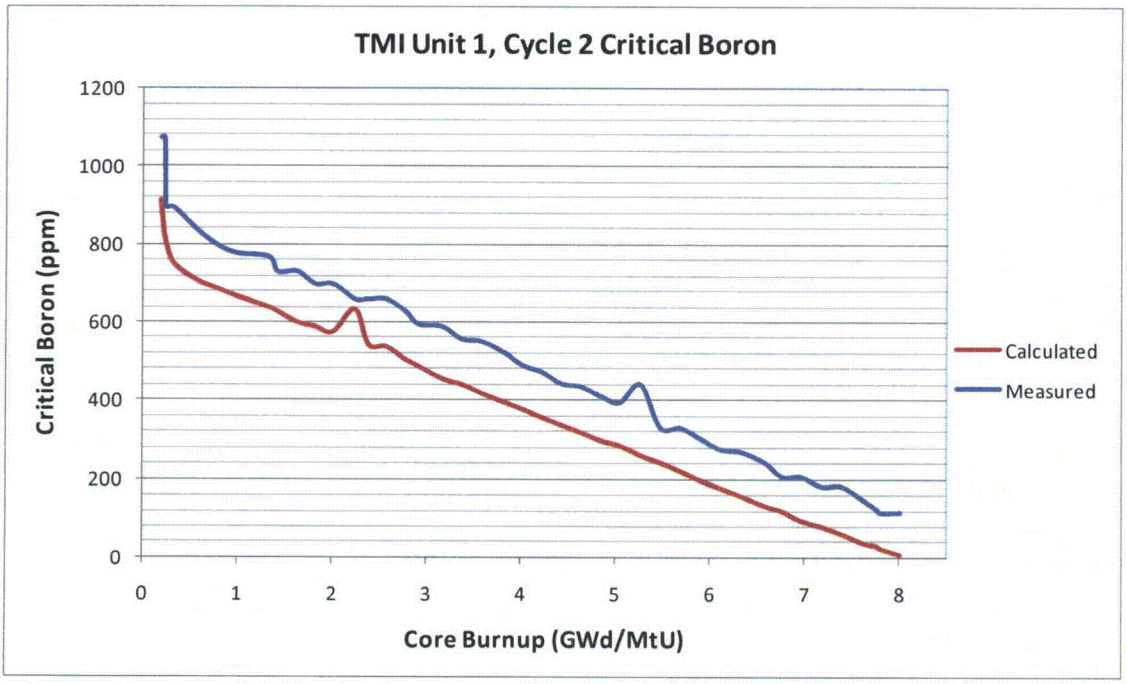

3.3.2.3 Radial Power Distribution Comparisons

The calculated two-dimensional radial power distributions for Cycles 1 and 2 are compared to measured power distributions at various points in the operating cycle. The signal–to-power conversion technique summary is described in Section 4 with details of this process given in Appendix C. Figure 3-11 and Figure 3-12 summarize the comparative analysis for Cycles 1 and 2. The measured power distribution for Cycles 1 and 2 were processed from the SPND signals contained in Reference 1. In general, the measured and calculated radial power distributions are in good agreement, with an average standard deviation between 0.03 and 0.04. Two representative radial power distributions are given in Figure 3-11 and Figure 3-12 and the power distributions for all state points during Cycles 1 and 2 are given in Appendix C.

Figure 3-11: TMI-1, Cycle 1 Radial Power Distribution Comparison at 1756 MWd/MtU

	H-8	H-9	H-10	H-11	H-12	H-13	H-14	H-15
Measured	1.023	1.270	1.401	1.354	1.291	1.204	1.290	0.821
Calculated	1.083	1.355	1.383	1.415	1.252	1.238	1.261	0.796
Difference	0.060	0.085	-0.018	0.060	-0.039	0.035	-0.029	-0.026

	K-9	K-10	K-11	K-12	K-13	K-14	K-15
	1.336	1.398	1.353	1.207	1.139	0.949	0.688
	1.355	1.433	1.328	1.268	1.100	0.947	0.684
	0.019	0.034	-0.025	0.061	-0.039	-0.002	-0.004

	L-10	L-11	L-12	L-13	L-14	L-15
	1.329	1.272	1.014	0.955	0.631	0.442
	1.352	1.325	1.012	0.980	0.645	0.423
	0.023	0.054	-0.003	0.025	0.013	-0.019

	M-11	M-12	M-13	M-14
	1.136	1.130	0.926	0.670
	1.160	1.096	0.870	0.652
	0.024	-0.034	-0.056	-0.018

	N-12	N-13	N-14
	0.994	0.794	0.458
	0.936	0.775	0.447
	-0.058	-0.019	-0.011

	O-13
	0.518
	0.506
	-0.012

STD DEV = 0.0378

Figure 3-12: TMI-1, Cycle 1 Radial Power Distribution Comparison at 3223 MWd/MtU

	H-8	H-9	H-10	H-11	H-12	H-13	H-14	H-15
Measured	1.012	1.261	1.395	1.323	1.278	1.210	1.255	0.797
Calculated	1.056	1.344	1.350	1.405	1.230	1.239	1.228	0.775
Difference	0.044	0.083	-0.045	0.081	-0.048	0.028	-0.027	-0.022
		K-9	K-10	K-11	K-12	K-13	K-14	K-15
		1.288	1.386	1.321	1.211	1.125	0.963	0.678
		1.324	1.422	1.304	1.273	1.095	0.950	0.674
		0.035	0.036	-0.016	0.062	-0.030	-0.013	-0.004
			L-10	L-11	L-12	L-13	L-14	L-15
			1.293	1.269	1.013	0.981	0.630	0.448
			1.326	1.326	1.016	1.000	0.641	0.422
			0.033	0.057	0.003	0.019	0.010	-0.026
				M-11	M-12	M-13	M-14	
				1.117	1.158	0.936	0.681	
				1.156	1.123	0.888	0.660	
				0.039	-0.035	-0.048	-0.021	
					N-12	N-13	N-14	
					1.005	0.837	0.476	
					0.959	0.808	0.461	
					-0.046	-0.029	-0.014	
						O-13		
						0.550		
						0.527		
						-0.022		

STD DEV = 0.0396

3.3.2.4 Axial Power Distribution Comparisons

A comparison of the calculated-to-measured axial power distributions for the two representative state points of Cycles 1 and 2 given above are summarized in Figure 3-13 and Figure 3-14 for two representative points in the operating cycle. As shown, the measured axial distribution for Cycles 1 and 2 were processed from the SPND signals contained in Reference 1. Overall the calculated axial power shapes data are in excellent agreement with the measured results.

Figure 3-13: TMI-1, Cycle 1 Axial Power Distribution Comparison at 1756 MWd/MtU

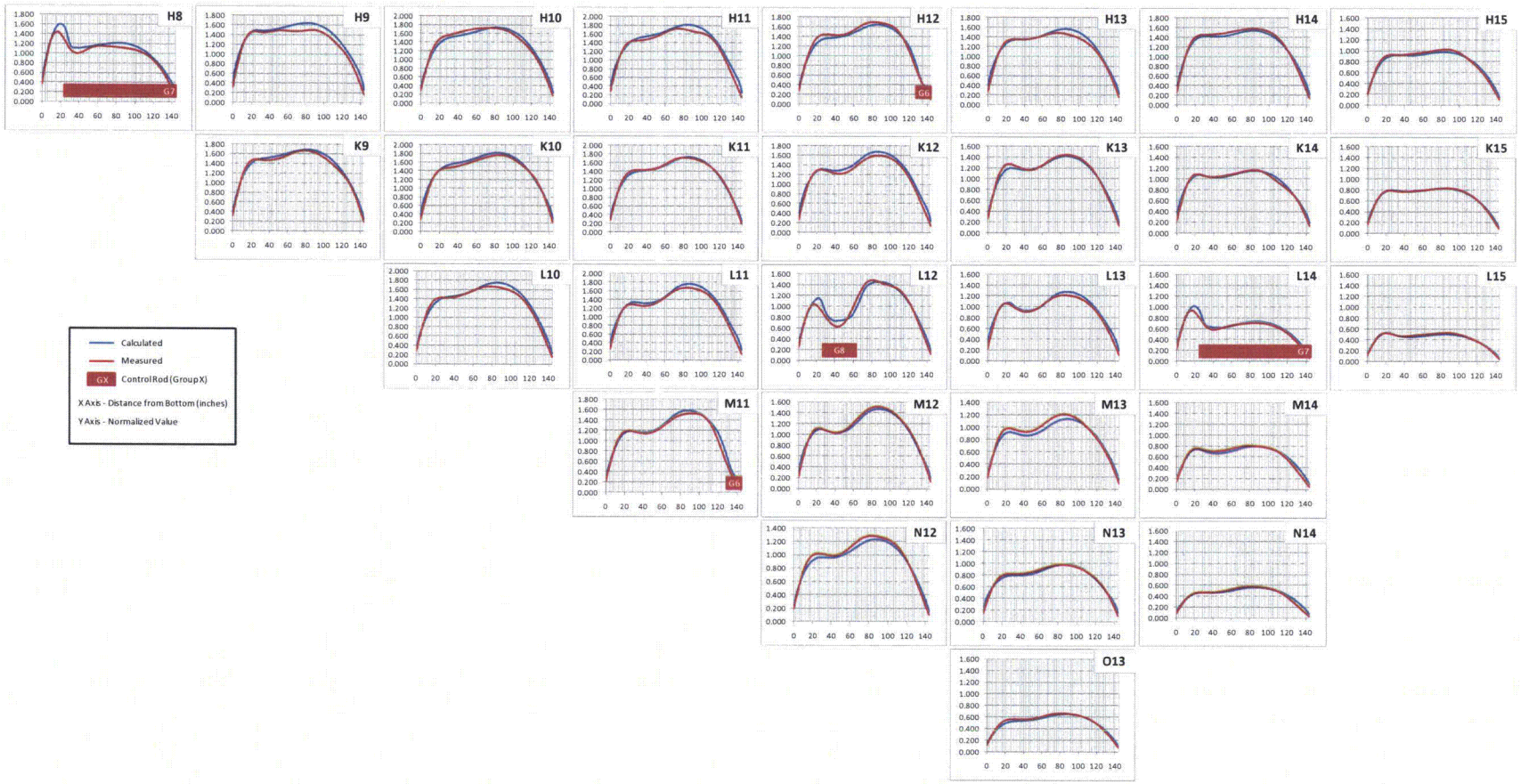

Figure 3-14: TMI-1, Cycle 1 Axial Power Distribution Comparison at 3223 MWd/MtU

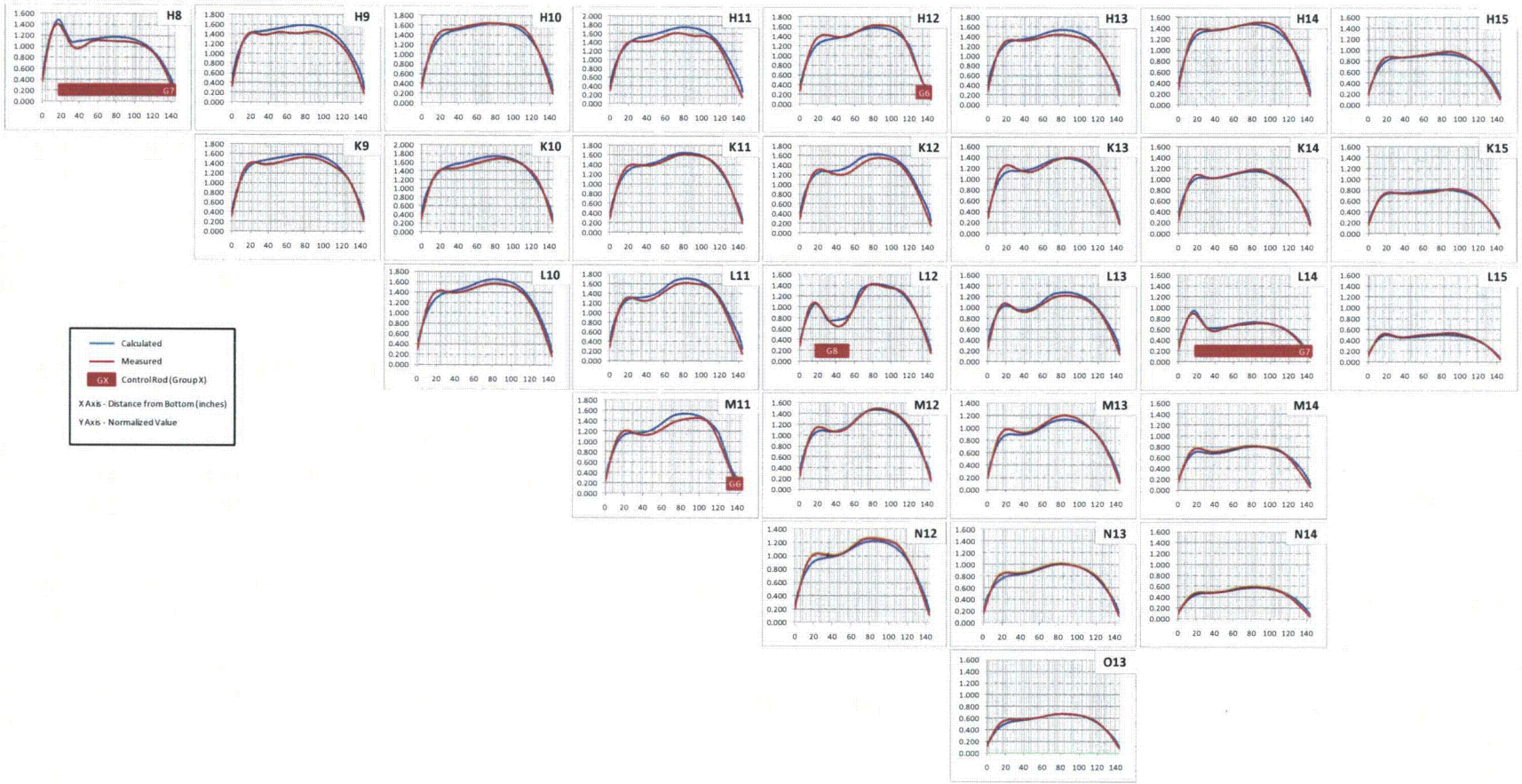

4.0 Summary of Results, Applicability of the Comparative Analysis, and Conclusions

4.1 Summary of the Comparative Analysis Results

The intent of this Topical Report is to validate the nuclear computational methodology that will be used in performing nuclear design calculations for the B&W mPower reactor core by comparing measured results from cold, clean, critical experiment data and reactor core operating data from 40 state points of TMI-1 Cycles 1 and 2 to computational models. The core physics qualification analysis was performed with the StudsvikScandpower CMS code suite, which is a state-of-the-art, industry standard, computer code package for comprehensive neutronic simulation of light water reactors.

The StudsvikScandpower CMS package consists of the two-dimensional transport code ***CASMO-5***, which is used to generate homogenized cross-section data and heterogeneous pin-by-pin form functions, which are subsequently used in the two-group three-dimensional nodal diffusion code ***SIMULATE-3*** for whole core coupled neutronic-thermal-hydraulic analysis. The link between ***CASMO-5*** and ***SIMULATE-3*** is accomplished by the auxiliary utility processing and functionalization code ***CMS-LINK***, which generates a binary macroscopic cross-section library accessible to ***SIMULATE-3*** from the data generated by ***CASMO-5***.

The core physics qualification analysis performed for the cold, critical experiments included: (1) 17 critical experiments with UO_2 fuel conducted at the B&W LRC as part of the Physics Verification Program; (2) 17 critical experiments containing UO_2-Gd_2O_3 bearing assemblies performed at LRC as part of the Urania-Gadolinia Critical Experiment Benchmark Program; and (3) six UO_2-PuO_2 (2 wt%) critical experiments carried out in the Plutonium Recycle Critical Facility at PNNL. The calculated eigenvalues and local pin power distribution within a fuel assembly were compared to the measured results from the critical experiments to determine the accuracy of the ***CASMO-5/SIMULATE-3*** computational methodology.

The overall comparisons between calculated and measured data were in very good agreement for the 17 critical experiments with UO_2. The predicted eigenvalues agreed very closely with measured k_{eff} inferred from boron concentration measurements. The highest biases were recorded for Loadings 8 and 9 (0.00431 and 0.00422 respectively), which had the lowest boron concentrations and the highest number of Pyrex rods. The standard deviation of all eigenvalues was 0.00202. Furthermore, the average bias on pin powers was less than 1%, with maximums in the low 3 – 4% range, without considering estimated uncertainties. With uncertainties taken into account, even better agreement was obtained. The total standard deviation for the pin powers considered in these experiments was 0.01615.

Similarly, the calculated core eigenvalues and pin powers for the critical experiments containing UO_2-Gd_2O_3 bearing assemblies are in good agreement with the measured results. The average k_{eff} was 0.99811 ± 0.00056 with a standard deviation between the calculated and measured results of 0.00056. The total standard deviation for the calculated and measured eigenvalues for the combined 34 UO_2 and UO_2-Gd_2O_3 critical assemblies performed at LRC was 0.00148. Additionally, the standard deviation on pin powers for the analyzed Urania-Gadolinia core indicates very good agreement with measurements. Specifically, the standard deviation for Cores 5 and 14 were 0.008 and 0.012 respectively, and the total standard deviation for the all Urania-Gadolinia pin powers considered in the comparative analysis was 0.01736.

The comparative analysis for six UO_2-PuO_2 (2 wt%) critical experiments performed at PNNL also indicated that both the calculated eigenvalues and pin powers were in excellent agreement with that inferred from experimental data. The standard deviation for the eigenvalues was on the order of 0.00155 and that for the pin powers was 0.03361. Furthermore, the total standard deviation on the pin powers for all 19 critical maps considered in this Topical was on the order of 0.02375. Table 4-1 summarizes the overall accuracy of the comparative analysis for the cold clean criticals. These results validate the ability of ***CASMO-5/SIMULATE-3*** to accurately calculate cross-sections in a very heterogeneous complex geometry, which is the basis for accurate calculation and prediction of power distribution within such geometries.

Table 4-1: Summary of the Clean Critical Data Analysis

Cold Clean Criticals Summary	
Criticals Eigenvalues Std. Deviation (σ_T)	
UO_2 σ_T =	0.00202
UO_2-Gd_2O_3 σ_T =	0.00056
Combined σ_T UO_2 + UO_2-Gd_2O_3 =	0.00148
UO_2-PuO_2 CASMO-5 σ_T =	0.00155
UO_2-PuO_2 MCNP-5 σ_T =	0.00101
UO_2-PuO_2 Experimental σ_m =	0.00025
Criticals Relative Power Distribution Std Dev (σ_T)	
UO_2 σ_T =	0.01615
UO_2-Gd_2O_3 σ_T =	0.01736
UO_2-PuO_2 σ_T =	0.03361
Combined RPD σ_T =	0.02375

The nuclear computational methodology was also validated by comparing computed and measured critical boron concentrations, local and core-wide power distributions, temperature coefficients, boron and control rod worths using data from TMI-1 startup of Cycles 1 and 2, and for core follow for Cycles 1 and 2. In general, there was very good agreement between predicted and measured cycle critical boron concentrations, temperature coefficients, and boron and control rod worths. The Appendices of this Topical contain a complete set of all measured data for TMI-1, Cycles 1 and 2, used for this analysis and the corresponding calculated values using the ***CASMO-5/SIMULATE-3*** methodology.

Forty state points of the TMI-1 Cycles 1 & 2 core follow analysis, in which measured radial power distributions were compared to the calculated radial power distributions, provided 1160 variance points that were analyzed to determine the accuracy of the comparison. The accuracy

of the comparative analysis is summarized in Table 4-2. The combined total standard deviation σ_T is 0.03453. A histogram of the calculated-to-measured variance is shown in the table in blue and an equivalent normal distribution is shown in red. The comparison of these two histograms indicates that the distribution of the variances of the calculated to measured data is close to normal.

Sixteen symmetrical ICDAs were arranged in one outer ring and one inner ring (8 ICDAs per ring) of the core. Each ICDA has 7 SPNDs, which were used to estimate the standard deviation of the measured data. The variance from the average of the eight signals within each plane of SPNDs in each ring provided a total of 4480 data points (excluding outliers and including a 2.0% correction for quadrant power tilt) that were used to determine the estimated measured standard deviation σ_m as 0.0239. Consequently, the calculated standard deviation σ_c for the RPD is .02711. The histogram for the measured symmetrical SPND variance data is shown in Table 4-2. These results show excellent results and again validate of the method and models used in ***CASMO-5/SIMULATE-3*** for reactor core design.

Table 4-2: Summary of the TMI-1 Cycles 1 and 2 Data Analysis

TMI-1 Cycles 1 & 2 Summary of σ_T & σ_m	
TMI-1 Estimate of Measurement σ_m Using 4480 Symmetrical Detectors Reading Assuming Tilt of 2% Correction	
σ_m using 4480 points =	0.03094
σ_m using 4480 points excluding points > .1 and <-.1 =	0.02139
TM-1 Relative Power Distribution Std Dev (σ)	
Cycle 1 σ_T =	0.03589
Cycle 1 σ_T =	0.03326
Combined Total Cycle 1 and Cycle 2 σ_T =	0.03453
Combined Calculational Cycle 1 and Cycle 2 σ_c =	0.02711

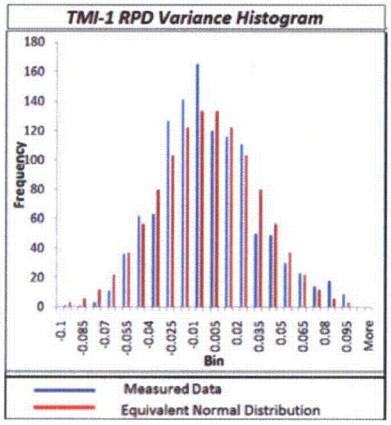

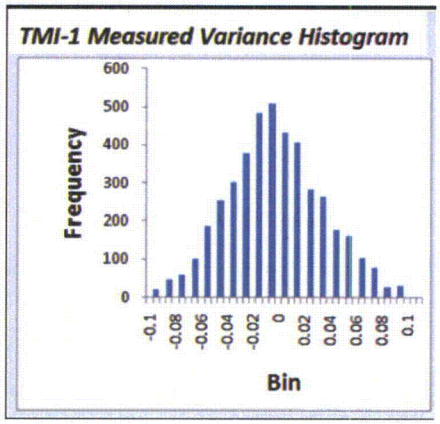

4.2 Applicability of the Comparative Analysis to the B&W mPower Core Design Concept

The scope of the selected cold, clean, critical experiments and TMI-1 reactor core startup and cycles operating data used for the nuclear methodology qualification analysis was designed to encompass a wide range of both geometric and material configurations to span the breadth of the core physics embodied by the design concept of the B&W mPower reactor core.

4.2.1 Brief Description of the B&W mPower Reactor Core Concept

The B&W mPower reactor is a passively safe, pressurized water reactor with the steam generator, pressurizer, reactor coolant pumps, and control rod drives internal to the pressure vessel. The reactor is designed for thermal power output of 425 MW(th) with an operating steam dome pressure of 1900 psi, a coolant inlet and outlet temperature of 568.4 F° and 609 F°, respectively, and a core mass flow rate of 25.4 Mlbm/hr.

The B&W mPower reactor has a rated power output of approximately 125 MWe; and the reactor is designed for a one batch, four year operating cycle between refueling, with a total reactor design life of 60 years. The reactor core consists of 69 mechanically identical fuel assemblies arranged in a pattern which approximates a right circular cylinder. The fuel assemblies are surrounded by a stainless steel core former which is supported by a stainless steel core basket.

The B&W mPower fuel assembly is a 17x17 pin array on a 12.6 mm (0.496-in) square pitch. In the baseline design concept, the fuel pins consist of UO_2 pellets enriched to 4.95 wt% and fuel rod clad of zircaloy-4. To suppress the large excess reactivity at the BOL required for an extended operating cycle, the B&W mPower fuel assemblies employ Al_2O_3-B_4C non-integral burnable poison rods (BPR) containing anywhere from 1 to 8 wt% B_4C. The non-integral BPRs are located geometrically within the fuel assembly to minimize power peaking within the assembly and deplete in concert with the fuel rods to maintain a relatively flat power profile during the burn cycle. Selected fuel assemblies contain fuel rods doped with Gd_2O_3 at 3 wt% (integral FBPRs) to minimize assembly-to-assembly peaking. In order to reduce the peak linear heat rate of the Gd_2O_3–doped fuel rods, the uranium enrichment of the integral FBPR pellets is 1% lower (3.95 wt%) than the enrichment of the non-doped uranium rods loaded in the same assembly. The axial active fuel length is 202.5 cm (79.724 inch) and the resulting low average linear power density of 3.8 kW/ft allows flexible core and fuel management with improved thermal margins. The core is loaded with sufficient excess reactivity to

meet core design lifetime (cycle length) and the design discharge burnup requirements of approximately 36 MWd/MTU.

The B&W mPower reactor does not use soluble boron poison (chemical shim) during normal operation and reactivity control is provided solely by 61 full-length control rod assemblies (CRA) which are located in guide tubes within the fuel assemblies. The CRAs consist of either 24 or 23 control rodlets. For those with 23 control rodlets, the remaining guide tube within the assembly is occupied by an in-core instrument assembly or the primary or secondary neutron source. The eight peripheral fuel assemblies on the corners of the core do not have CRAs.

The CRAs are divided into banks that are used for either core hot excess reactivity control during the operating cycle, axial power shape control, or shutdown. The CRA banks that are designated shutdown banks remain out of the core at all times during full power operation. These CRA groups are used primarily for reactor shutdown. The remaining CRA banks that are used to control the core excess reactivity and the axial power shape augment the shutdown banks to ensure that the required shutdown margin is maintained under cold conditions. The control rod system has enough reactivity to compensate for rapid reactivity fluctuations during operation and for the transition from full power to the hot zero power conditions. In addition, the control rods possess sufficient negative worth to ensure cold shutdown margin with the most reactive control rod stuck out.

Because the B&W mPower core is designed for a one batch extended cycle operation, the power distributions control and fuel burnup are managed over the operating cycle with BPRs, FBPRs and mechanical shim using CRAs. In the B&W mPower core design concept, the core wide power distribution is managed over the extended operating cycle by use of multiple control rod assembly sequences, which are exchanged periodically in order to re-distribute and flatten the core power and burn profiles.

4.2.2 Comparison of the Selected Data Used for the Nuclear Methodology Analysis and the B&W mPower Core Design

One of the constraints placed on the nuclear data used in this Topical is that no proprietary data could be used. This restricts the available data for the analysis considerably, since most of the data for the current PWR operating fleet is owned by the utilities or the reactor vendors. As a result, only publicly available information, such as government or EPRI sponsored program reports, could be used for the cold critical experiments and reactor core startup and operation cycle data.

The selection of the UO_2 and UO_2-Gd_2O_3 criticals from the Physics Verification Program and Urania-Gadolinia Critical Experiment Benchmark, were key to verifying the BOL lattice physics for the B&W mPower core design. As discussed previously, a typical B&W mPower fuel lattice consists of a varying number of UO_2 fuel rods, non-integral Al_2O_3-B_4C BPRs and integral UO_2-Gd_2O_3 FBPRs. This mixture of various types of fissile, and parasitic points integrated within the fuel lattice is well represented by the selected criticals in which the UO_2 and UO_2-Gd_2O_3 critical experiments utilize various UO_2 fuel rods enrichments (2.46 wt% ^{235}U and 4.02 wt% ^{235}U) with a variety of both non-integral BPRs and integral FBPRs including: (1) unclad Pyrex glass rods containing 12.6 wt% B_2O_3; (2) clad vicor glass rods containing 3 wt% B_2O_3 in pure silica; (3) aluminum oxide (Al_2O_3) rods; (4) Ag-In-Cd poison rods; (5) B_4C rods; and (6) solid and annular UO_2-Gd_2O_3 fuel pellets containing approximately 4 wt% gadolinia and UO_2 enriched in ^{235}U to 1.944 wt%. In addition, water and void rods were used in strategic locations within the lattice to vary the neutron spectrum. Note that the BPRs represented in items 1, 2, 3, and 5 above have the same effects and behavior as Al_2O_3-B_4C BPRs used in the mPower reactor design concept. The combination of the BPRs, FBPRs, water, and void rods within the criticals' fuel lattice verified the ability of the core physics to accurately handle sharp discontinuities and spectral shifts in the lattice neutron flux.

The B&W mPower core is designed for a boron free, 4-year operating cycle without fuel shuffle. Consequently the core excess reactivity over the operating cycle is managed by a combination of burnable poisons and mechanical shim using control rod assemblies. The combination use of BPRs, FBPRs and control rod insertion will displace water, resulting in a harder spectrum, which will result in substantial amount of plutonium generated in the fuel assemblies. The selection of the UO_2-PuO_2 (2 wt%) critical experiments was designed to provide rods-in and rods-out local power distribution data that simulated an extreme core burnup condition (similar to EOL conditions) when the plutonium isotopes have accumulated in the fuel over an extended burnup period. In addition, the six UO_2-PuO_2 (2 wt%) critical experiments selected for analysis consisted of core configurations with three lattices of different fuel rods pitches. The lattice pitches were selected to provide configurations that were under-moderated, near optimum moderation, or over-moderated conditions, and which had approximately the same water-to-fuel volume ratio for all fuel types in each degree of moderation.

TMI-1 Cycles 1 and 2 were selected for analysis because of the similarities of the fuel assembly composition, core heterogeneities, and operating rod configurations to that of the B&W mPower reactor core design. More specifically, the core loading for TMI-1 Cycle 1 consisted of 60 interior fuel assemblies enriched to 2.75 wt% ^{235}U loaded with 1.09, 1.26, or 1.43 wt% Al_2O_3-B_4C BPR assemblies. The periphery of the core also contained 8 fuel assemblies enriched to 3.05 wt% ^{235}U and containing 1.26 wt% Al_2O_3-B_4C BPR assemblies. The interspersed mixing of fuel assemblies with and without BPR assemblies is consistent, from a core physics point of view, with the B&W mPower reactor core, where the 69 assemblies have various degrees of BPR loading to control the excess reactivity over the operating cycle.

With respect to the TMI-1 Cycle 1 burnup control configuration, although the TMI-1 core used chemical shim to assist reactivity control, control authority was imposed over the cycle operation by the use of multiple control banks whose percent insertion varies from

deep to shallow. During Cycle 2, the burnable poisons rods were removed and the guide tubes were used for control rod insertion to varying degrees. Additionally, in Cycle 2, all the control banks were reconfigured. The use of rodded core configurations in the TMI Cycles 1 and 2 is consistent with the B&W mPower reactor design concept, where the core wide power distribution is re-distributed over the extended cycle by use of multiple control rod assembly sequences. Thus the TMI-1 Cycles 1 and 2 core follow radial power distribution and axial core power shape comparisons over the operating cycles are a good indicator of the accuracy and applicability of the core physics methods when used for designs in which core power is re-distributed with control rod allocation such as that envisioned for the B&W mPower reactor core concept.

Although the B&W mPower reactor core differs geometrically from the TMI-1 core configuration, the commonality in fuel assembly materials and layout, as well as the control authority philosophy, makes the selection of the TMI-1 Cycles 1 and 2 a good candidate to verify the fundamental core physics expected in the mPower reactor core. Another good verification of the core physics of the B&W mPower reactor core design prior to commissioning will be a detailed comparison to a well recognized audit code with the same cross-section library as the one used in ***CASMO-5/SIMULATE-3*** code suite, such as the newest version of ***MCNP*** with the ENDF/B-VII cross-section library. Presently, a comparative benchmark analysis of the B&W mPower core operating cycle calculated with the CMS code suite ***CASMO-5/SIMULATE-3*** and the newest versions of the Monte Carlo codes ***MCNP6*** and ***SCALE6*** is scheduled for late 2011.

4.3 Conclusion

In conclusion, the overall results from the comparative analysis between predicted and measured data from the cold, clean, critical experiments and the TMI-1 operating reactor cores have demonstrated that the ***CASMO-5/SIMULATE-3*** methods and model used for the calculation can accurately predict: (1) criticality conditions and localized pin power distributions of various heterogeneous configurations and (2) critical boron concentrations, local and core-

wide power distributions, temperature coefficients, and boron and control rod worths for various TMI-1 reactor core operating and burnup states. The scope of the subject nuclear methodology qualification analysis encompassed a wide range of both geometric and material configurations, and will adequately represent the core physics characteristics of the B&W mPower reactor core design.

5.0 References

1 "Reactor Core Physics Design and Operating Data for Cycles 1 and 2 of TMI Unit 1", EPRI NP-1410, Volumes 1 and 2.

2 BAW-3647-18, "Physics Verification Program, Part III, Task 4 – Quarterly Technical Report, April – June 1970", M. N. Baldwin, M. E. Stern, September 1970.

3 BAW-3647-20, "Physics Verification Program, Part III, Task 4 – Summary Report", M. N. Baldwin, M. E. Stern, March 1971.

4 BAW-1810, "Urania-Gadolinia: Nuclear Model Development and Critical Experiment Benchmark," L.W. Newman et al, April 1984.

5 "Clean Critical Experiment Benchmarks for Plutonium Recycle in LWR's", EPRI NP-196, Final Report, April 1976.

6 "CASMO-5/CASMO-5M - A Fuel Assembly Burnup Program User's Manual", SSP-07/431, Rev. 0, August 2007.

7 "CMS-LINK User's Manual", SOA-97, Rev2.

8 "SIMULATE-3 Advanced Three Dimensional Two-Group Reactor Analysis Code", SSP-05/15 Rev. 4, September 2007.

9 LEU-COMP_THERM-008, "Critical Lattices of UO_2 Fuel Rods and Perturbing Rods in Borated Water", Russell D. Mosteller, Los Alamos National Laboratory.

Appendix A Details of Cold Critical Experiments

The predicted and measured results from numerous critical experiments were analyzed to determine the accuracy of the ***CASMO-5/SIMULATE-3*** computational methodology. Detailed models were used to calculate the local pin power distribution within a fuel assembly. The cold, critical experiments included: (1) 17 critical experiments containing UO_2 fuel; (2) 17 critical experiments containing UO_2-Gd_2O_3 bearing assemblies; and (3) six critical experiments employing mixed fuel, UO_2-PuO_2 (2 wt%).

A.1 Critical Experiments at the B&W Critical Experiment Laboratory Facility

The 17 UO_2 critical experiments from the Physics Verification Program provide local power distribution data covering all possible fuel assembly configurations at beginning-of-life (BOL) conditions. The 17 critical experiments from the Urania-Gadolinia Critical Experiment Benchmark Study that were selected for study were a subset of the DOE Extended-Burnup Program performed by B&W in 1984.

A.1.1 The B&W Critical Experiment Laboratory Facility

The facility used for both the Physics Verification Program and the Urania-Gadolinia Critical Experiment Benchmark Program was located in the B&W Critical Experiment Laboratory of the LRC. The various core configurations were constructed inside a 5-foot inside diameter (ID) by 6.5-foot high core tank with 0.5-inch thick aluminum walls as shown in Figure A-15.

Figure A-15: Vertical Section through the Core Tank

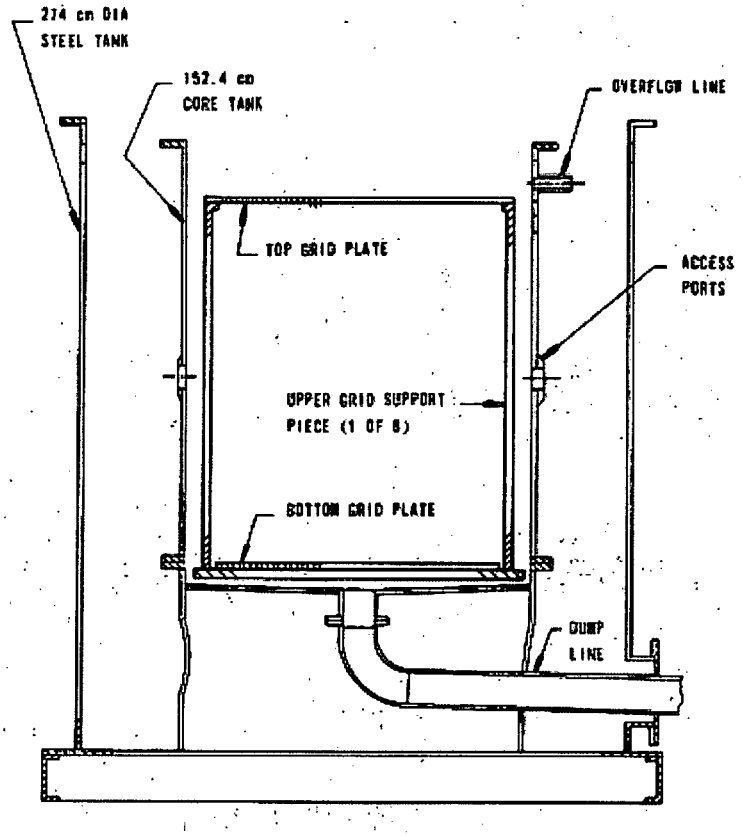

The core tank is located inside a steel tank 9 feet in diameter and is supported on a skirt that holds it about 30 inches above the base of the larger tank. The top and bottom "egg-crate" grid plates consist of 1.0-inch wide slotted aluminum strips interlocked to form a square matrix. The strips are 0.160-inch thick and are spaced on 0.644 ± 0.002-inch centers. A 2-inch thick aluminum base plate one inch above the bottom of the core tank supports the fuel rods. Moderator heights are referenced from the top of this base plate. Criticality was achieved by adjusting the moderator level. Figure A-16 shows the moderator fill system used. The maximum pump capacity is about 35 gpm. Except for the 4,500-gallon dump tank, which is constructed of amercoated carbon steel, the moderator system components are either aluminum or stainless steel.

Figure A-16: Moderator Fill System

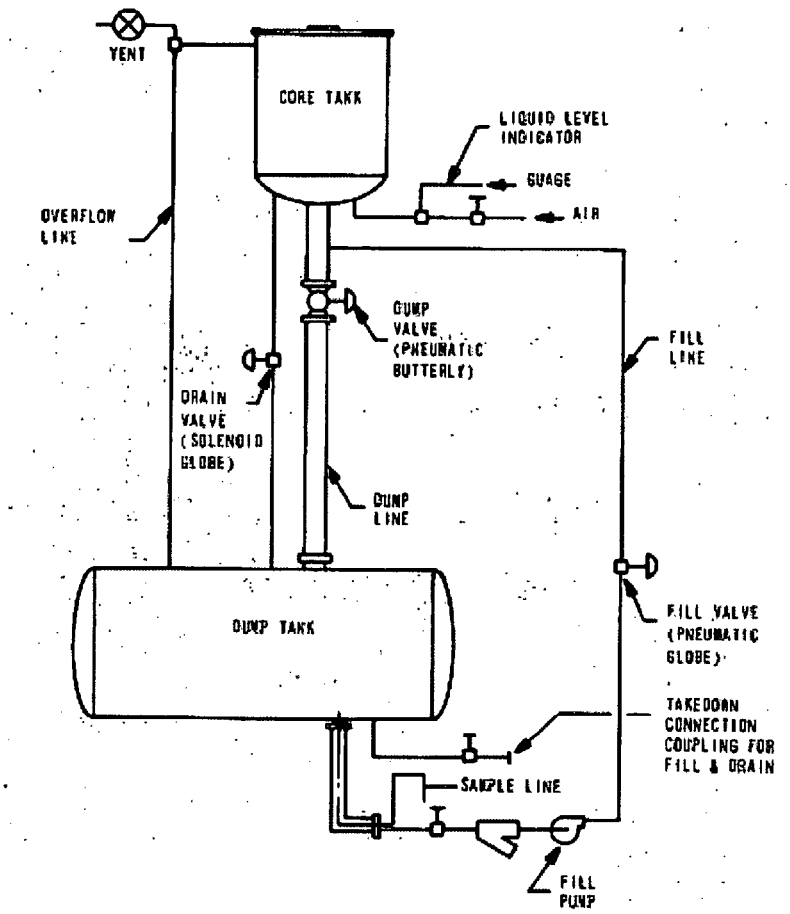

The safety blades are 0.08-inch thick boral, 7.9 inches wide by 70.9 inches long. All blades are thin enough to pass between the rows of fuel rods, and webs are cut in the top grid to allow blade entry. During these experiments, the blades perform a safety function only and are fully withdrawn during operation and held in a cocked position above the fueled region of the core to avoid perturbations during the measurements.

The nuclear instrumentation and control system is basically the same as that used in earlier light water experiments. The neutron detectors are conventional pulse counters and ionization chambers located at the outside wall of the core tank in

standpipes. The moderator level in the core tank is sensed by a remotely operated conductivity probe. The probe is moved by a Selsyn motor driven by a manually operated Selsyn transmitter at the control console. The moderator level indicated at the console by a Veeder Root counter is calibrated to an accuracy of ± 0.1-inch. Incremental changes in moderator level can be measured to an accuracy of ±0.01 inch.

Excess reactivity was controlled by dissolving boric acid (H3BO3) in the demineralized water moderator. The boron concentration in parts per million (ppm) is defined as the grams of natural boron per 106 cm3 of moderator at 25°C. The boron concentration was determined by titration against a standard KOH solution.

A.1.2 Fuel and Control Rod Description

A.1.2.1 UO2 Fuel Rods

Two types of UO_2 fuel rods were used in critical experiments. The first fuel rod type, which was used both in the Physics Verification Program and the Urania-Gadolinia Critical Experiment Benchmark Program, was a 0.475 inch outer diameter, 0.032-inch thick clad 6061 aluminum tube filled with sintered UO_2 pellets enriched to 2.46 wt% ^{235}U. The finished rods are 61.59 inches long with 0.125-inch thick aluminum plugs welded to the ends to seal the tubes. The one-inch space between the top pellet and the end plug is filled with Kaowool.

Table A-3 contains a summary of the physical properties of the fuel rods based on measurements of randomly selected samples. The uncertainties listed are standard deviations from the mean obtained from vendor's quality control data and check measurements on 50 to 100 randomly selected samples. The impurities are given as the summation of $N_i\sigma_i$ where N_i is the concentration of each impurity per cubic centimeter of the oxide fuel, and σ_i is the corresponding

microscopic absorption cross-section at 2200 m/s. The physical and chemical properties of the fuel rods reported herein are taken from References 2 and 3.

Table A-3: 2.46 wt% ^{235}U Fuel Rod

Parameter	Value[1]	
Fuel Composition	UO_2	
Fuel Pellet Density (g/cm^3)	10.24 ± 0.04	
Enrichment, wt % ^{235}U	2.459 ± 0.002	
Weight Percent of U in UO_2	88.13 ± 0.01	
Fuel Pellet Diameter (in, cm)	0.4054 ± 0.0005	1.0297 ± 0.00127
Fuel Clad Material	Aluminum 6061	
Fuel Rod OD (in, cm)	0.4748 ± 0.0006	1.206 ± 0.0015
Fuel Clad Wall Thickness (in, cm)	0.032 ± 0.001	0.0813 ± 0.0025
Active Fuel Length (in, cm)	60.37 ± 0.16	153.34 ± 0.4
Total Length of Fuel Rod (in, cm)	61.59 ± 0.35	156.44 ± 0.89
Weight of ^{235}U (g/rod)	28.29 ± 0.02	
Weight of Fuel Rod (g/rod)	1305.5 ± 1.0	
$\Sigma N_i \sigma_i$ (cm^2/cm^3 Oxide)	< 0.001	

Notes: 1. The standard deviations assigned by the experimenters to concentrations, dimensions, densities, etc., have not been used in the specifications for the benchmark models; only the listed mean values were used.

The second type of fuel rod, used primarily in the Urania-Gadolinia Critical Experiment Benchmark program, was a 0.4755-inch outer diameter, 71.5-inch long UO_2 fuel rod with fuel pellets enriched to 4.02 wt% ^{235}U and swaged in 0.016-inch thick 304 stainless steel tubes. The physical and chemical properties of these rods are summarized in Table A-4.

As in the previous case for the 2.46 wt% enriched fuel rods, the uncertainties are one standard deviation of the mean obtained from vendor quality control data and check measurements on randomly selected samples where the impurities are

given as the summation of the product of the concentration of each impurity per cm^3 of the oxide fuel and the corresponding microscopic absorption cross-section at 2200 m/s. Since the fuel rods were swaged and, thus, have no fuel gap, the fuel diameters were obtained by measuring the cladding outside and wall thicknesses. Although the outside diameter was constant, the wall thickness, which was determined using a conductivity measurement, was appreciably larger near the ends of the rod. The average cladding thickness between 15 and 55 inches was 15.9 ±0.5 mils, but the average between 4 and 67 inches was 16.6 ±0.6 mils. The value listed in Table A-4 is the cosine-squared-weighted average between 4 and 67 inches. The top and bottom end caps of the fuel rods are each approximately 2.35 inches long and consist of stainless steel thimbles filled with either aluminum or stainless steel plugs. Approximately 20% of the end caps are stainless steel. No distinction is being made in the experiments since the reactivity differences were shown to be negligible.

Table A-4: 4.02 wt% ^{235}U Fuel Rod

Parameter	Value	
Fuel Composition	UO_2	
Fuel Pellet Density (g/cm^3)	9.46 ± 0.10	
Enrichment, wt % ^{235}U	4.020 ± 0.005	
Fuel Pellet Diameter (in, cm)	0.4755 ± 0.0015	1.2078 ± 0.00381
Fuel Clad Material	Stainless Steel 304	
Fuel Rod OD (in, cm)	0.444 ± 0.002	1.206 ± 0.0015
Fuel Clad Wall Thickness (in, cm)	0.016 ± 0.0005[1]	0.0406 ± 0.0013
Active Fuel Length (in, cm)	66.70 ± 0.3	169.42 ± 0.76
Total Length of Fuel Rod (in, cm)	71.5	181.61
Weight of ^{235}U (g/rod)	56.61 ± 0.1	
Weight of Uranium (g/rod)	1408 ± 2.0	
Weight of Fuel Rod (g/rod)	1600 ± 2.0	
$\Sigma N_i \sigma_i$ (cm^2/cm^3 Oxide)	< 0.0005	

Notes: 1. Cosine-squared-Weighted Average

A.1.2.2 $UO_2 - Gd_2O_3$ Fuel Rods

The solid UO_2-Gd_2O_3 fuel rods are aluminum tubes filled with sintered fuel pellets containing approximately 4 wt% gadolinia and 96 wt% uranium nominally enriched in ^{235}U to 1.944 wt% (the variation was from 1.929 to 1.956 wt% ^{235}U). The fuel pellets are 0.4055 ± 0.001-inch in diameter by 0.59 ± 0.10-inch long. The 63-inch long tubes have an outer diameter of 0.475 inch and a 0.032 inch wall of type 6063 aluminum. Aluminum plugs 1/8-inch thick are welded at the ends to seal the tubes. The minimum pellet stack length is 60.4 inches and the space between the top pellet and the end plug is void.

In addition to solid UO_2-Gd_2O_3 fuel rod, annular UO_2-Gd_2O_3 fuel rods are used in the Gadolinia-Urania Critical Experiment Benchmark Program. These fuel rods are identical to the solid UO_2-Gd_2O_3 fuel rods except that they contain annular pellets with an inner diameter of 0.130 ± 0.005-inch. Table A-5 and Table A-6 summarize the physical and chemical properties of the solid and annular UO_2-Gd_2O_3 fuel rods, respectively.

Table A-5: Solid Gadolinia Fuel Rod

Parameter	Value	
Fuel Composition	UO_2- Gd_2O_3	
Fuel Pellet Density (g/cm^3)	10.11 ± 0.10	
Enrichment, wt % ^{235}U	1.944 (Nominal)	
Gadolina Weight Percent in Pellet, wt %	4 (Nominal)	
Fuel Pellet Diameter (in, cm)	0.4055 ± 0.001	1.2078 ± 0.00381
Fuel Clad Material	Aluminum 6063	
Fuel Clad Density (g/cm3)	2.7	
Fuel Rod OD (in, cm)	0.4748 ± 0.0006	1.206 ± 0.0015
Fuel Clad Wall Thickness (in, cm)	0.032 ± 0.001	0.0813 ± 0.0025
Active Fuel Length (in, cm)	60.40 ± 0.3	153.42 ± 0.76

Table A-6: Annular Gadolinia Fuel Rod

Parameter	Value	
Fuel Composition	UO_2- Gd_2O_3	
Fuel Pellet Density (g/cm^3)	10.11 ± 0.10	
Enrichment, wt % ^{235}U	1.944 (Nominal)	
Gadolina Weight Percent in Pellet, wt %	4 (Nominal)	
Fuel Pellet Inner Diameter (in, cm)	0.1300 ± 0.005	0.3302 ± 0.0127
Fuel Pellet Outer Diameter (in, cm)	0.4055 ± 0.001	1.2078 ± 0.00381
Fuel Clad Material	Aluminum 6063	
Fuel Clad Density (g/cm^3)	2.7	
Fuel Rod OD (in, cm)	0.4748 ± 0.0006	1.206 ± 0.0015
Fuel Clad Wall Thickness (in, cm)	0.032 ± 0.001	0.0813 ± 0.0025
Active Fuel Length (in, cm)	60.40 ± 0.3	153.42 ± 0.76

A.1.2.3 Poison Rods

The poison rods used in the various critical experiments consist of: (1) unclad Pyrex glass rods containing B_2O_3; (2) clad Vicor glass rods containing B_2O_3; (3) aluminum oxide rods clad in aluminum tubes; (4) Ag-In-Cd poisons rods; and (5) B_4C rods. The Pyrex rods represent LBP rods of high boron concentration that should not be exceeded in the design of any practical PWR fuel cycle. The Pyrex glass rods are slightly smaller than the fuel rods and contain 12.6 wt% B_2O_3. These poison rods are 188 cm long and have a Maxwell-averaged macroscopic cross-section of approximately 3.2 cm^{-1}.

The Vicor glass rods contain about 3 wt% B_2O_3 in pure silica. Their Maxwell-averaged macroscopic cross-section is about 0.76 cm^{-1}. Two 3-foot-long rods are loaded into 6061 aluminum tubes 6 feet long by 7/16-inch OD by 0.035-inch wall. Each tube is sealed at the bottom by a 3/8-inch-thick aluminum plug (welded in place) and at the top by a removable cork plug.

The aluminum oxide pins consist of reagent grade anhydrous Al_2O_3 powder in 0.437-inch outer diameter by 0.035-inch wall thickness 6061 aluminum tubes.

The Al_2O_3 filled rods represent depleted LBP rods. Each tube is sealed at the bottom by a 0.37-inch-thick aluminum plug (welded in place) and at the top by a removable cork plug. The Al_2O_3 is packed in the tube to a density of 1.31 g/cm (33% of the theoretical density).

The Ag-in-Cd absorber rods are 0.400 inch in diameter by 62.03 inches long and have a nominal composition of 80 wt% Ag, 15 wt% In, and 5 wt% Cd. The calculated macroscopic thermal cross-section is about 13.6 cm^{-1}. Depending on the selected experiment, the alloy rods are clad either with 0.441-inch outer diameter by 0.018-inch wall thickness 304 stainless steel (Physics Verification Program), or 0.475-inch outer diameter by 0.032-inch wall thickness type 6063 aluminum (Urania-Gadolinia Critical Experiment Benchmark Program). In the former case, the stainless steel tubes are sealed at the bottom by a 1/8-inch thick stainless steel plug. In the latter case, the aluminum tube is sealed at the bottom by a 1/8-inch thick aluminum plug (welded in place) and at the top by a removable cork. Table A-7 through Table A-9 summarize the physical and dimensional characteristics of the poison rods used in the various critical experiments.

Table A-7: Physical Properties of the Poison Pins

Perturbing Medium	Material	Clad	Density (g/cm^3)	Mass (g)	Pellet Diam. (cm)	Length (cm)
Pyrex Glass	12.615 ±.007% B_2O_3 81.385% SiO_2 4% Na2O 2% Al	No	2.23	453.6 ± 0.6	1.170± 0.001	188± 0.1
Vicor	3.035 wt % B_2O_3 96.965wt % SiO_2	Yes	2.19	214.5± 0.5	0.825± 0.002	183± 0.3
Ag-In-Cd	79.68 wt % Ag 15.09 wt % In 5.02 wt% Cd	Yes	10.16	1296± 5	1.016	157.6
Al2O3	Al2O3	Yes	1.31	138.8± 0.8	0.933± 0.001	154.6

Table A-26: Physical Properties of Cladding Tubing

Pellet Material	Clad Material	Outside Diameter (cm)	Inside Diameter (cm)	Thickness (cm)
Pyrex Glass				
Vicor	Aluminum 6061	1.115± 0.001	0.935± 0.001	0.09
Ag-In-Cd	Stainless Steel 304/ Aluminum 6063	1.120± 0.001	1.028± 0.001	0.046
Al2O3	Aluminum 6061	1.11± 0.001	0.932± 0.001	0.089

Table A-9: Material Composition of Aluminum 6061

Element	Al	Si	Fe	Cu	Mn	Mg	Cr	Zn	Ti
Fraction (wt. %)	96.55	0.6	0.7	0.25	0.15	1.15	0.2	0.25	0.15

The B_4C absorber rods are 0.438-inch outer diameter by 0.035-inch wall thickness aluminum tubes filled with natural B_4C powder ranging from 30 to 50 mesh. The bottom ends are sealed with welded aluminum plugs and the top ends with a removable cork plug. Each rod contains 156 grams of B_4C, which constitutes a column long enough to span the full core height. The space within the rod above the B_4C is void and extends about 1 foot above the level of the moderator. In all rods, the B_4C is compacted to 2.233 ±0.003 g/inch. A certified chemical analysis of the B_4C is given in Table A-28.

Table A-28: Physical Properties of the B_4C Rod

Parameter	Value	
Absorber Composition	B_4C	
Absorber Density (g/cm^3)	1.328	
Absorber Diameter (in, cm)	0.3681	0.935
Absorber Active Length (in, cm)	69.862	177.44
Clad Material	Aluminum 6063	
Clad Density (g/cm^3)	2.7	
Absorber Rod OD (in, cm)	0.438	1.113
Clad Wall Thickness (in, cm)	0.035	0.089
Total Boron (%)	77.8 (Average)	
Total Carbon (%)	20.8 (Average)	
Anhydrous B_2O_3 (%)	0.1 (Average)	
Boron Plus Carbon (%)	98.6 (Average)	

Notes: 1. B_4C powder is filled and compacted into tube.
2. Active length is based on 156 g column loading and 2.233 g/in. compacted density

A.1.2.4 Void Rods

Two types of void rods are used in the critical experiments at the B&W Critical Experiment Laboratory. The first type of void rod is a 1/4-inch outer diameter by 0.035-inch wall thickness Inconel-600 tube sealed at the bottom to exclude water. The tube is 157 cm in length and is fitted with 0.475-inch outer diameter 304 stainless steel sleeves at the bottom and near the top to center it in its top and bottom grid position. Pertinent parameters and compositions for this void rod are given in Table A-29.

Table A-29: Physical Properties of the Void Rods Used in the Physics Verification Program

Parameter	Value	
Material	Void (Air)	
Density (g/cm^3)	0.0012	
Diameter (in, cm)	0.018± 0.0005	0.457 ± 0.001
Length (in, cm)	61.42± 0.2	156.0 ± 0.5
Clad Material	Inconel 600	
Rod OD (in, cm)	0.25± 0.0005	0.635 ± 0.001
Clad Wall Thickness (in, cm)	0.035	0.089

The second type of void rod, which is used in the Urania-Gadolinia Critical Benchmarks, consists of 0.475-inch outer diameter by 0.032-inch wall thickness type 6063 aluminum tubes 63-inches long. The tubes are sealed by a 1/8-inch thick aluminum plug welded in place at the bottom to exclude water. The tops are sealed with O-ring fitted lead weights, which also prevents the tubes from floating. These weights are located well above the moderator level in the core. Table A-30 summarizes the pertinent physical properties of the void rods used in the Urania-Gadolinia Critical Benchmark Experiments.

Table A-30: Physical Properties of the Void Rods Used in the Urania-Gadolinia Critical Experiment Benchmark Program

Parameter	Value	
Material	Void (Air)	
Density (g/cm^3)	0.0012	
Length (in, cm)	63	160.02
Clad Material	Aluminum 6063	
Rod OD (in, cm)	0.4748 ± 0.0006	1.206 ± 0.0015
Clad Wall Thickness (in, cm)	0.032 ± 0.001	0.0813 ± 0.0025

A.1.3 Core Loadings

A.1.3.1 B&W Physics Verification Program Core Loadings

The basic critical assembly, designated as Core XI, used to provide data for the comparative analysis performed as part of this Topical is shown in Figure 2-1 and the composition of some of the different arrays of control and instrument lattice positions that are part of the Core XI critical experiments is shown in Figure 2-2.

The configuration for Loading 16, which is illustrated in Figure A-17, is different from the preceding 15 loadings, in that parallel lines of water holes, separated by 7 lines of fuel rods, run the entire length of the central region of the core.

Figure A-17: Loading 16, Core XI

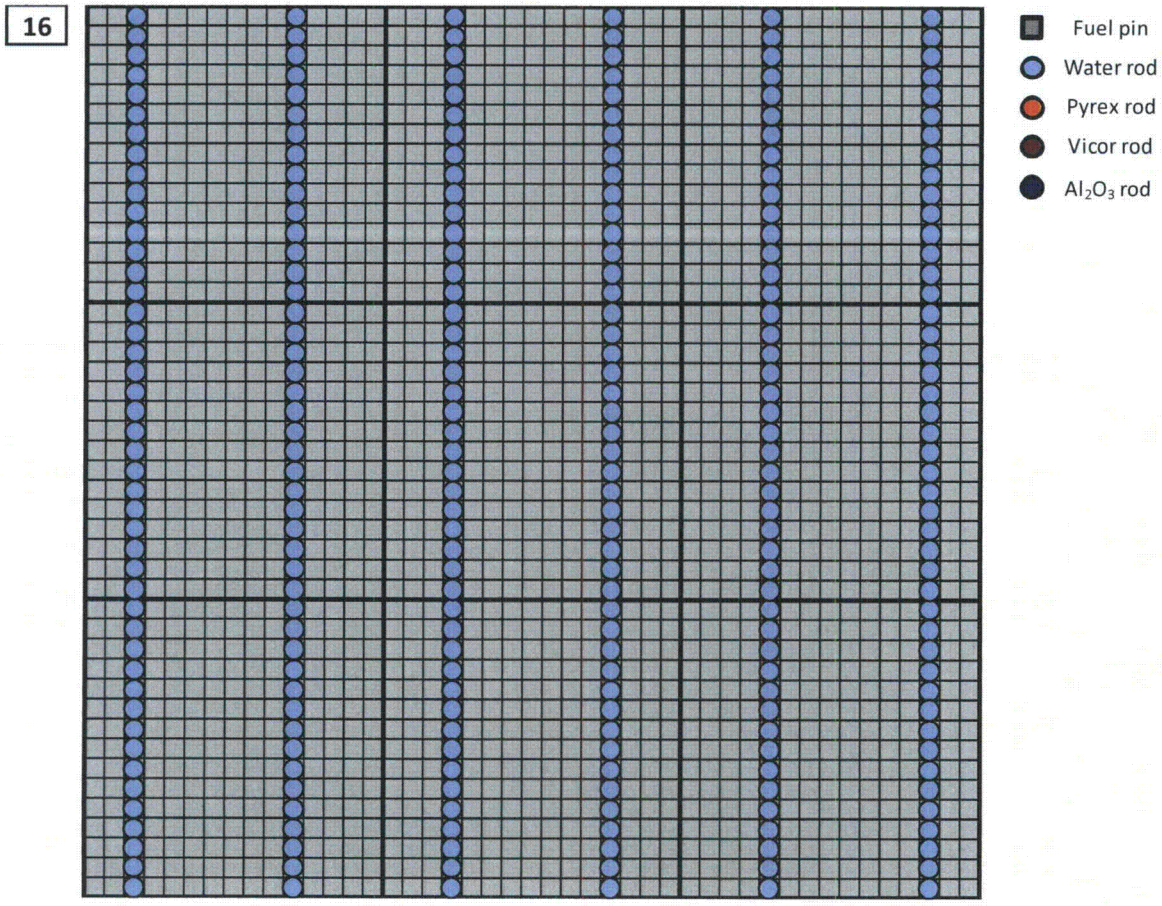

Loading 17, shown in Figure A-18, is similar to loading 16 except that parallel lines of water holes run from left to right as well as front to back.

Figure A-18: Loading 17, Core XI

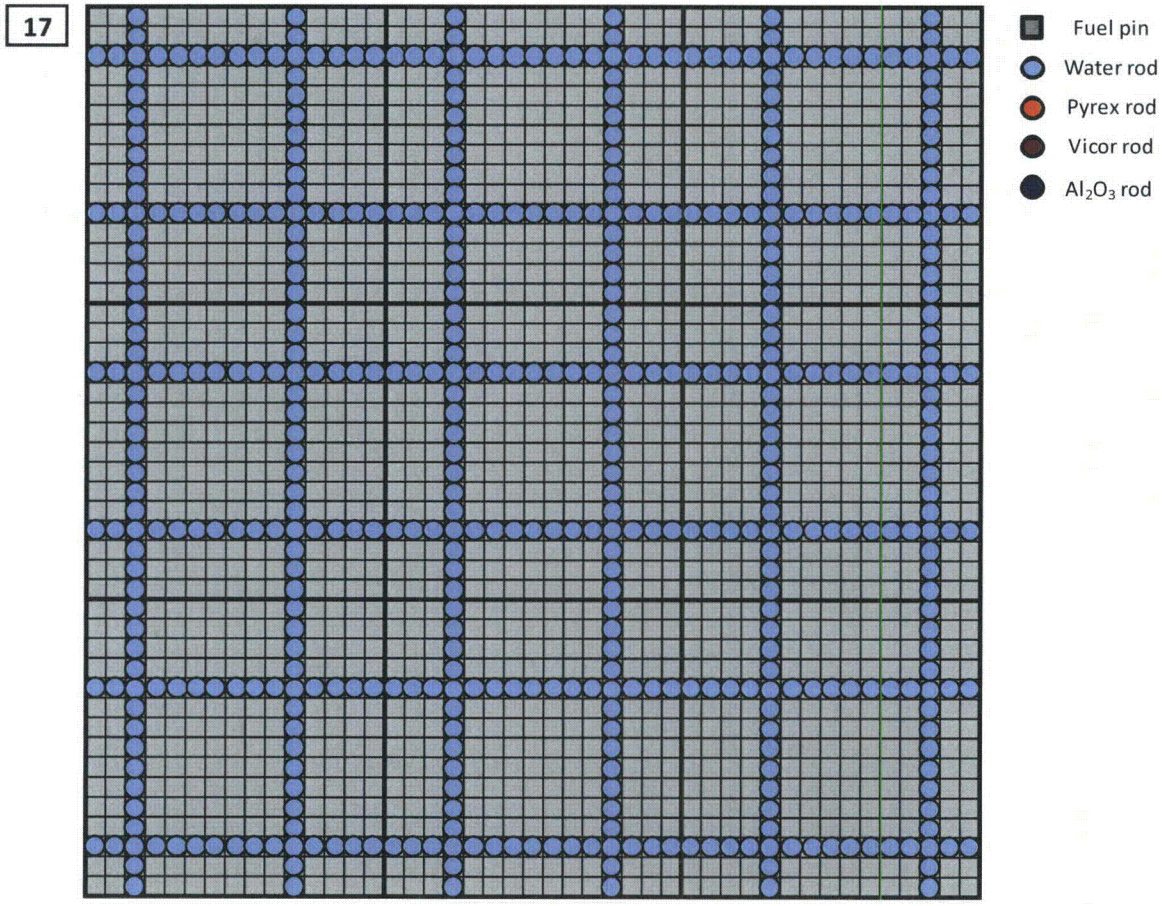

All 17 experiments for Core XI are constructed with a uniform square pitch of 1.63576 cm and are axially uniform. The outer radius of the water reflector is 76.2 cm.

The vertical dimensions of Core XI are given in Figure A-19. As shown, the top and bottom grid plates align the fuel, control, and instrumentation tube rods vertically. The grid plates are 1-inch wide slotted aluminum strips interlocked to

form a square matrix. The strips are 0.160 inch thick and are spaced on centers of 0.664 ± 0.001 inches.

Figure A-19: Vertical Core Dimensions

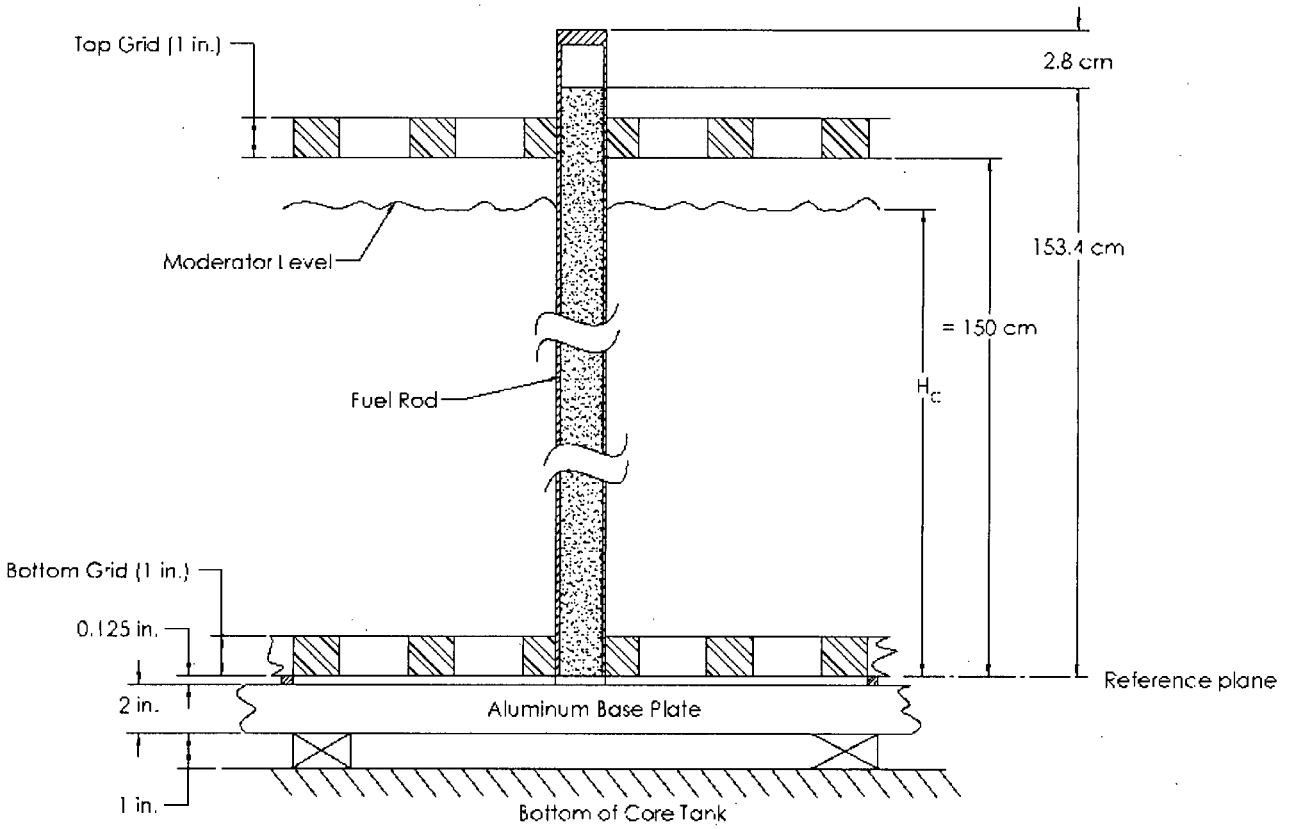

The fuel rods are supported on a 2-inch thick aluminum base plate, which is raised about 1 inch above the bottom of the 5-foot diameter tank. The intervening space is filled with moderator. Moderator levels are reported relative to the bottom of the active fuel. The fuel rods and perturbing rods are uniformly spaced at intervals of the lattice pitch and are loaded to approximate a cylindrical geometry.

The lattice configurations, various attributes, and measured critical boron concentrations for the 17 UO_2 critical experiments selected for analysis are summarized in Table 2-1.

A.1.3.2 Urania-Gadolinia Critical Experiment Benchmark Program Core Loadings

A total of 23 cores were assembled in the Urania-Gadolinia Critical Experiment Benchmark Program. In 22 of the 23 cores studied, UO_2-Gd_2O_3, B_4C rods, void tubes and water holes were spaced on selected patterns in an otherwise uniform clean lattice in order to study their effect on reactivity, power distribution and incore detector signal. To provide generic data germane to all domestic PWR designs, each core loading was a variation of two basic configurations, namely:

Babcock & Wilcox Configurations

- ***15x15 Fuel Rods per Assembly Using 2.46 wt% Enriched Fuel:***

  The basic core (Core 1) used for the 15x15 configuration measurements consists of 4808 fuel rods. Imaginary lines divide the center of the core into nine fuel assemblies, 15 lattice pitches square. A pattern of vacant fuel rod positions in each fuel assembly simulates an instrument hole and 16 control rod guide tube positions. Cores 2 through 10 are variations of the basic core.

- ***15x15 Fuel Rods per Assembly Using 2.46 and 4.02 wt% Enriched Fuel***

  The basic core (Core 12) used is similar to the one described above, except that the central zone contains 4.02 wt% ^{235}U fuel rods and the outer portion contains 2.46 wt% ^{235}U fuel rods. Cores 13 through 17 are variations of this basic Core 12

Combustion Engineering Configuration

The basic core (Core 18) used is a 16x16 configuration and consists of 4620 fuel rods. Imaginary lines divide the center of the core into nine identical fuel assemblies, 16 lattice pitches square. Large water holes

have been created by omitting multiple fuel rods. Cores 19 and 20 are variations of this basic core.

The remaining core, designated Core 11, was a special core assembled for the resonance integral measurements. The core contained a total of 554 2.46 wt% ^{235}U enriched fuel rods loaded on a square pitch of 0.644 inch. To provide a central water region, 36 fuel rod positions in the center of the core are unoccupied by fuel rods. A 0.625-inch outer diameter by 0.65-inch thick wall aluminum tube, sealed at the bottom to exclude water, is located along the core's axial centerline with the open end extending well above the moderator level.

Seventeen (17) of the cores (15x15 B&W type lattice) were selected for evaluation with ***CASMO-5/SIMULATE-3.*** A cross-sectional layout of the critical experiments identifying the axial dimensions of the pins and grids is shown in Figure A-20 and the loading configurations for the various critical are illustrated in Figure A-21. The configurations of these cores are summarized in Table 2-2. The measured pin power distributions for Cores 1, 5, 12 and 14 were compared to the ***CASMO-5/SIMULATE-3*** pin power reconstruction calculations.

Figure A-20: Critical Experiment Axial Dimensions of Pins and Grids

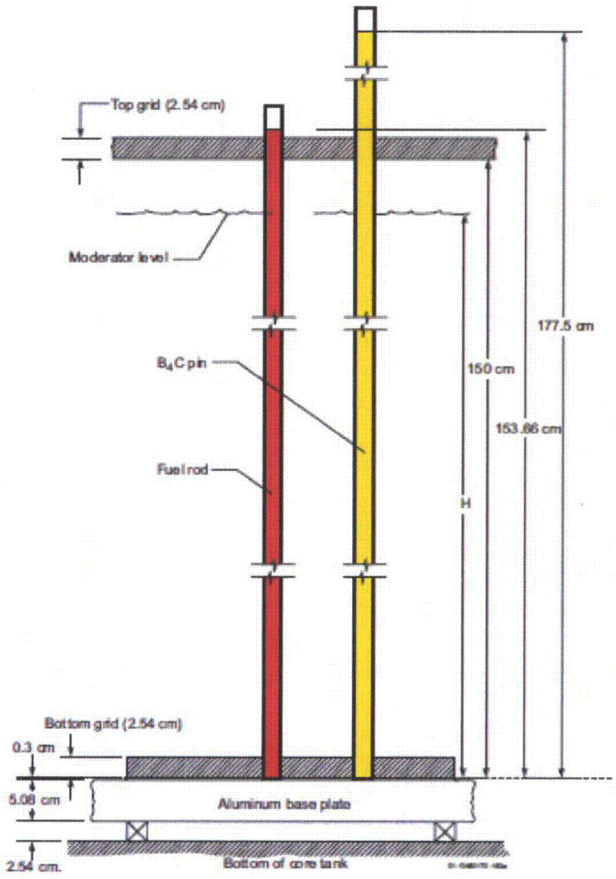

Figure A-21: B&W Urania-Gadolinia Critical Experiment Core Loading Diagrams

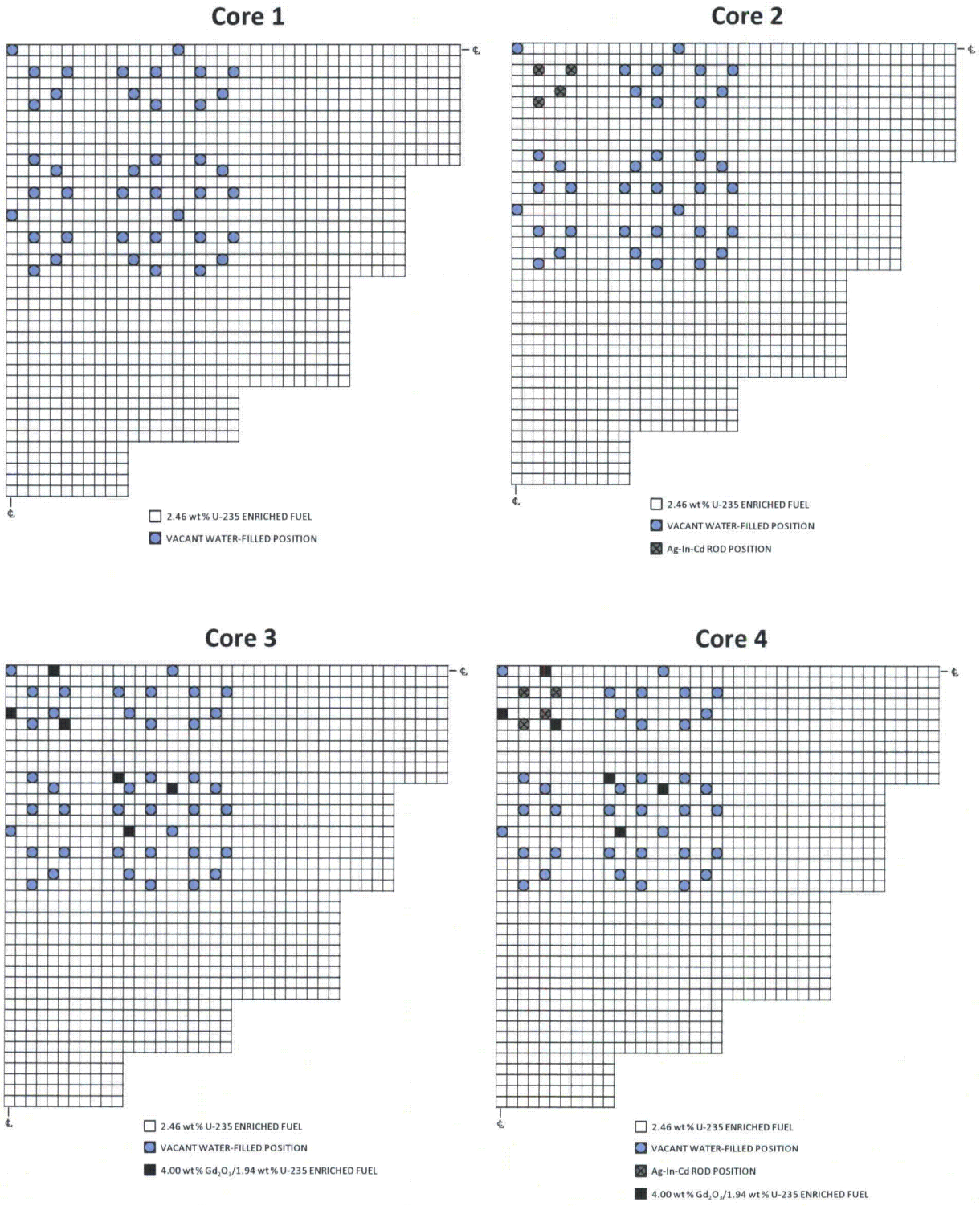

Figure A-21 (continued)

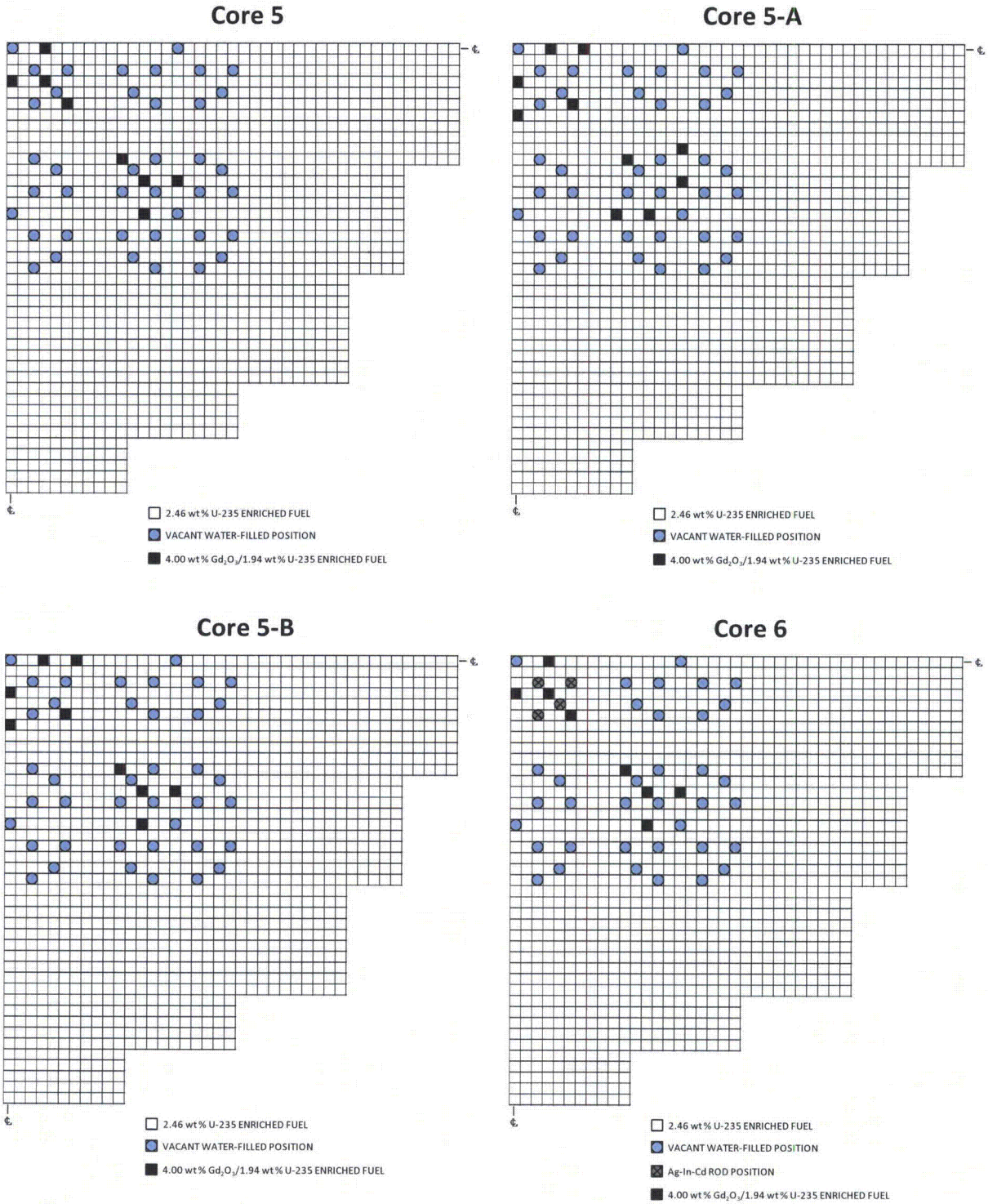

Figure A-21 (continued)

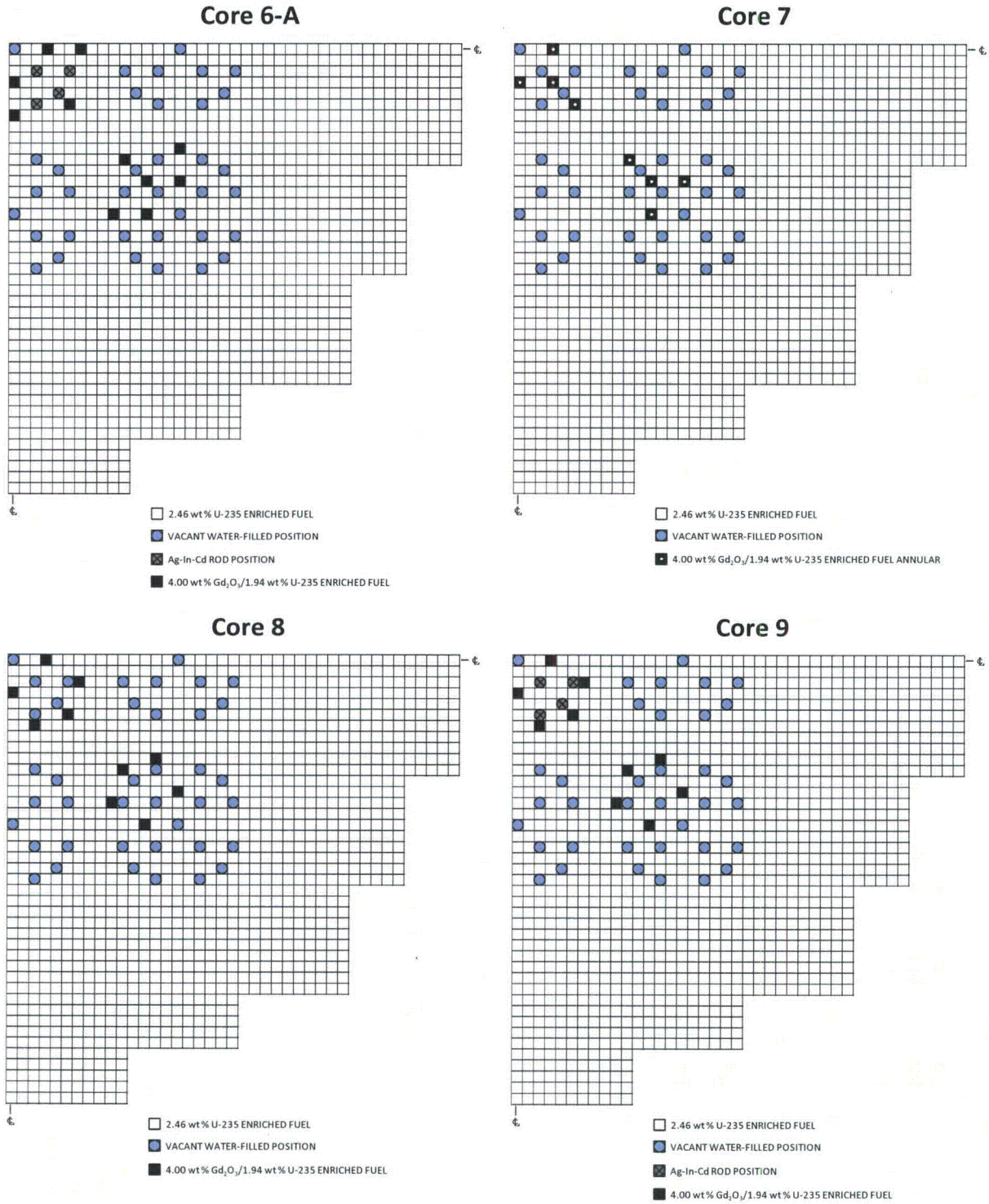

Figure A-21 (continued)

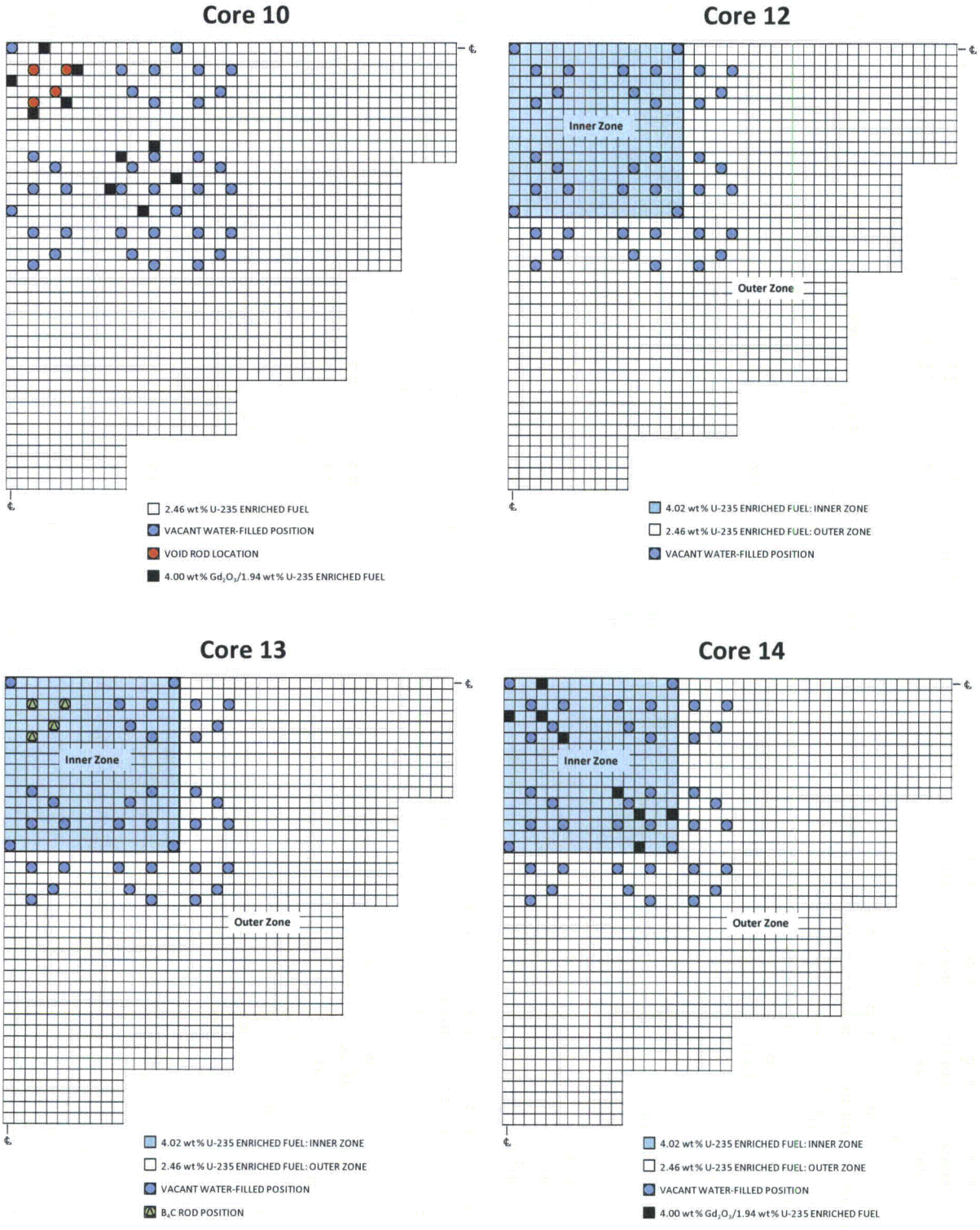

Figure A-21 (continued)

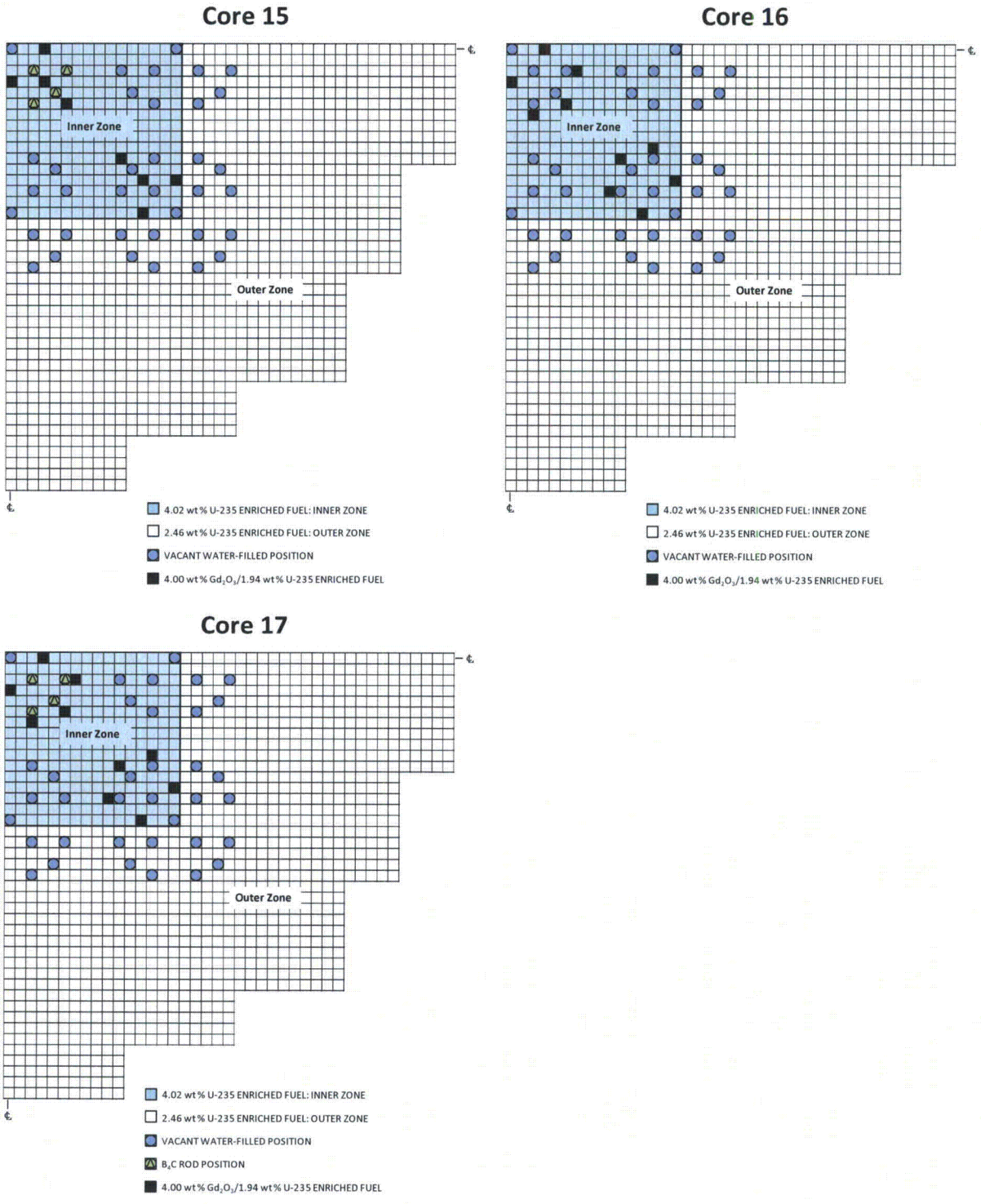

A.1.4 Measurement Techniques

A.1.4.1 B&W Physics Verification Program Critical experiments Measurement Techniques

Using various patterns of simulated LBP, control, and instrument rods, the UO_2 fueled critical assemblies were all adjusted to a k_{eff} of about 1.0007 with the moderator height at 145 cm. This was accomplished by adjusting, the soluble boron concentration until the critical water height was about 139 cm for all eight critical assemblies. The boron concentration is determined by titration against a standard KOH solution and is given in units of parts per million (ppm), which is defined as the grams of natural boron per 10^6 cm^3 of moderator at 25 C°. The boron concentration measurements have a standard deviation $\pm$ 3 ppm.

Axial power distributions were measured on the fuel rods constituting a one-eighth core symmetric volume of the central 15 by 15 simulated fuel assemblies. The relative power distribution was determined by counting collimated fission product gammas from activated fuel rods with an NaI(TI) scintillation counter. Photons with energies less than 200 keV were discriminated out. The collimator consisted of a 1-inch diameter hole in the 2-inch thick lead shield placed between the fuel rod and the counter. Four inches of lead above and below the detector and 2 inches along the sides provided shielding from other portions of the fuel rod.

To perform all fuel rod activations at a constant moderator height, the boron concentration was adjusted to make the assembly critical at a moderator height of about 139 cm. Activations were then made on an exponential period obtained by raising the moderator height to 145 cm. The integrated exposure was approximately 1 kW-minute. The counting time varied from 8 to 50 seconds, and the total count collected at each rod position varied from 60,000 to 80,000

counts. The background activity was kept low by loading essentially unirradiated fuel rods in the positions to be studied.

Decay corrections were obtained from a master fuel rod, which was irradiated simultaneously with the rods to be scanned, and then counted in a second counting system. The second system was identical to the first in collimation and electronics. A standard fuel rod, recounted at frequent intervals, provided data to correct for any small changes in either system.

All power density data were normalized to a reference point 74.4 cm from the top of the fuel region on the standard rod. Detailed lattice descriptions and measured critical boron concentrations are listed in Table 2-2 for each of the UO_2 critical experiments.

A.1.4.2 Urania-Gadolinia Critical Experiment Benchmark Measurement Techniques

The change in the moderator boron concentration is used as a measure of reactivity change since boron concentration can be readily and accurately measured. Excess reactivity is controlled by dissolving boric acid (H_3BO_3) in the moderator (demineralized water). The boron concentration in parts per million (ppm) is defined as the grams of natural boron per million cm^3 of moderator at 25°C; it is determined by titration against a standard KOH solution.

The moderator boron concentrations for the 17 critical experiments selected for analysis in this Topical are given in Table 2-1. All of them produce a critical condition when the moderator is at a height of 57.1 inches and the safety blades are fully withdrawn (i.e., they are above the moderator). In addition to the standard deviation shown for the boron concentration, a systematic bias which may be as large as 0.2% existed. This bias cancels when differences are calculated.

Relative midplane power distribution measurements were made for the base configurations either 2.46 wt% or 4.02 wt% ^{235}U in the 15x15 design, and the 16x16 design (Cores 1, 12, and 18). Also measured were three cores similar to the base configuration but having UO_2-Gd_2O_3 fuel, Cores 5 and 14 with 12 UO_2-Gd_2O_3 fuel rods per assembly, and Core 20 with 16 UO_2-Gd_2O_3 fuel rods per assembly. An incore detector assembly was loaded along the axial centerline of these cores. The incore detector assembly is similar to that used in B&W designed PWRs and contains seven rhodium detectors (almost equally spaced along the vertical axis of the core), a background detector, a thermocouple, and a central calibration tube. Stainless steel filler rods are located between the end cap of the assembly and the ends of the detectors. The outer sheath is 0.316-inch OD and has a 0.031-inch wall thickness. The calibration tube is 0.125-inch OD by 0.093-inch ID.

The relative power profiles within the cores were determined by counting collimated fission product gammas from activated fuel rods with an NaI(Tl) scintillation counter. Gamma photons less than 250 keV were discriminated out. The collimator consisted of a 1-inch diameter hole in a 2-inch thick lead shield placed between the fuel rod and the detector so that only the gammas from a 1-inch segment of the rod were counted. The detector was surrounded by at least 4 inches of lead, and other portions of the fuel rod were shielded from the detector by at least another 5 inches of lead. The rods were rotated while being counted to provide data that were independent of rod orientation. So that all fuel rod activations could be performed at a constant moderator height, the boron concentration was adjusted to make the core critical at a moderator height of approximately 55 inches. Activations were then made on an exponential period obtained by raising the moderator height to 57.10 ±0.05 inches. The integrated exposure was about 1 kW-minute. The background activity was kept

low by always loading essentially unirradiated fuel rods in the positions to be studied.

Decay corrections were obtained from a "master" fuel rod, irradiated simultaneously with the rods to be scanned, and then counted in a second counting system. The second system was identical to the first in collimation and electronics. Counts were taken on the two systems simultaneously, and the master rod was never moved during the data acquisition of a given run. A standard fuel rod, recounted at frequent intervals, provided data to correct for any small changes in either system.

The basic rod scan data are presented in Reference 4 where the average value for each fuel rod position tabulated is the result of three reactor runs (See Tables 4-6 through 4-11 in Reference 4). Additionally, Tables 4-12 through 4-20 in Reference 4 have been corrected for the difference in counting efficiency of the various types of fuel rods. In essence, the counting efficiency is due to the differences in the radial power profile through the types of fuel pellets, cladding material, and thickness. This difference has been evaluated by dissolving fuel from each fuel rod type, determining the fission product activity of the solution, and comparing the results with a fuel rod scan. Correction factors derived from these comparisons were then applied to the fuel rod scan data. In addition, the data has been normalized so that the average power of the fuel rods within the center assembly is unity.

A.2 Description of Critical Experiments at the Plutonium Recycle Critical Facility (PRCF)

A series of twelve lattice experiments were performed at PNNL to provide benchmark neutronics data for use in assessing the accuracy of neutronics analysis methods for slightly enriched uranium lattices and for mixed oxide (UO_2-PuO_2) lattices. However, since UO_2 critical experiments have previously been analyzed as

part of the B&W Physics Verification Program, only the six UO_2-PuO_2 (2 wt%) core configurations were analyzed here to provide rods-in and rods-out local power distribution data that simulated an extreme core burnup condition. This was done to obtain the uncertainty in the ***CASMO-5/SIMULATE-3*** calculational model under EOL fuel burnup conditions.

A.2.1 The Plutonium Recycle Critical Facility

The Plutonium Recycle Critical Facility (PRCF) is a low-power (< 15 kW thermal) experimental reactor designed for studying neutronics phenomena in liquid-moderated reactor cores. The aluminum reactor tank is 6 feet in diameter and 9 feet deep; it has a cadmium wrapper and thermal insulation on its cylindrical surface. The lattice plates are made of 6061-T6 aluminum alloy 0.75 inch thick. Two of the plates are drilled on a 0.75-inch square pitch to position the fuel rods, and a third, located beneath the lower lattice plate, is essentially solid. The fuel rods are supported so that the bottom of the fuel column is flush with the top surface of the lower lattice plate. The upper surface of the upper lattice plate is positioned 1 inch below the top of the fuel column. The physical layout of the tank, lattice plates and support structure, and fuel rods is shown in Figure A-22.

The neutron sensing chambers of the reactor instrumentation system were positioned at the core midplane in the radial reflector with a minimum distance of about 5.5 inches between the core periphery and a chamber. The lattice support posts, made of 6061-T6 aluminum alloy, were located about 1.5 inches from the core periphery. The effect of these chambers on the core reactivity status was measured and found to be negligible. The measured reactivity effect of the lattice support rods was also negligible.

The reactor was controlled using moderator level and cadmium control rods with fuel followers. The rod follower sets occupied normal lattice positions so that the followers completed the local lattice array with the rods fully withdrawn.

Figure A-22: PRCF Lattice Support Structures

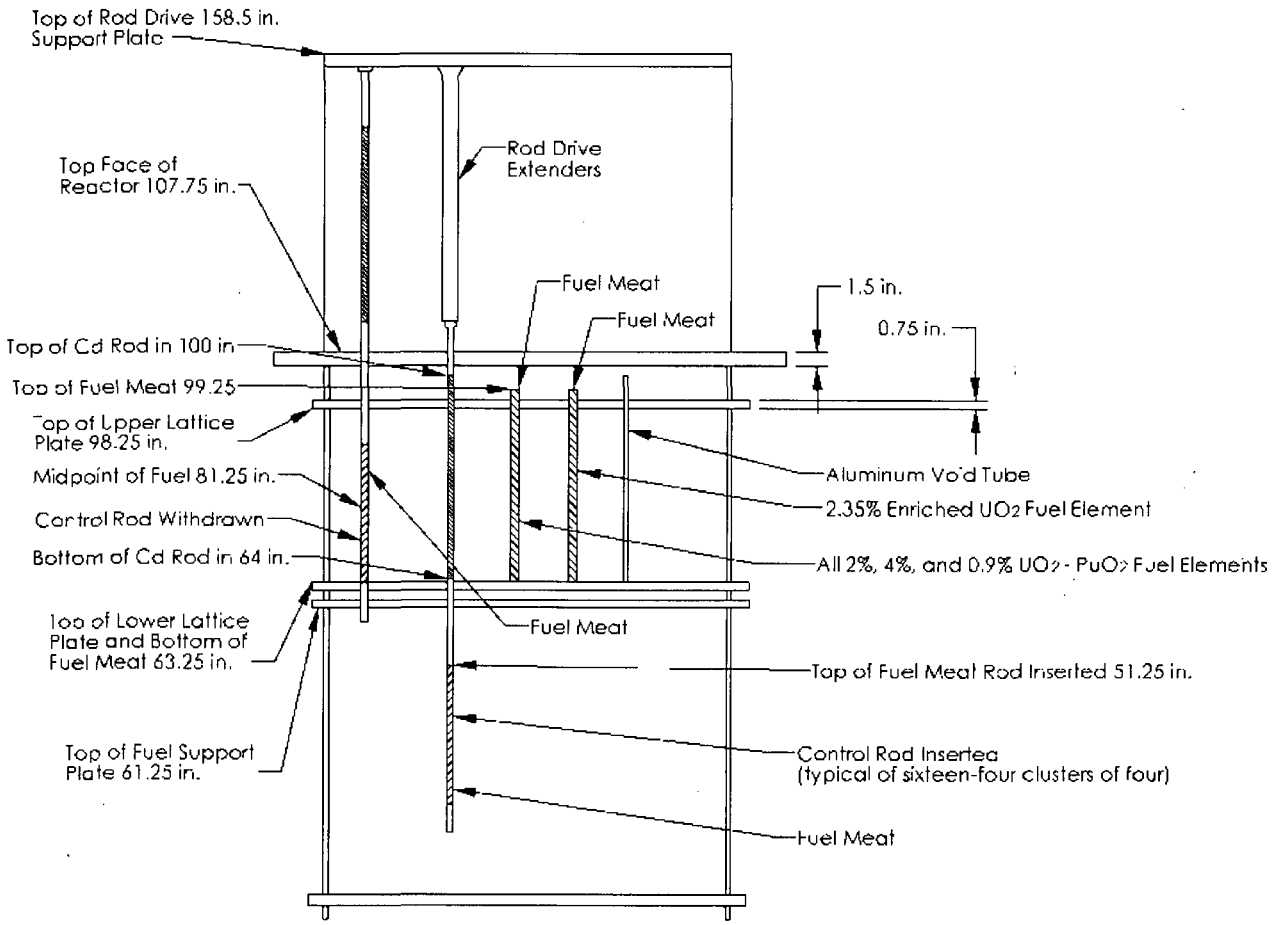

A.2.2 Fuel Rod Description

The six core configurations analyzed as part of this report consist of UO_2 (2 wt%) - PuO_2 (8% ^{240}Pu) fuel rods clad in zircaloy-2 clad. A sufficient number of rods of each fuel type were available to permit assembly of cores with large radii, thus reducing the influence of radial leakage on measured results. A detailed drawing with the pertinent dimensions and material types for the fuel rod is given in Figure A-35. The

fuel followers for the UO_2 (2 wt%) - PuO_2 (8% ^{240}Pu) fuel are identical with the fuel rods of that type.

Figure A-35: Description of UO_2-PuO_2 (2 wt%) Fuel Rods

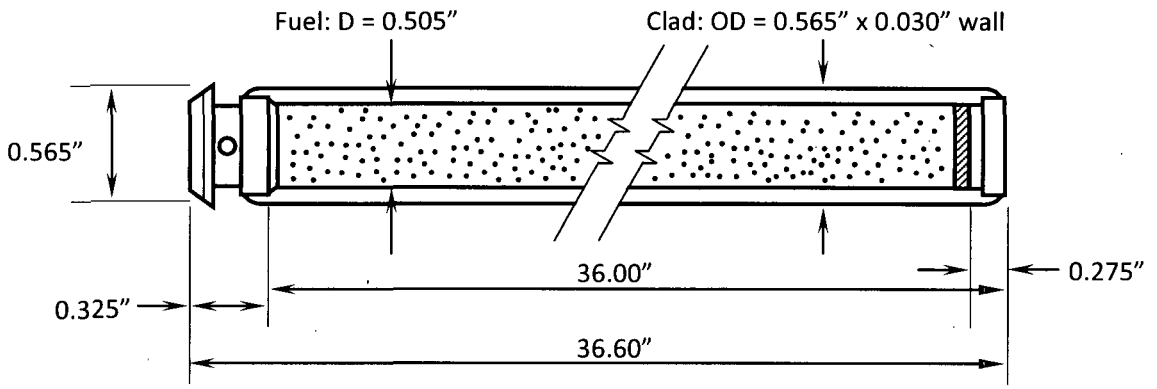

1. Rod dimensions	Fuel OD = 0.505" (1.2827 cm), r_{fuel} = 0.64135 cm (for CASMO-5 use) Clad OD = 0.565" (1.4351 cm), r_{clad} = 0.71755 cm (for CASMO-5 use) Clad wall thickness = 0.030"
2. Cladding	Zircalloy-2 tubing
3. Rod total weight	1340 g (average)
4. Fuel loading	Mixed $PuO_2 - UO_2$ vibrationaly compacted
5. Fuel weight	1128 g/rod (average)
6. Composition (wt%)	Pu/PuO_2 = 88.1, Pu/MOX = 1.760
7. Total Pu in MOX	2 wt%
8. Fuel density	9.54 g/cm^3

9. Isotopic distribution of Pu at analysis date, January 1965

^{239}Pu	91.615 wt%
^{240}Pu	7.654 wt%
^{241}Pu	0.701 wt%
^{242}Pu	0.031 wt%
^{241}Am	unknown

10. Separation date: April 1962

A.2.3 Core Loadings

The six UO_2-PuO_2 (2 wt%) critical experiments selected for analysis consisted of core configurations with three lattices of different fuel rods pitches, namely 0.7-inch, 0.87-inch, and 0.99-inch. Loading maps of each of the lattice types are illustrated in Figure A-35 through Figure A-37. All cores were loaded to be as nearly cylindrical as possible, within the constraints of keeping the fuel follower rods within the core boundary. The heavy line on each map denotes the actual boundary of the core loading.

Figure A-35: 0.7-inch Pitch Lattice Core Configuration

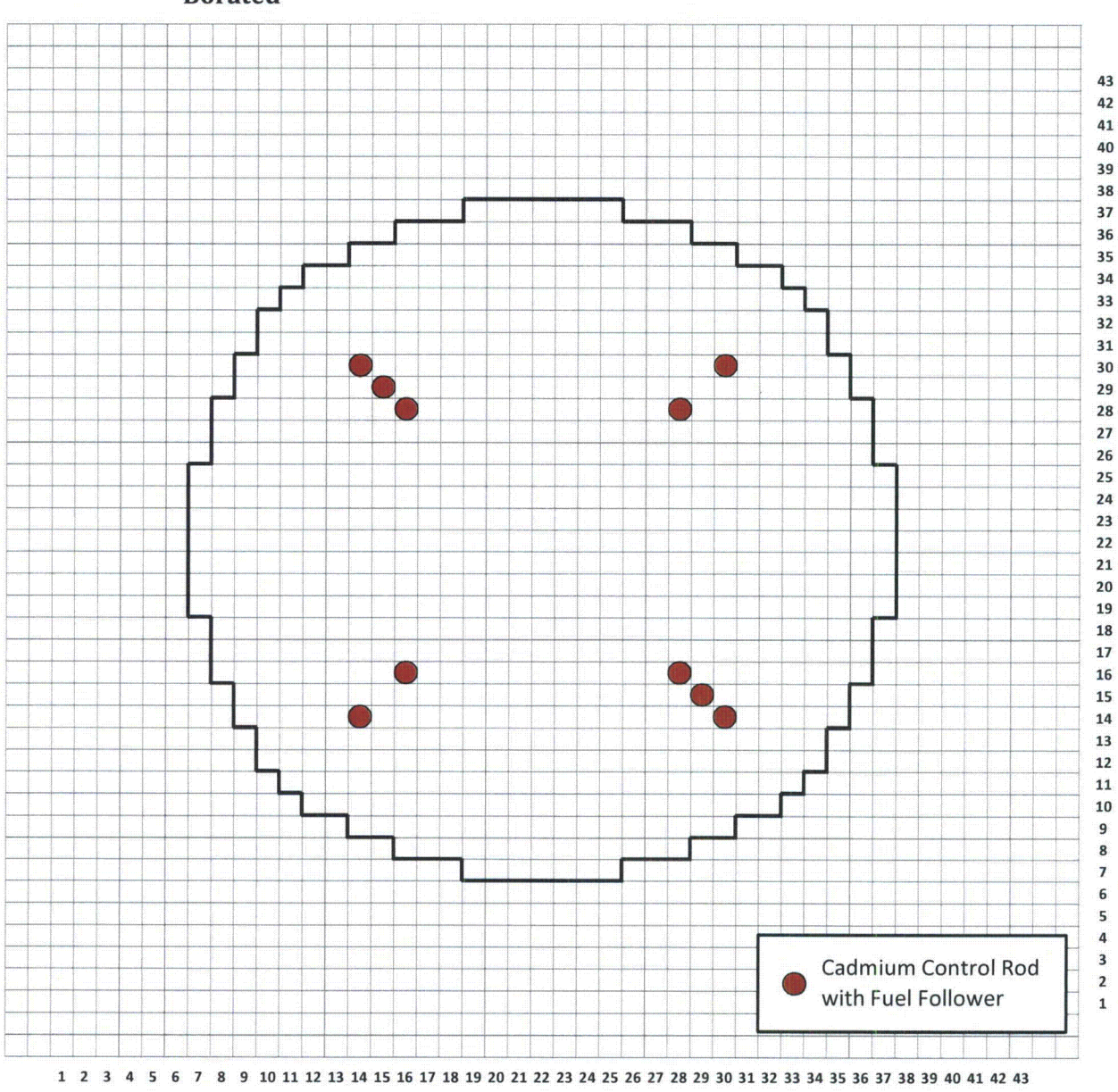

Unborated

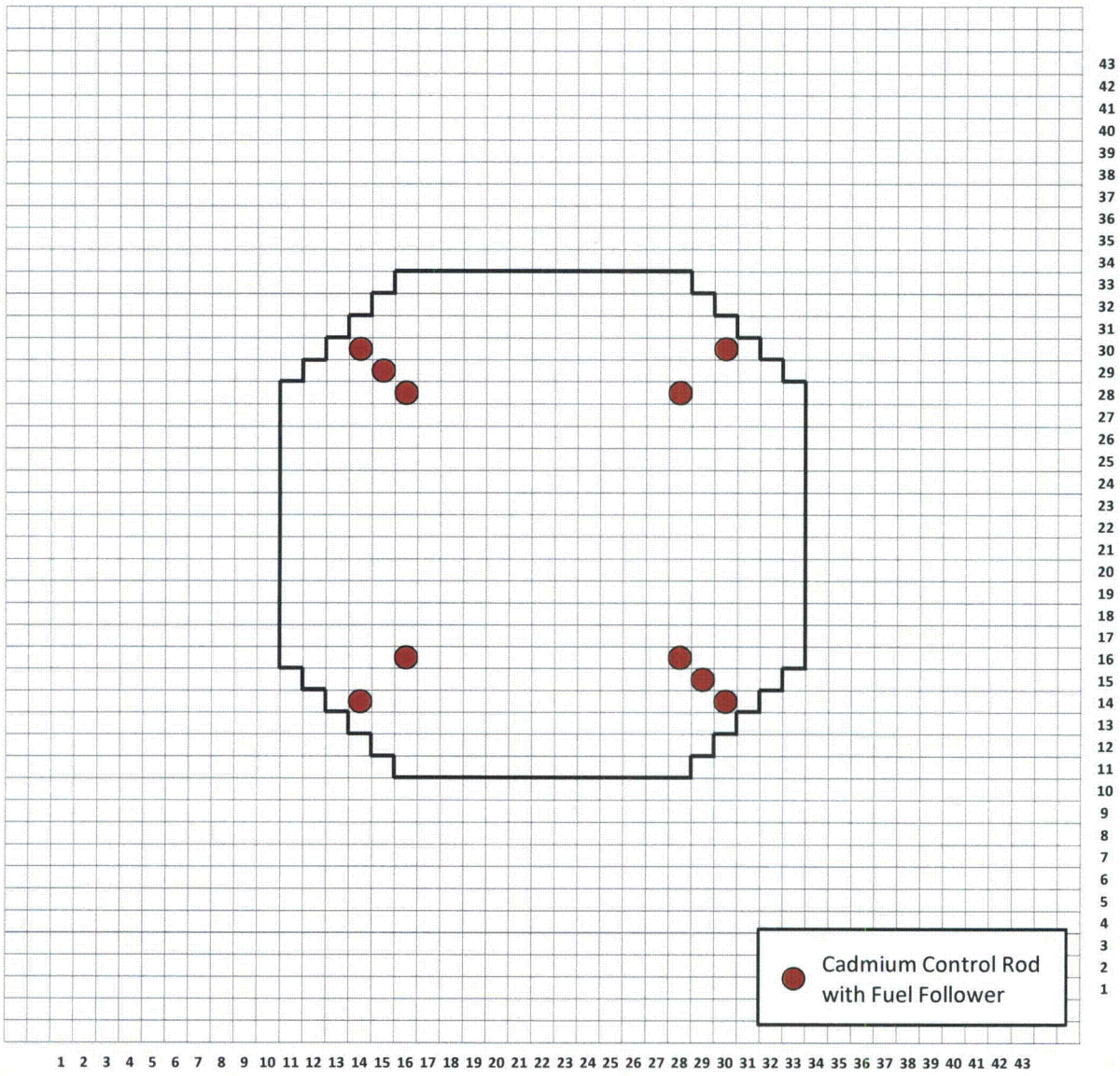

Figure A-25: 0.87-inch Pitch Lattice Core Configuration

Borated

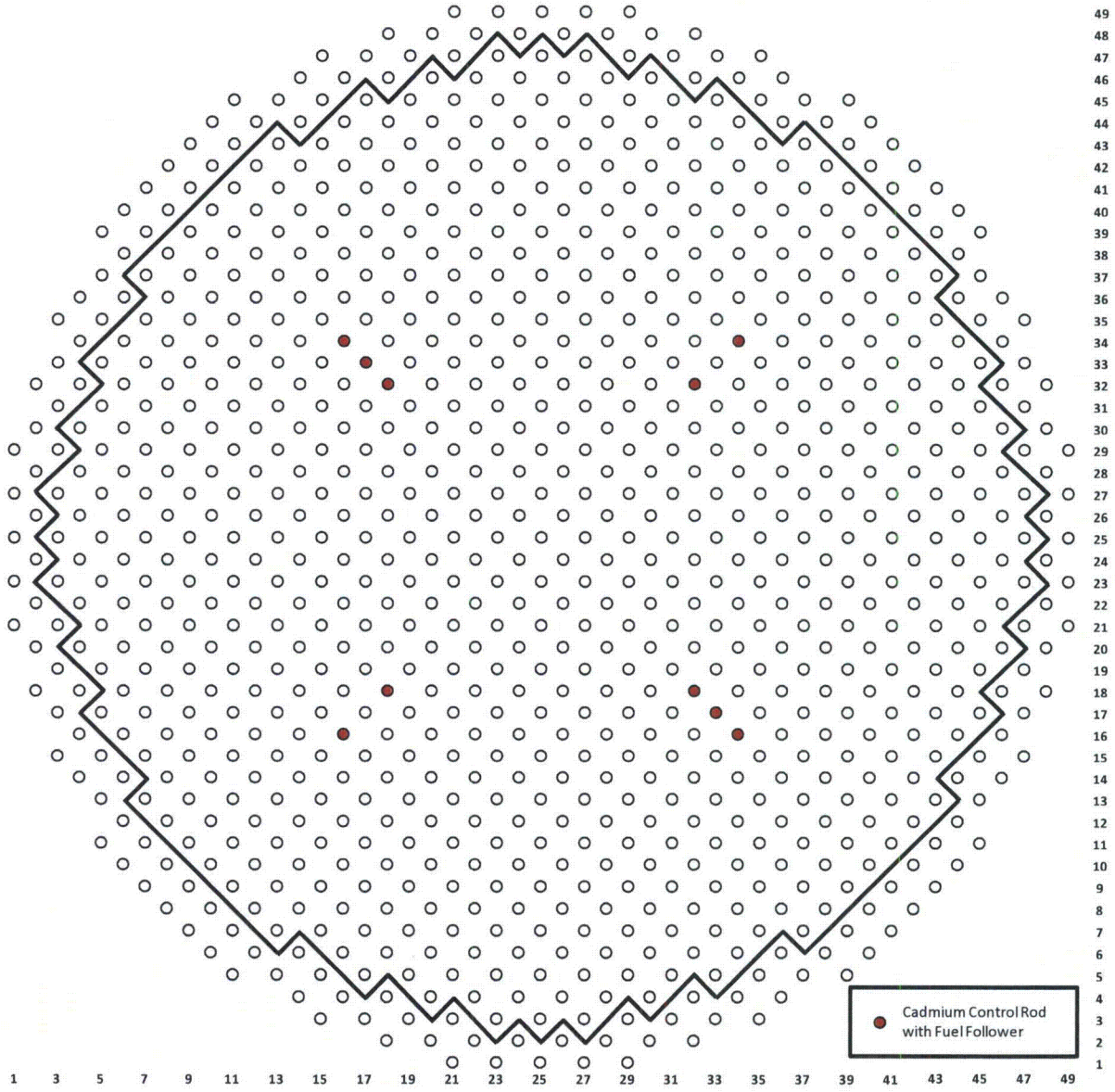

Unborated

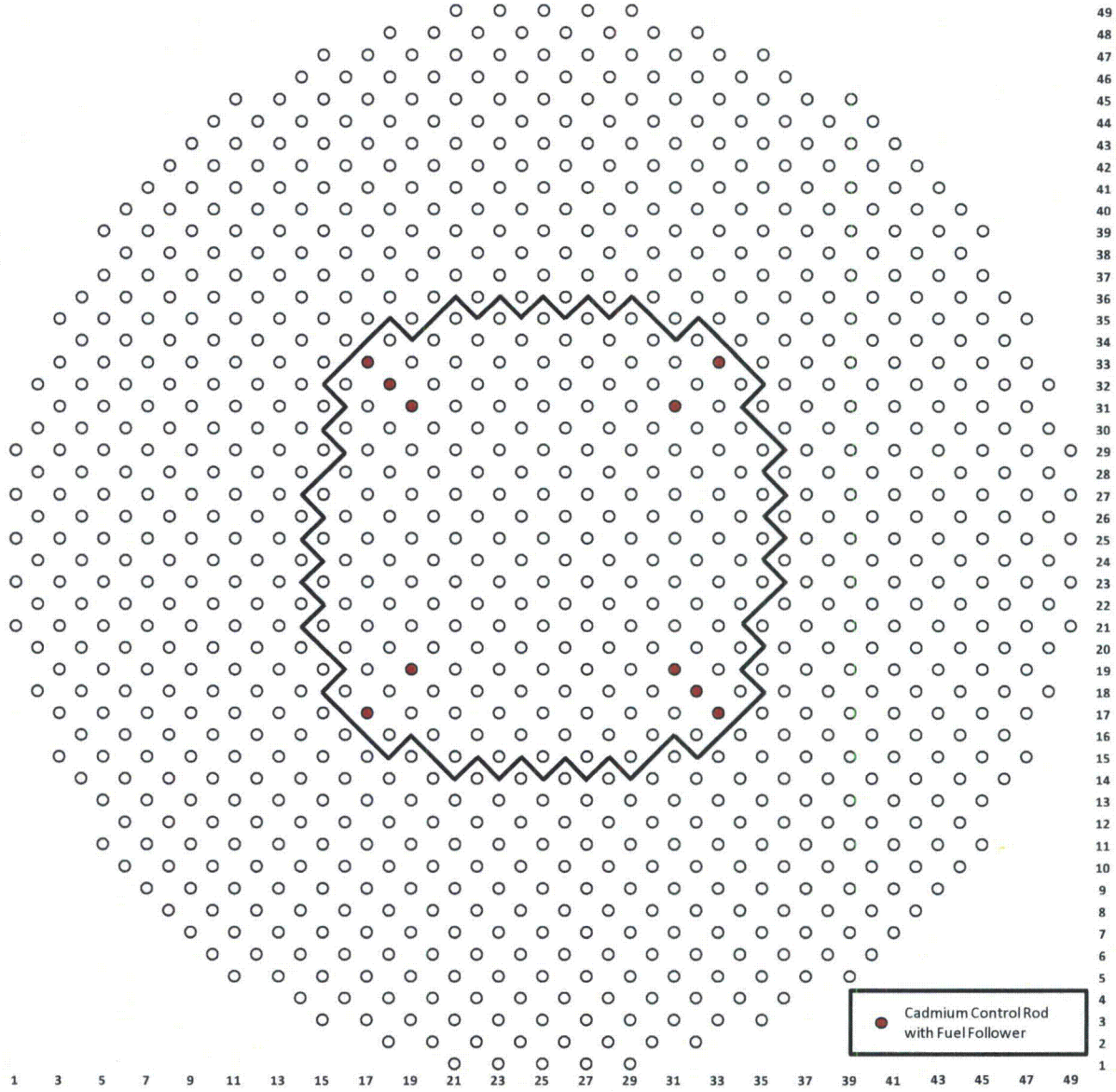

Figure A-37: 0.99-inch Pitch Lattice Core Configuration

Borated

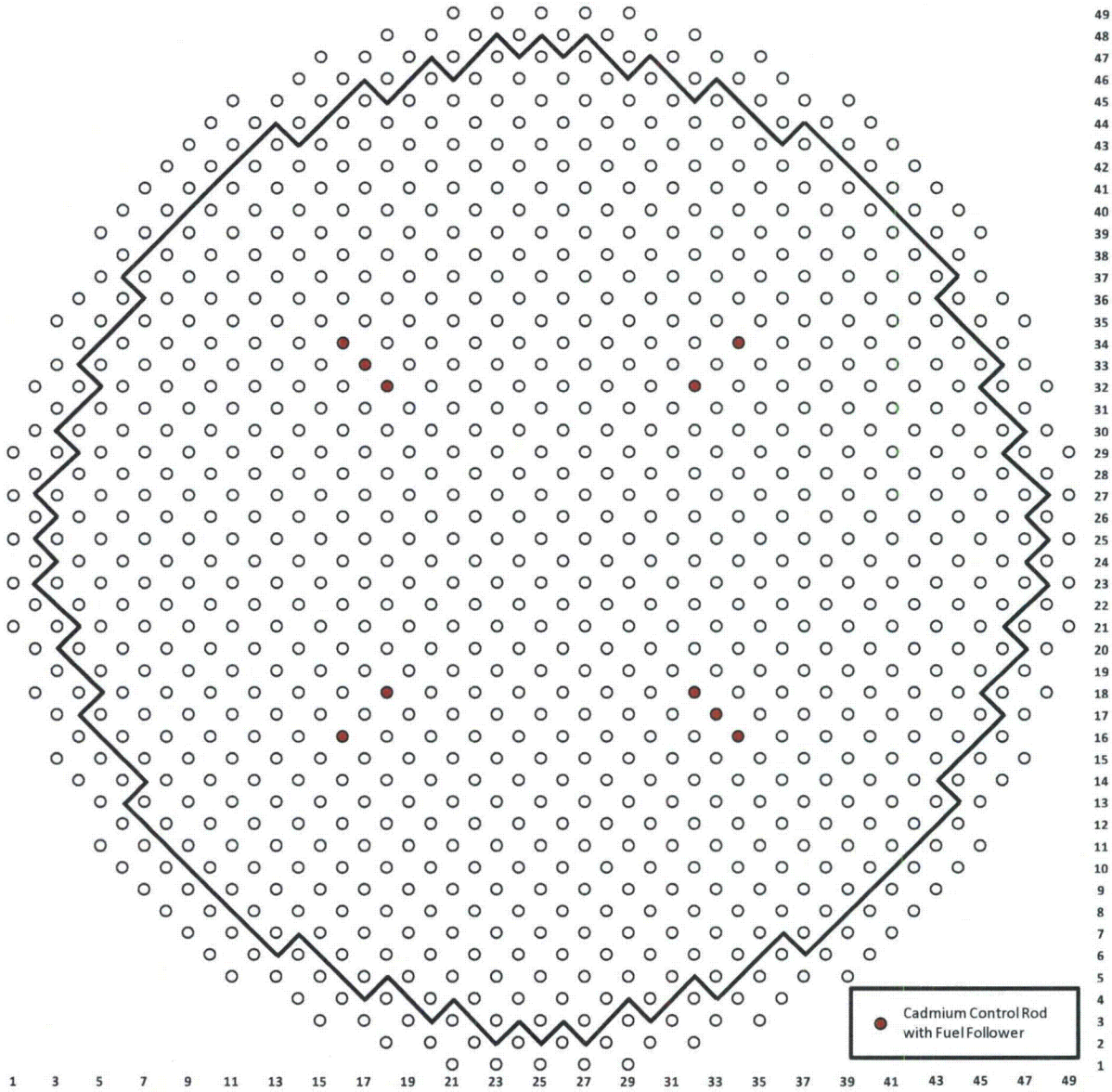

Unborated

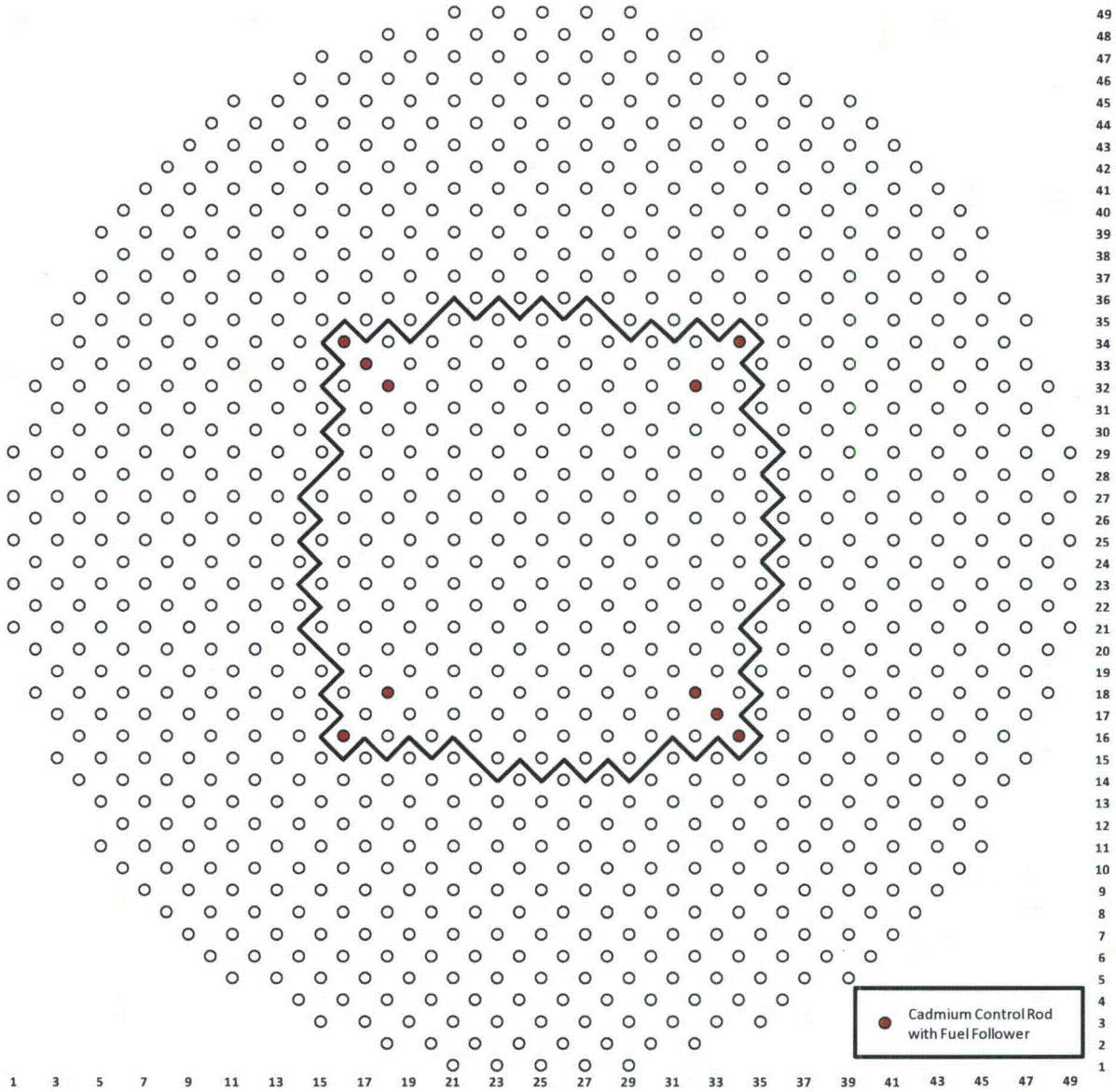

A.2.4 Measurement Techniques

The initial phase in each core configuration was to achieve criticality, either by incremental fuel additions if unborated, or by adjustment of the boron concentration in the moderator with the core size held constant if borated. Each measurement of relative power distribution was made by irradiating the core on a very slowly rising reactor period, with the core fully reflected and all control rods fully withdrawn.

The relative power distribution in a given array was determined from an analysis of measurements of the intensity of fission product gamma rays from the fuel, rod-to-rod, throughout each array. Each fuel rod selected for measurement was counted on a dual channel counting system which automatically corrected for fission product decay during the measurement period.

The system employed two matched counting systems, one measured the rods of interest (called the traverse system), and another provided a means of correcting the measurements for radioactive decay during counting (called the decay system). A fuel rod of similar exposure history to those being measured was placed in the decay system at the start of the measurement and left there for the duration of the measurements. The decay system was electronically arranged to stop the traverse system after a preset number of counts had been obtained from the decay rod, thereby correcting for decay. Both systems were matched according to gain and energy discrimination. An integral counting method was used; only gammas with energies greater than 0.470 MeV were counted.

The fuel rods were rotated at about 20 rpm about their longitudinal axis in the traverse system during the counting periods in order to average the circumferential fuel rod activity. The decay rod was not rotated. The collimator aperture on the traverse system was rectangular, 0.375 in. x 0.75 in., such that a 0.375 in. long axial

segment of the fuel rod was scanned at each point. Each rod was counted at its axial mid-plane to obtain the rod-to-rod power distribution within the array. Two rods in each array were traversed in 2 in. intervals to obtain the axial power shapes. The worths of peripheral fuel rods and/or the worths of small changes in boron concentration were measured in each core configuration to permit extrapolation to the just critical condition (keff = 1.000) from the slightly super critical conditions of the measurements.

The reactivity worth of a fuel rod on the periphery of the core was determined from the difference in rising reactor period with and without a fuel rod on the core periphery. The measurement of boron sensitivity was accomplished by determining the change in rising reactor period produced by an addition of a small amount of water. While the absolute value of the boron concentration was uncertain by ± 2 ppm, small changes in the concentration could be made with good precision, using the relationship $\Delta C=\Delta V C_0/(V_0+\Delta V)$ where C_0 is initial boron concentration, V_0 is the initial volume of the moderator in the system and ΔV is the volume of clean H_2O added to the system.

A key measurement in the total program was the determination of the boron concentration in the moderator for each borated critical array. These determinations were made by performing an acid-base titration analysis of moderator samples drawn after each irradiation or other measurement. Multiple samples were drawn and duplicate analyses were formed on the samples. The analysis equipment was calibrated against solution standards traceable to the National Bureau of Standards. Experience with the equipment has shown that the expected uncertainty on measurements of standards in the range 300 to 1000 weight parts per million (wppm) boron in water is about 0.5%. The isotopic analysis of the boric acid powder used to borate the moderator was ^{10}B = 19.8 ± 0.1 atom percent.

A.2.5 Data Analysis Methods

An automated data processing and analysis code was available to handle the large volume of counting data generated during this program. The basic data collected are the number of counts C_{ij} from the traverse rod collected in the time interval t_{ij} that was required to collect C_0 counts from the decay rod, and the time T_{ij} elapsed between the end of the irradiation and the start of the counting interval t_{ij}, where the subscripts ij indicate the i^{th} rod of the j^{th} type and C_0 is a constant, usually 40,000. Also measured were backgrounds for each detector system, and residual back-grounds for each fuel rod due to previous irradiation histories. One rod, designated the normalization rod, was counted at selected intervals throughout each measurement period. The corrected data from the set of observations from the normalization rod are fitted to a linear function of time, N(T). Each corrected value, C_{ij}, is divided by the value of N(T) calculated at the time of observation, to correct for any electronic drifts occurring during the measurement period. If more than one observation was made on a given rod, the corrected and normalized values are averaged. Symmetric points are also averaged. The final result is a list of relative power values within a given array together with their one sigma statistical uncertainties given in units of percent.

The data from each axial traverse were fitted by least squares with a cosine function of the form $A(X)=A_1\cos[(A_2(X-A_3)]$ where A_1 is the peak relative power at position X = A_3 and A_2 is the square root of the axial buckling in inverse inches. Each point in a traverse was weighted by the inverse of its variance.

A.3 Determination of Measured to Calculated Data Accuracy

The combination of critical assembly power distribution data from the Physics Verification Program and the Urania-Gadolinia Critical Experiment Benchmark Program provides an overall data base sufficient to determine the accuracy of the ***CASMO-5/SIMULATE-3*** calculational model at both BOL and EOL conditions. However, to make the required

comparisons between the measured and calculated data the measurement uncertainty for the pin powers must be established. In this regard, the sets of symmetric fuel pins from Core XII, loading 1 and loading 2, were analyzed to determine the uncertainty on the measured pin power value.

In this topical the total uncertainty σ_t will be used for conservatism of measured to calculate values. Note that the standard deviation associated with the comparisons of measured to calculated data is the combined total uncertainty, σ_t, which is defined by the square root of the sum of the squares of the measurement and calculation uncertainties, σ_m and σ_c, respectively:

$$\sigma_t = \sqrt{\sigma_m^2 + \sigma_c^2}$$

Therefore, the use of the total standard deviation (σ_t) would conservatively represent the accuracy of the ***CASMO-5/SIMULATE-3*** calculational model and its ability to predict the eigenvalues and power distributions of very heterogeneous geometry configurations.

A.4 Calculated Versus Measured Results

This section describes the calculated values used as a base for the evaluation of the computational methodology using the CMS code suite ***CASMO-5/CMS-LINK/SIMULATE-3***. Comparisons are made between calculated and measured parameters for the cold clean critical experiments from: (1) the B&W Physics Verification Program; (2) the Urania-Gadolinia Critical Experiment Benchmark Program; and (3) the UO_2-PuO_2 critical experiments from the Plutonium Recycle Critical Facility.

A.4.1 B&W Physics Verification Program UO_2 Critical Experiments

The 17 candidate loadings described previously in subsection 1.2.1.3.1 were modeled for computational methodology evaluation. Although sufficient information for the 17 loading was available for the critical eigenvalue comparative analysis, only nine loadings were adequate for the pin power comparisons. Only

loadings 2 through 9 and 11 from References 2 and 3 were used in the pin power comparative analysis.

A.4.1.1 Computational Model

The candidate core loadings described previously were modeled for computational methodology evaluation. Specifically, cross-sections and discontinuity factors for interior zone fuel lattice types (segments), one exterior zone lattice and one reflector configuration were computed with ***CASMO-5***. The ***CASMO-5*** lattice segments were created based on the 15x15 fuel assembly layout in the interior zone of the cores using eighth-core lattice symmetry.

A.4.1.2 Eigenvalue Comparisons

A.4.1.2.1 Uncertainties in the Critical Eigenvalue Calculation

The modeling-induced biases, boron concentration uncertainties and overall uncertainties in the eigenvalue calculations for the UO_2 critical experiments were discussed in detail in Subsection 2.4.1.2.1 of the main body of this Topical Report. It was concluded that a bias of ± 0.0045 Δk should account for all uncertainties identified in Table 2-3 of Subsection 2.4.1.2.1. The resulting benchmark-model critical eigenvalue for all of the UO_2 cases is then: 1.0007 ± 0.0045.

A.4.1.2.2 Calculated Versus Measured Critical Eigenvalues

Table 2-4summarizes the cold critical k_{eff} calculated with ***SIMULATE-3*** for all 17 critical experiments. Comparisons are presented between three data sets: ***SIMULATE-3***, The Physics Verification Program (as reported in References 2 and 3) and the ***MCNP*** benchmark described in Reference 7.

A.4.1.2.3 Pin Power Comparisons

Pin powers for Loadings 2 through 9 and 11 were calculated with ***SIMULATE-3*** and compared to the B&W Physics Verification Program (References 2 and 3)

measured data. Figure A-38 through Figure A-46 summarizes the results of the comparative analysis. All experimentally measured data was properly renormalized to a quarter-core lattice, consistent with ***SIMULATE-3*** methodology, for a correct comparison.

Figure A-38: Pin Powers Comparison for Loading 2

MEAS	0.000	1.071	0.993	0.968	0.992	0.993	0.948	0.951
CALC	0.000	1.079	1.028	1.003	0.996	0.995	0.963	0.942
DIFF	0.000	0.008	0.035	0.035	0.004	0.002	0.015	-0.009
		1.033	1.040	1.002	1.013	1.062	0.993	0.970
		1.052	1.072	1.021	1.015	1.046	0.984	0.946
		0.019	0.032	0.019	0.002	-0.016	-0.009	-0.024
			0.000	1.080	1.082	0.000	1.035	0.930
			0.000	1.083	1.076	0.000	1.033	0.952
			0.000	0.003	-0.006	0.000	-0.002	0.022
				1.056	1.108	1.096	0.999	0.894
				1.055	1.092	1.071	0.989	0.943
				-0.001	-0.016	-0.025	-0.010	0.049
					0.000	1.073	0.974	0.942
					0.000	1.051	0.962	0.939
					0.000	-0.022	-0.012	-0.003
						0.982	0.941	0.939
						0.982	0.940	0.919
						0.000	-0.001	-0.020
							0.939	0.919
							0.922	0.909
							-0.017	-0.010
								0.890
								0.900
								0.010

MAX DIFF	0.049
ST DEV	0.019

UO2 rod

Water rod

Pyrex rod

Vicor rod

Al2O3 rod

Figure A-28: Pin Powers Comparison for Loading 3

Figure A-29: Pin Powers Comparison for Loading 4

MEAS	0.000	0.987	0.909	0.922	0.994	1.039	1.007	0.992
CALC	0.000	0.995	0.916	0.935	0.977	1.008	1.000	0.984
DIFF	0.000	0.008	0.007	0.013	-0.017	-0.031	-0.007	-0.008
		0.902	0.830	0.914	0.970	1.071	1.066	0.993
		0.923	0.859	0.918	0.999	1.069	1.022	0.989
		0.021	0.029	0.004	0.029	-0.002	-0.044	-0.004
			0.000	0.880	1.041	0.000	1.097	0.983
			0.000	0.890	1.061	0.000	1.077	0.998
			0.000	0.010	0.020	0.000	-0.020	0.015
				1.000	1.113	1.101	1.025	0.978
				0.985	1.103	1.115	1.035	0.992
				-0.015	-0.010	0.014	0.010	0.014
					0.000	1.077	0.999	0.991
					0.000	1.097	1.011	0.983
					0.000	0.020	0.012	-0.008
						1.050	1.010	1.006
						1.032	0.993	0.975
						-0.018	-0.017	-0.031
							0.990	0.985
							0.978	0.967
							-0.012	-0.018
								0.952
								0.961
								0.009

MAX DIFF	0.029
ST DEV	0.018

UO2 rod

Water rod

Pyrex rod

Vicor rod

Al2O3 rod

Figure A-30: Pin Powers Comparison for Loading 5

MEAS	0.000	1.119	1.038	1.008	1.029	1.041	1.005	0.997
CALC	0.000	1.125	1.058	1.027	1.019	1.021	1.001	0.982
DIFF	0.000	0.006	0.020	0.019	-0.010	-0.020	-0.004	-0.015
		1.076	1.085	1.038	1.036	1.088	1.035	0.986
		1.094	1.110	1.049	1.039	1.077	1.020	0.984
		0.018	0.025	0.011	0.003	-0.011	-0.015	-0.002
			0.000	1.077	1.067	0.000	1.071	0.980
			0.000	1.087	1.069	0.000	1.050	0.985
			0.000	0.010	0.002	0.000	-0.021	0.005
				0.964	0.893	1.026	0.978	0.947
				0.991	0.922	1.008	0.990	0.967
				0.027	0.029	-0.018	0.012	0.020
					0.000	0.879	0.931	0.958
					0.000	0.873	0.944	0.951
					0.000	-0.006	0.013	-0.007
						0.922	0.944	0.966
						0.909	0.939	0.943
						-0.013	-0.005	-0.023
							0.961	0.966
							0.942	0.941
							-0.019	-0.025
								0.937
								0.937
								0.000

MAX DIFF	0.029
ST DEV	0.016

UO2 rod

Water rod

Pyrex rod

Vicor rod

Al2O3 rod

Figure A-31: Pin Powers Comparison for Loading 6

MEAS	0.000	1.025	0.943	0.969	1.008	1.062	1.043	1.019
CALC	0.000	1.027	0.948	0.965	1.008	1.044	1.050	1.030
DIFF	0.000	0.002	0.005	-0.004	0.000	-0.018	0.007	0.011
		0.924	0.847	0.949	1.001	1.106	1.072	1.031
		0.958	0.877	0.949	1.022	1.095	1.062	1.033
		0.034	0.030	0.000	0.021	-0.011	-0.010	0.002
			0.000	0.908	1.048	0.000	1.117	1.043
			0.000	0.891	1.042	0.000	1.098	1.037
			0.000	-0.017	-0.006	0.000	-0.019	-0.006
				0.906	0.916	1.041	1.025	1.006
				0.912	0.915	1.034	1.039	1.022
				0.006	-0.001	-0.007	0.014	0.016
					0.000	0.925	0.993	1.006
					0.000	0.913	0.995	1.009
					0.000	-0.012	0.002	0.003
						0.982	1.011	1.019
						0.959	0.996	1.006
						-0.023	-0.015	-0.013
							1.016	0.996
							1.005	1.008
							-0.011	0.012
								0.986
								1.008
								0.022

MAX DIFF	0.034
ST DEV	0.014

UO2 rod

Water rod

Pyrex rod

Vicor rod

Al2O3 rod

Figure A-32: Pin Powers Comparison for Loading 7

MEAS	0.000	1.142	1.066	1.024	0.997	0.965	0.965	0.977
CALC	0.000	1.160	1.091	1.029	0.986	0.949	0.961	0.966
DIFF	0.000	0.018	0.025	0.005	-0.011	-0.016	-0.004	-0.011
		1.113	1.107	1.021	0.950	0.884	0.957	0.977
		1.127	1.136	1.047	0.958	0.887	0.936	0.953
		0.014	0.029	0.026	0.008	0.003	-0.021	-0.024
			0.000	1.088	0.913	0.000	0.901	0.956
			0.000	1.084	0.928	0.000	0.882	0.956
			0.000	-0.004	0.015	0.000	-0.019	0.000
				1.065	1.046	0.928	0.947	0.960
				1.056	1.043	0.934	0.962	0.976
				-0.009	-0.003	0.006	0.015	0.016
					0.000	1.068	1.000	1.006
					0.000	1.074	1.007	0.998
					0.000	0.006	0.007	-0.008
						1.061	1.026	1.038
						1.042	1.025	1.008
						-0.019	-0.001	-0.030
							1.004	1.031
							1.015	1.010
							0.011	-0.021
								1.014
								1.009
								-0.005

MAX DIFF	0.029
ST DEV	0.016

UO2 rod

Water rod

Pyrex rod

Vicor rod

Al2O3 rod

Figure A-33: Pin Powers Comparison for Loading 8

Figure A-34: Pin Powers Comparison for Loading 9

MEAS	0.000	1.107	1.003	1.016	1.011	1.011	1.058	1.072
CALC	0.000	1.123	1.015	1.008	1.008	1.009	1.045	1.075
DIFF	0.000	0.016	0.012	-0.008	-0.003	-0.002	-0.013	0.003
		1.013	0.901	0.961	0.958	0.931	1.036	1.070
		1.036	0.936	0.971	0.974	0.938	1.016	1.068
		0.023	0.035	0.010	0.016	0.007	-0.020	-0.002
			0.000	0.882	0.900	0.000	0.954	1.056
			0.000	0.899	0.903	0.000	0.955	1.056
			0.000	0.017	0.003	0.000	0.001	0.000
				0.932	0.968	0.925	0.993	1.055
				0.950	0.955	0.923	1.003	1.063
				0.018	-0.013	-0.002	0.010	0.008
					0.956	0.960	1.018	1.082
					0.961	0.920	1.009	1.070
					0.005	-0.040	-0.009	-0.012
						0.000	0.996	1.096
						0.000	0.972	1.072
						0.000	-0.024	-0.024
							1.045	1.094
							1.048	1.098
							0.003	0.004
								1.105
								1.119
								0.014

MAX DIFF	0.035
ST DEV	0.015

UO2 rod

Water rod

Pyrex rod

Vicor rod

Al2O3 rod

Figure A-46: Pin Powers Comparison for Loading 11

The average bias on pin powers was less than 1%, with maximums in the low 3 – 4% range, without considering the uncertainties listed in Tables 4 through 12 in References 2 and 3. When those uncertainties are taken into account, an even better agreement is obtained.

A.4.2 UO_2–Gd_2O_3 Experiments from the Urania-Gadolinia Critical Benchmark Program

As discussed previously in Section 2.1.1.2, a total of 23 cores were assembled in the Urania-Gadolinia Critical Experiment Benchmark Program. In 22 of the 23 cores,

UO_2-Gd_2O_3, B_4C rods, void tubes and water holes were spaced on selected patterns in an otherwise uniform clean lattice in order to study their effect on reactivity, power distribution and incore detector signal. Seventeen of the cores (15x15 B&W type lattice) were used in the computational analysis with ***CASMO-5/SIMULATE-3.*** The configurations of these cores are summarized in Table 2-2. The measured pin power distributions for Cores 1, 5, 12 and 14 were compared to the ***CASMO-5/SIMULATE-3*** pin power reconstruction calculations

A.4.2.1 Computational Model

Cross-sections and discontinuity factors for fifteen interior zone fuel lattice types (segments), one exterior zone lattice and one reflector configuration were computed with ***CASMO-5***. These cases are shown in Table 2-5.

A.4.2.2 Eigenvalue Comparisons

A.4.2.2.1 Uncertainties in the Critical Eigenvalue Calculation

Reference 4 indicates that the soluble boron given in Table 2-6 of this report is that for critical (k=1.0) when the moderator height is at 145 cm and the temperature is at 77 °F. Uncertainty in moderator boron was reported to be on average ± 1 ppm for the Urania-Gadolinia experiments. Based on this and the uncertainty in the physical parameters of the 2.46 wt % enriched fuel rods such as density and enrichment, an evaluation was made of experimental uncertainties on the critical eigenvalues. Also the impact of modeling fewer rods due to core periphery and use of axial buckling on critical eigenvalue was made. Table 2-6 summarizes the evaluation of experimental uncertainties in the calculation of the critical eigenvalue by the various uncertainties in physical parameters and idealizations (axial buckling and core geometry approximation) made in modeling of the experimental cores.

The principal physical parameters which introduce uncertainty are the fuel density, fuel enrichment temperature and boron concentration. The standard deviation on the critical eigenvalue for these physical parameters is ± 0.00070. This implies the benchmark critical eigenvalues are 1.00000 ± 0.00070 (0.99930 to 1.00070). Note the ***SIMULATE-3*** Core 1 eigenvalue is within this range.

The bias introduced by the model approximation in the core periphery and the resultant 11 fewer rods than the actual loading was found to be 0.00008 Δk. This is small but should be added to the results of Table 2-7. The uncertainty introduced by assuming an axial buckling was found to be 0.00114 Δk. Note that Reference 4 does not give a measured axial buckling. The axial buckling assumed in these evaluations is inferred from earlier measurements given in References 2 and 3.

Figure A-36: Estimated Uncertainties in the Critical Eigenvalue Calculation

	Parameter	Uncertainty/bias	Average	High	ΔK
1	Fuel Density	± 0.04 g/cc	10.24	10.28	
			0.99939	1.00006	+0.00067
2	Fuel Enrichment	± 0.002 wt %	2.459	2.461	
			0.99939	0.99952	+0.00013
3	Temperature	± 1 F	77	78	
			0.99939	0.99940	+0.00001
4	Buckling Bias	± 0.00031 cm^{-2}	$4.41x10^{-4}$	$4.1x10^{-4a}$	
			0.99939	1.00053	+0.00114
5	Boron Conc.	± 1 ppm	1138	1139	
			0.99939	0.99923	-0.00016
6	Modeling Bias	-11 rods	1925	1936	
			0.99939	0.99947[b]	+0.00008

Notes: [a] Studsvik recommended value based on 150 cm active fuel zone.
[b] Computed from eigenvalue due to the addition of one quadrant of 52 fuel rods scaled down to 11 additional rods

A.4.2.2.2 Calculated Versus Measured Critical Eigenvalues

The Urania-Gadolinia core eigenvalues are summarized in Table 2-7. The average k_{eff} is 0.99811 ± 0.00056. These eigenvalues are consistent, i.e. no apparent trends, over the range of experimental variables.

A.4.2.3 Pin Power Comparisons

Comparisons of calculated to measured central assembly pin powers are shown in Figure A-48 through Figure A-51.

Figure A-48: Core 1 Central Assembly Pin Powers Calculated to Measured

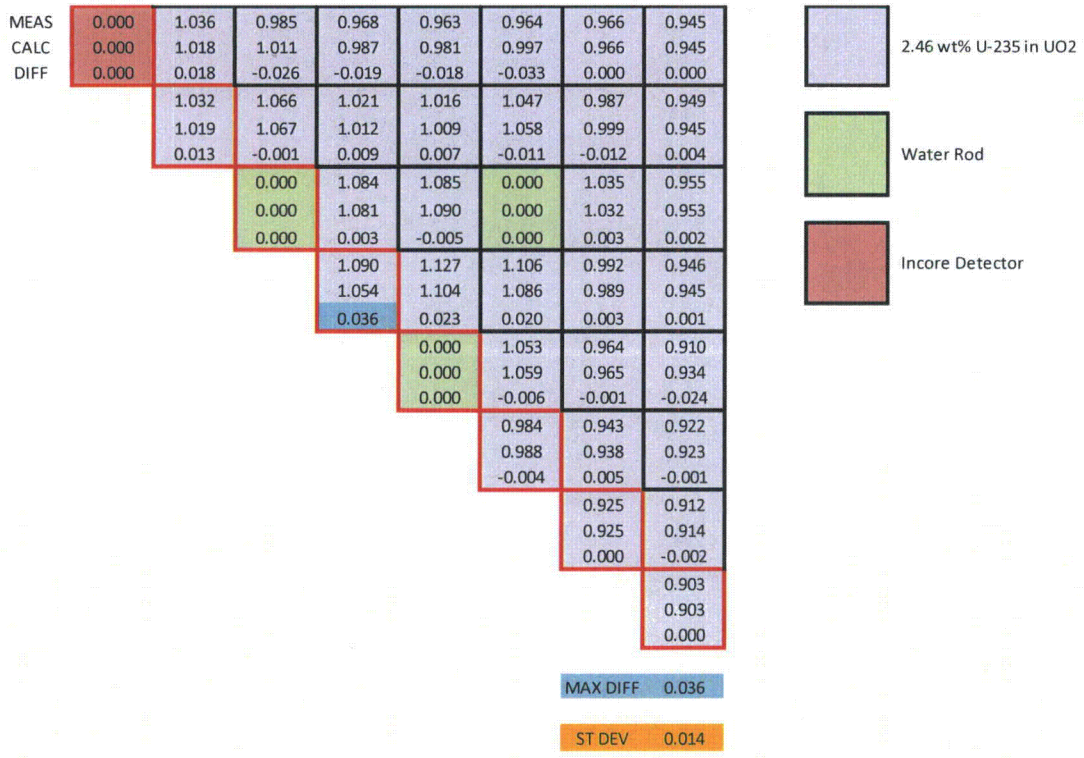

Figure A-38: Core 5 Central Assembly Pin Powers Calculated to Measured

Figure A-39: Core 12 Central Assembly Pin Powers Calculated to Measured

Figure A-51: Core 14 Central Assembly Pin Powers Calculated to Measured

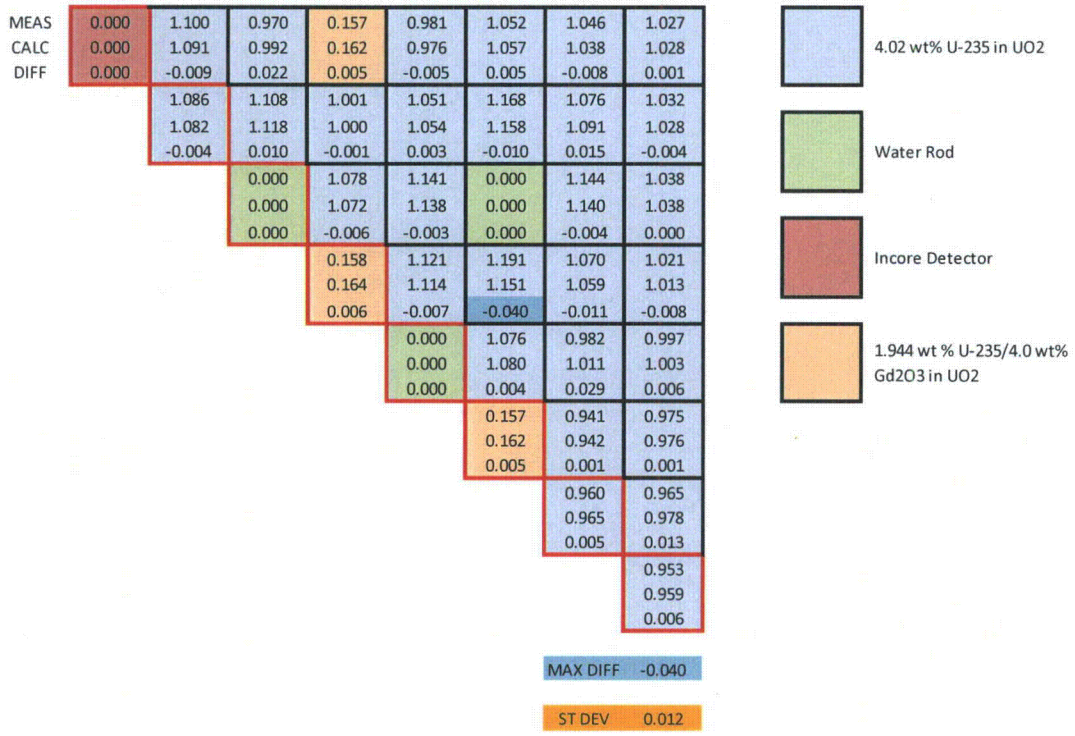

A.4.3 UO_2–PuO_2 Critical Experiments from the Plutonium Recycle Critical Facility

Six mixed oxide (UO_2-PuO_2) core configurations were selected from the Critical Experiment Benchmarks for the Plutonium Recycle Program and were analyzed to provide rods-in and rods-out local power distribution data that simulated an extreme core burnup condition. The six cases encompass three different lattice pitches providing simulated under-moderated, near optimum moderation, and over-moderated configurations. For each type of lattice, two experiments were conducted, one with unborated water and one with borated water as moderator. Table 2-8, above, summarizes the general characteristics of the critical experiments evaluated with ***CASMO-5.***

A.4.3.1 Computational Model

Details of the computational model were presented previously in section 2.4.3.1

A.4.3.2 Eigenvalue/k-infinite Comparisons

Since the calculations were performed employing only ***CASMO-5***, the k-infinite for each model was compared to the eigenvalues computed from the fully reflected excess reactivity and effective β values listed in Reference 5 for each experiment.

A.4.3.2.1 Uncertainties in the k-infinite Calculation

The fuel pin modeling-induced uncertainties, the plutonium isotopic composition and concentration uncertainties, boron concentration uncertainties, buckling uncertainties, and overall uncertainties in the eigenvalue calculations for the UO_2-PuO_2 (2%) critical experiments were discussed in detail in Subsection 2.4.3.2.1 of the main body of this Topical Report. It was concluded that a bias of ± 0.0029 Δk should account for all uncertainties identified in Table 2-9, of Subsection 2.4.3.2.1.

A.4.3.2.2 Calculated Versus Measured Multiplication Factors

Table 2-10 in subsection 2.4.3.2.1 summarizes the k-infinite calculated with ***CASMO-5*** for all 6 experimental configurations presented in Table 2-8. Comparisons are presented between three data sets: 1) ***CASMO-5***, 2) k-effective calculated from the experimental data in Reference 5 (fully reflected excess reactivity, in cents, listed for each experiment, and β-effective, listed as 3.45×10^{-3} for all MOX cores) and 3) MCNP-5 values (based on three-dimensional models that include additional axial details).

Overall, the ***CASMO-5*** calculated k-infinite was in very good agreement with both ***MCNP*** k_{eff} and the k_{eff} inferred from experimental data (excess reactivity and β-effective). For all but one computer run, the eigenvalue differences were well within the estimated uncertainties. The highest bias was recorded for CORE-3, which is consistent with other recent publications (R. D. Mosteller).

A.4.3.2.3 Pin Power Comparisons

The pin powers are insensitive to the benchmark assumptions that affect k_{eff}. The pin powers comparisons from the ***CASMO-5*** calculations and experimentally measured data are presented in Figure A-52 through Figure A-57. Data from Reference 5 was used for comparison for all the loadings, including the uncertainties listed in Reference 5. Measured values listed in the figures below are nominal, i.e. they do not include the measurement uncertainties. All experimentally measured data, presented above, was properly renormalized to quarter-core lattice, consistent with Studsvik methodology, for a correct comparison. Measurement uncertainties are included in the comparisons.

Figure A-52: Pin Powers Comparison for CORE-1

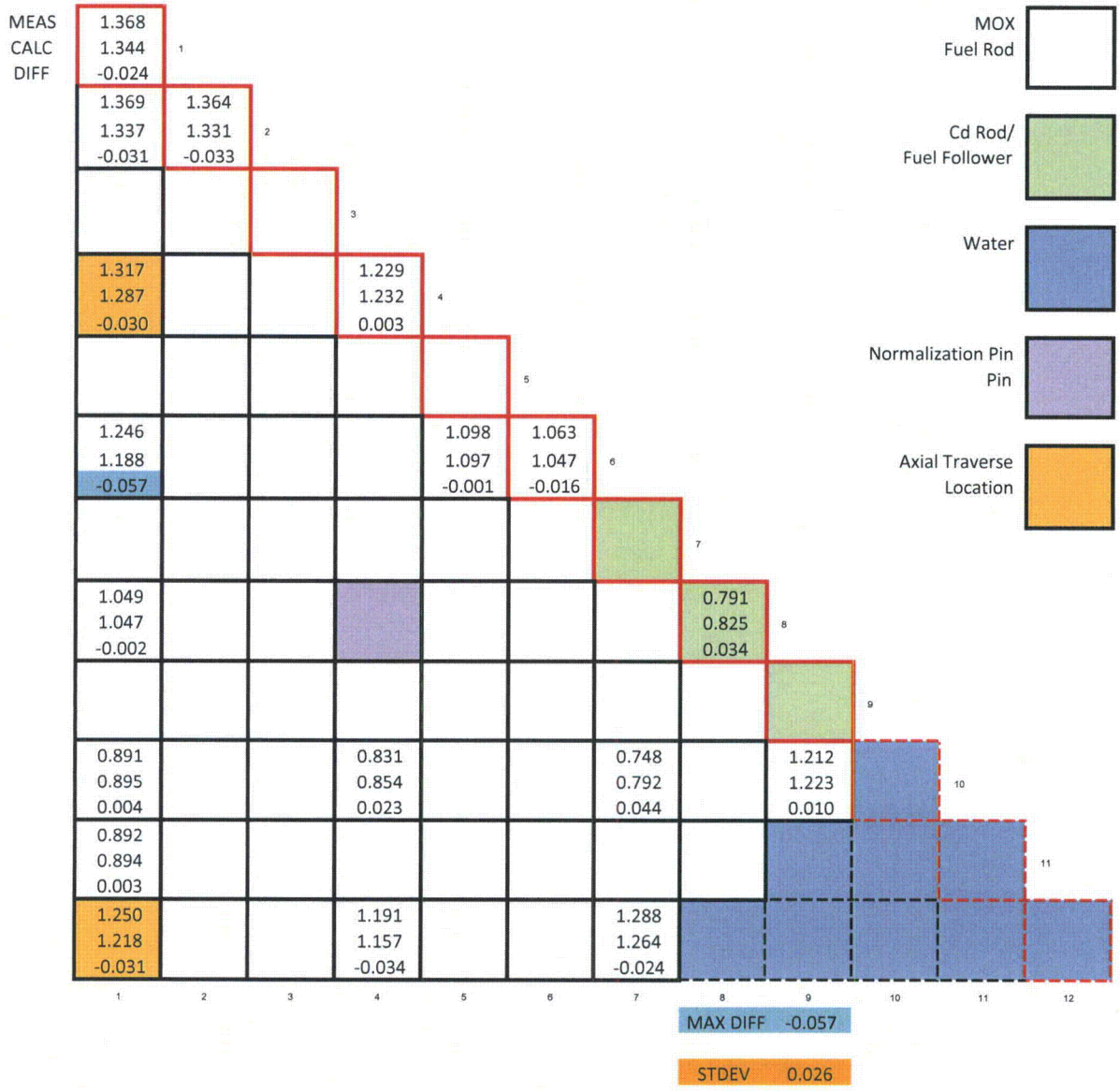

Figure A-42: Pin Powers Comparison for CORE-2

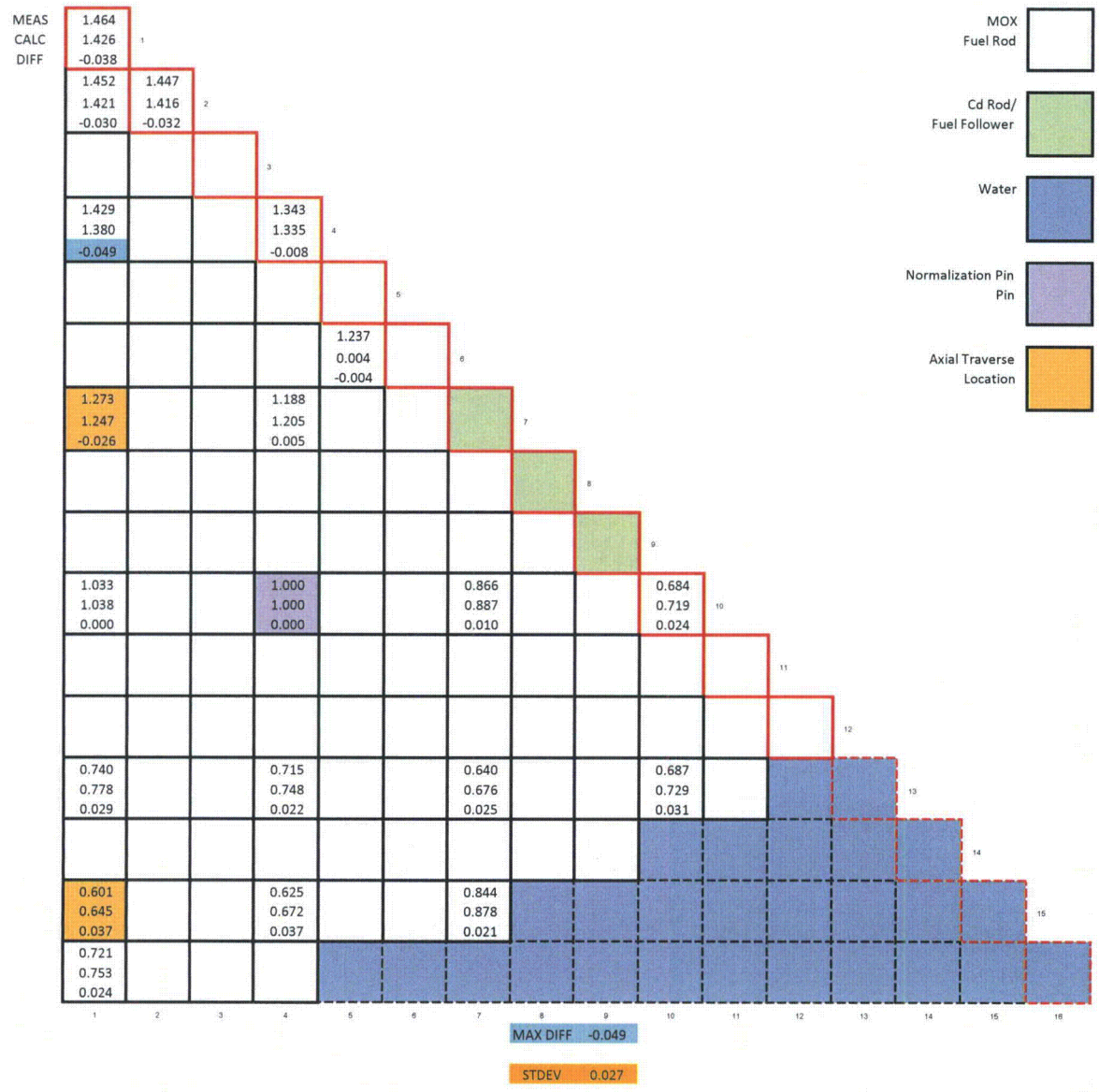

Figure A-43: Pin Powers Comparison for CORE-3

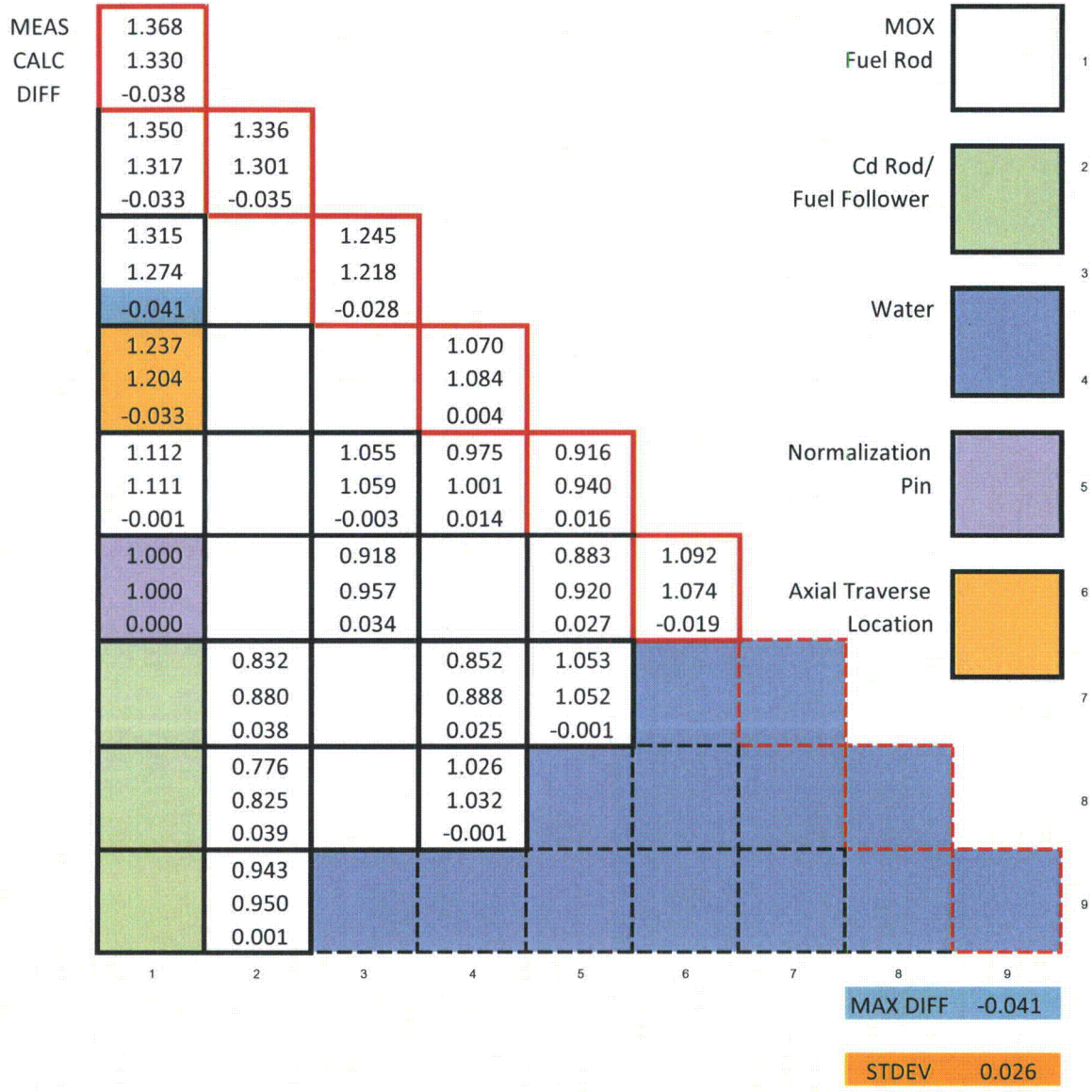

Figure A-44: Pin Powers Comparison for CORE-4

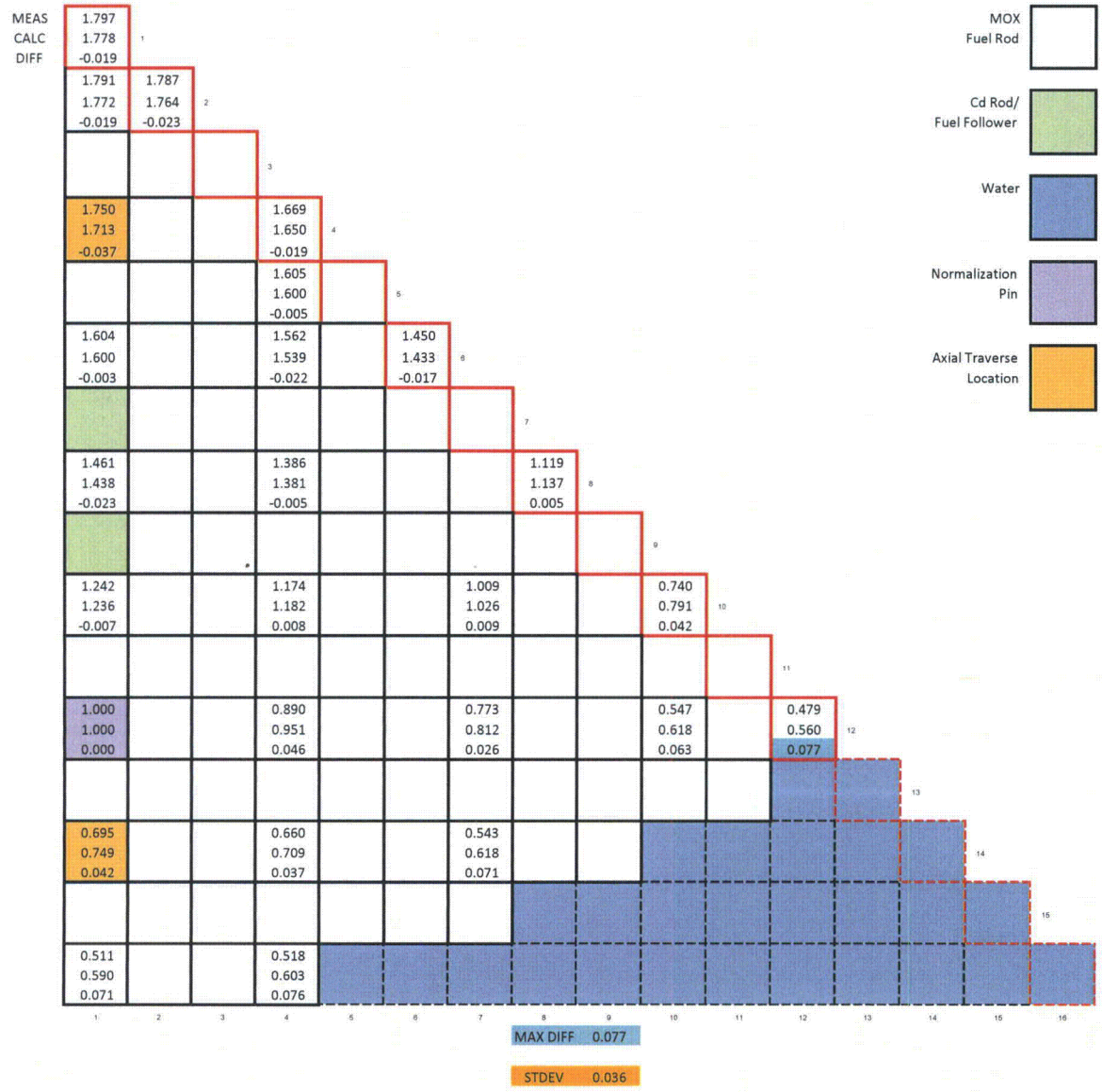

Figure A-45: Pin Powers Comparison for CORE-5

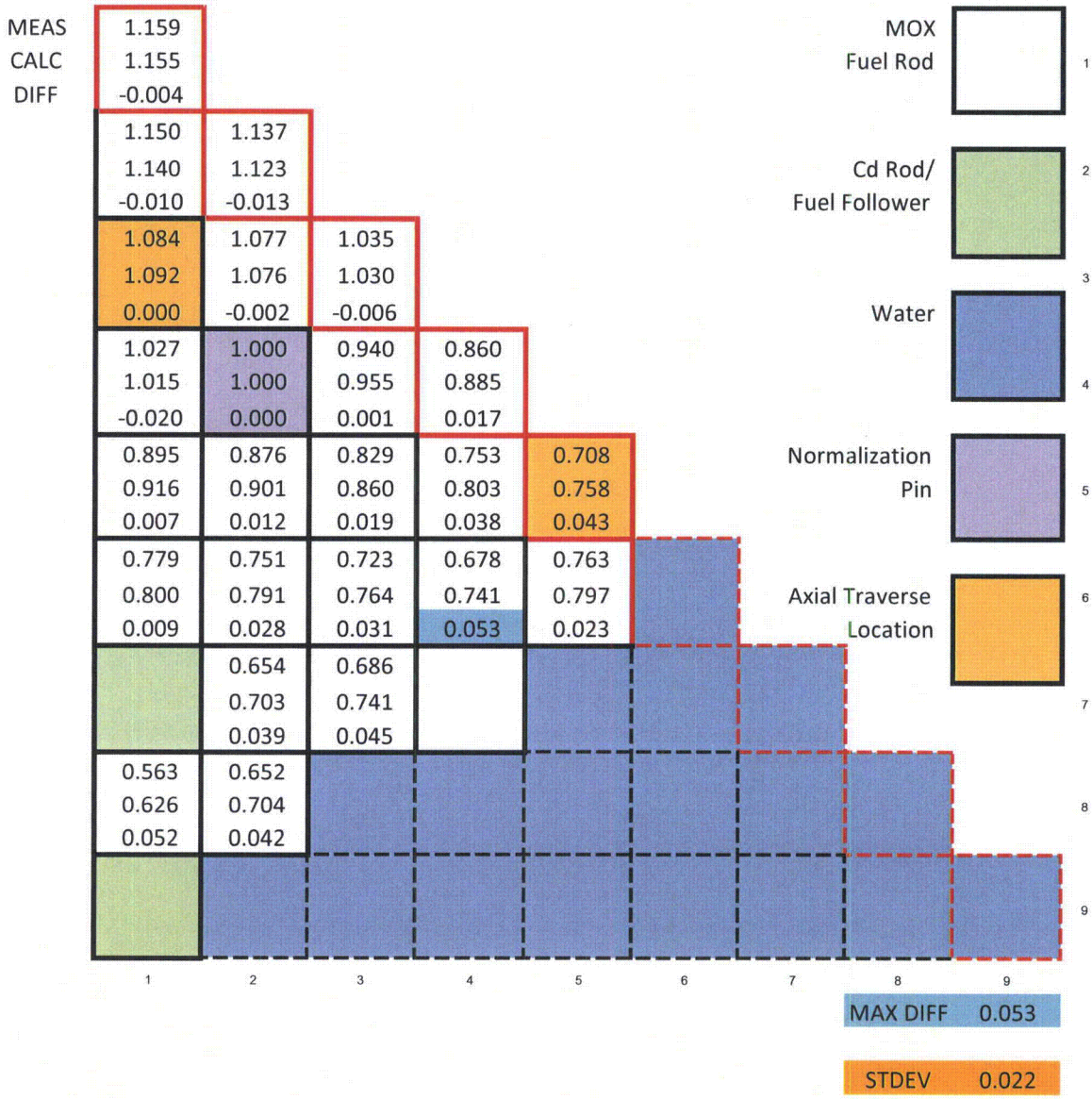

Figure A-57: Pin Powers Comparison for CORE-6

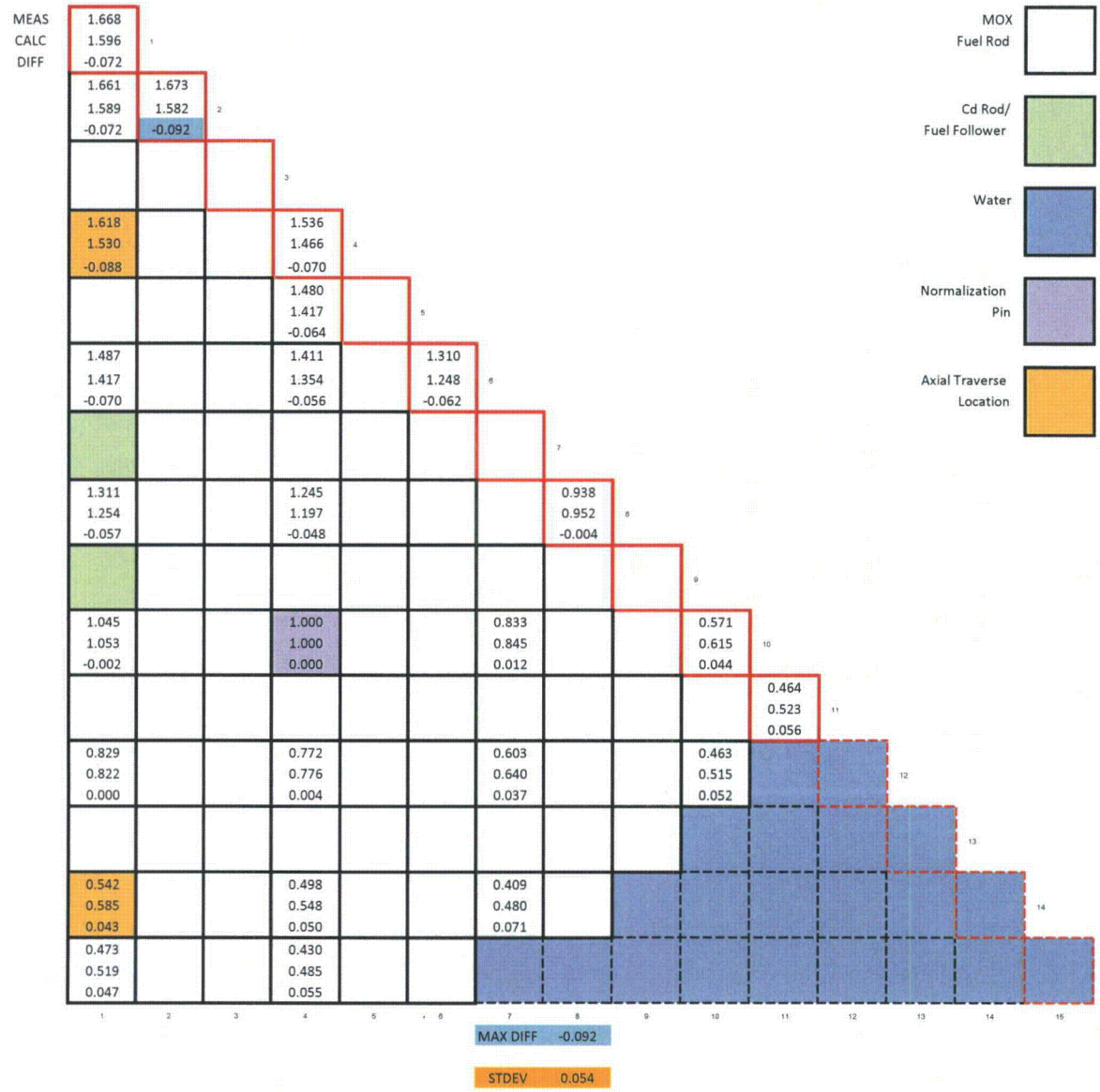

Appendix B TMI Measured Data Analysis

B.1 General Description

The analytical performance of ***CASMO-5/SIMULATE-3*** in the prediction of assembly power distribution for TMI-1 Cycles 1 and 2 was determined by comparison of "measured" assembly power to calculated assembly power. However, the measured assembly power was inferred from fixed incore Rhodium SPND signals that correspond to the neutron flux at the SPND location. These signals were converted to measured power by multiplying by power to signal ratios determined by analytical techniques, i.e., ***CASMO-5/SIMULATE-3***. The measured powers at the fixed SPND locations were processed to compute assembly power. The details of these computations are given in subsequent paragraphs. The approach outlined in this report is implemented using ***EXCEL*** software. It can also be used in future core follow benchmarking of the B&W mPower reactor.

The axial measured power shapes and radial power distributions were analyzed using an ***EXCEL*** spreadsheet that mimics in a simplified way the processing performed by a nuclear application system used in operating reactors. It was possible to develop this ***EXCEL*** spreadsheet because the measured signals from TMI-1 Cycles 1 and 2, reported in the Reference 1 were already corrected for the following effects:

1) instrument-independent Rhodium signal from SPND
2) detector leakage
3) detector depletion

Since analysis of the core follow of the TMI-1 Cycles 1 & 2 were made in one-eighth core symmetry it was necessary to adjust the signals to correct for quarter core power tilt. Simplified correction factors calculated from the 16 symmetric ICDAs were used compared to what is typically used in commercial nuclear application software. A small number of suspect SPNDs signals were corrected using substitution from their equivalent symmetric signals.

A signal to power conversion factor for each SPND location in the core was calculated using the ***CASMO-5/SIMULATE-3*** computer package. The Rhodium SPNDs were explicitly modeled in the three-dimensional TMI-1 calculation. The reaction rate resulting from the thermal flux absorption in the Rhodium SPNDs was directly proportional to the measured nano-amp signal obtained from the incore system in the plant.

B.2 Core/Model Description

The signal data reported in Reference 1 were given in nano-amps at seven axial SPND locations for each of the fifty-two assemblies (of 177) containing ICDAs. These data were provided at a number of state points in both Cycles 1 and 2. Figure B-47 presents the layout of the core, indicating ICDA locations. This arrangement allows for an eighth-core representation to be constructed, providing enough data to predict the behavior of the whole core.

Figure B-47: Core Cross-Section with Highlighted ICDAs

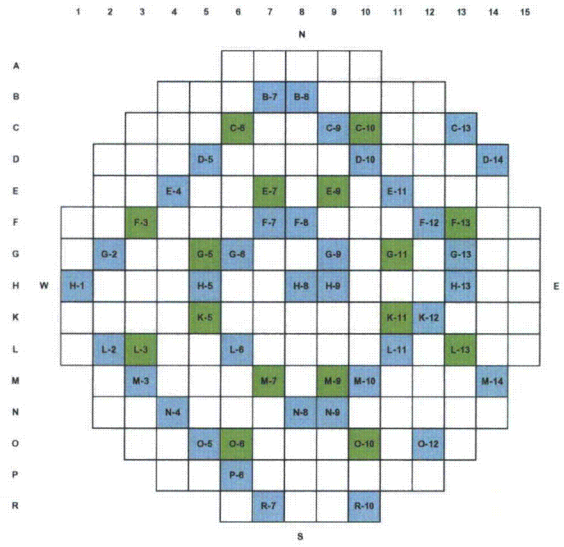

A detailed core follow ***SIMULATE-3*** calculation was performed for both cycles. The output files were post-processed for the calculated signals and corresponding nodal powers. Figure B-48 provides a representation of how each assembly was axially divided into twenty-one nodes to eliminate nodal weighting as each SPND (4.75 inches in length) would

be fully encompassed by a single node. The seven SPNDs in each ICDA were located 10.29, 30.86, 51.42, 72.00, 92.57, 113.14, and 133.71 inches from the bottom, corresponding to the 2nd, 5th, 8th, 11th, 14th, 17th, and 20th nodes, respectively.

Figure B-48: SPND/Nodal Representation

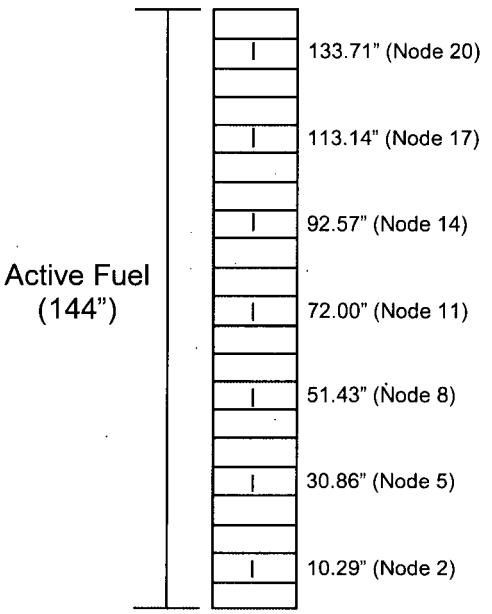

B.3 Processing SPND Signals and SIMULATE Core Follow Data

The following output data from ***SIMULATE-3*** were input into the ***EXCEL*** spread sheets: a) control rod withdrawal data, b) seven (7) axial positions of simulated signal data represented by SPND reaction rates, and c) nodal powers data. The equivalent measured data to ***CASMO-5/SIMULATE-3*** from Reference 1 were also input to the ***EXCEL*** spreadsheets. Figure B-49 shows the flow of data processing with measured data coming from Reference 1 and calculated data coming from ***CASMO-5/SIMULATE-3***.

Once all of the data was input into the ***EXCEL*** files, the subsequent calculations were automatically performed. The data was organized into a one-eighth core configuration by "folding" the data for the assemblies throughout the core into a set representative of the 29 assemblies comprising one-eighth of the core. In Figure B-50, the inner and outer symmetrical rings (consisting of 8 ICDAs each) where the average reading of all 8 SPNDs is used are highlighted in green. The locations where the average of two symmetrical SPNDs at a given elevation from different parts of the core was used for the assembly reading are highlighted in teal. Additionally, the data were corrected for tilt (see section B-6.1, "Simplified Tilt Correction") and the total core-average power was calculated based on the weighting of each assembly represented (see section B-6.2, "Full Core Weighting", below).

Figure B-49: EXCEL Processing Flowchart

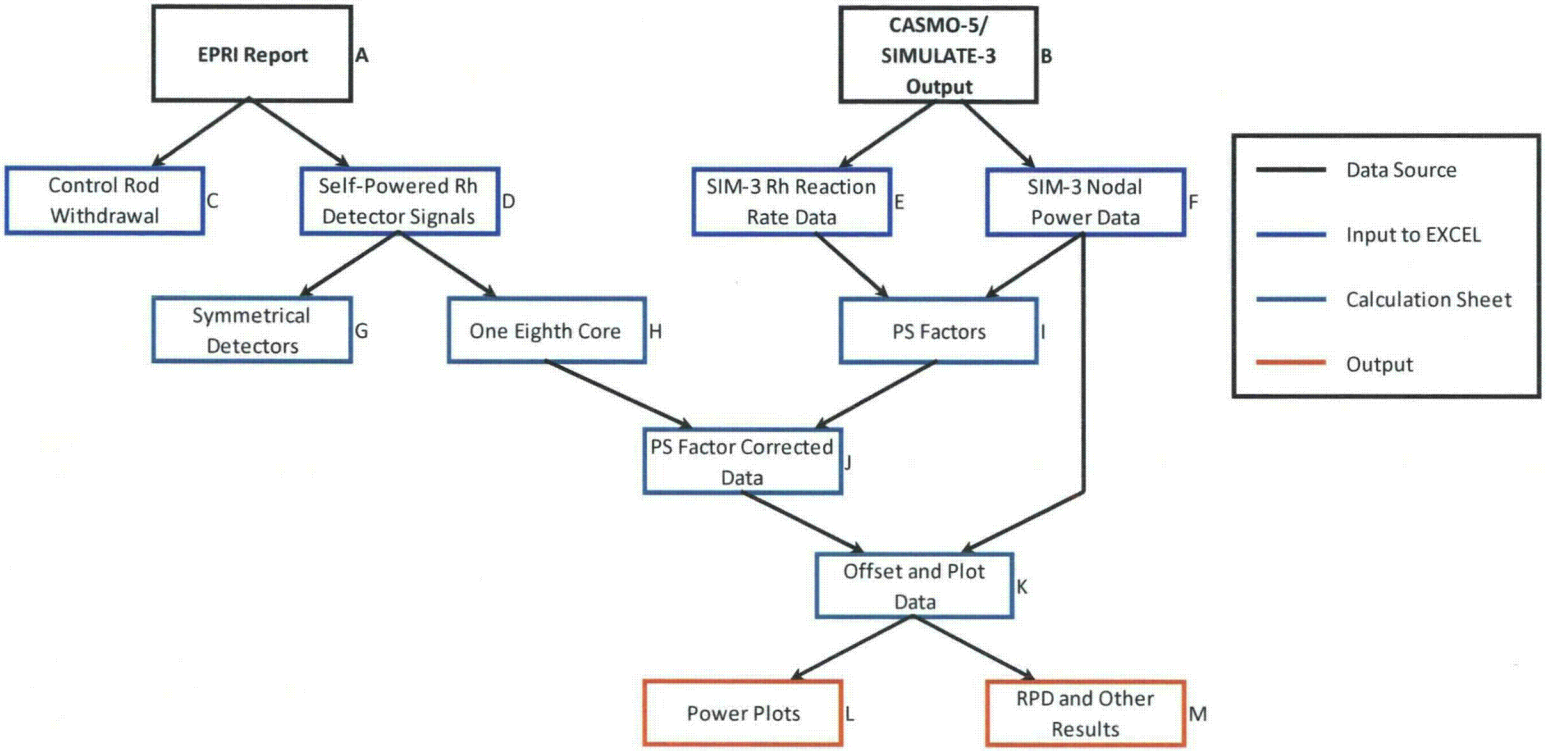

Figure B-50: One-Eighth Core Representation

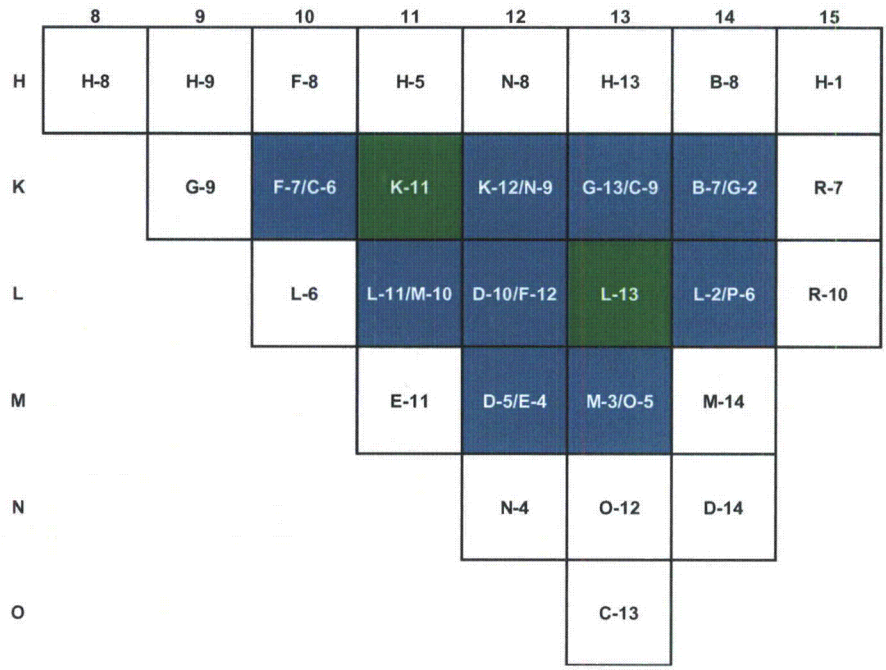

B.4 Formulation of the Signal-to-Power Ratios

To convert the measured signals to measured powers, a signal-to-power ratio can be determined from the calculated power density in the node and calculated signals, which are proportional to the reaction rates within the rhodium. The equation below demonstrates the calculation of this simple factor, which is the basis of the power conversion.

$$\left(\frac{Power_{calculated}}{Reaction\ Rate_{calculated}}\right)$$

B.5 Processing the Normalized SPND Signals into Measured Powers

B.5.1 Multiplication of Normalized Signals and Signal-to-Power Ratios

The normalized measured signal data were then multiplied by the calculated signal-to-power ratios. Since the multiplication of the signal data by the signal-to-power factor does not guarantee the normality of the resulting powers, the assembly

powers were renormalized post-power conversion using a full core weighted normalization factor,

$$P_{m\,i,j,k} = S_{m\,i,j,k} \times \left(\frac{P_c}{S_c}\right)_{i,j,k}$$

where

P_m = measured Power
S_m = measured Signal
P_c = Calculated Power
S_c = Calculated Signal (equal reaction rate)

B.5.2 Axial Power Integration of the Measured Powers with Spline Interpolation

The seven data points were then expanded to 21 points using a normal cubic spline function (in ***EXCEL*** through the XIXtrFun add-in), using -3 and 147 inches as the zero points. The shapes between 0 inches and 144 inches represent the axial power distribution; the integration of the axial power shapes provide the measured radial power distribution, similar to that calculated by ***SIMULATE-3***. The core axial offset was also calculated (discussed in greater detail in section B-6.3, "Core Offset", below).

B.6 Supporting Calculation Methods

The following sections provide more detailed descriptions of some methods used that, to this point, have only been described briefly above.

B.6.1 Simplified Tilt Correction

Radially, the results from ***CASMO-5/SIMULATE-3*** represent a fully eighth-core symmetric design. There are no factors that might lead to core tilt in the simulated model as the control rod heights are input as the average of the rods in each bank (from Reference 1). However, due to the actual variation of control rod height within each bank, there is a slight tilt in the real core, as can be seen through the data from the symmetrical ICDAs (highlighted in green in Figure B-50). When the

data from the SPNDs is organized into an eight core configuration, the tilt in the system may be an additional source of error and needs to be taken into account.

To correct for the tilt, the data from the four symmetrical ICDAs in each quadrant were averaged by plane and normalized based on the planar average of the data from all of the symmetrical ICDAs:

$$Tilt\ Factor_{i,j} = \frac{\sum_{i,j} avg.symm.det.signal\ in\ quad.\ i, plane\ j}{\sum_{i=1,j}^{i=4,j} avg.symm.det.signal\ in\ quad.\ i, plane\ j}$$

The data in each SPND were then divided by the corresponding tilt factor. For those SPNDs lying on the boundary of multiple quadrants, the average of the tilt factors affecting the SPND were used. This correction technique essentially operates under the assumption that the tilt is zero at the center of the core (tilt factor = 1 at center). Since the tilt is typically less than a few percent, the tilt correction does not have a strong impact on the data, though it is necessary to ensure the integrity of the comparison.

B.6.2 Full Core Weighting

Figure B-50 is an illustration of how the full core data is folded into an eighth core configuration. If a full core average is to be calculated from this, data from the assemblies needs to be weighted according to how many assemblies are represented by each eighth-core assembly if expanded into a full core configuration. For example, in the unfolding process, the center assembly (H-8) would only represent itself and only needs to be multiplied by a factor of one. However, the assemblies on the top edge (H-9 though H-15) and the diagonal (K-9, L-10, M-11, N-12, and O-13) would be seen four times in the full core and have a weighting of four. All of the other assemblies represent eight assemblies in the full core and need to be multiplied by eight. Using this technique, the appropriate normalization routines

can be executed versus simply taking the average of the data without the necessary weighting.

B.6.3 Core Offset

The calculation of the core offset for the measured and calculated cases were determined using the following equation:

$$Offset = \frac{Power_{top} - Power_{bottom}}{Power_{total}}$$

Since the data was expanded to twenty-one points in both cases, the offset was calculated as the summation of the top ten points plus half of the middle point minus the summation of the bottom ten points plus half of the middle point divided by the summation of all of the points, ensuring the weight for full core representation.

B.6.4 Radial Power Distribution

The normalized, power-converted, tilt-corrected data represent the power density data for each assembly. These seven points were fit using a cubic spline function within ***EXCEL***, thereby expanding from seven measured points to twenty-one points, corresponding to the number of nodal data points generated by ***SIMULATE-3*** for an equivalent graphical and analytical comparison of the data. Since the data was expanded to the same number of points represented by the twenty-one nodes, essentially a nodal configuration was set up for the measured data where the sum of all the nodes could be taken as the integral of the data, as is done in ***SIMULATE-3*** for the calculated data. Once the integration value was divided by the number of data points (twenty-one) and the average of the integration values (weighted for full core), the normalized measured radial power density (measured RPD) is determined.

The calculated radial power density (calculated RPD) distribution from ***CASMO-5/SIMULATE-3*** can be obtained straight from the output in the 2RPF output or by averaging the nodal data for each assembly from the 3RPF output.

B.7 Symmetrical ICDA Rings

An ***EXCEL*** worksheet containing detailed data for the two rings of symmetrical ICDAs (eight ICDAs each), as discussed in the eighth core folding. The data include signal and power data normalized by planar average of the symmetrical SPNDs and plots of the normalized power to represent the variation throughout the core.

B.8 Determination of the Measured Signal Accuracy

The estimated measured signal accuracy was determined by evaluating the data collected from the inner and outer rings of symmetrical ICDAs, consisting of eight ICDAs each. This involved calculating the variation between the ICDAs and the planar average for the eight ICDAs of the inner and outer circle. A histogram was constructed using these data from 40 state points over the two operating cycles (see Figure B-51).

The standard deviation was calculated for each cycle, with a resulting value of 0.03589 for Cycle 1 and 0.03326 for Cycle 2. The combined standard deviation for both cycles was 0.03453. These values represent the errors resulting from both the core tilt (which is relatively small) and the detection accuracy.

Figure B-51: TMI-1, Cycle 1 Symmetrical SPND Difference Histogram

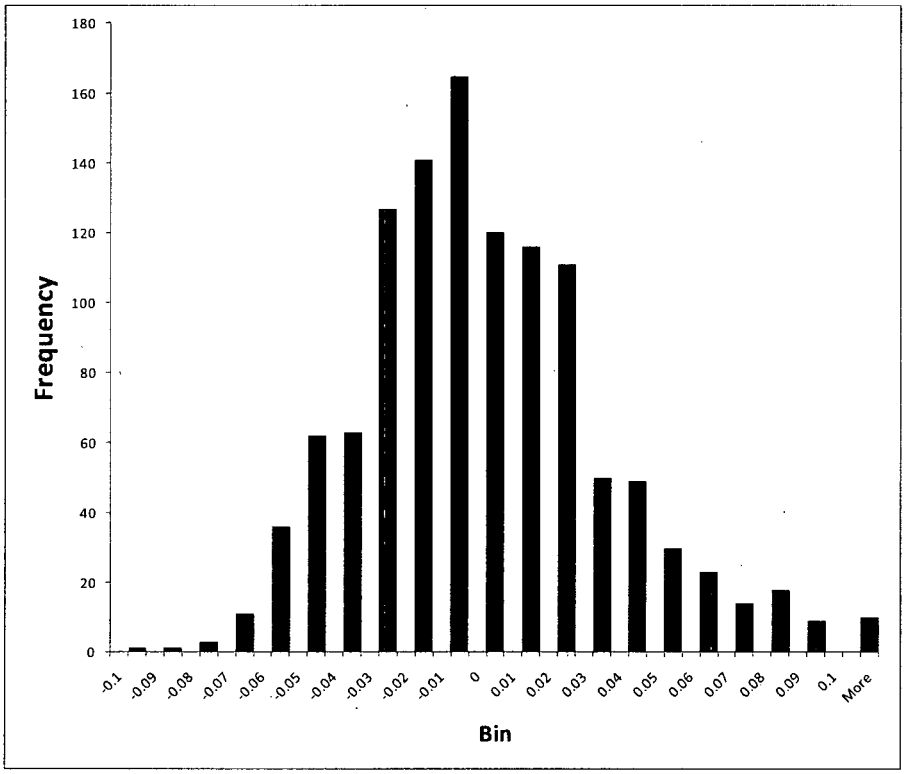

Appendix C Details of Three Mile Island Unit 1 Cycles 1 and 2 HZP Startup and Core Follow

In this Appendix, a detailed comparative analysis between the predicted and measured results from Three Mile Island Unit 1 (TMI-1) Cycles 1 and 2 hot zero power startup and core cycle operation are documented to quantify the accuracy of the ***CASMO-5/SIMULATE-3*** computational methodology. Detailed models were used to calculate: (1) Hot zero power critical boron, control rod worths, and reactivity coefficients, and (2) core follow eigenvalues, critical boron, and assembly radial and axial power distributions.

C.1 Brief Description of TMI-1 Cycles 1 and 2

As discussed previously in Section 3.0 of this Topical Report, TMI-1 is two-loop PWR with each reactor coolant loop containing a vertical once-through straight-tube-and-shell steam generator and two coolant pumps. One loop includes a pressurizer. The reactor is designed for a thermal power of 2535 MW(th) with a nominal operating pressure of 2185 psi. The reactor core consists of 177 mechanically identical fuel assemblies arranged in a pattern that approximates a right circular cylinder. Each fuel assembly consists of a 15×15 lattice containing 208 fuel rods, 16 control/safety rod guide tubes, and one instrument tube. Reactivity control authority is maintained by 61 full-length Ag-In-Cd control rod assemblies and soluble boron shim. Eight partial-length Ag-In-Cd control rods are used to control the axial power distribution.

C.1.1 Fuel Assembly Data

The TMI-1 core utilizes the B&W Mark B 15x15 fuel assembly design. Each fuel assembly lattice contains 208 fuel rods consisting of uranium dioxide pellets contained in cold-worked zircaloy-4 cladding tubes on a 0.568-inch pitch. The pellets are 0.370-inch diameter and 0.7-inch long, and the fuel cladding is 0.430-inch OD and 0.0265-inch thick. The gap between the pellet and the cladding is pressurized to approximately 350 psi initial pressure. The active fuel length is 144 inches.

There are eight spacer grids per assembly (six in the active fuel length) and the assembly-to-assembly pitch spacing is 8.587 inches. Table C-1 and Table C-2 summarize the fuel assembly design and the dimensions and materials of construction. Figure C-52 through Figure C-54 illustrate the fuel rod arrangement and axial extent.

Table C-1: Fuel Assembly Design

Parameter	Value
Lattice Array	15 x 15
Number of Fuel Rods	208
Number of Guide Tubes	16
Number of Instrument Tubes in Selected Assemblies	1
Assembly Pitch	8.587

Table C-2: Fuel Assembly Rod Dimensions and Compositions

Fuel Rod	**inch or lb/in^3**	**cm or g/cm^3**	**Radius, cm**
Pitch	0.568	1.443	
Clad OD	0.43	1.092	0.5461
Clad ID	0.377	0.958	0.4788
Material	Zirc-4		
Density	0.238	6.588	
Pellet OD	0.37	0.94	0.4699
Material	UO_2		
Stack Density			
Active Length	144	365.76	
Guide Tubes	**inch or lb/in^3**	**cm or g/cm^3**	**Radius, cm**
Material	Zirc-4		
Density	0.238	6.588	
Tube OD	0.53	1.346	0.6731
Tube ID	0.498	1.265	0.6325
Instrument Tube + Sleeve	**inch or lb/in^3**	**cm or g/cm^3**	**Radius, cm**
Tube OD	0.493	1.252	0.6261
Tube ID	0.441	1.12	0.5601
Material	Zirc-4		
Density	0.238	6.588	
Sleeve OD	0.554	1.407	0.7036
Sleeve ID	0.502	1.275	0.6375
Grid Spacer	**inch or lb/in^3**	**cm or g/cm^3**	**Radius, cm**
No. of Grids in Active	6		
Grid Mass, lbs	1.6	725.584	
Grid Material	Inconel 718		
Density, lb/in^3	0.297	8.221	
Density, gm/active length		11.9031	

1 - **Spacer Density** $\left(\frac{g}{cm}\right) = \frac{No.Grids \times mass\ per\ grid\ (lb) \times 453.59\ \frac{g}{lb}}{active\ fuel\ length\ (cm)}$

Figure C-52: 15x15 Mark B Fuel Assembly Pin Layout

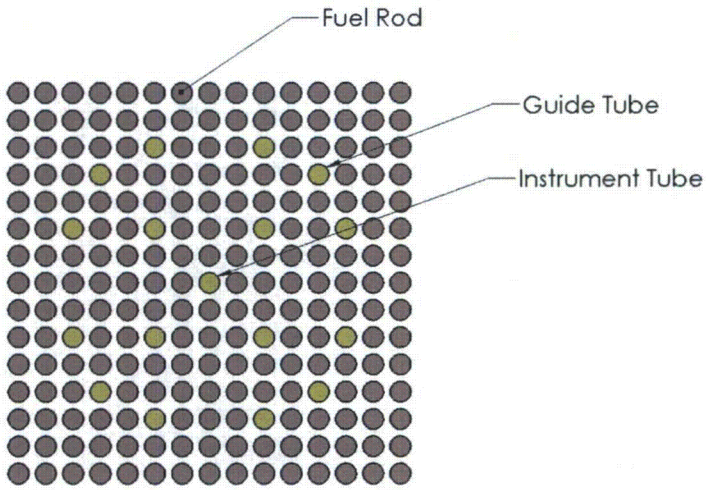

Figure C-65: Mark B Fuel Assembly Axial Extent

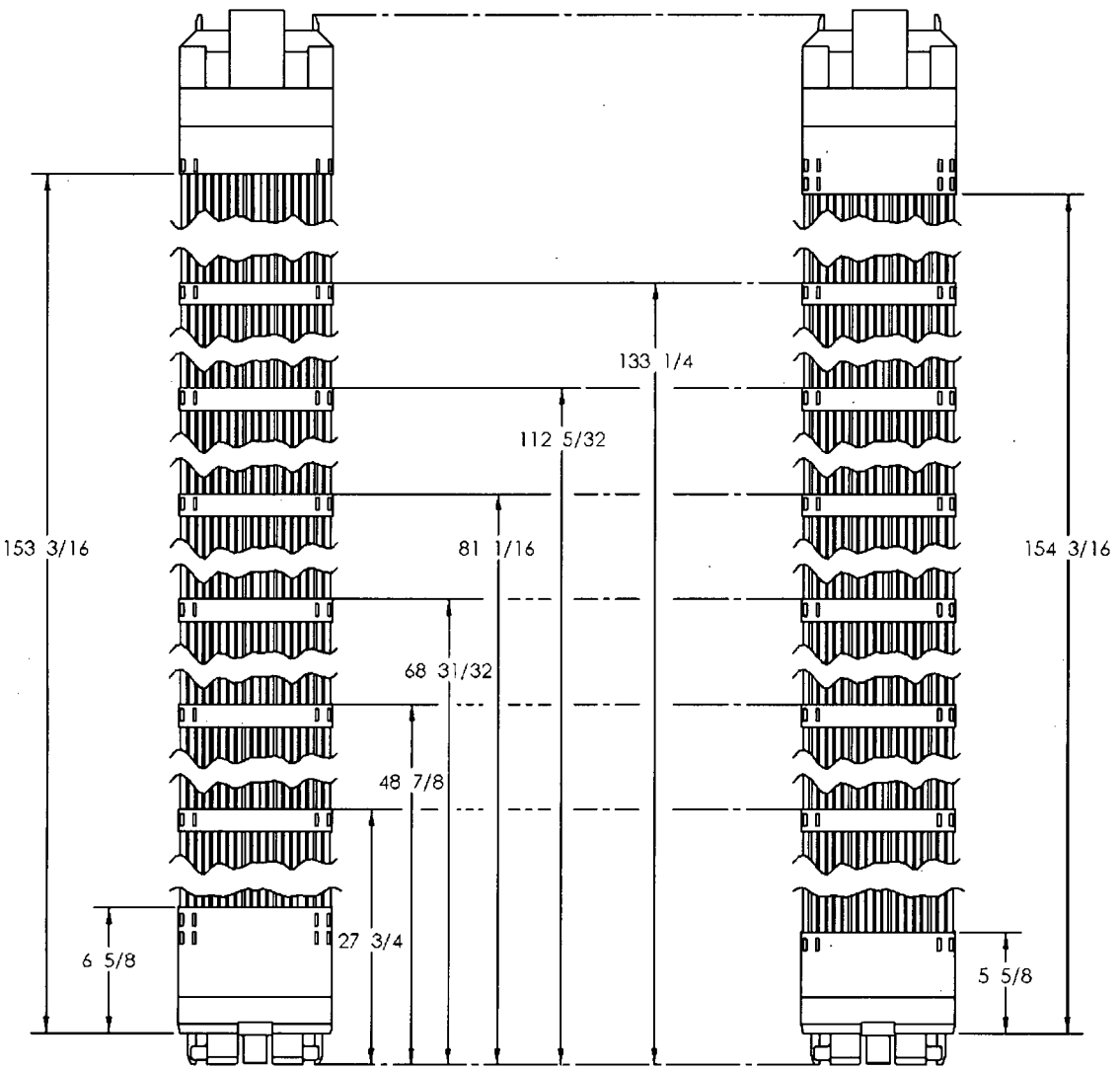

NOTE: ALL DIMENSIONS IN INCHES

Figure C-54: Relative Axial Positions of Active Assembly Components

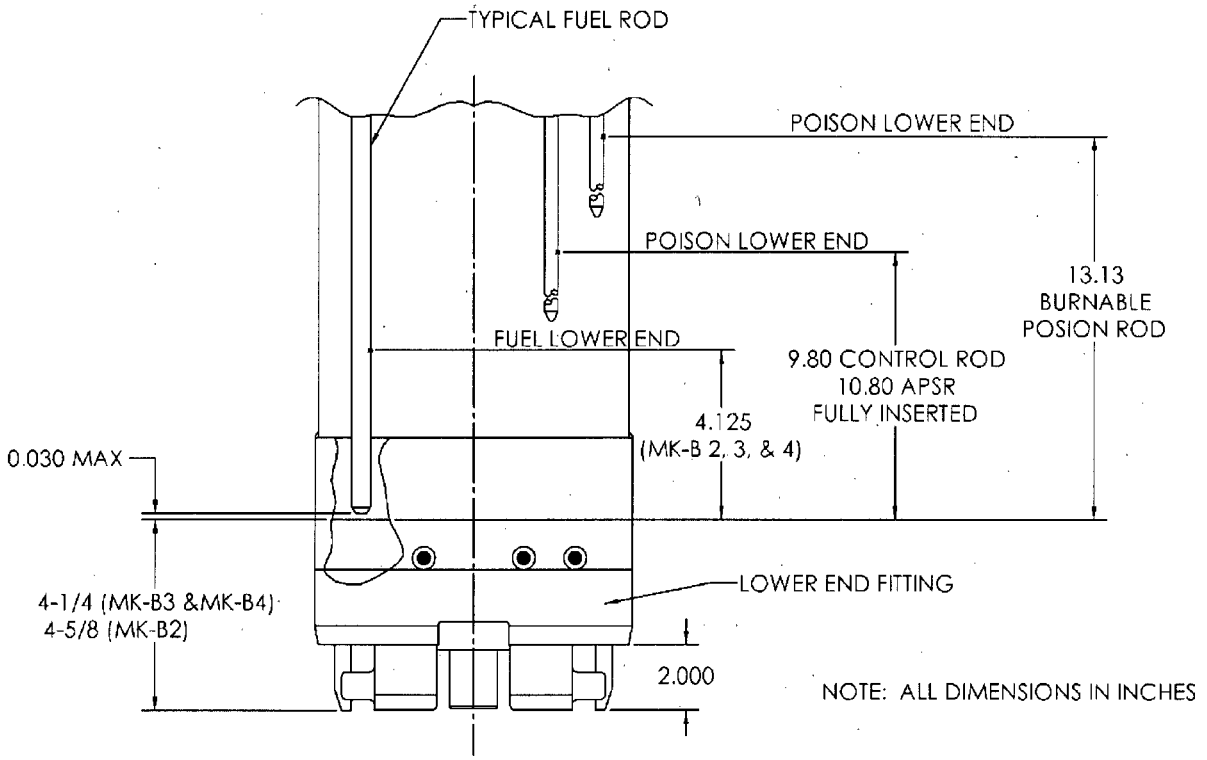

Eight different fuel assembly lattice designs (combinations of enrichments and burnable poisons) were used in the Cycles 1 and 2 loading patterns. These are summarized in Table C-3. The Cycles 1 and 2 fuel batch loadings and stack densities are summarized in Table C-4. The active fuel length is 144 inches, except for the batch 4 fuel which is 142.5 inches. The stack density for this batch is adjusted accordingly to preserve the uranium loading.

Table C-3: Cycles 1 and 2 Fuel Lattice Data

Batch	Designator	wt % 235	No. BP	wt % B4C	Cycle 1	Cycle 2[1]
1	A00	2.06	0	0	56	
2	B00	2.75	0	0	1	1
	B01	2.75	16	1.43	20	20
	B02	2.75	16	1.26	24	24
	B03	2.75	16	1.09	16	16
3	C00	3.05	0	0	52	52
	C01	3.05	16	1.26	8	8
4	D00	2.64	0	0		56

Notes: 1. Batch 2 and 3 BPs removed in Cycle 2.

Table C-4: Cycles 1 and 2 Batch Fuel Loadings and Stack Densities

Batch	U-238 (g)	U-235 (g)	Stack Density (g/cm^3)[1,2]	U Loading (MtU)
1	454723	9551	9.98	0.4643
2	451118	12742	9.9711	0.4639
3	449992	14149	9.9772	0.4641
4	451942	12248	9.9782	0.4642

Notes: 1. Stack Density (g/cm^3) = $\frac{U_{\frac{mass}{.8815\ gU/gUO2}}}{\text{number fuel rods}*\pi*\text{pellet radius(cm)}^2*\text{active length(cm)}}$

2. Stack Density based on a 144 inch (365.76 cm) active fuel length for all batches

C.1.2 Lumped Burnable Poison (LBP) Rod Data

A significant number of BP rods are utilized in the batch 2 and 3 fuel assemblies of TMI Cycle 1 for power distribution and reactivity control. The BP rod data is shown in Table C-5. The BP rods are inserted into the 16 guide tubes. Based on the BP active length and end position given in Figure C-54 the BP active zone is cut back 9 inches (22.86 cm) top and bottom in relation to the active fuel zone.

Table C-5: Lumped Burnable Poison Rod Data

BP Rod Parameter	Inch	cm	Radius (cm)
Clad OD	0.43	1.092	0.5461
Clad ID	0.36	0.914	0.4572
Material	Zirc-4		
Density	0.238	6.588	
Pellet OD	0.34	0.864	0.4318
Material	Al_2O_3-B_4C		
Density	0.119	3.294	
Active Length	126 wt %	320.04 mg/cm^2	
B_4C Loading, Wt %	1.43	3.98	
	1.26	3.507	
	1.09	3.033	

C.1.3 Control Rod and Control Rod Group Data

As discussed previously, each control rod assembly is made up of 16 control rods attached to a single Type 304 stainless steel spider. Each control rod consists of a absorber section of silver-indium-cadmium (Ag-In-Cd) poison clad with solid-worked Type 304 stainless steel tubing (0.44-in outer diameter and 0.021-inch thick walls) and Type 304 stainless steel upper and lower end pieces, which are welded to the cladding to form a water and pressure tight container for the poison. The control rods are loosely attached to the spider to permit maximum conformance to the channels provided by the guide tunes. The control rod assemblies are inserted through the upper end fitting of the fuel assembly, each control rod being guided by an incore guide tube. Guide tubes are also provided in the upper plenum assembly above the core so that full length guidance of the control rods is provided throughout the stroke. The control rod assembly cannot be withdrawn far enough to cause disengagement of the control rods from the incore guide tubes.

The TMI-1 core reactivity is controlled by 69 control rod assemblies and soluble boron. Of the 69 control rod assemblies, 61 control assemblies are full-length and

are used to control reactor power level and are properly called safety rods. The remaining eight control rod assemblies are part-length control rods, designated as APSR, and contain a concentration of neutron poison (Ag-In-Cd) in the lower quarter of the rod. These control rod assemblies are used to control the axial power distribution. The design input data for the control rods is shown in Table C-6. The elevation of the control rod tip with respect to the bottom of the active fuel is shown in Figure C-54.

Table C-6: Control Rod Data

Control Rod	inch	cm	Radius (cm)
Full Length Control Rods			
Clad OD	0.44	1.118	0.5588
Clad ID	0.398	1.011	0.5055
Material	SS-304		
Density	0.29	8.027	
Pellet OD	0.392	0.996	0.4978
Material	Ag-In-Cd	80/15/5	
Density	0.367	10.158	
Full Length	134	340.36	
Partial Length Control Rods			
Clad OD	0.44	1.118	0.5588
Clad ID	0.398	1.011	0.5055
Material	SS-304		
Density	0.29	8.027	
Pellet OD	0.375	0.9525	0.4763
Material	Ag-In-Cd	80/15/5	
Density	0.367	10.158	
Part Length	36	91.44	

The control rod clusters are arranged into control rod groups. The TMI-1 core has 8 control rod groups. Groups 1 through 4 are the safety (shutdown) groups and are fully withdrawn during power operation. Groups 5 through 8 can be used for power and reactivity control. Groups 1 through 7 utilize full-length Ag-In-Cd, and Group 8 utilizes the part length Ag-In-Cd type of control rod. The core group arrangements

are shown in Figure C-67, Figure C-68, and Figure C-69. It is important to note that there was some re-assignment of the control rod groups during cycles 1 and 2.

Figure C-67: TMI-1 Cycle 1 Control Rod Group Configuration 0-250 EFPD

		1	2	3	4	5	6	7	8	9	10	11	12	13	14	15	
A																	
B							7		4		7						
C						5		3		3		5					
D					4		8		6		8		4				
E				5		6		1		1		6		5			
F			7		8		2		2		2		8		7		
G				3		1		5		5		1		3			
H			4		6		2		7		2		6		4		
K				3		1		5		5		1		3			
L			7		8		2		2		2		8		7		
M				5		6		1		1		6		5			
N					4		8		6		8		4				
O						5		3		3		5					
P							7		4		7						
R																	

Figure C-68: TMI-1 Cycle 1 Control Rod Group Configuration 250-466 EFPD

		1	2	3	4	5	6	7	8	9	10	11	12	13	14	15	
A																	
B							4		7		4						
C						5		3		3		5					
D					7		8		6		8		7				
E				5		6		1		1		6		5			
F			4		8		2		2		2		8		4		
G				3		1		5		5		1		3			
H			7		6		2		7		2		6		7		
K				3		1		5		5		1		3			
L			4		8		2		2		2		8		4		
M				5		6		1		1		6		5			
N					7		8		6		8		7				
O						5		3		3		5					
P							4		7		4						
R																	

Figure C-69: TMI-1 Cycle 2 Control Rod Group Configuration

		1	2	3	4	5	6	7	8	9	10	11	12	13	14	15	
A																	
B							4		5		4						
C						2		7		7		2					
D					6		8		3		8		6				
E				2		3		1		1		3		2			
F			4		8		5		6		5		8		4		
G				7		1		3		3		1		7			
H			5		3		6		4		6		3		5		
K				7		1		3		3		1		7			
L			4		8		5		6		5		8		4		
M				2		3		1		1		3		2			
N					6		8		3		8		6				
O						2		7		7		2					
P							4		5		4						
R																	

C.1.4 Core Baffle and Reflector Material Data

The TMI-1 exterior materials are required for ***CASMO-5*** reflector cross-section data calculations. This exterior data is given in Table C-7 below.

Table C-7: Core Baffle and Reflector Thickness and Material Volume Fraction Data

Region	Thickness (cm)	Void	Zirc Cladding	Stainless Steel	Water
1 – Bottom Nozzle	15.24	--	--	0.426	0.574
2 – Bottom Plenum	15.24	0.315	0.102	--	0.583
3 – Baffle Region	5.842	--	--	0.330	0.670
4 – Outer Reflector	20+	--	--	0.198	0.802
5 – Top Plenum	15.24	0.315	0.102	--	0.583
6 – Top Nozzle	15.24	--	--	0.196	0.803

C.1.5 TMI Unit 1 Operational Data

The TMI-1 Cycles 1 and 2 reactor core loadings, control configurations, and operational data were discussed previously in subsections 3.1.2 through 3.1.6 of this Topical Report and will not be repeated in this Appendix.

C.2 TMI-1 Calculated Versus Measured Results

The ***CASMO-5/SIMULATE-3*** computational models for the comparative analysis of the TMI-1, Cycles 1 and 2 hot zero power startup tests and core follow were presented previously in subsection 3.3.1 of this Topical Report. Furthermore, the results of the comparative analyses, including all rods out (ARO) critical boron, various temperature coefficient, boron and rod worths, core follow eigenvalues and critical boron were presented in both tabular and graphical form in subsections 3.3.2.1 and 3.3.2.2 of this document.

The calculated two-dimensional radial power distributions and Cycles 1 and 2 were compared to measured power distribution in subsection 3.3.2.3 for various points in the operating cycle. Likewise, a comparison of the calculated-to-measured axial power distributions for the two representative state points of Cycles 1 and 2 given above are

summarized in subsection 3.3.2.4 of this Topical Report. The measured power distribution for Cycles 1 and 2 were processed from the SPND signals contained in Reference 1. In essence, the measured assembly power was inferred from fixed incore rhodium SPND signals which respond to the neutron flux at the SPND location. These signals were then converted to measured power by multiplying by signal-to-power ratios, which were determined by analytical techniques. The methodology used in this Topical for converting the reaction rate signal to power was similar to that incorporated into reactor control systems in that it used the reaction rate and relative nodal power fraction data from ***CASMO-5/SIMULATE-3*** to calculate a unique signal-to-power factor for each SPND. This was necessary since the factor is influenced by the various fuel enrichments and burnable poison concentrations, which will differ both from assembly to assembly and axially as the burnup will induce fuel and BP variation within the same assembly over time.

Although, the results for comparative analyses of the Cycles 1 and 2 hot zero power startup tests and core follow eigenvalues and critical boron concentrations were documented in the main body of this report, only a few representative radial and axial power distribution comparisons were quantified in tabular and graphical form to demonstrate to illustrate the excellent agreement between the calculated and measured results. To complete the comparative qualification analysis for the nuclear computation methodology, a comprehensive set of calculated two-dimensional radial power distributions and axial power shapes for Cycles 1 and 2 are compared to measured power distribution for various points in the operating cycle. Figure C-70 through Figure C-109 summarize the Cycles 1 and 2 comparative analysis for the two-dimensional radial power distribution, and Figure C-110 through Figure C-149 summarize the calculated-to-measured axial power distributions for Cycles 1 and 2.

Figure C-70: TMI-1, Cycle 1 Radial Power Distribution Comparison at 655 MWd/MtU

	H-8	H-9	H-10	H-11	H-12	H-13	H-14	H-15
Measured	1.063	1.231	1.404	1.327	1.347	1.195	1.318	0.868
Calculated	1.085	1.314	1.356	1.380	1.255	1.242	1.319	0.843
Difference	0.022	0.083	-0.049	0.053	-0.092	0.048	0.001	-0.024

K-9	K-10	K-11	K-12	K-13	K-14	K-15
1.334	1.340	1.341	1.188	1.152	0.937	0.722
1.328	1.388	1.309	1.250	1.112	0.970	0.722
-0.007	0.048	-0.032	0.062	-0.040	0.033	0.000

L-10	L-11	L-12	L-13	L-14	L-15
1.327	1.247	1.012	0.939	0.688	0.461
1.329	1.296	1.005	0.980	0.679	0.447
0.002	0.049	-0.007	0.041	-0.009	-0.014

M-11	M-12	M-13	M-14
1.150	1.084	0.940	0.714
1.156	1.080	0.874	0.672
0.006	-0.003	-0.066	-0.041

N-12	N-13	N-14
0.988	0.770	0.460
0.929	0.772	0.454
-0.058	0.002	-0.006

O-13
0.507
0.507
0.000

STD DEV = 0.0413

Figure C-71: TMI-1, Cycle 1 Radial Power Distribution Comparison at 986 MWd/MtU

	H-8	H-9	H-10	H-11	H-12	H-13	H-14	H-15
Measured	1.021	1.260	1.419	1.358	1.302	1.200	1.309	0.847
Calculated	1.072	1.332	1.375	1.400	1.257	1.240	1.294	0.823
Difference	0.051	0.072	-0.043	0.043	-0.045	0.041	-0.014	-0.025
		K-9	K-10	K-11	K-12	K-13	K-14	K-15
		1.352	1.384	1.364	1.201	1.148	0.935	0.703
		1.345	1.413	1.325	1.260	1.107	0.955	0.704
		-0.007	0.028	-0.039	0.059	-0.041	0.020	0.001
			L-10	L-11	L-12	L-13	L-14	L-15
			1.348	1.267	1.018	0.941	0.637	0.444
			1.347	1.312	1.009	0.976	0.652	0.433
			-0.001	0.046	-0.010	0.035	0.016	-0.011
				M-11	M-12	M-13	M-14	
				1.143	1.104	0.930	0.677	
				1.160	1.087	0.870	0.660	
				0.016	-0.017	-0.060	-0.017	
					N-12	N-13	N-14	
					0.991	0.774	0.454	
					0.933	0.772	0.450	
					-0.059	-0.002	-0.005	
						O-13		
						0.507		
						0.506		
						-0.001		

STD DEV = 0.0356

Figure C-72: TMI-1, Cycle 1 Radial Power Distribution Comparison at 1756 MWd/MtU

	H-8	H-9	H-10	H-11	H-12	H-13	H-14	H-15
Measured	1.023	1.270	1.401	1.354	1.291	1.204	1.290	0.821
Calculated	1.083	1.355	1.383	1.415	1.252	1.238	1.261	0.796
Difference	0.060	0.085	-0.018	0.060	-0.039	0.035	-0.029	-0.026

	K-9	K-10	K-11	K-12	K-13	K-14	K-15
	1.336	1.398	1.353	1.207	1.139	0.949	0.688
	1.355	1.433	1.328	1.268	1.100	0.947	0.684
	0.019	0.034	-0.025	0.061	-0.039	-0.002	-0.004

	L-10	L-11	L-12	L-13	L-14	L-15
	1.329	1.272	1.014	0.955	0.631	0.442
	1.352	1.325	1.012	0.980	0.645	0.423
	0.023	0.054	-0.003	0.025	0.013	-0.019

	M-11	M-12	M-13	M-14
	1.136	1.130	0.926	0.670
	1.160	1.096	0.870	0.652
	0.024	-0.034	-0.056	-0.018

	N-12	N-13	N-14
	0.994	0.794	0.458
	0.936	0.775	0.447
	-0.058	-0.019	-0.011

	O-13
	0.518
	0.506
	-0.012

STD DEV = 0.0378

Figure C-73: TMI-1, Cycle 1 Radial Power Distribution Comparison at 2248 MWd/MtU

	H-8	H-9	H-10	H-11	H-12	H-13	H-14	H-15
Measured	1.021	1.268	1.390	1.347	1.288	1.204	1.276	0.810
Calculated	1.078	1.355	1.375	1.414	1.243	1.237	1.247	0.786
Difference	0.057	0.087	-0.015	0.067	-0.045	0.033	-0.030	-0.024
		K-9	K-10	K-11	K-12	K-13	K-14	K-15
		1.320	1.399	1.344	1.209	1.133	0.953	0.682
		1.348	1.433	1.321	1.271	1.097	0.946	0.679
		0.028	0.034	-0.022	0.062	-0.035	-0.006	-0.003
			L-10	L-11	L-12	L-13	L-14	L-15
			1.315	1.272	1.033	0.963	0.630	0.442
			1.345	1.327	1.015	0.986	0.643	0.422
			0.030	0.055	-0.018	0.023	0.014	-0.020
				M-11	M-12	M-13	M-14	
				1.130	1.143	0.925	0.670	
				1.158	1.105	0.875	0.654	
				0.028	-0.038	-0.050	-0.016	
					N-12	N-13	N-14	
					0.992	0.807	0.461	
					0.943	0.785	0.451	
					-0.050	-0.022	-0.011	
						O-13		
						0.526		
						0.512		
						-0.015		

STD DEV = 0.0383

Figure C-74: TMI-1, Cycle 1 Radial Power Distribution Comparison at 2763 MWd/MtU

	H-8	H-9	H-10	H-11	H-12	H-13	H-14	H-15
Measured	1.023	1.268	1.411	1.334	1.282	1.210	1.263	0.803
Calculated	1.078	1.351	1.360	1.410	1.242	1.239	1.236	0.779
Difference	0.055	0.083	-0.051	0.075	-0.041	0.030	-0.027	-0.024

K-9	K-10	K-11	K-12	K-13	K-14	K-15
1.303	1.390	1.329	1.210	1.128	0.961	0.680
1.334	1.426	1.311	1.273	1.096	0.949	0.675
0.032	0.036	-0.018	0.063	-0.032	-0.012	-0.005

L-10	L-11	L-12	L-13	L-14	L-15
1.300	1.277	1.015	0.974	0.633	0.445
1.334	1.327	1.015	0.994	0.650	0.423
0.034	0.050	0.001	0.020	0.017	-0.022

M-11	M-12	M-13	M-14
1.120	1.151	0.930	0.674
1.161	1.113	0.879	0.656
0.041	-0.038	-0.050	-0.018

N-12	N-13	N-14
0.998	0.820	0.467
0.948	0.793	0.454
-0.050	-0.027	-0.013

O-13
0.536
0.516
-0.020

STD DEV = 0.0397

Figure C-75: TMI-1, Cycle 1 Radial Power Distribution Comparison at 3223 MWd/MtU

	H-8	H-9	H-10	H-11	H-12	H-13	H-14	H-15
Measured	1.012	1.261	1.395	1.323	1.278	1.210	1.255	0.797
Calculated	1.056	1.344	1.350	1.405	1.230	1.239	1.228	0.775
Difference	0.044	0.083	-0.045	0.081	-0.048	0.028	-0.027	-0.022
		K-9	**K-10**	**K-11**	**K-12**	**K-13**	**K-14**	**K-15**
		1.288	1.386	1.321	1.211	1.125	0.963	0.678
		1.324	1.422	1.304	1.273	1.095	0.950	0.674
		0.035	0.036	-0.016	0.062	-0.030	-0.013	-0.004
			L-10	**L-11**	**L-12**	**L-13**	**L-14**	**L-15**
			1.293	1.269	1.013	0.981	0.630	0.448
			1.326	1.326	1.016	1.000	0.641	0.422
			0.033	0.057	0.003	0.019	0.010	-0.026
				M-11	**M-12**	**M-13**	**M-14**	
				1.117	1.158	0.936	0.681	
				1.156	1.123	0.888	0.660	
				0.039	-0.035	-0.048	-0.021	
					N-12	**N-13**	**N-14**	
					1.005	0.837	0.476	
					0.959	0.808	0.461	
					-0.046	-0.029	-0.014	
						O-13		
						0.550		
						0.527		
						-0.022		

STD DEV = 0.0396

Figure C-76: TMI-1, Cycle 1 Radial Power Distribution Comparison at 4055 MWd/MtU

	H-8	H-9	H-10	H-11	H-12	H-13	H-14	H-15
Measured	0.982	1.239	1.351	1.304	1.263	1.216	1.248	0.794
Calculated	1.035	1.327	1.324	1.391	1.220	1.240	1.218	0.772
Difference	0.053	0.088	-0.028	0.087	-0.043	0.025	-0.029	-0.023
		K-9	**K-10**	**K-11**	**K-12**	**K-13**	**K-14**	**K-15**
		1.254	1.366	1.300	1.208	1.128	0.973	0.682
		1.297	1.405	1.285	1.272	1.094	0.957	0.675
		0.043	0.040	-0.015	0.063	-0.035	-0.016	-0.007
			L-10	**L-11**	**L-12**	**L-13**	**L-14**	**L-15**
			1.268	1.261	1.018	0.997	0.642	0.456
			1.305	1.319	1.016	1.012	0.644	0.426
			0.037	0.058	-0.002	0.015	0.002	-0.030
				M-11	**M-12**	**M-13**	**M-14**	
				1.111	1.172	0.949	0.689	
				1.154	1.136	0.900	0.669	
				0.043	-0.035	-0.049	-0.020	
					N-12	**N-13**	**N-14**	
					1.016	0.855	0.490	
					0.975	0.830	0.473	
					-0.042	-0.026	-0.017	
						O-13		
						0.569		
						0.543		
						-0.026		

STD DEV = 0.0408

Figure C-77: TMI-1, Cycle 1 Radial Power Distribution Comparison at 5082 MWd/MtU

	H-8	H-9	H-10	H-11	H-12	H-13	H-14	H-15
Measured	0.980	1.231	1.317	1.277	1.239	1.214	1.239	0.790
Calculated	1.023	1.303	1.287	1.364	1.199	1.240	1.214	0.775
Difference	0.043	0.072	-0.030	0.087	-0.039	0.026	-0.026	-0.015
		K-9	**K-10**	**K-11**	**K-12**	**K-13**	**K-14**	**K-15**
		1.227	1.346	1.274	1.201	1.128	0.981	0.692
		1.263	1.376	1.256	1.263	1.093	0.972	0.684
		0.036	0.031	-0.018	0.063	-0.035	-0.009	-0.009
			L-10	**L-11**	**L-12**	**L-13**	**L-14**	**L-15**
			1.238	1.275	1.018	1.012	0.658	0.466
			1.272	1.302	1.012	1.029	0.664	0.439
			0.034	0.027	-0.006	0.017	0.006	-0.027
				M-11	**M-12**	**M-13**	**M-14**	
				1.105	1.178	0.958	0.700	
				1.143	1.148	0.917	0.687	
				0.039	-0.030	-0.041	-0.012	
					N-12	**N-13**	**N-14**	
					1.018	0.873	0.503	
					0.990	0.858	0.490	
					-0.028	-0.016	-0.013	
						O-13		
						0.585		
						0.563		
						-0.022		

STD DEV = 0.0354

Figure C-78: TMI-1, Cycle 1 Radial Power Distribution Comparison at 5727 MWd/MtU

	H-8	H-9	H-10	H-11	H-12	H-13	H-14	H-15
Measured	0.950	1.201	1.274	1.239	1.208	1.192	1.215	0.776
Calculated	1.010	1.287	1.266	1.350	1.192	1.241	1.211	0.776
Difference	0.060	0.086	-0.008	0.110	-0.016	0.048	-0.004	0.000
		K-9	**K-10**	**K-11**	**K-12**	**K-13**	**K-14**	**K-15**
		1.236	1.219	1.344	1.108	1.259	1.202	0.765
		1.287	1.266	1.350	1.192	1.241	1.211	0.776
		0.050	0.047	0.005	0.084	-0.018	0.009	0.012
			L-10	**L-11**	**L-12**	**L-13**	**L-14**	**L-15**
			1.205	1.214	0.993	1.003	0.652	0.465
			1.254	1.292	1.011	1.038	0.672	0.445
			0.049	0.078	0.017	0.035	0.019	-0.020
				M-11	**M-12**	**M-13**	**M-14**	
				1.065	1.163	0.954	0.692	
				1.141	1.155	0.926	0.696	
				0.076	-0.008	-0.027	0.004	
					N-12	**N-13**	**N-14**	
					1.016	0.866	0.501	
					1.000	0.874	0.500	
					-0.016	0.008	-0.001	
						O-13		
						0.583		
						0.575		
						-0.008		

STD DEV = 0.0380

Figure C-79: TMI-1, Cycle 1 Radial Power Distribution Comparison at 6549 MWd/MtU

	H-8	H-9	H-10	H-11	H-12	H-13	H-14	H-15
Measured	0.966	1.218	1.282	1.248	1.218	1.212	1.230	0.788
Calculated	0.988	1.265	1.242	1.332	1.183	1.240	1.208	0.779
Difference	0.021	0.047	-0.040	0.084	-0.035	0.028	-0.022	-0.009
		K-9	**K-10**	**K-11**	**K-12**	**K-13**	**K-14**	**K-15**
		1.197	1.320	1.250	1.192	1.128	0.994	0.693
		1.217	1.338	1.223	1.253	1.093	0.990	0.694
		0.020	0.017	-0.027	0.062	-0.035	-0.004	0.001
			L-10	**L-11**	**L-12**	**L-13**	**L-14**	**L-15**
			1.216	1.228	1.010	1.033	0.677	0.482
			1.234	1.281	1.010	1.048	0.678	0.453
			0.018	0.053	-0.001	0.015	0.001	-0.029
				M-11	**M-12**	**M-13**	**M-14**	
				1.092	1.185	0.980	0.716	
				1.138	1.163	0.938	0.708	
				0.046	-0.022	-0.042	-0.009	
					N-12	**N-13**	**N-14**	
					1.044	0.918	0.524	
					1.013	0.896	0.513	
					-0.030	-0.021	-0.011	
						O-13		
						0.603		
						0.592		
						-0.010		

STD DEV = 0.0330

Figure C-80: TMI-1, Cycle 1 Radial Power Distribution Comparison at 7199 MWd/MtU

	H-8	H-9	H-10	H-11	H-12	H-13	H-14	H-15
Measured	0.962	1.207	1.260	1.225	1.227	1.215	1.225	0.790
Calculated	0.993	1.247	1.216	1.309	1.172	1.238	1.210	0.786
Difference	0.031	0.041	-0.044	0.084	-0.055	0.023	-0.016	-0.004
		K-9	K-10	K-11	K-12	K-13	K-14	K-15
		1.186	1.297	1.227	1.182	1.136	1.001	0.707
		1.195	1.312	1.201	1.243	1.093	1.004	0.705
		0.008	0.016	-0.026	0.061	-0.043	0.003	-0.002
			L-10	L-11	L-12	L-13	L-14	L-15
			1.189	1.214	1.011	1.040	0.692	0.498
			1.210	1.264	1.004	1.059	0.706	0.468
			0.022	0.050	-0.006	0.018	0.014	-0.030
				M-11	M-12	M-13	M-14	
				1.081	1.186	0.980	0.728	
				1.131	1.165	0.948	0.723	
				0.050	-0.021	-0.032	-0.005	
					N-12	N-13	N-14	
					1.038	0.944	0.537	
					1.020	0.912	0.525	
					-0.018	-0.032	-0.012	
						O-13		
						0.607		
						0.603		
						-0.003		

STD DEV = 0.0337

Figure C-81: TMI-1, Cycle 1 Radial Power Distribution Comparison at 7711 MWd/MtU

	H-8	H-9	H-10	H-11	H-12	H-13	H-14	H-15
Measured	0.947	1.200	1.289	1.211	1.216	1.207	1.212	0.803
Calculated	0.988	1.234	1.200	1.296	1.166	1.236	1.209	0.789
Difference	0.042	0.034	-0.089	0.084	-0.050	0.030	-0.003	-0.014

	K-9	K-10	K-11	K-12	K-13	K-14	K-15
	1.161	1.277	1.217	1.208	1.169	1.011	0.690
	1.179	1.297	1.188	1.238	1.093	1.011	0.711
	0.019	0.020	-0.029	0.030	-0.075	0.001	0.021

	L-10	L-11	L-12	L-13	L-14	L-15
	1.187	1.193	1.000	1.041	0.703	0.498
	1.196	1.254	1.002	1.065	0.719	0.475
	0.010	0.061	0.002	0.025	0.015	-0.023

	M-11	M-12	M-13	M-14
	1.087	1.176	0.993	0.743
	1.129	1.167	0.955	0.732
	0.042	-0.008	-0.038	-0.010

	N-12	N-13	N-14
	1.018	0.950	0.541
	1.026	0.924	0.533
	0.007	-0.027	-0.008

	O-13
	0.603
	0.613
	0.010

STD DEV = 0.0376

Figure C-82: TMI-1, Cycle 1 Radial Power Distribution Comparison at 8549 MWd/MtU

	H-8	H-9	H-10	H-11	H-12	H-13	H-14	H-15
Measured	0.936	1.178	1.238	1.191	1.177	1.120	0.793	0.698
Calculated	0.951	1.207	1.175	1.267	1.128	1.139	0.799	0.693
Difference	0.016	0.029	-0.063	0.076	-0.050	0.019	0.006	-0.005
		K-9	K-10	K-11	K-12	K-13	K-14	K-15
		1.148	1.265	1.198	1.178	1.154	1.047	0.742
		1.154	1.268	1.162	1.223	1.109	1.054	0.751
		0.006	0.003	-0.036	0.045	-0.045	0.007	0.009
			L-10	L-11	L-12	L-13	L-14	L-15
			1.159	1.165	0.999	1.174	1.216	0.682
			1.160	1.206	0.990	1.198	1.217	0.649
			0.002	0.041	-0.009	0.023	0.001	-0.033
				M-11	M-12	M-13	M-14	
				0.978	1.050	1.009	0.896	
				1.027	1.035	0.970	0.893	
				0.049	-0.015	-0.038	-0.004	
					N-12	N-13	N-14	
					0.611	0.783	0.544	
					0.618	0.797	0.540	
					0.007	0.014	-0.004	
						O-13		
						0.517		
						0.520		
						0.003		

STD DEV = 0.0311

Figure C-83: TMI-1, Cycle 1 Radial Power Distribution Comparison at 9133 MWd/MtU

	H-8	H-9	H-10	H-11	H-12	H-13	H-14	H-15
Measured	0.929	1.165	1.220	1.178	1.177	1.122	0.802	0.706
Calculated	0.949	1.196	1.163	1.257	1.128	1.141	0.809	0.700
Difference	0.020	0.031	-0.058	0.079	-0.048	0.019	0.007	-0.007
		K-9	**K-10**	**K-11**	**K-12**	**K-13**	**K-14**	**K-15**
		1.135	1.249	1.187	1.172	1.155	1.051	0.748
		1.142	1.255	1.153	1.220	1.107	1.057	0.753
		0.007	0.006	-0.034	0.047	-0.048	0.006	0.005
			L-10	**L-11**	**L-12**	**L-13**	**L-14**	**L-15**
			1.146	1.158	1.001	1.176	1.212	0.682
			1.151	1.202	0.990	1.196	1.207	0.648
			0.005	0.044	-0.011	0.020	-0.005	-0.033
				M-11	**M-12**	**M-13**	**M-14**	
				0.985	1.058	1.014	0.897	
				1.034	1.044	0.975	0.893	
				0.049	-0.013	-0.039	-0.005	
					N-12	**N-13**	**N-14**	
					0.625	0.801	0.553	
					0.635	0.813	0.548	
					0.010	0.012	-0.005	
						O-13		
						0.529		
						0.534		
						0.005		

STD DEV = 0.0313

Figure C-84: TMI-1, Cycle 1 Radial Power Distribution Comparison at 10187 MWd/MtU

	H-8	H-9	H-10	H-11	H-12	H-13	H-14	H-15
Measured	0.920	1.160	1.210	1.167	1.163	1.117	0.806	0.714
Calculated	0.933	1.182	1.149	1.242	1.115	1.137	0.808	0.706
Difference	0.013	0.022	-0.061	0.075	-0.048	0.019	0.002	-0.008

		K-9	K-10	K-11	K-12	K-13	K-14	K-15
		1.132	1.240	1.179	1.164	1.154	1.058	0.753
		1.129	1.241	1.142	1.211	1.104	1.061	0.759
		-0.003	0.001	-0.037	0.047	-0.050	0.003	0.006

			L-10	L-11	L-12	L-13	L-14	L-15
			1.142	1.151	0.996	1.180	1.207	0.685
			1.140	1.193	0.988	1.198	1.203	0.654
			-0.002	0.042	-0.008	0.018	-0.004	-0.031

				M-11	M-12	M-13	M-14
				0.981	1.061	1.027	0.899
				1.030	1.050	0.985	0.900
				0.048	-0.011	-0.042	0.001

					N-12	N-13	N-14
					0.644	0.798	0.566
					0.646	0.836	0.564
					0.002	0.038	-0.002

						O-13
						0.547
						0.555
						0.007

STD DEV = 0.0314

Figure C-85: TMI-1, Cycle 1 Radial Power Distribution Comparison at 10814 MWd/MtU

	H-8	H-9	H-10	H-11	H-12	H-13	H-14	H-15
Measured	0.916	1.148	1.195	1.156	1.164	1.119	0.814	0.722
Calculated	0.936	1.170	1.135	1.230	1.115	1.138	0.825	0.715
Difference	0.020	0.022	-0.061	0.074	-0.048	0.019	0.012	-0.007
		K-9	**K-10**	**K-11**	**K-12**	**K-13**	**K-14**	**K-15**
		1.115	1.226	1.171	1.160	1.153	1.064	0.759
		1.115	1.225	1.132	1.205	1.102	1.065	0.764
		0.000	-0.001	-0.039	0.045	-0.051	0.001	0.005
			L-10	**L-11**	**L-12**	**L-13**	**L-14**	**L-15**
			1.132	1.147	0.999	1.180	1.202	0.685
			1.129	1.186	0.987	1.195	1.196	0.655
			-0.003	0.039	-0.012	0.015	-0.006	-0.030
				M-11	**M-12**	**M-13**	**M-14**	
				1.000	1.070	1.031	0.898	
				1.037	1.058	0.990	0.901	
				0.036	-0.012	-0.041	0.004	
					N-12	**N-13**	**N-14**	
					0.656	0.805	0.572	
					0.668	0.853	0.572	
					0.012	0.048	0.000	
						O-13		
						0.559		
						0.568		
						0.009		

STD DEV = 0.0314

Figure C-86: TMI-1, Cycle 1 Radial Power Distribution Comparison at 11808 MWd/MtU

	H-8	H-9	H-10	H-11	H-12	H-13	H-14	H-15
Measured	0.905	1.135	1.189	1.141	1.152	1.115	0.820	0.729
Calculated	0.924	1.158	1.124	1.215	1.099	1.132	0.824	0.723
Difference	0.019	0.023	-0.064	0.074	-0.052	0.016	0.004	-0.007
		K-9	**K-10**	**K-11**	**K-12**	**K-13**	**K-14**	**K-15**
		1.106	1.217	1.164	1.153	1.156	1.073	0.763
		1.106	1.213	1.122	1.195	1.099	1.068	0.771
		0.000	-0.004	-0.042	0.041	-0.057	-0.005	0.008
			L-10	**L-11**	**L-12**	**L-13**	**L-14**	**L-15**
			1.124	1.138	0.996	1.185	1.197	0.690
			1.120	1.176	0.985	1.195	1.194	0.662
			-0.004	0.038	-0.011	0.010	-0.003	-0.027
				M-11	**M-12**	**M-13**	**M-14**	
				0.979	1.077	1.042	0.902	
				1.028	1.061	0.999	0.911	
				0.049	-0.016	-0.043	0.009	
					N-12	**N-13**	**N-14**	
					0.667	0.807	0.587	
					0.677	0.874	0.588	
					0.011	0.067	0.001	
						O-13		
						0.574		
						0.589		
						0.014		

STD DEV = 0.0338

Figure C-87: TMI-1, Cycle 1 Radial Power Distribution Comparison at 12850 MWd/MtU

	H-8	H-9	H-10	H-11	H-12	H-13	H-14	H-15
Measured	0.898	1.126	1.183	1.126	1.147	1.109	0.825	0.733
Calculated	0.920	1.145	1.111	1.199	1.090	1.128	0.834	0.733
Difference	0.022	0.019	-0.072	0.073	-0.058	0.020	0.009	0.001
		K-9	**K-10**	**K-11**	**K-12**	**K-13**	**K-14**	**K-15**
		1.097	1.206	1.159	1.150	1.155	1.074	0.768
		1.093	1.197	1.110	1.184	1.096	1.072	0.780
		-0.004	-0.009	-0.048	0.034	-0.059	-0.002	0.012
			L-10	**L-11**	**L-12**	**L-13**	**L-14**	**L-15**
			1.117	1.130	1.003	1.185	1.190	0.691
			1.108	1.165	0.980	1.193	1.191	0.669
			-0.009	0.035	-0.023	0.008	0.001	-0.022
				M-11	**M-12**	**M-13**	**M-14**	
				0.980	1.081	1.048	0.902	
				1.026	1.065	1.007	0.918	
				0.046	-0.016	-0.041	0.016	
					N-12	**N-13**	**N-14**	
					0.676	0.822	0.595	
					0.694	0.895	0.602	
					0.018	0.073	0.007	
						O-13		
						0.590		
						0.609		
						0.019		

STD DEV = 0.0354

Figure C-88: TMI-1, Cycle 1 Radial Power Distribution Comparison at 13745 MWd/MtU

	H-8	H-9	H-10	H-11	H-12	H-13	H-14	H-15
Measured	1.241	1.102	1.042	1.002	1.111	1.156	1.262	0.874
Calculated	1.248	1.118	0.980	1.056	1.032	1.180	1.247	0.876
Difference	0.006	0.016	-0.062	0.055	-0.079	0.023	-0.015	0.002

		K-9	K-10	K-11	K-12	K-13	K-14	K-15
		1.025	1.061	1.023	1.058	1.142	1.153	0.835
		1.006	1.049	0.979	1.095	1.088	1.158	0.847
		-0.018	-0.012	-0.044	0.037	-0.055	0.006	0.012

			L-10	L-11	L-12	L-13	L-14	L-15
			0.984	1.028	0.971	1.134	1.151	0.687
			0.974	1.061	0.943	1.150	1.163	0.667
			-0.011	0.033	-0.028	0.016	0.012	-0.020

				M-11	M-12	M-13	M-14
				0.987	1.137	1.047	0.871
				1.024	1.122	1.019	0.896
				0.037	-0.014	-0.028	0.026

					N-12	N-13	N-14
					1.045	0.937	0.609
					1.042	1.006	0.617
					-0.004	0.069	0.008

						O-13
						0.660
						0.686
						0.026

STD DEV = 0.0340

Figure C-89: TMI-1, Cycle 2 Radial Power Distribution Comparison at 188 MWd/MtU

	H-8	H-9	H-10	H-11	H-12	H-13	H-14	H-15
Measured	1.100	1.022	1.032	1.050	1.239	0.867	0.810	0.604
Calculated	1.088	1.013	0.984	1.060	1.188	0.867	0.786	0.583
Difference	-0.011	-0.009	-0.047	0.010	-0.051	0.000	-0.025	-0.021
		K-9	**K-10**	**K-11**	**K-12**	**K-13**	**K-14**	**K-15**
		1.157	1.223	1.176	1.323	0.654	0.710	0.592
		1.172	1.188	1.141	1.274	0.640	0.700	0.573
		0.014	-0.035	-0.035	-0.050	-0.014	-0.009	-0.019
			L-10	**L-11**	**L-12**	**L-13**	**L-14**	**L-15**
			1.072	1.103	1.176	1.016	1.032	0.531
			1.088	1.129	1.196	1.027	0.993	0.492
			0.016	0.025	0.020	0.011	-0.039	-0.039
				M-11	**M-12**	**M-13**	**M-14**	
				1.331	1.406	1.313	0.962	
				1.453	1.421	1.370	0.955	
				0.121	0.015	0.057	-0.007	
					N-12	**N-13**	**N-14**	
					1.058	1.136	0.662	
					1.128	1.187	0.663	
					0.070	0.052	0.001	
						O-13		
						0.704		
						0.726		
						0.023		

STD DEV = 0.0391

Figure C-90: TMI-1, Cycle 2 Radial Power Distribution Comparison at 572 MWd/MtU

	H-8	H-9	H-10	H-11	H-12	H-13	H-14	H-15
Measured	1.122	1.033	1.028	1.056	1.243	0.886	0.852	0.652
Calculated	1.097	1.022	0.985	1.063	1.187	0.886	0.830	0.631
Difference	-0.024	-0.011	-0.043	0.007	-0.055	0.001	-0.022	-0.022
		K-9	**K-10**	**K-11**	**K-12**	**K-13**	**K-14**	**K-15**
		1.173	1.225	1.162	1.309	0.662	0.741	0.640
		1.173	1.184	1.138	1.264	0.645	0.737	0.616
		0.000	-0.040	-0.024	-0.045	-0.017	-0.004	-0.024
			L-10	**L-11**	**L-12**	**L-13**	**L-14**	**L-15**
			1.090	1.088	1.134	1.013	1.054	0.560
			1.083	1.112	1.151	1.024	1.019	0.523
			-0.007	0.024	0.016	0.010	-0.035	-0.036
				M-11	**M-12**	**M-13**	**M-14**	
				1.284	1.359	1.301	0.961	
				1.403	1.371	1.341	0.965	
				0.119	0.011	0.040	0.004	
					N-12	**N-13**	**N-14**	
					1.035	1.095	0.667	
					1.096	1.168	0.670	
					0.061	0.073	0.003	
						O-13		
						0.693		
						0.729		
						0.035		

STD DEV = 0.0385

Figure C-91: TMI-1, Cycle 2 Radial Power Distribution Comparison at 788 MWd/MtU

	H-8	H-9	H-10	H-11	H-12	H-13	H-14	H-15
Measured	1.116	1.035	1.047	1.053	1.239	0.898	0.866	0.655
Calculated	1.097	1.023	0.992	1.064	1.186	0.889	0.835	0.636
Difference	-0.019	-0.012	-0.056	0.011	-0.053	-0.009	-0.031	-0.019
		K-9	**K-10**	**K-11**	**K-12**	**K-13**	**K-14**	**K-15**
		1.174	1.228	1.169	1.307	0.678	0.752	0.638
		1.173	1.183	1.135	1.263	0.648	0.741	0.622
		-0.002	-0.045	-0.033	-0.044	-0.030	-0.010	-0.016
			L-10	**L-11**	**L-12**	**L-13**	**L-14**	**L-15**
			1.072	1.084	1.095	1.019	1.050	0.564
			1.081	1.108	1.147	1.023	1.022	0.527
			0.009	0.024	0.052	0.004	-0.027	-0.037
				M-11	**M-12**	**M-13**	**M-14**	
				1.288	1.363	1.281	0.960	
				1.395	1.365	1.336	0.965	
				0.107	0.002	0.055	0.005	
					N-12	**N-13**	**N-14**	
					1.029	1.097	0.671	
					1.098	1.165	0.671	
					0.069	0.068	-0.001	
						O-13		
						0.707		
						0.729		
						0.023		

STD DEV = 0.0396

Figure C-92: TMI-1, Cycle 2 Radial Power Distribution Comparison at 1000 MWd/MtU

	H-8	H-9	H-10	H-11	H-12	H-13	H-14	H-15
Measured	1.109	1.029	1.041	1.048	1.234	0.897	0.871	0.662
Calculated	1.092	1.020	0.989	1.062	1.185	0.892	0.842	0.644
Difference	-0.016	-0.009	-0.052	0.014	-0.050	-0.005	-0.029	-0.018
		K-9	K-10	K-11	K-12	K-13	K-14	K-15
		1.170	1.227	1.163	1.304	0.674	0.758	0.645
		1.168	1.179	1.133	1.263	0.650	0.748	0.630
		-0.001	-0.048	-0.030	-0.041	-0.023	-0.011	-0.015
			L-10	L-11	L-12	L-13	L-14	L-15
			1.043	1.081	1.136	1.016	1.052	0.572
			1.077	1.104	1.144	1.023	1.029	0.533
			0.034	0.024	0.008	0.008	-0.024	-0.039
				M-11	M-12	M-13	M-14	
				1.304	1.357	1.250	0.964	
				1.388	1.358	1.332	0.968	
				0.084	0.001	0.083	0.004	
					N-12	N-13	N-14	
					1.024	1.100	0.672	
					1.094	1.162	0.672	
					0.069	0.062	0.000	
						O-13		
						0.707		
						0.730		
						0.022		

STD DEV = 0.0376

Figure C-93: TMI-1, Cycle 2 Radial Power Distribution Comparison at 1333 MWd/MtU

	H-8	H-9	H-10	H-11	H-12	H-13	H-14	H-15
Measured	1.103	1.025	1.040	1.052	1.240	0.910	0.884	0.675
Calculated	1.084	1.014	0.987	1.059	1.185	0.902	0.856	0.657
Difference	-0.019	-0.011	-0.053	0.007	-0.055	-0.008	-0.028	-0.018
		K-9	**K-10**	**K-11**	**K-12**	**K-13**	**K-14**	**K-15**
		1.168	1.218	1.165	1.307	0.689	0.770	0.580
		1.161	1.172	1.128	1.264	0.664	0.759	0.641
		-0.007	-0.046	-0.037	-0.043	-0.024	-0.011	0.061
			L-10	**L-11**	**L-12**	**L-13**	**L-14**	**L-15**
			1.065	1.068	1.126	1.022	1.066	0.580
			1.070	1.097	1.140	1.025	1.036	0.540
			0.006	0.029	0.013	0.002	-0.030	-0.039
				M-11	**M-12**	**M-13**	**M-14**	
				1.274	1.342	1.267	0.968	
				1.375	1.347	1.324	0.968	
				0.101	0.005	0.057	0.000	
					N-12	**N-13**	**N-14**	
					1.033	1.105	0.677	
					1.089	1.155	0.672	
					0.056	0.050	-0.005	
						O-13		
						0.709		
						0.728		
						0.019		

STD DEV = 0.0380

Figure C-94: TMI-1, Cycle 2 Radial Power Distribution Comparison at 1637 MWd/MtU

	H-8	H-9	H-10	H-11	H-12	H-13	H-14	H-15
Measured	1.089	1.011	1.011	1.040	1.226	0.907	0.892	0.692
Calculated	1.080	1.010	0.972	1.055	1.181	0.900	0.867	0.674
Difference	-0.008	-0.001	-0.039	0.015	-0.045	-0.006	-0.025	-0.018

		K-9	K-10	K-11	K-12	K-13	K-14	K-15
		1.153	1.207	1.153	1.294	0.676	0.777	0.673
		1.156	1.167	1.125	1.260	0.651	0.768	0.657
		0.003	-0.041	-0.028	-0.034	-0.025	-0.010	-0.016

			L-10	L-11	L-12	L-13	L-14	L-15
			1.055	1.070	1.099	1.019	1.076	0.593
			1.069	1.095	1.130	1.024	1.049	0.553
			0.014	0.025	0.031	0.005	-0.027	-0.040

				M-11	M-12	M-13	M-14
				1.260	1.335	1.276	0.978
				1.368	1.338	1.323	0.977
				0.107	0.004	0.047	0.000

					N-12	N-13	N-14
					1.012	1.095	0.683
					1.072	1.153	0.678
					0.060	0.058	-0.005

						O-13
						0.712
						0.731
						0.020

STD DEV = 0.0352

Figure C-95: TMI-1, Cycle 2 Radial Power Distribution Comparison at 2011 MWd/MtU

	H-8	H-9	H-10	H-11	H-12	H-13	H-14	H-15
Measured	1.126	1.009	1.029	1.042	1.230	0.900	0.907	0.703
Calculated	1.077	1.011	0.986	1.055	1.182	0.914	0.879	0.683
Difference	-0.048	0.002	-0.043	0.013	-0.048	0.013	-0.028	-0.020

		K-9	K-10	K-11	K-12	K-13	K-14	K-15
		1.138	1.174	1.152	1.281	0.695	0.794	0.683
		1.154	1.164	1.120	1.260	0.676	0.778	0.665
		0.016	-0.011	-0.032	-0.021	-0.018	-0.016	-0.018

			L-10	L-11	L-12	L-13	L-14	L-15
			1.051	1.058	1.100	1.026	1.080	0.594
			1.062	1.087	1.126	1.024	1.049	0.557
			0.011	0.029	0.026	-0.002	-0.031	-0.038

				M-11	M-12	M-13	M-14
				1.252	1.337	1.264	0.968
				1.353	1.327	1.311	0.971
				0.101	-0.010	0.047	0.003

					N-12	N-13	N-14
					1.026	1.097	0.682
					1.079	1.145	0.674
					0.053	0.048	-0.008

						O-13
						0.712
						0.729
						0.017

STD DEV = 0.0342

Figure C-96: TMI-1, Cycle 2 Radial Power Distribution Comparison at 2574 MWd/MtU

	H-8	H-9	H-10	H-11	H-12	H-13	H-14	H-15
Measured	0.925	0.843	0.676	0.981	1.261	0.988	0.998	0.807
Calculated	0.942	0.862	0.682	1.008	1.233	0.984	0.987	0.781
Difference	0.016	0.019	0.007	0.027	-0.028	-0.005	-0.011	-0.026
		K-9	K-10	K-11	K-12	K-13	K-14	K-15
		0.989	1.071	1.126	1.328	0.702	0.888	0.790
		1.018	1.056	1.110	1.318	0.700	0.863	0.755
		0.028	-0.015	-0.016	-0.010	-0.002	-0.025	-0.035
			L-10	L-11	L-12	L-13	L-14	L-15
			0.968	1.065	1.141	1.091	1.194	0.678
			1.044	1.110	1.192	1.082	1.140	0.620
			0.076	0.045	0.052	-0.009	-0.055	-0.058
				M-11	M-12	M-13	M-14	
				1.251	1.293	1.296	1.036	
				1.355	1.285	1.317	1.011	
				0.104	-0.007	0.022	-0.025	
					N-12	N-13	N-14	
					0.743	1.027	0.694	
					0.786	1.060	0.668	
					0.043	0.033	-0.026	
						O-13		
						0.671		
						0.669		
						-0.001		

STD DEV = 0.0369

Figure C-97: TMI-1, Cycle 2 Radial Power Distribution Comparison at 2913 MWd/MtU

	H-8	H-9	H-10	H-11	H-12	H-13	H-14	H-15
Measured	1.075	1.003	1.022	1.030	1.212	0.917	0.922	0.723
Calculated	1.083	1.017	0.986	1.054	1.172	0.912	0.897	0.709
Difference	0.008	0.014	-0.037	0.024	-0.040	-0.005	-0.025	-0.014
		K-9	K-10	K-11	K-12	K-13	K-14	K-15
		1.135	1.185	1.138	1.284	0.688	0.803	0.703
		1.158	1.163	1.116	1.248	0.665	0.791	0.690
		0.022	-0.022	-0.023	-0.037	-0.023	-0.012	-0.013
			L-10	L-11	L-12	L-13	L-14	L-15
			1.038	1.056	1.080	1.016	1.083	0.612
			1.062	1.082	1.113	1.019	1.060	0.575
			0.024	0.026	0.034	0.003	-0.022	-0.037
				M-11	M-12	M-13	M-14	
				1.230	1.311	1.287	0.972	
				1.337	1.310	1.300	0.976	
				0.107	-0.001	0.013	0.004	
					N-12	N-13	N-14	
					1.014	1.087	0.684	
					1.066	1.139	0.680	
					0.052	0.052	-0.004	
						O-13		
						0.757		
						0.734		
						-0.023		

STD DEV = 0.0328

Figure C-98: TMI-1, Cycle 2 Radial Power Distribution Comparison at 3373 MWd/MtU

	H-8	H-9	H-10	H-11	H-12	H-13	H-14	H-15
Measured	1.070	0.999	1.026	1.028	1.209	0.926	0.938	0.738
Calculated	1.074	1.010	0.980	1.050	1.171	0.921	0.911	0.724
Difference	0.004	0.011	-0.046	0.022	-0.038	-0.004	-0.026	-0.014
		K-9	**K-10**	**K-11**	**K-12**	**K-13**	**K-14**	**K-15**
		1.133	1.184	1.134	1.255	0.701	0.817	0.701
		1.150	1.155	1.110	1.247	0.677	0.803	0.703
		0.017	-0.029	-0.024	-0.008	-0.024	-0.014	0.002
			L-10	**L-11**	**L-12**	**L-13**	**L-14**	**L-15**
			1.036	1.051	1.105	1.025	1.090	0.617
			1.056	1.077	1.113	1.021	1.066	0.584
			0.020	0.026	0.008	-0.004	-0.024	-0.034
				M-11	**M-12**	**M-13**	**M-14**	
				1.226	1.310	1.268	0.970	
				1.327	1.300	1.292	0.975	
				0.101	-0.010	0.024	0.005	
					N-12	**N-13**	**N-14**	
					1.017	1.080	0.687	
					1.058	1.132	0.680	
					0.041	0.052	-0.007	
						O-13		
						0.714		
						0.732		
						0.018		

STD DEV = 0.0306

Figure C-99: TMI-1, Cycle 2 Radial Power Distribution Comparison at 3832 MWd/MtU

	H-8	H-9	H-10	H-11	H-12	H-13	H-14	H-15
Measured	1.070	1.002	1.040	1.024	1.210	0.931	0.948	0.747
Calculated	1.075	1.012	0.981	1.050	1.169	0.927	0.923	0.737
Difference	0.005	0.010	-0.058	0.026	-0.041	-0.004	-0.024	-0.010
		K-9	**K-10**	**K-11**	**K-12**	**K-13**	**K-14**	**K-15**
		1.135	1.172	1.132	1.249	0.703	0.835	0.728
		1.150	1.154	1.108	1.243	0.681	0.813	0.715
		0.015	-0.018	-0.024	-0.006	-0.022	-0.022	-0.013
			L-10	**L-11**	**L-12**	**L-13**	**L-14**	**L-15**
			1.032	1.051	1.089	1.018	1.089	0.626
			1.056	1.074	1.107	1.020	1.070	0.592
			0.024	0.023	0.018	0.002	-0.019	-0.034
				M-11	**M-12**	**M-13**	**M-14**	
				1.222	1.296	1.258	0.969	
				1.317	1.289	1.283	0.974	
				0.094	-0.006	0.025	0.004	
					N-12	**N-13**	**N-14**	
					1.009	1.078	0.691	
					1.052	1.125	0.680	
					0.043	0.047	-0.010	
						O-13		
						0.718		
						0.732		
						0.013		

STD DEV = 0.0303

Figure C-100: TMI-1, Cycle 2 Radial Power Distribution Comparison at 4231 MWd/MtU

	H-8	H-9	H-10	H-11	H-12	H-13	H-14	H-15
Measured	1.070	1.003	1.044	1.023	1.208	0.939	0.960	0.757
Calculated	1.078	1.016	0.983	1.050	1.165	0.927	0.930	0.746
Difference	0.008	0.013	-0.060	0.027	-0.042	-0.011	-0.030	-0.010
		K-9	**K-10**	**K-11**	**K-12**	**K-13**	**K-14**	**K-15**
		1.132	1.180	1.129	1.247	0.708	0.837	0.731
		1.152	1.155	1.107	1.238	0.678	0.818	0.724
		0.020	-0.025	-0.022	-0.010	-0.030	-0.019	-0.008
			L-10	**L-11**	**L-12**	**L-13**	**L-14**	**L-15**
			1.025	1.052	1.081	1.027	1.086	0.634
			1.056	1.072	1.101	1.018	1.073	0.598
			0.032	0.021	0.020	-0.008	-0.013	-0.036
				M-11	**M-12**	**M-13**	**M-14**	
				1.212	1.297	1.234	0.970	
				1.311	1.283	1.279	0.974	
				0.099	-0.013	0.045	0.004	
					N-12	**N-13**	**N-14**	
					1.004	1.080	0.689	
					1.048	1.122	0.682	
					0.043	0.043	-0.007	
						O-13		
						0.717		
						0.733		
						0.016		

STD DEV = 0.0326

Figure C-101: TMI-1, Cycle 2 Radial Power Distribution Comparison at 4628 MWd/MtU

	H-8	H-9	H-10	H-11	H-12	H-13	H-14	H-15
Measured	1.073	1.005	1.027	1.027	1.207	0.942	0.965	0.763
Calculated	1.075	1.014	0.982	1.049	1.165	0.935	0.941	0.757
Difference	0.002	0.010	-0.045	0.022	-0.042	-0.008	-0.024	-0.007
		K-9	**K-10**	**K-11**	**K-12**	**K-13**	**K-14**	**K-15**
		1.129	1.178	1.131	1.242	0.713	0.842	0.743
		1.149	1.151	1.105	1.236	0.688	0.826	0.733
		0.020	-0.026	-0.026	-0.005	-0.024	-0.015	-0.010
			L-10	**L-11**	**L-12**	**L-13**	**L-14**	**L-15**
			1.032	1.050	1.074	1.022	1.094	0.635
			1.054	1.069	1.098	1.019	1.075	0.604
			0.021	0.019	0.024	-0.003	-0.018	-0.031
				M-11	**M-12**	**M-13**	**M-14**	
				1.206	1.290	1.236	0.966	
				1.303	1.275	1.272	0.972	
				0.097	-0.015	0.035	0.006	
					N-12	**N-13**	**N-14**	
					1.009	1.076	0.687	
					1.042	1.116	0.681	
					0.033	0.040	-0.006	
						O-13		
						0.717		
						0.732		
						0.015		

STD DEV = 0.0295

Figure C-102: TMI-1, Cycle 2 Radial Power Distribution Comparison at 5042 MWd/MtU

	H-8	H-9	H-10	H-11	H-12	H-13	H-14	H-15
Measured	1.080	1.016	1.054	1.024	1.214	0.946	0.972	0.763
Calculated	1.079	1.019	0.994	1.050	1.165	0.941	0.947	0.760
Difference	-0.002	0.004	-0.060	0.026	-0.050	-0.005	-0.026	-0.003
		K-9	**K-10**	**K-11**	**K-12**	**K-13**	**K-14**	**K-15**
		1.140	1.177	1.125	1.234	0.721	0.842	0.743
		1.152	1.153	1.103	1.234	0.700	0.831	0.736
		0.012	-0.024	-0.021	0.000	-0.021	-0.011	-0.007
			L-10	**L-11**	**L-12**	**L-13**	**L-14**	**L-15**
			1.030	1.046	1.091	1.019	1.087	0.634
			1.052	1.066	1.096	1.018	1.073	0.605
			0.022	0.020	0.005	-0.002	-0.014	-0.028
				M-11	**M-12**	**M-13**	**M-14**	
				1.206	1.279	1.228	0.960	
				1.295	1.269	1.263	0.967	
				0.089	-0.010	0.036	0.007	
					N-12	**N-13**	**N-14**	
					1.004	1.072	0.687	
					1.047	1.112	0.679	
					0.043	0.040	-0.008	
						O-13		
						0.719		
						0.731		
						0.011		

STD DEV = 0.0293

Figure C-103: TMI-1, Cycle 2 Radial Power Distribution Comparison at 5469 MWd/MtU

	H-8	H-9	H-10	H-11	H-12	H-13	H-14	H-15
Measured	1.077	1.009	1.057	1.026	1.213	0.951	0.981	0.776
Calculated	1.081	1.023	0.996	1.051	1.161	0.941	0.952	0.769
Difference	0.004	0.014	-0.061	0.025	-0.051	-0.010	-0.028	-0.008
		K-9	**K-10**	**K-11**	**K-12**	**K-13**	**K-14**	**K-15**
		1.131	1.173	1.126	1.229	0.722	0.854	0.756
		1.154	1.154	1.103	1.229	0.698	0.836	0.744
		0.023	-0.020	-0.023	0.000	-0.024	-0.018	-0.012
			L-10	**L-11**	**L-12**	**L-13**	**L-14**	**L-15**
			1.008	1.046	1.073	1.020	1.092	0.642
			1.053	1.065	1.092	1.016	1.074	0.611
			0.045	0.018	0.019	-0.004	-0.018	-0.032
				M-11	**M-12**	**M-13**	**M-14**	
				1.191	1.275	1.227	0.961	
				1.291	1.263	1.259	0.966	
				0.099	-0.012	0.032	0.005	
					N-12	**N-13**	**N-14**	
					1.007	1.075	0.687	
					1.044	1.109	0.680	
					0.037	0.035	-0.007	
						O-13		
						0.716		
						0.732		
						0.016		

STD DEV = 0.0319

Figure C-104: TMI-1, Cycle 2 Radial Power Distribution Comparison at 5906 MWd/MtU

	H-8	H-9	H-10	H-11	H-12	H-13	H-14	H-15
Measured	1.075	1.006	1.048	1.024	1.216	0.954	0.988	0.788
Calculated	1.077	1.018	0.984	1.048	1.160	0.945	0.964	0.783
Difference	0.002	0.012	-0.065	0.024	-0.056	-0.009	-0.024	-0.005
		K-9	**K-10**	**K-11**	**K-12**	**K-13**	**K-14**	**K-15**
		1.128	1.169	1.123	1.220	0.719	0.862	0.769
		1.149	1.149	1.100	1.226	0.697	0.845	0.757
		0.021	-0.020	-0.022	0.006	-0.022	-0.017	-0.012
			L-10	**L-11**	**L-12**	**L-13**	**L-14**	**L-15**
			1.029	1.045	1.058	1.019	1.095	0.653
			1.052	1.063	1.086	1.016	1.081	0.621
			0.023	0.018	0.028	-0.002	-0.014	-0.032
				M-11	**M-12**	**M-13**	**M-14**	
				1.186	1.269	1.223	0.962	
				1.284	1.255	1.255	0.969	
				0.097	-0.014	0.032	0.007	
					N-12	**N-13**	**N-14**	
					1.004	1.074	0.690	
					1.030	1.104	0.683	
					0.025	0.031	-0.007	
						O-13		
						0.716		
						0.733		
						0.017		

STD DEV = 0.0307

Figure C-105: TMI-1, Cycle 2 Radial Power Distribution Comparison at 6327 MWd/MtU

	H-8	H-9	H-10	H-11	H-12	H-13	H-14	H-15
Measured	1.076	1.006	1.050	1.025	1.215	0.958	0.994	0.792
Calculated	1.077	1.020	0.988	1.048	1.159	0.951	0.971	0.789
Difference	0.002	0.014	-0.062	0.023	-0.056	-0.007	-0.023	-0.003
		K-9	**K-10**	**K-11**	**K-12**	**K-13**	**K-14**	**K-15**
		1.126	1.166	1.121	1.216	0.725	0.868	0.774
		1.149	1.148	1.098	1.224	0.706	0.851	0.762
		0.023	-0.018	-0.022	0.008	-0.019	-0.017	-0.011
			L-10	**L-11**	**L-12**	**L-13**	**L-14**	**L-15**
			1.029	1.044	1.054	1.019	1.094	0.654
			1.051	1.060	1.083	1.016	1.081	0.625
			0.022	0.016	0.029	-0.003	-0.013	-0.030
				M-11	**M-12**	**M-13**	**M-14**	
				1.181	1.264	1.219	0.960	
				1.277	1.249	1.248	0.967	
				0.096	-0.016	0.029	0.007	
					N-12	**N-13**	**N-14**	
					1.005	1.075	0.689	
					1.029	1.100	0.682	
					0.023	0.025	-0.007	
						O-13		
						0.714		
						0.732		
						0.018		

STD DEV = 0.0300

Figure C-106: TMI-1, Cycle 2 Radial Power Distribution Comparison at 6758 MWd/MtU

	H-8	H-9	H-10	H-11	H-12	H-13	H-14	H-15
Measured	1.081	1.014	1.057	1.027	1.211	0.957	0.996	0.796
Calculated	1.084	1.027	0.995	1.050	1.156	0.949	0.973	0.792
Difference	0.002	0.012	-0.062	0.023	-0.055	-0.008	-0.023	-0.003
		K-9	K-10	K-11	K-12	K-13	K-14	K-15
		1.132	1.169	1.121	1.209	0.723	0.870	0.777
		1.154	1.152	1.099	1.219	0.701	0.852	0.765
		0.022	-0.018	-0.022	0.010	-0.022	-0.018	-0.012
			L-10	L-11	L-12	L-13	L-14	L-15
			1.031	1.044	1.052	1.017	1.090	0.655
			1.053	1.061	1.081	1.014	1.079	0.627
			0.022	0.017	0.029	-0.003	-0.010	-0.027
				M-11	M-12	M-13	M-14	
				1.180	1.261	1.216	0.958	
				1.275	1.246	1.244	0.965	
				0.094	-0.015	0.029	0.008	
					N-12	N-13	N-14	
					1.005	1.076	0.692	
					1.031	1.099	0.683	
					0.025	0.023	-0.009	
						O-13		
						0.716		
						0.735		
						0.019		

STD DEV = 0.0296

Figure C-107: TMI-1, Cycle 2 Radial Power Distribution Comparison at 7176 MWd/MtU

	H-8	H-9	H-10	H-11	H-12	H-13	H-14	H-15
Measured	1.083	1.016	1.058	1.028	1.205	0.961	1.000	0.801
Calculated	1.085	1.030	1.000	1.050	1.153	0.951	0.977	0.797
Difference	0.002	0.014	-0.058	0.022	-0.051	-0.010	-0.023	-0.004
		K-9	**K-10**	**K-11**	**K-12**	**K-13**	**K-14**	**K-15**
		1.132	1.170	1.121	1.205	0.725	0.876	0.781
		1.156	1.152	1.098	1.215	0.704	0.856	0.770
		0.023	-0.018	-0.022	0.011	-0.021	-0.020	-0.011
			L-10	**L-11**	**L-12**	**L-13**	**L-14**	**L-15**
			1.031	1.045	1.054	1.018	1.090	0.659
			1.053	1.060	1.078	1.012	1.079	0.631
			0.022	0.014	0.024	-0.006	-0.011	-0.028
				M-11	**M-12**	**M-13**	**M-14**	
				1.177	1.257	1.212	0.954	
				1.269	1.241	1.239	0.963	
				0.092	-0.016	0.027	0.010	
					N-12	**N-13**	**N-14**	
					1.005	1.071	0.691	
					1.032	1.097	0.684	
					0.027	0.026	-0.007	
						O-13		
						0.707		
						0.736		
						0.029		

STD DEV = 0.0292

Figure C-108: TMI-1, Cycle 2 Radial Power Distribution Comparison at 7609 MWd/MtU

	H-8	H-9	H-10	H-11	H-12	H-13	H-14	H-15
Measured	1.084	1.017	1.055	1.028	1.205	0.960	1.007	0.810
Calculated	1.086	1.030	0.997	1.050	1.151	0.951	0.982	0.805
Difference	0.002	0.014	-0.058	0.021	-0.054	-0.009	-0.025	-0.005
		K-9	**K-10**	**K-11**	**K-12**	**K-13**	**K-14**	**K-15**
		1.134	1.169	1.119	1.199	0.721	0.881	0.789
		1.156	1.151	1.097	1.211	0.701	0.860	0.778
		0.022	-0.017	-0.022	0.012	-0.021	-0.021	-0.012
			L-10	**L-11**	**L-12**	**L-13**	**L-14**	**L-15**
			1.032	1.046	1.047	1.017	1.091	0.663
			1.054	1.059	1.075	1.011	1.081	0.637
			0.022	0.013	0.028	-0.005	-0.010	-0.026
				M-11	**M-12**	**M-13**	**M-14**	
				1.173	1.253	1.207	0.955	
				1.266	1.236	1.236	0.965	
				0.092	-0.017	0.029	0.010	
					N-12	**N-13**	**N-14**	
					1.003	1.071	0.692	
					1.026	1.095	0.687	
					0.023	0.024	-0.006	
						O-13		
						0.710		
						0.738		
						0.028		

STD DEV = 0.0292

Figure C-109: TMI-1, Cycle 2 Radial Power Distribution Comparison at 8079 MWd/MtU

	H-8	H-9	H-10	H-11	H-12	H-13	H-14	H-15
Measured	1.083	1.015	1.053	1.029	1.211	0.967	1.011	0.812
Calculated	1.087	1.034	1.009	1.051	1.152	0.960	0.988	0.807
Difference	0.003	0.019	-0.045	0.022	-0.060	-0.007	-0.023	-0.005
		K-9	K-10	K-11	K-12	K-13	K-14	K-15
		1.132	1.165	1.118	1.200	0.732	0.885	0.793
		1.156	1.151	1.095	1.210	0.720	0.865	0.779
		0.025	-0.014	-0.023	0.011	-0.012	-0.020	-0.014
			L-10	L-11	L-12	L-13	L-14	L-15
			1.030	1.043	1.042	1.017	1.093	0.668
			1.051	1.055	1.073	1.011	1.078	0.637
			0.021	0.011	0.031	-0.005	-0.015	-0.030
				M-11	M-12	M-13	M-14	
				1.171	1.250	1.205	0.954	
				1.257	1.230	1.228	0.959	
				0.086	-0.020	0.022	0.004	
					N-12	N-13	N-14	
					1.003	1.072	0.693	
					1.031	1.090	0.684	
					0.029	0.019	-0.009	
						O-13		
						0.687		
						0.737		
						0.050		

STD DEV = 0.0292

Figure C-110: TMI-1, Cycle 1 Axial Power Distribution Comparison at 655 MWd/MtU

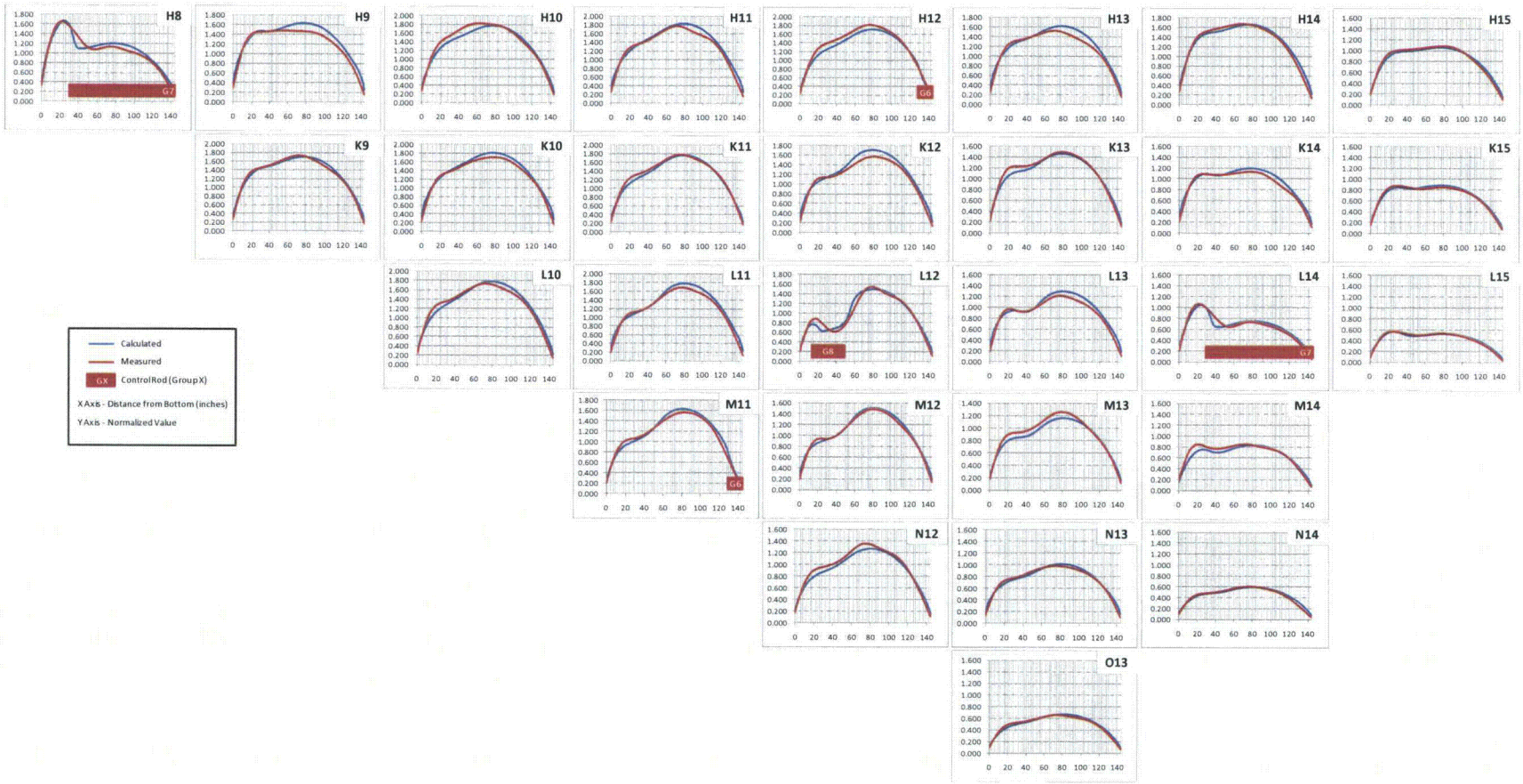

Figure C-111: TMI-1, Cycle 1 Axial Power Distribution Comparison at 986 MWd/MtU

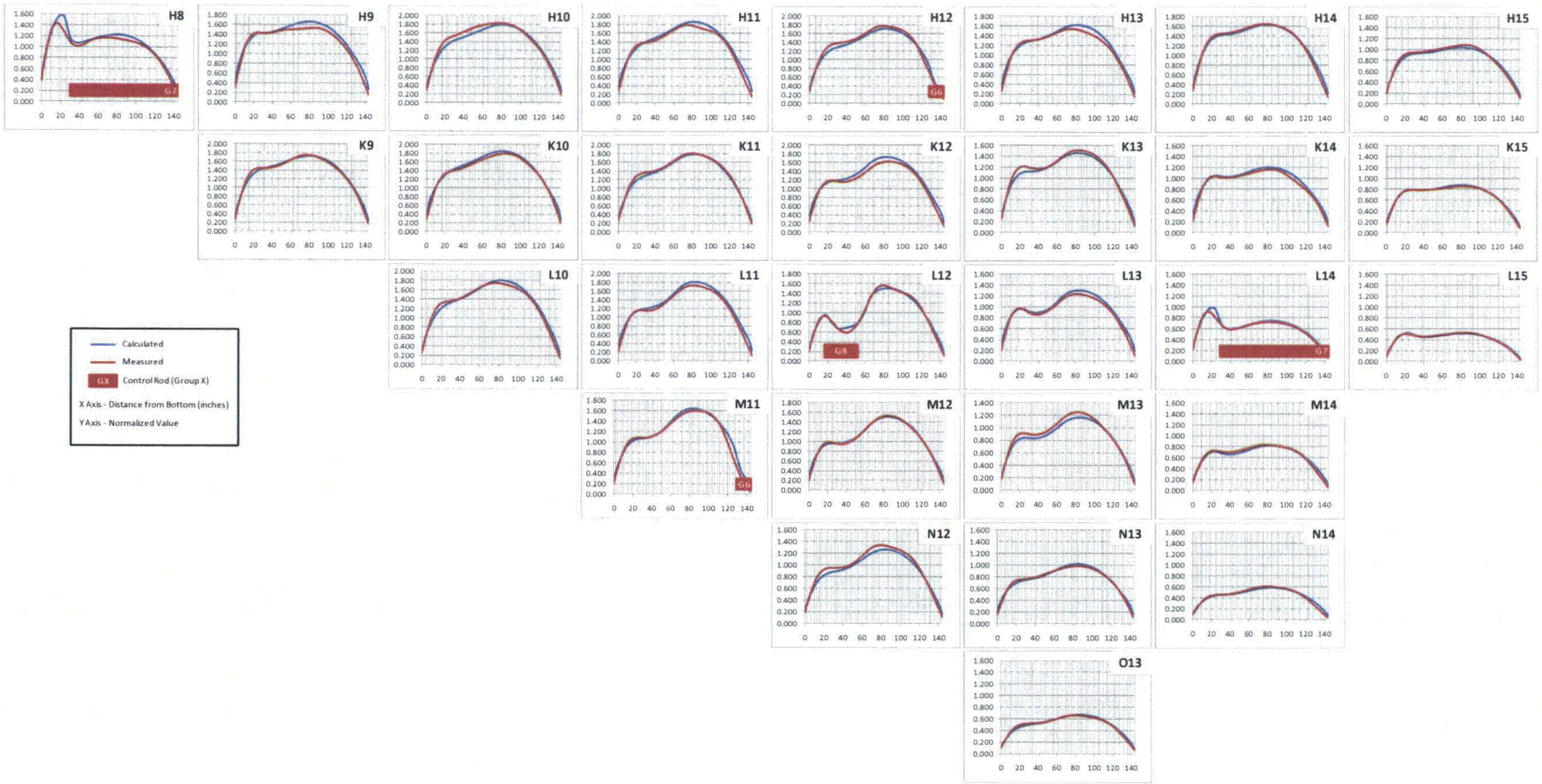

Figure C-112: TMI-1, Cycle 1 Axial Power Distribution Comparison at 1756 MWd/MtU

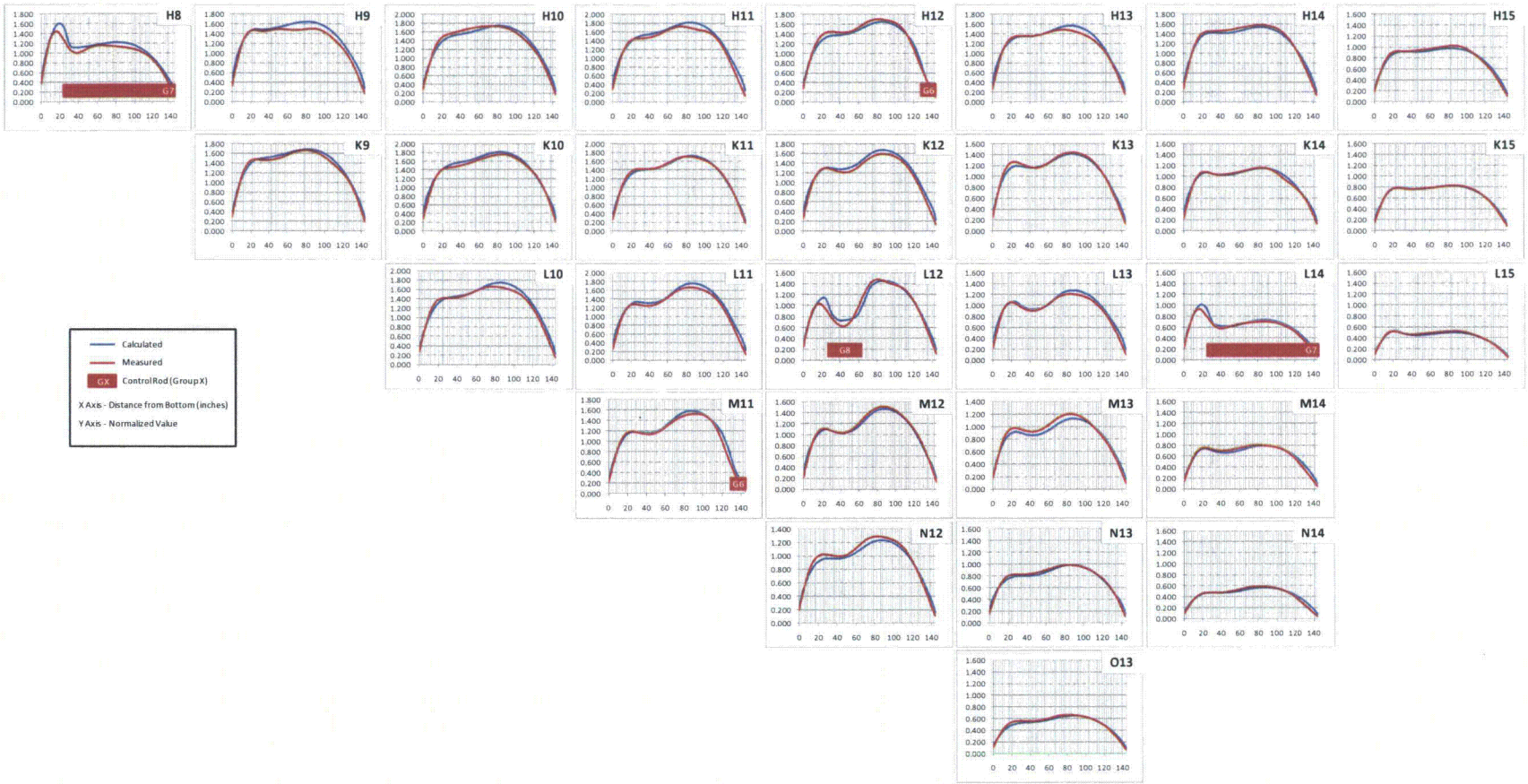

Figure C-113: TMI-1, Cycle 1 Axial Power Distribution Comparison at 2248 MWd/MtU

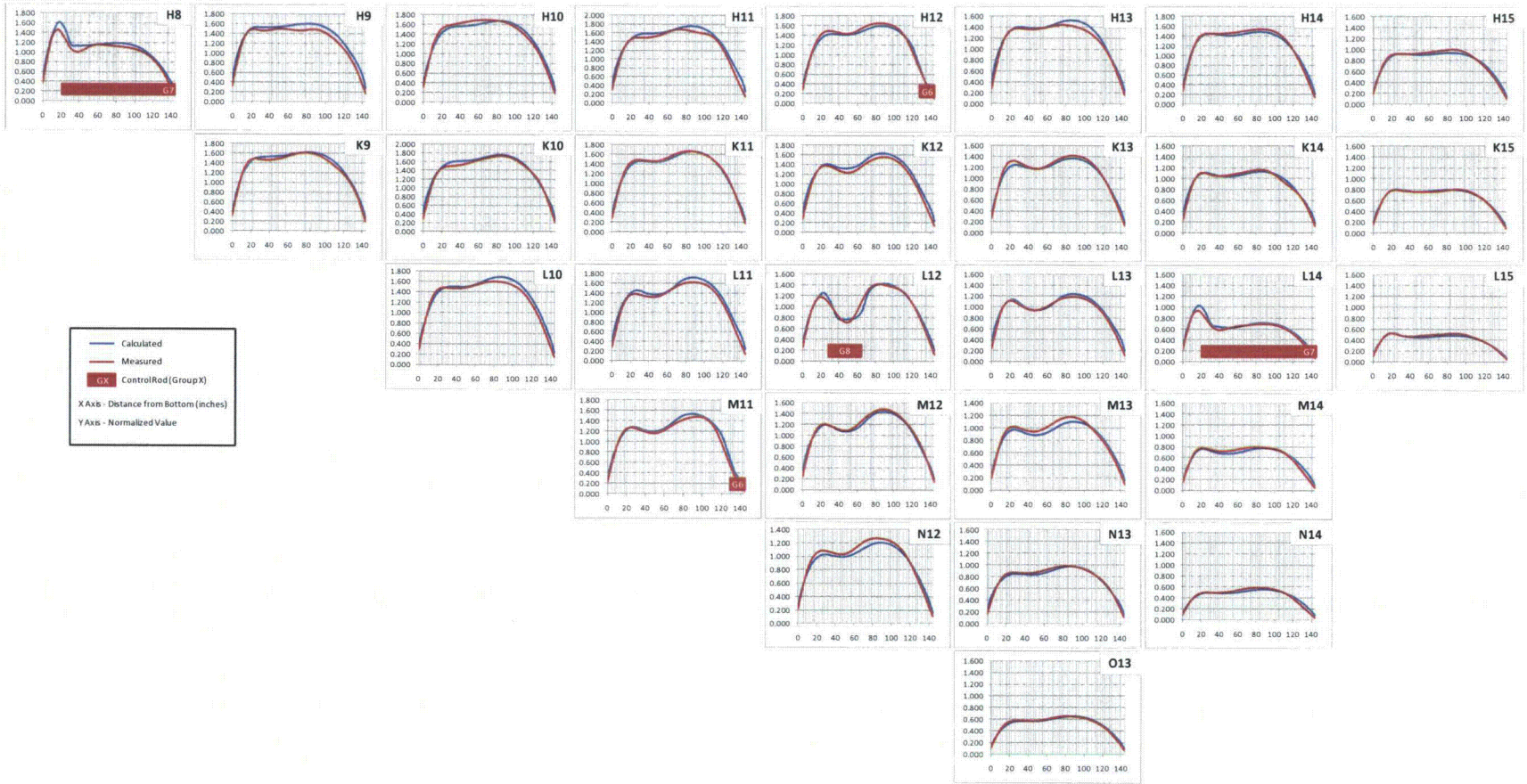

Figure C-114: TMI-1, Cycle 1 Axial Power Distribution Comparison at 2763 MWd/MtU

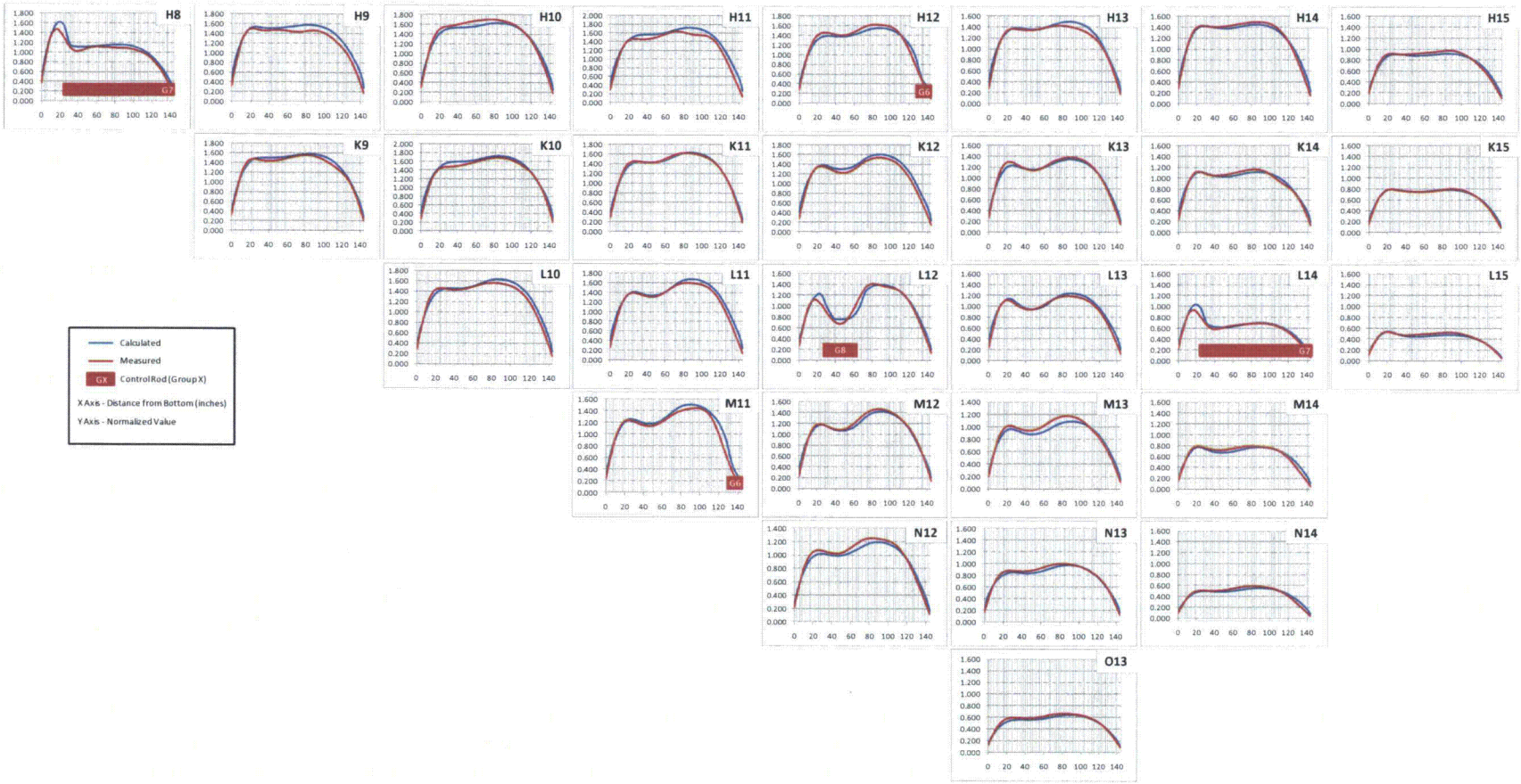

Figure C-115: TMI-1, Cycle 1 Axial Power Distribution Comparison at 3223 MWd/MtU

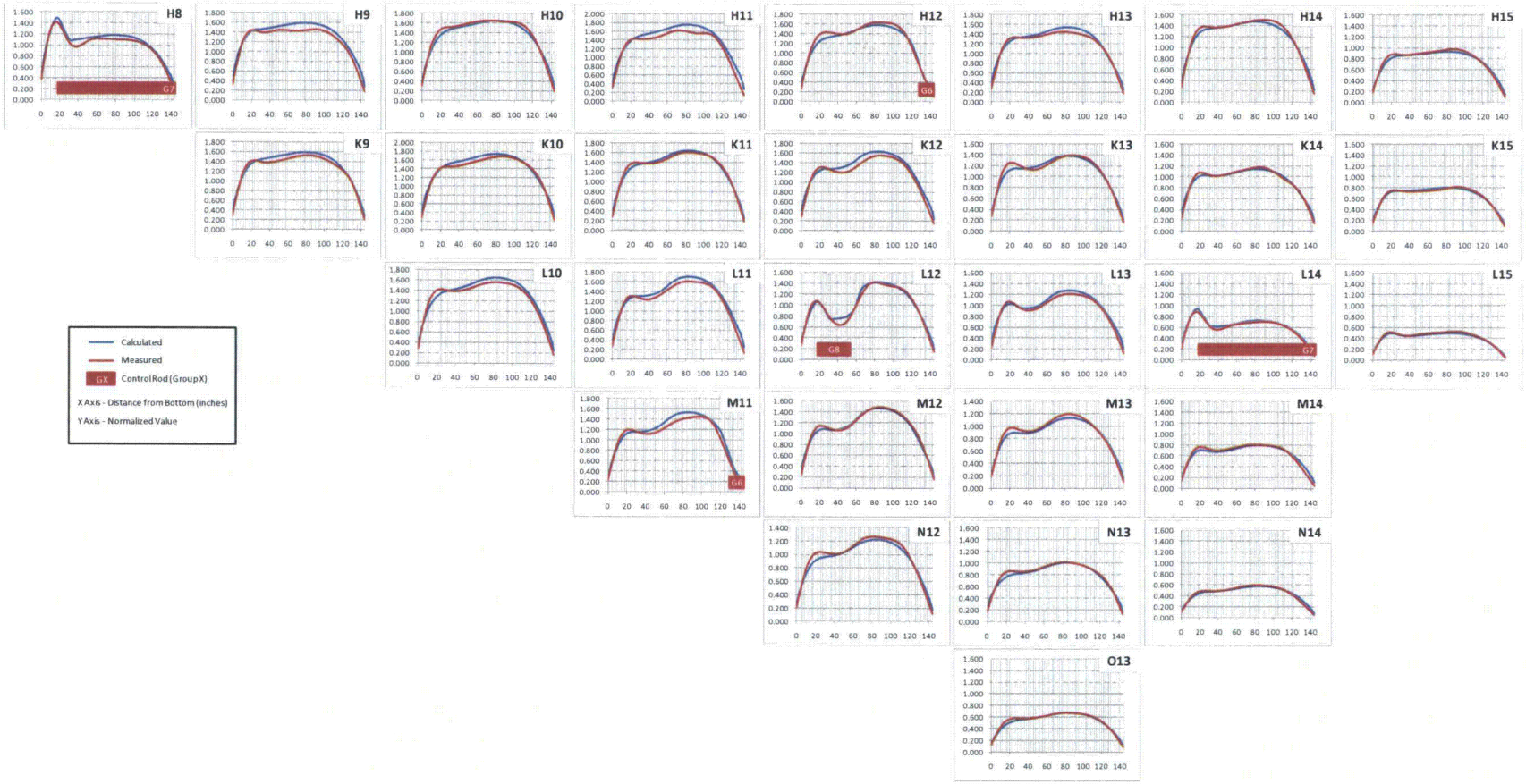

Figure C-116: TMI-1, Cycle 1 Axial Power Distribution Comparison at 4055 MWd/MtU

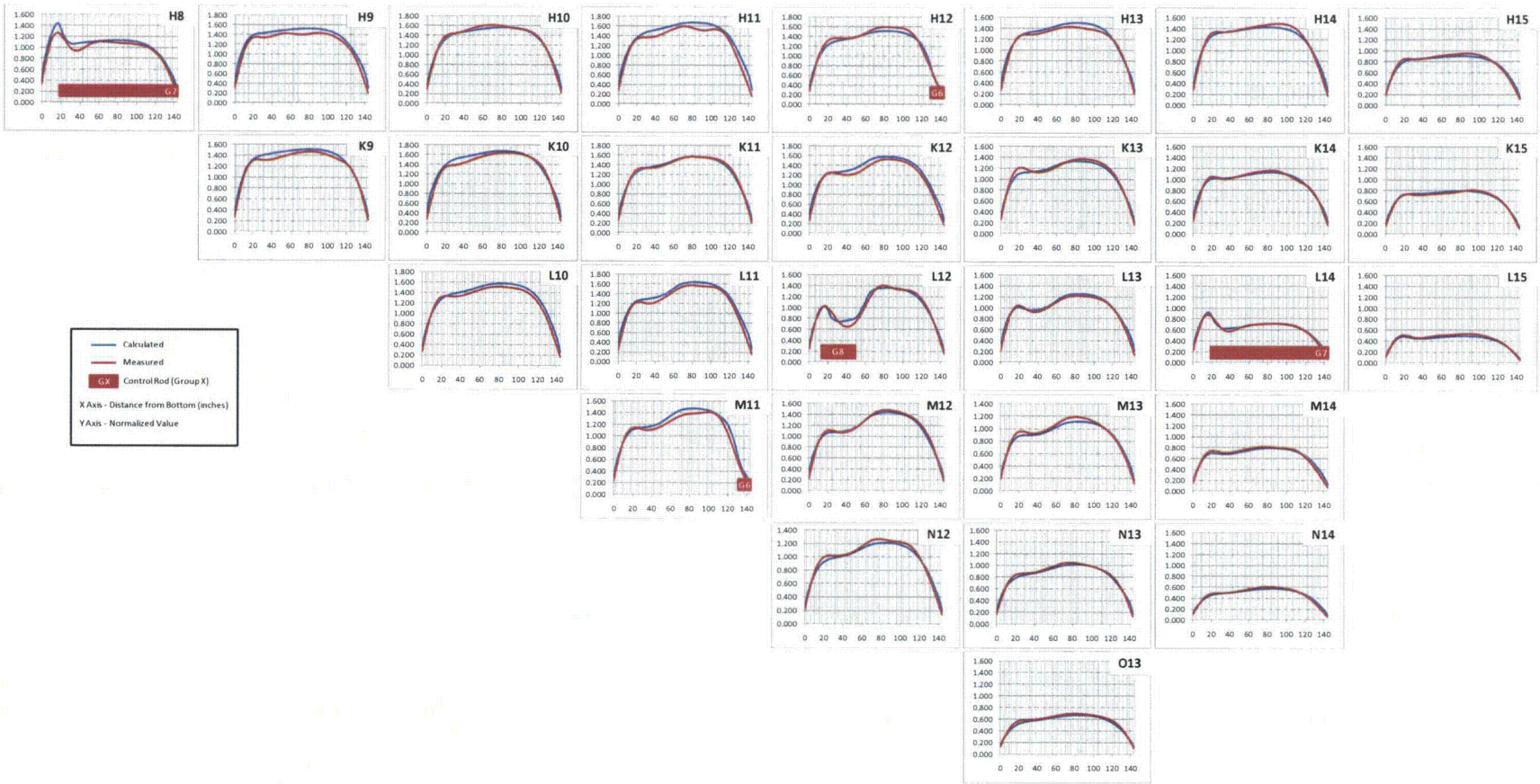

Figure C-117: TMI-1, Cycle 1 Axial Power Distribution Comparison at 5082 MWd/MtU

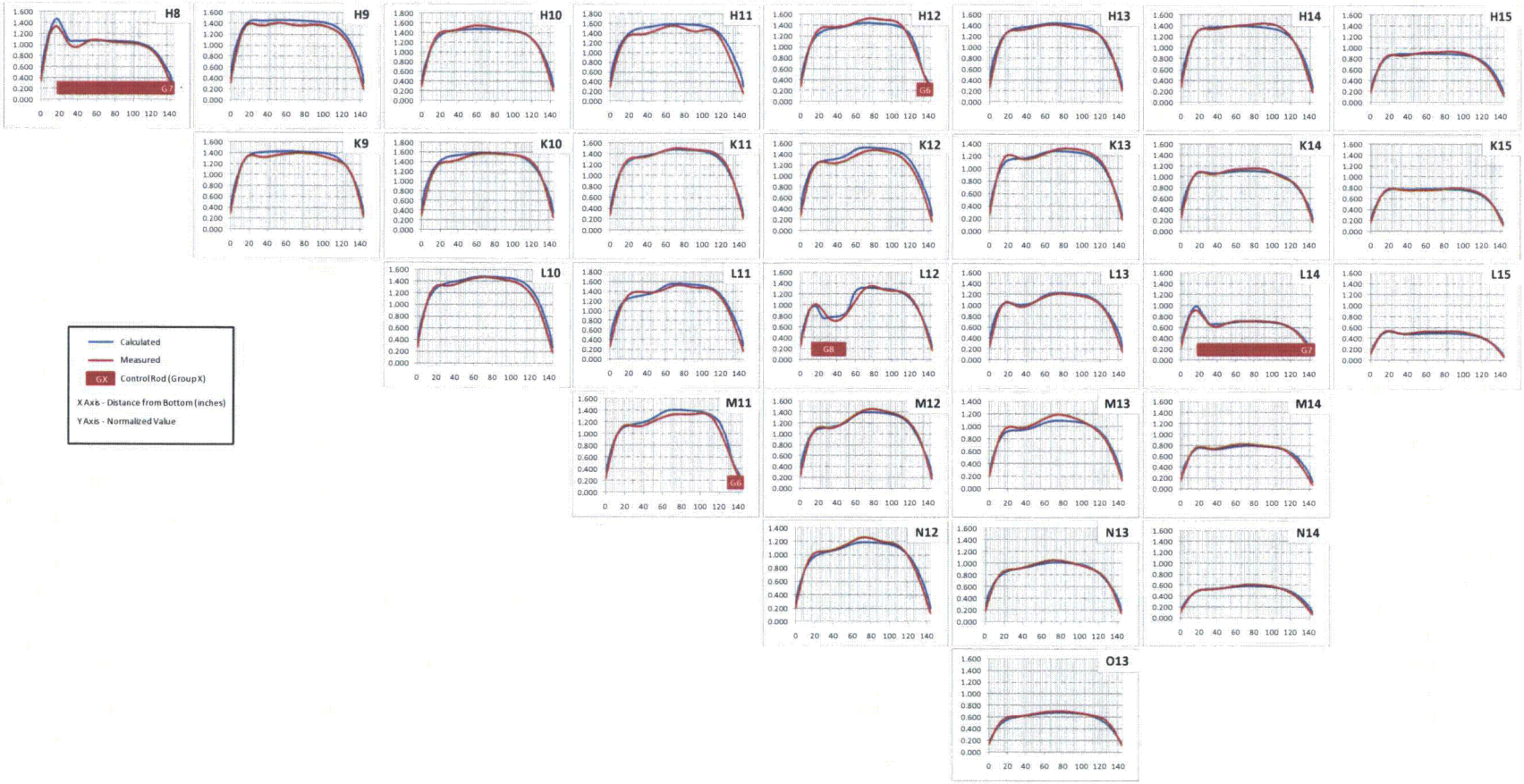

Figure C-118: TMI-1, Cycle 1 Axial Power Distribution Comparison at 5727 MWd/MtU

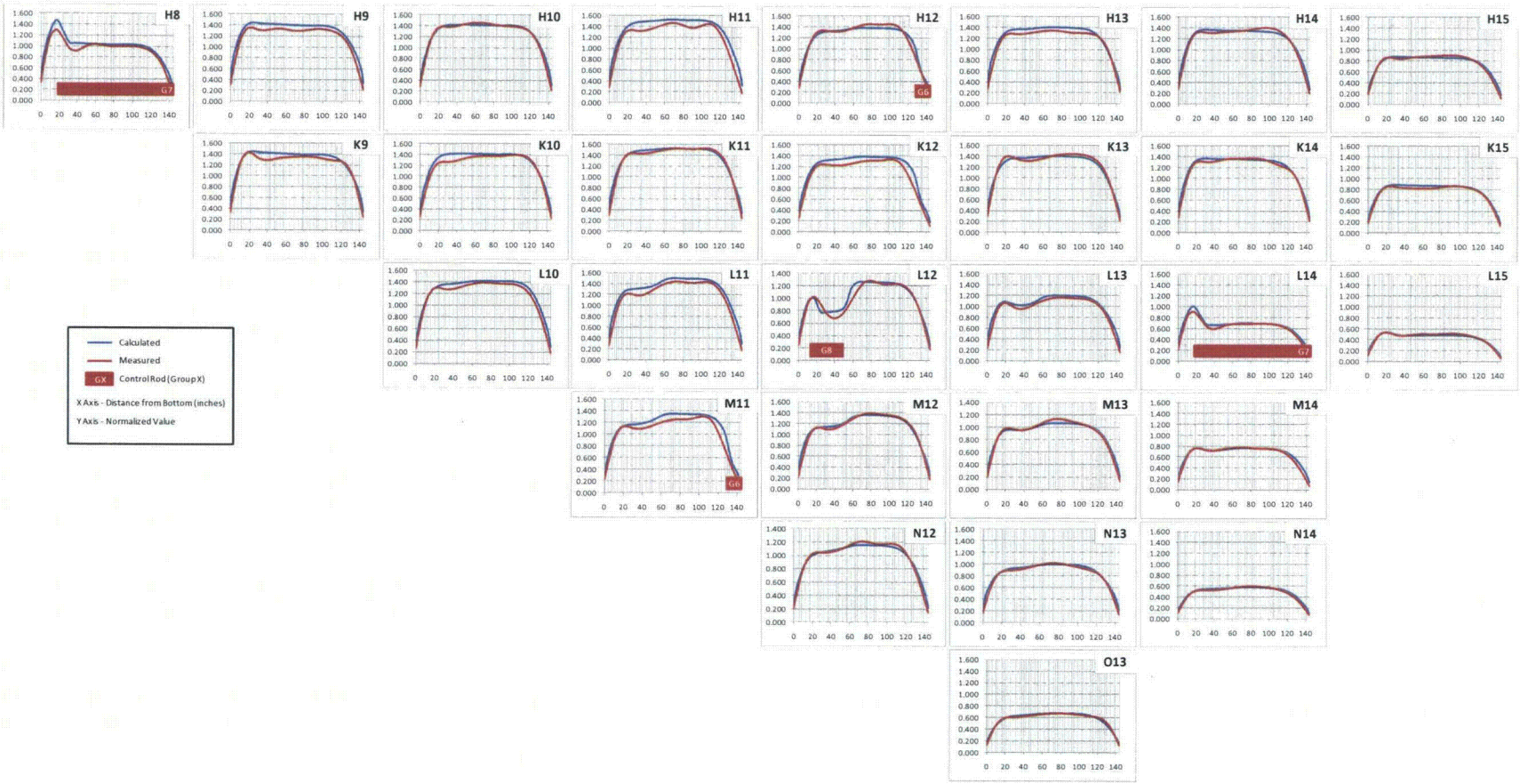

Figure C-119: TMI-1, Cycle 1 Axial Power Distribution Comparison at 6549 MWd/MtU

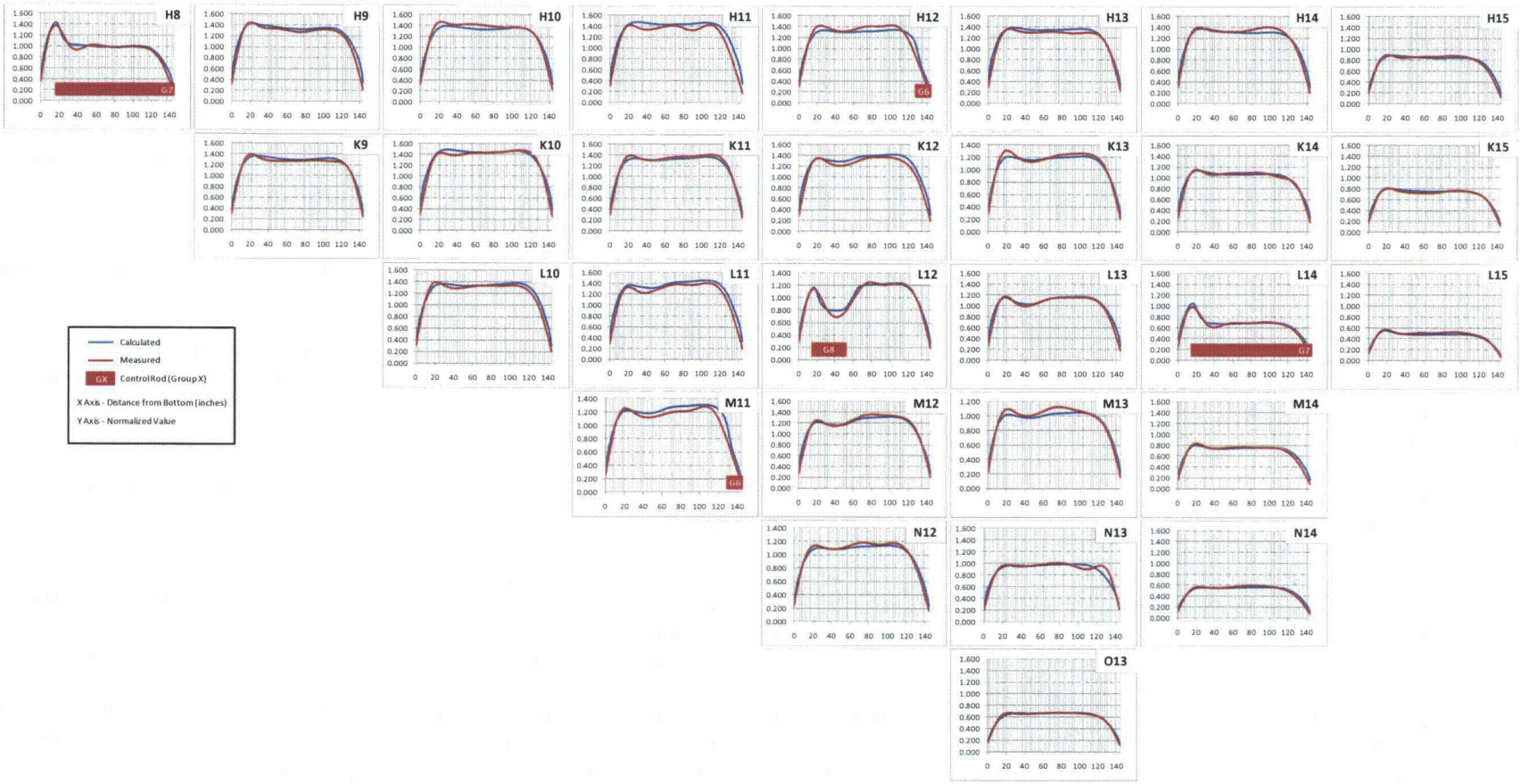

Figure C-120: TMI-1, Cycle 1 Axial Power Distribution Comparison at 7199 MWd/MtU

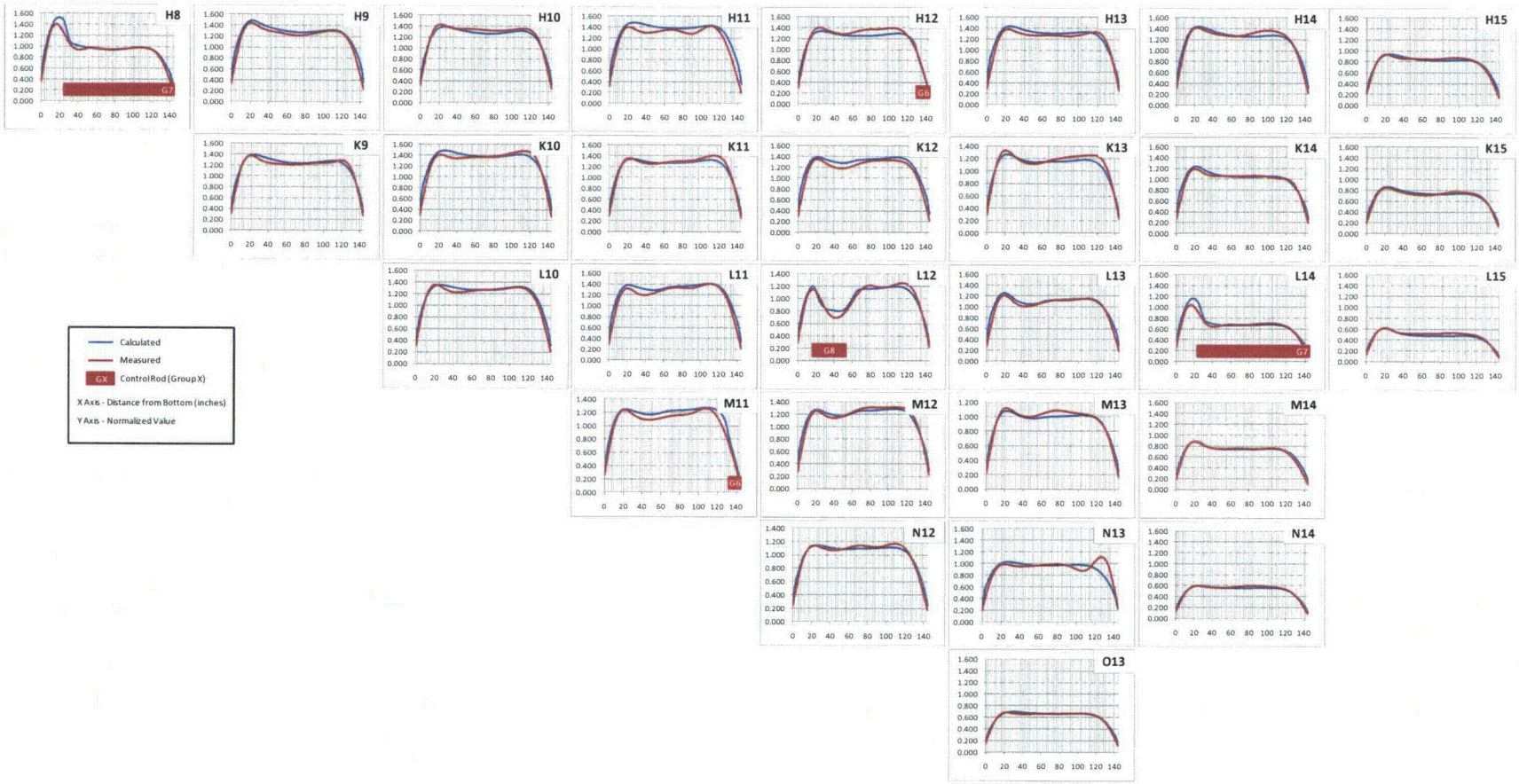

Figure C-121: TMI-1, Cycle 1 Axial Power Distribution Comparison at 7711 MWd/MtU

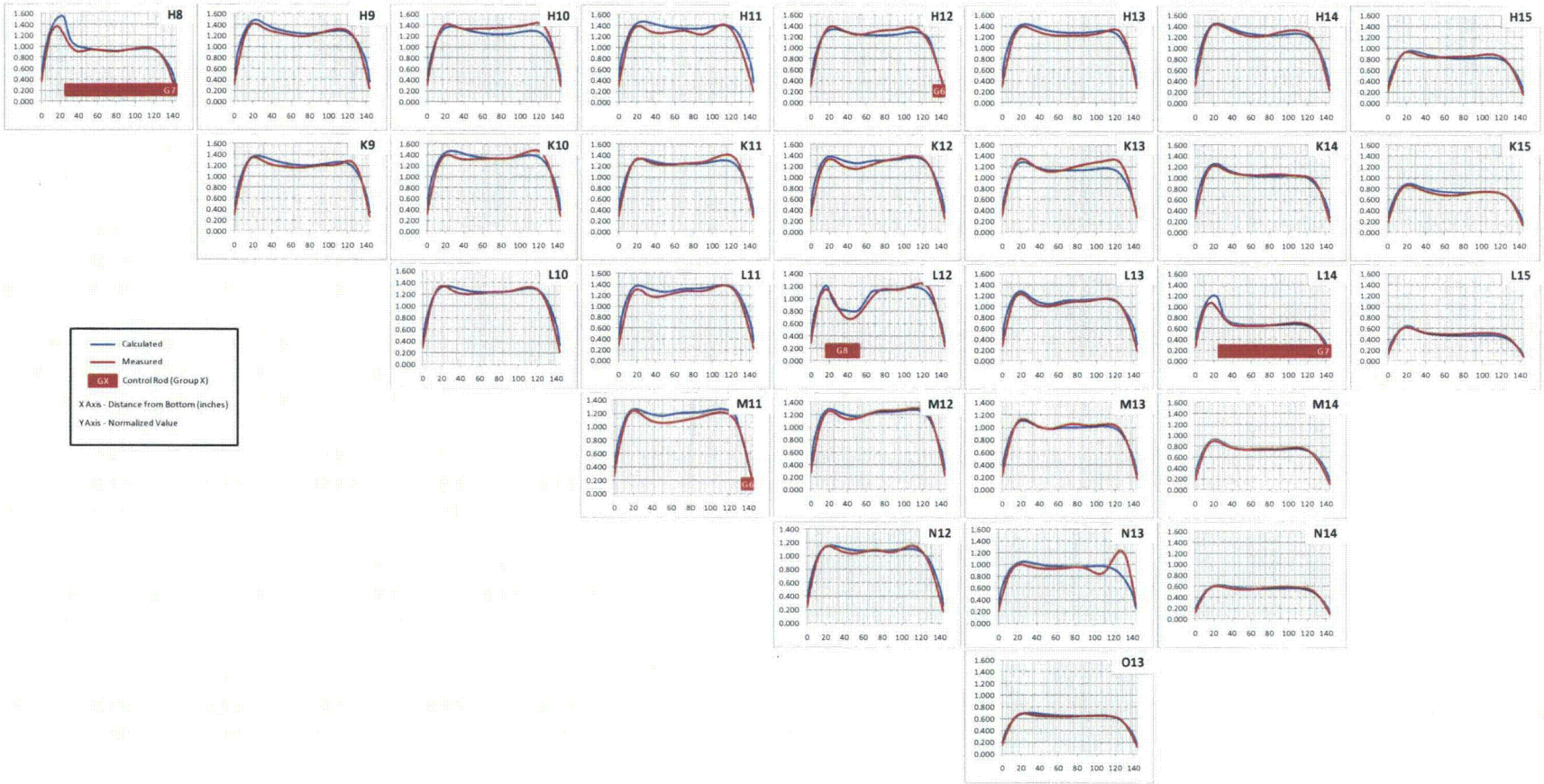

Figure C-122: TMI-1, Cycle 1 Axial Power Distribution Comparison at 8549 MWd/MtU

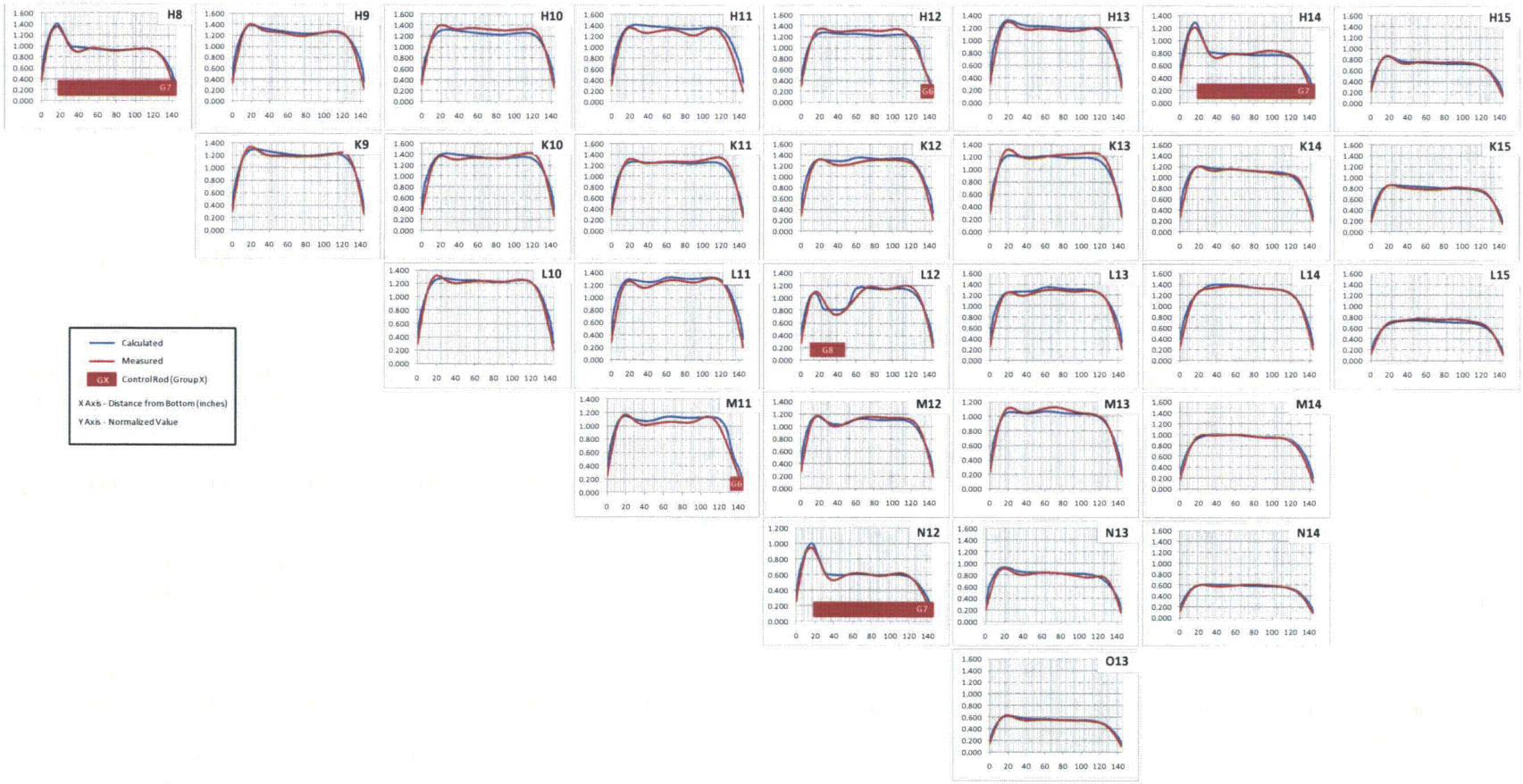

Figure C-123: TMI-1, Cycle 1 Axial Power Distribution Comparison at 9133 MWd/MtU

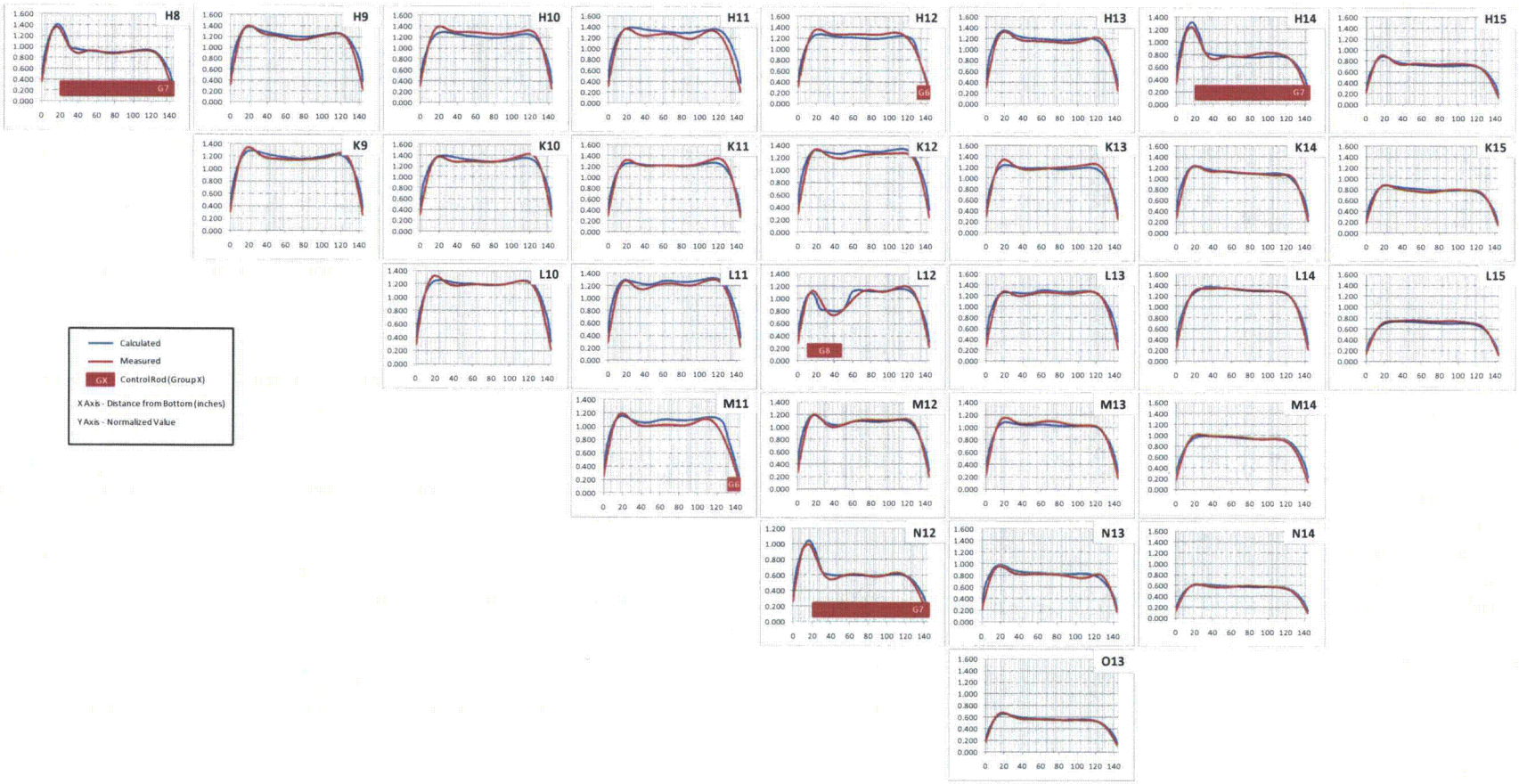

Figure C-124: TMI-1, Cycle 1 Axial Power Distribution Comparison at 10187 MWd/MtU

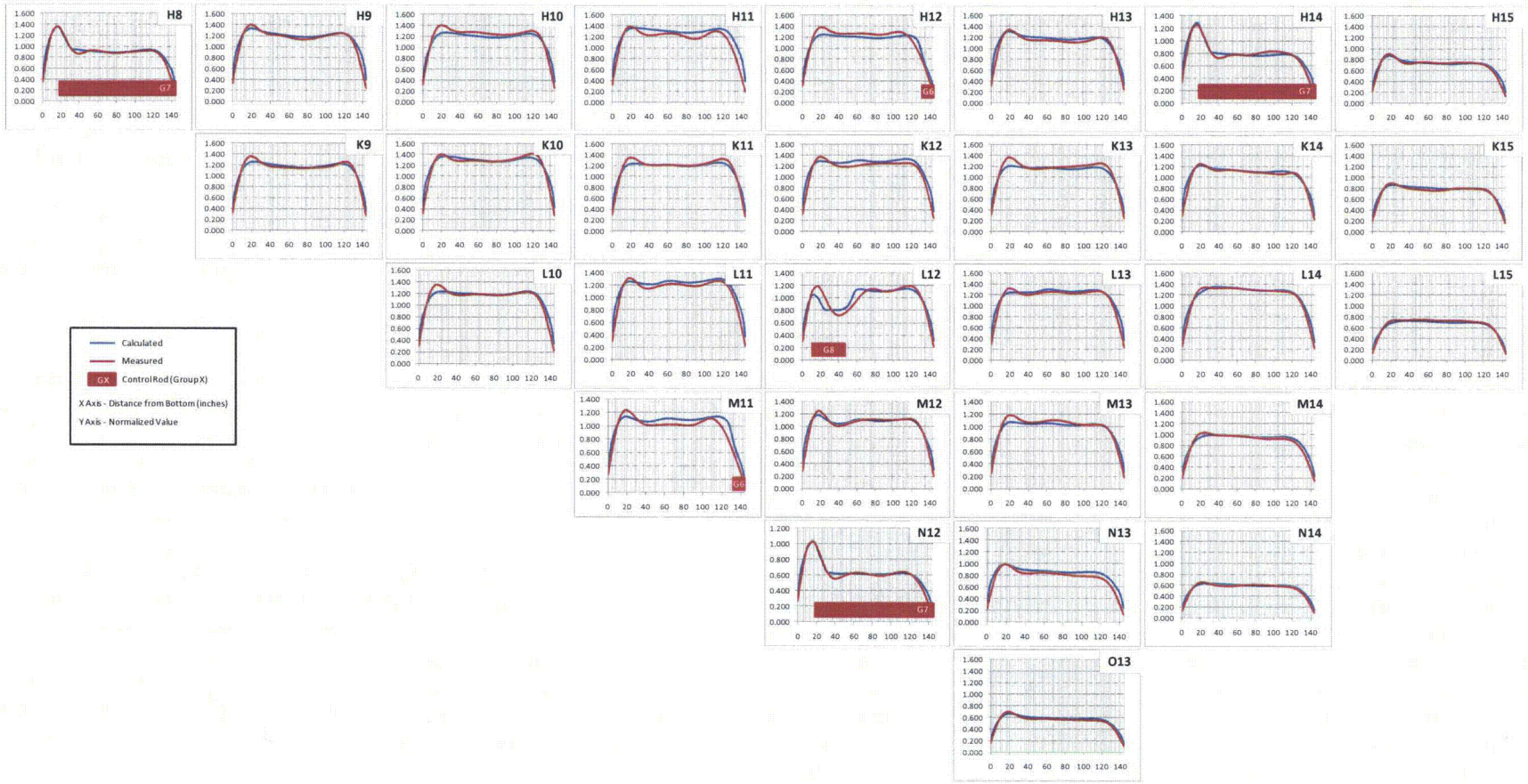

Figure C-125: TMI-1, Cycle 1 Axial Power Distribution Comparison at 10814 MWd/MtU

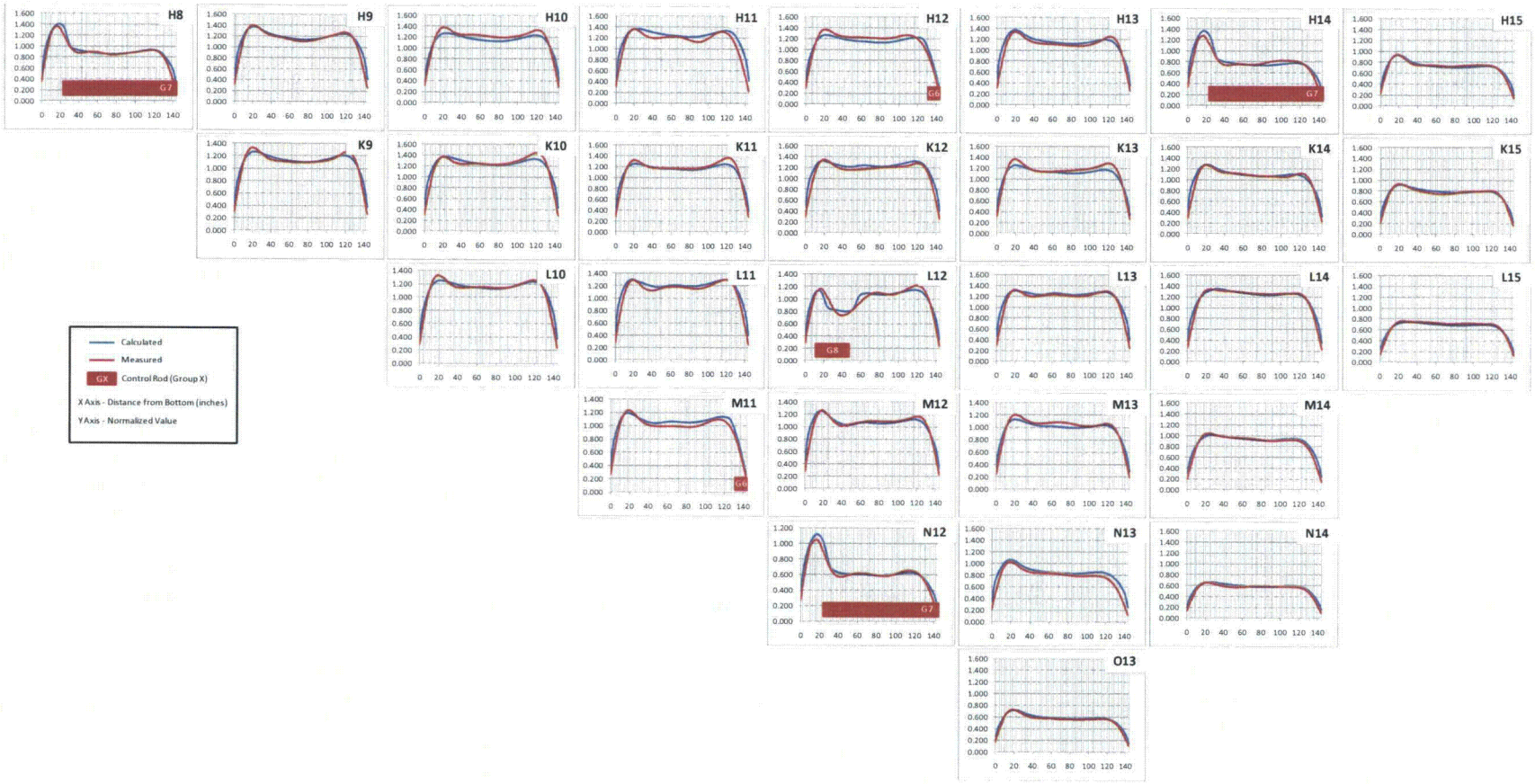

Figure C-126: TMI-1, Cycle 1 Axial Power Distribution Comparison at 11808 MWd/MtU

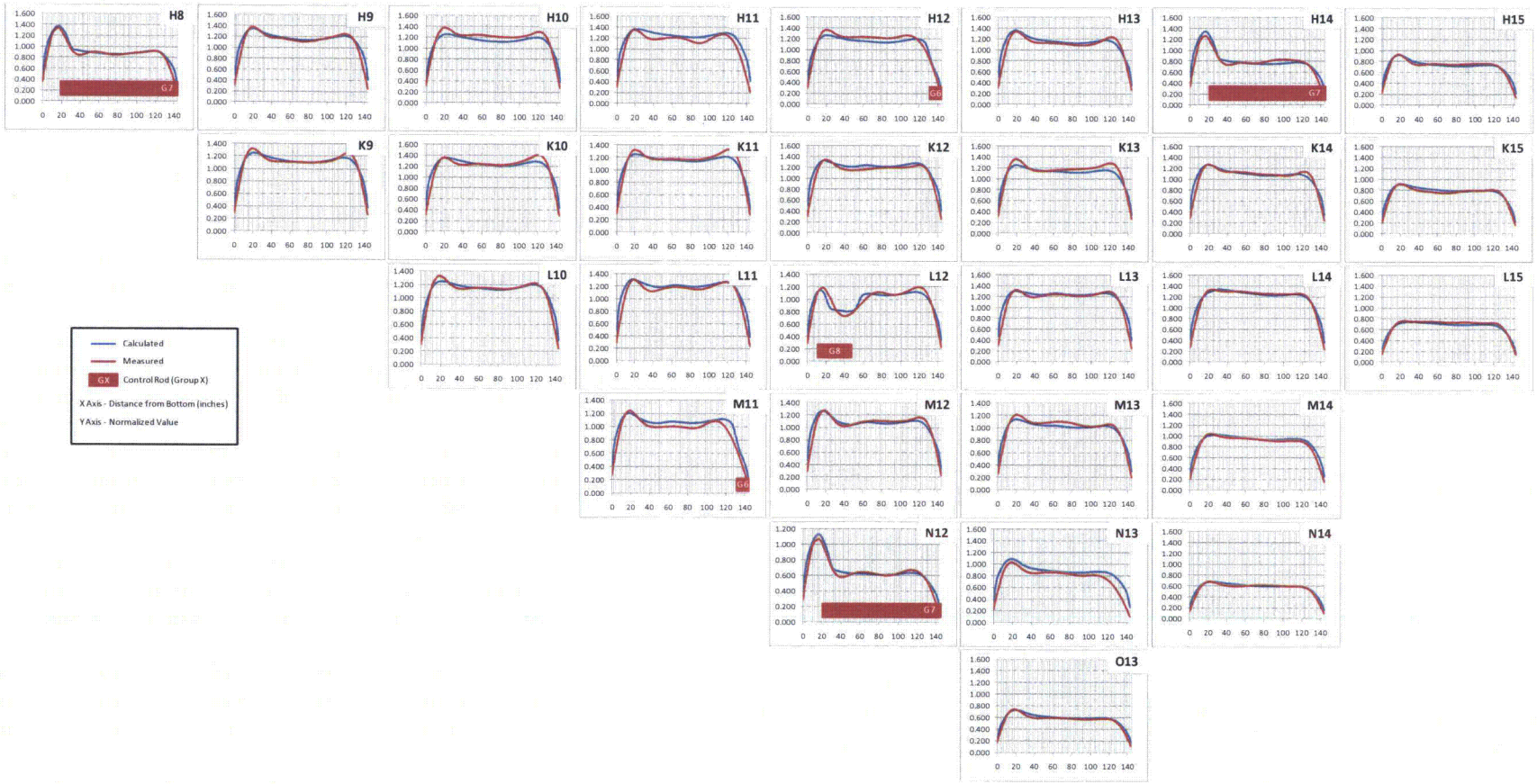

Figure C-127: TMI-1, Cycle 1 Axial Power Distribution Comparison at 12850 MWd/MtU

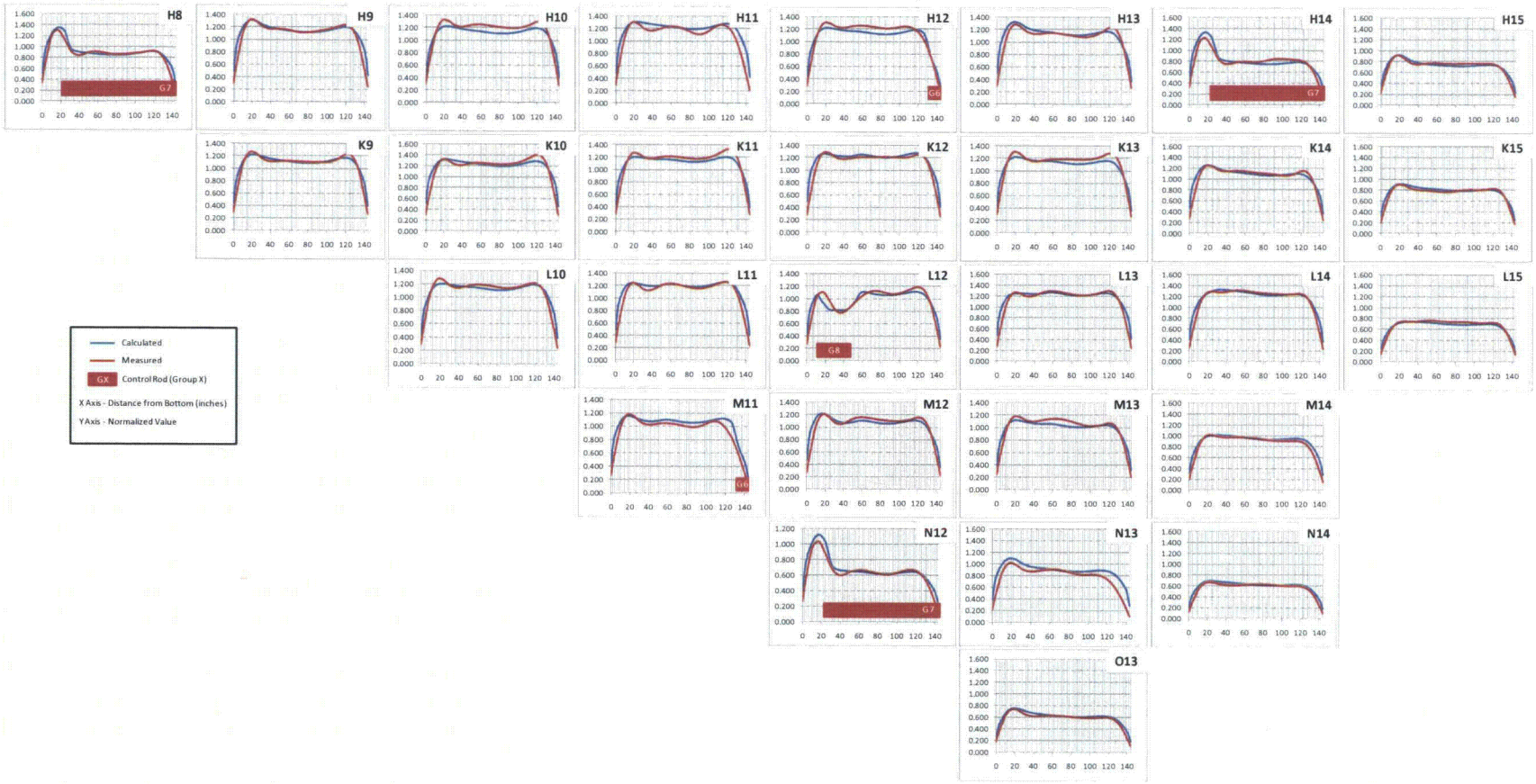

Figure C-128: TMI-1, Cycle 1 Axial Power Distribution Comparison at 13745 MWd/MtU

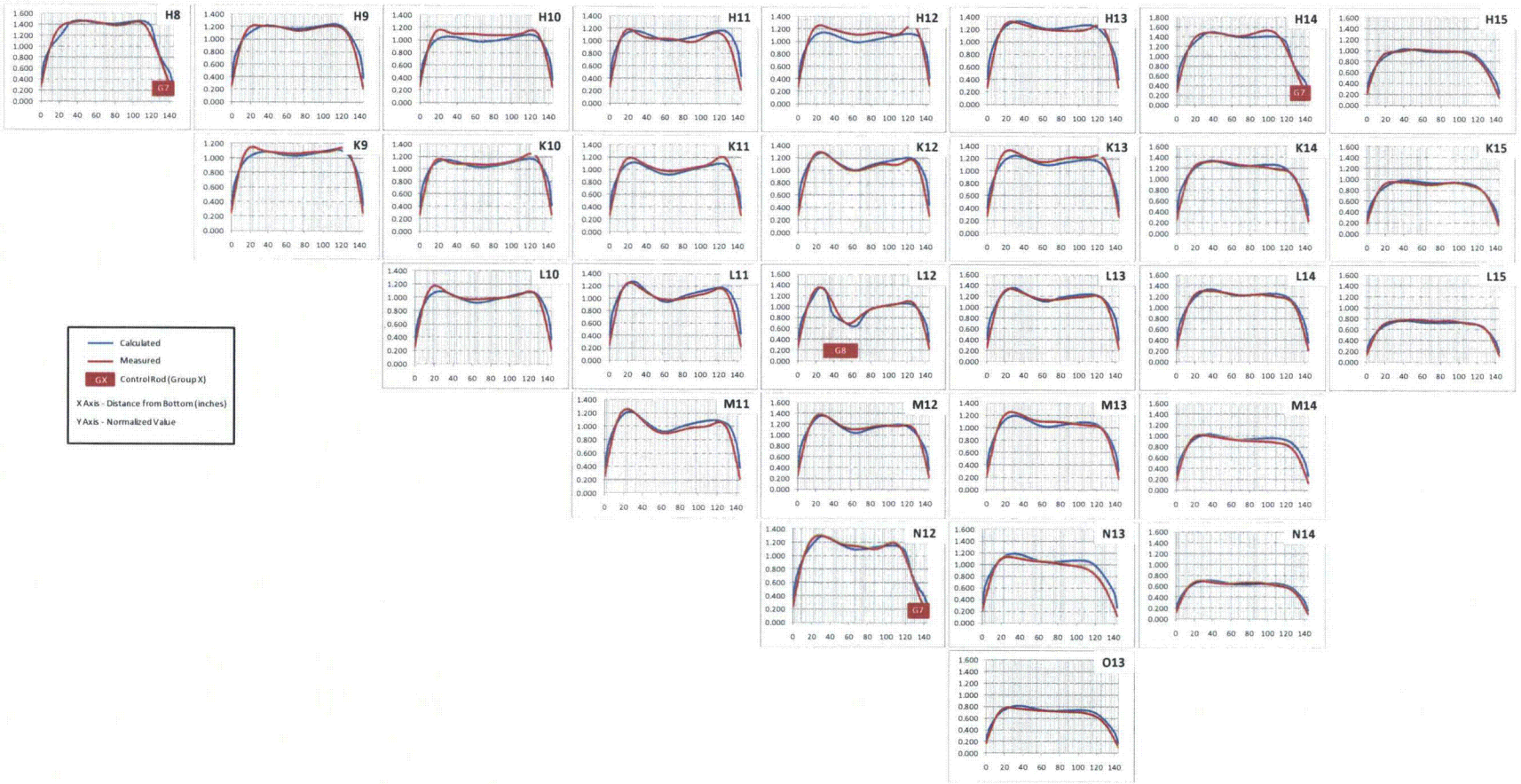

Figure C-129: TMI-1, Cycle 2 Axial Power Distribution Comparison at 188 MWd/MtU

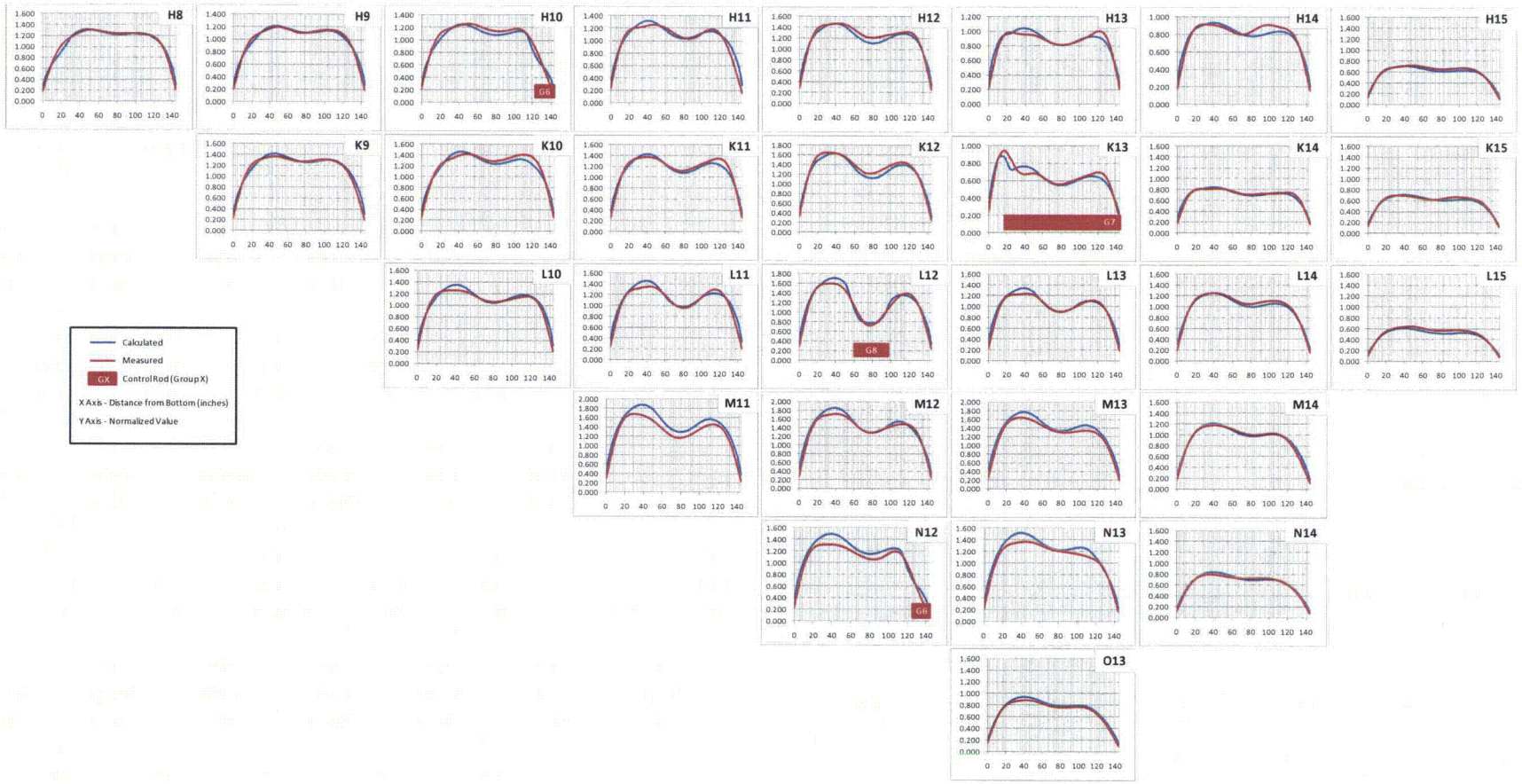

Figure C-130: TMI-1, Cycle 2 Axial Power Distribution Comparison at 572 MWd/MtU

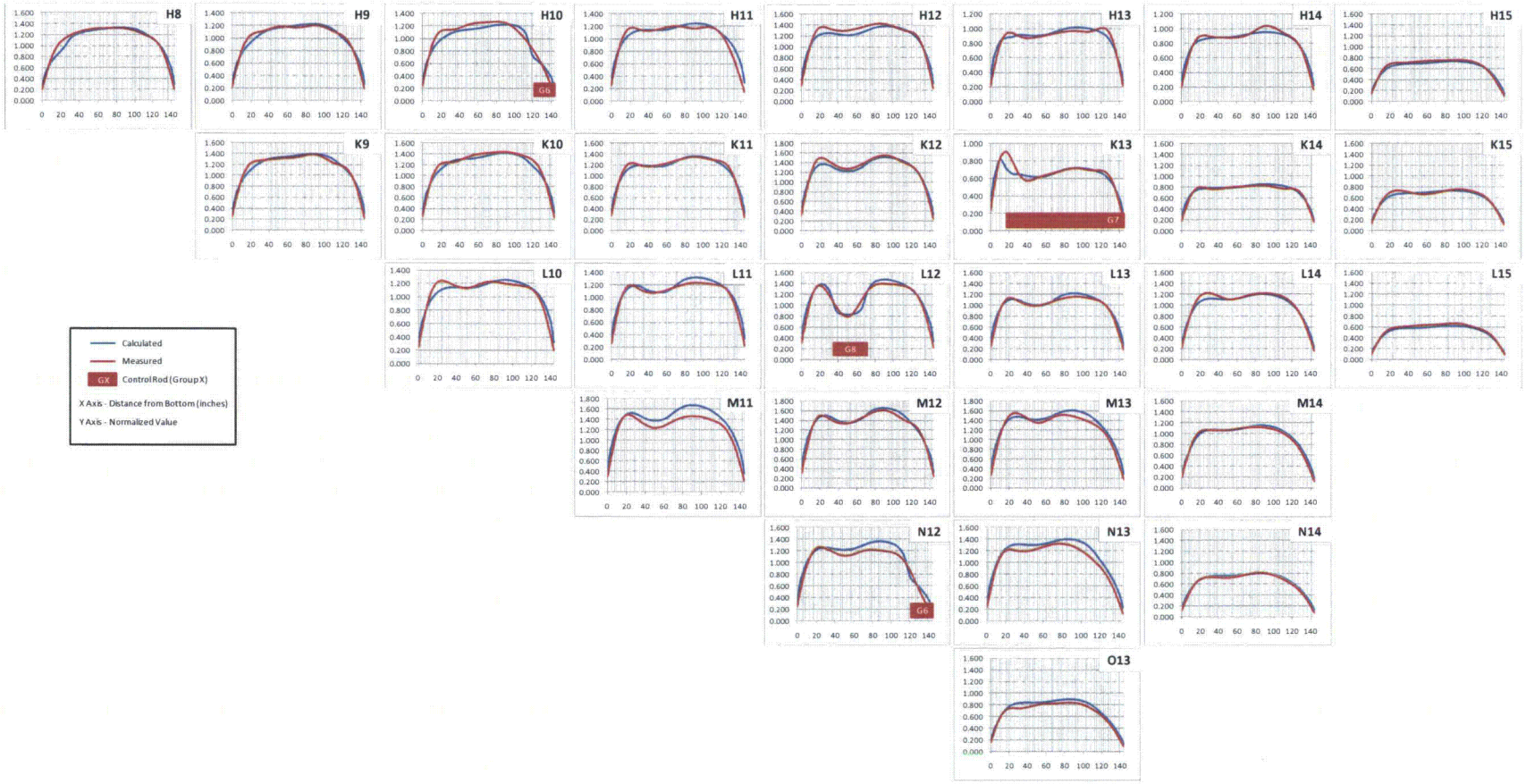

Figure C-131: TMI-1, Cycle 2 Axial Power Distribution Comparison at 788 MWd/MtU

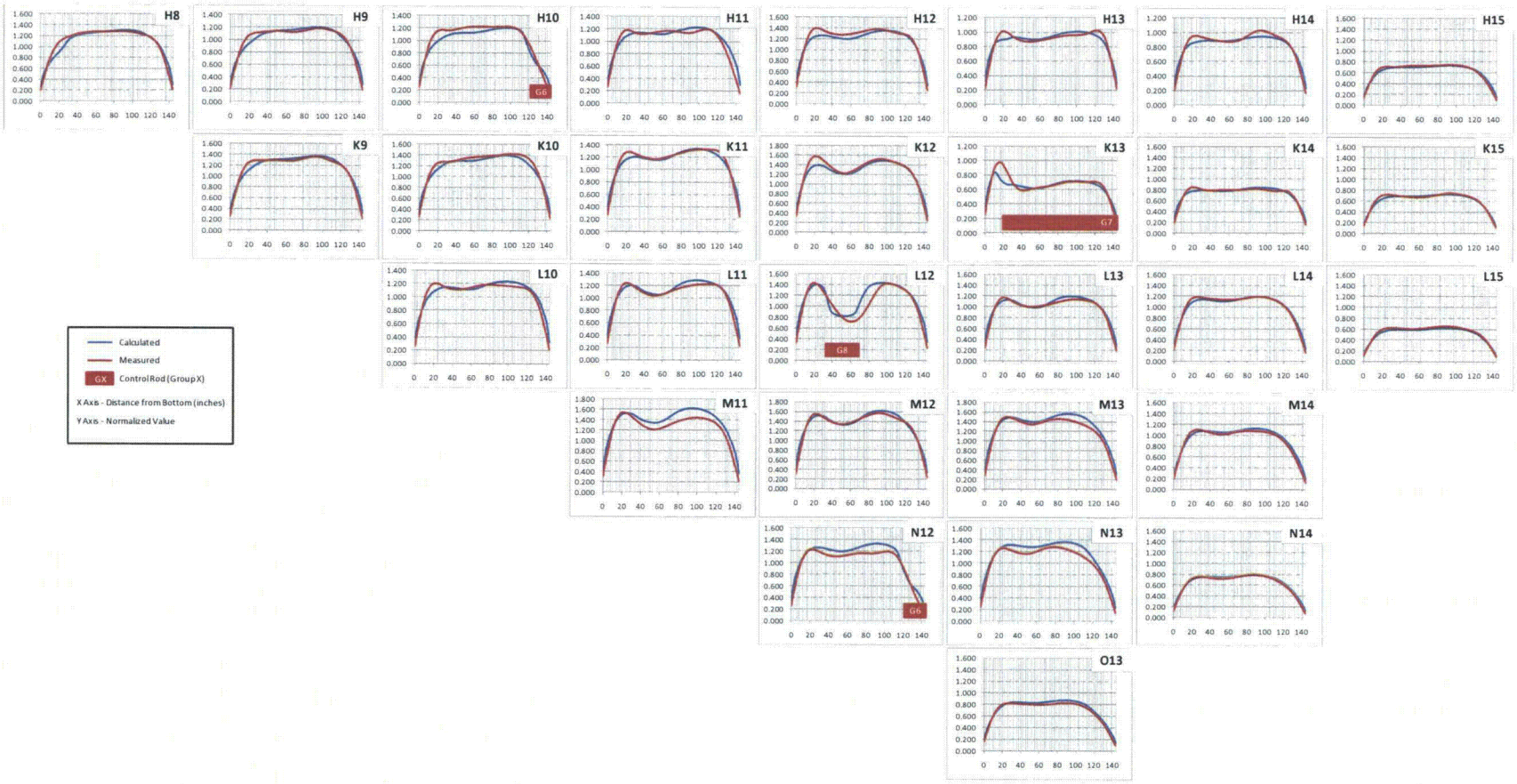

Figure C-132: TMI-1, Cycle 2 Axial Power Distribution Comparison at 1000 MWd/MtU

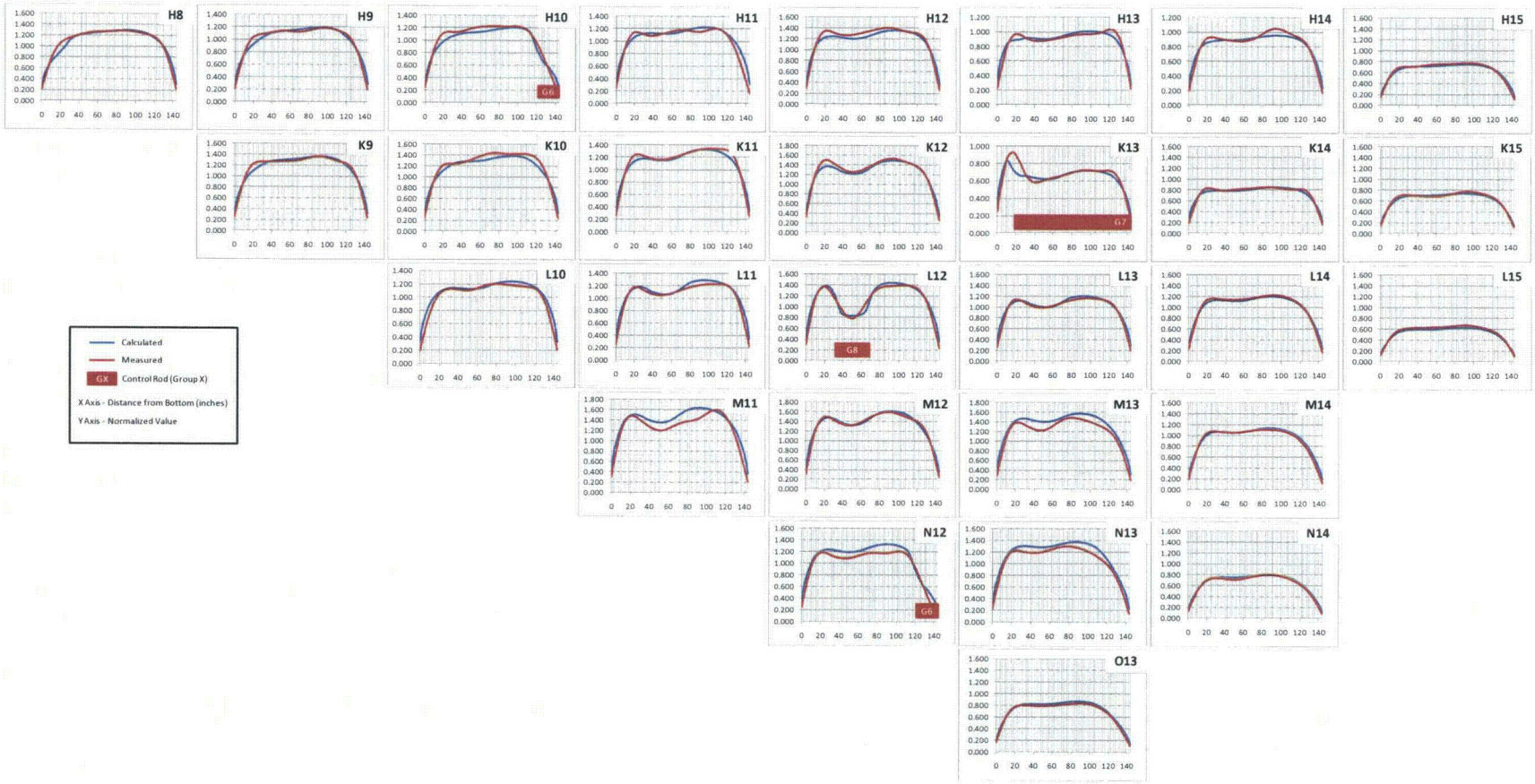

Figure C-133: TMI-1, Cycle 2 Axial Power Distribution Comparison at 1333 MWd/MtU

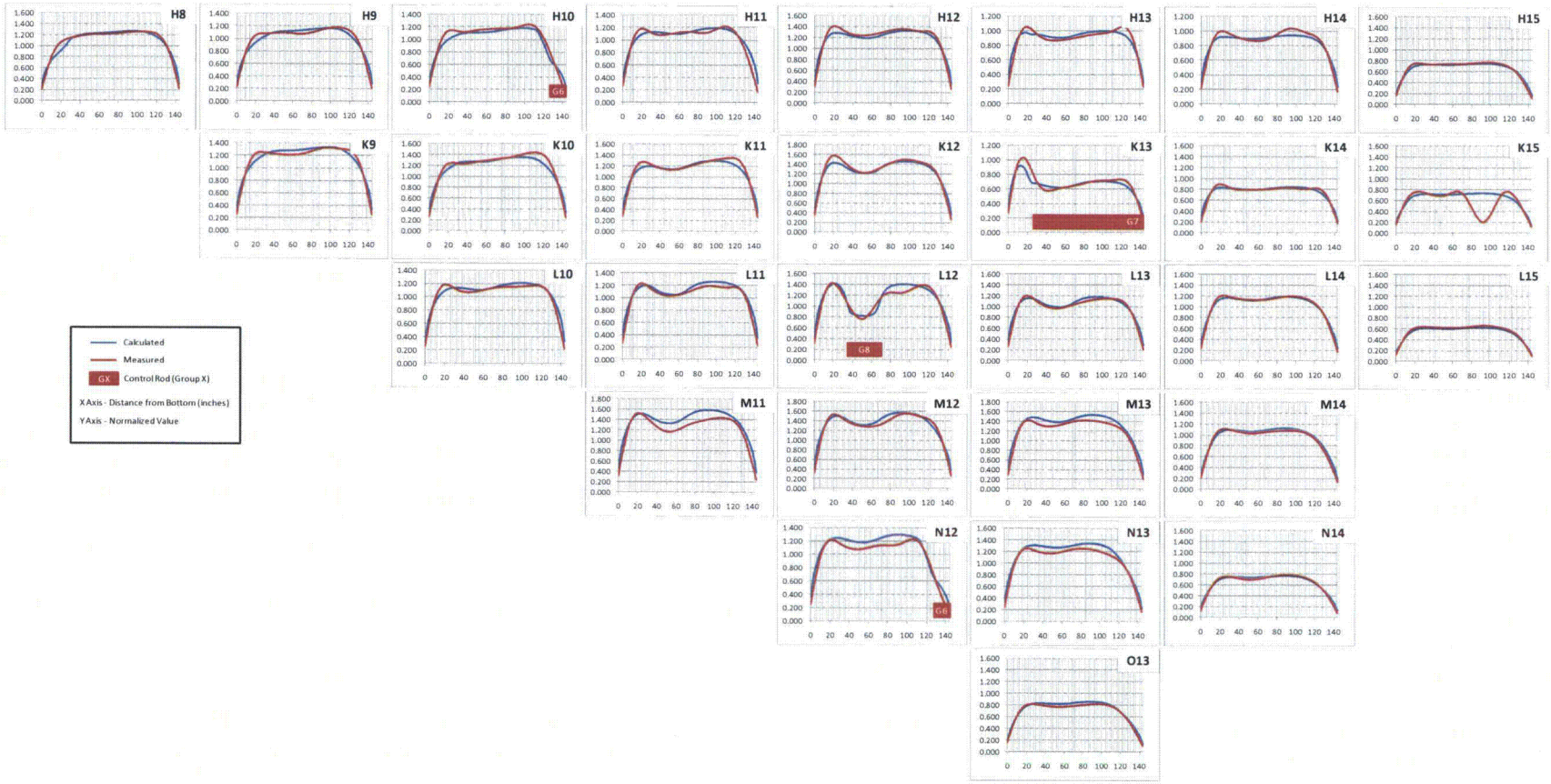

Figure C-134: TMI-1, Cycle 2 Axial Power Distribution Comparison at 1637 MWd/MtU

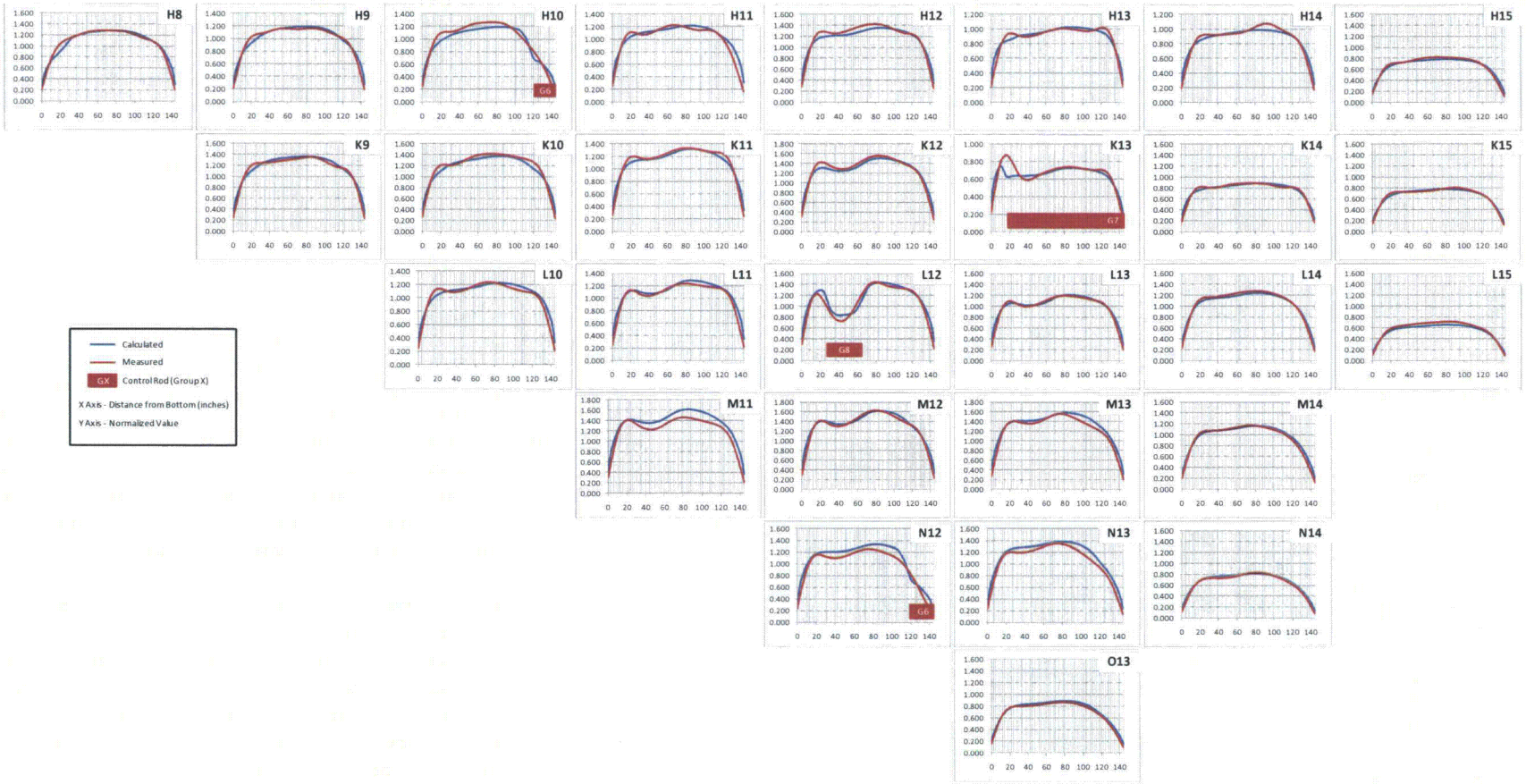

Figure C-135: TMI-1, Cycle 2 Axial Power Distribution Comparison at 2011 MWd/MtU

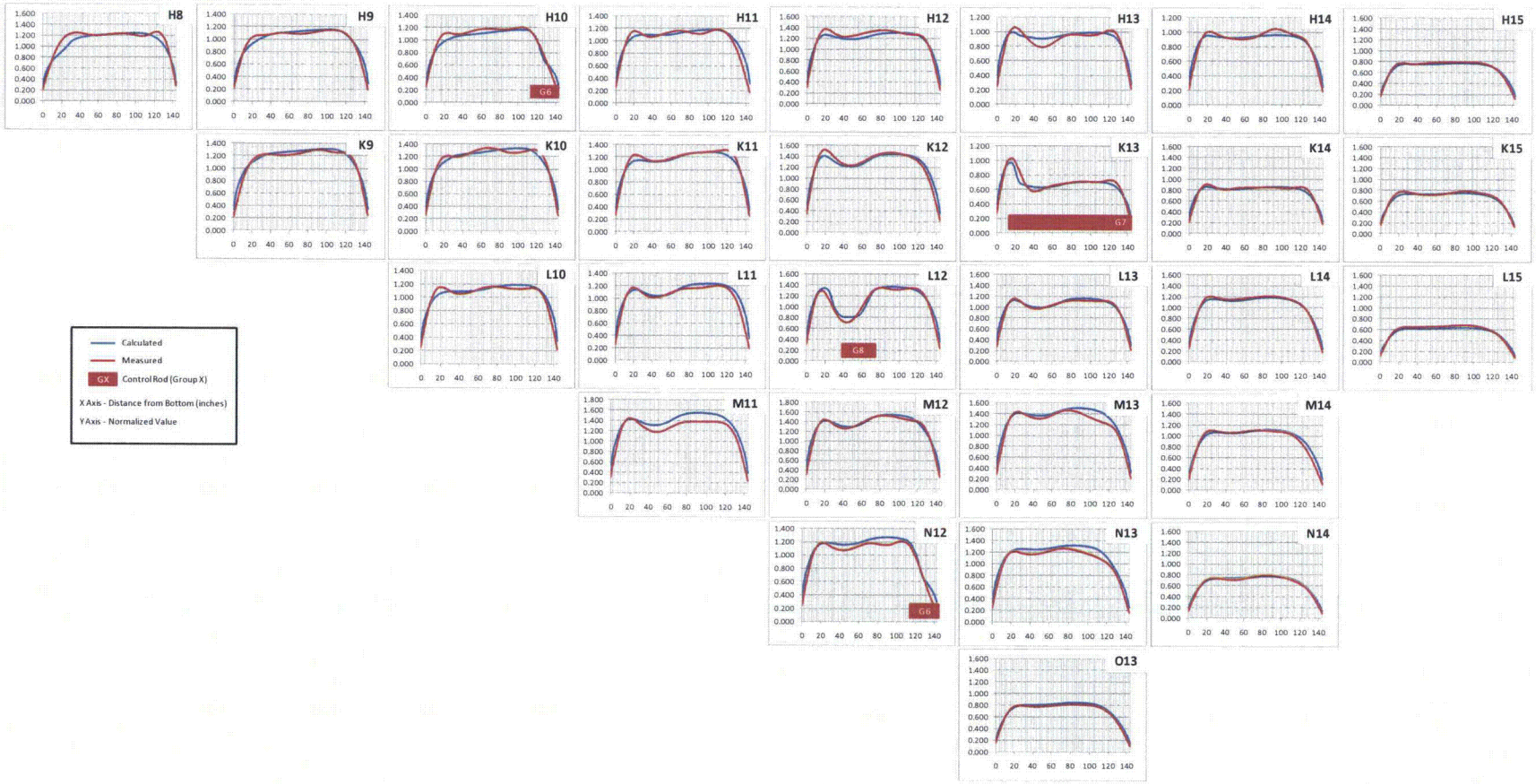

Figure C-136: TMI-1, Cycle 2 Axial Power Distribution Comparison at 2574 MWd/MtU

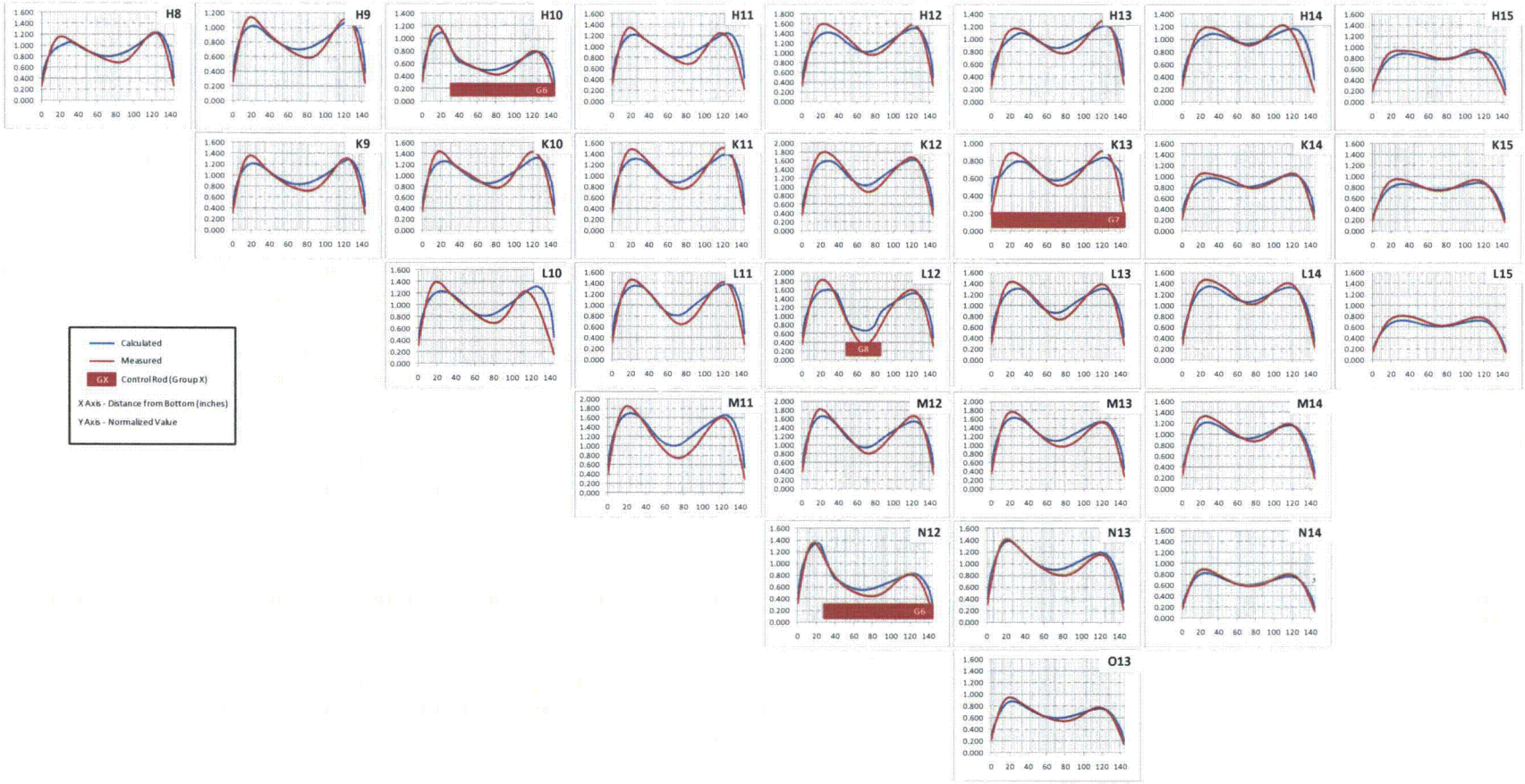

Figure C-137: TMI-1, Cycle 2 Axial Power Distribution Comparison at 2913 MWd/MtU

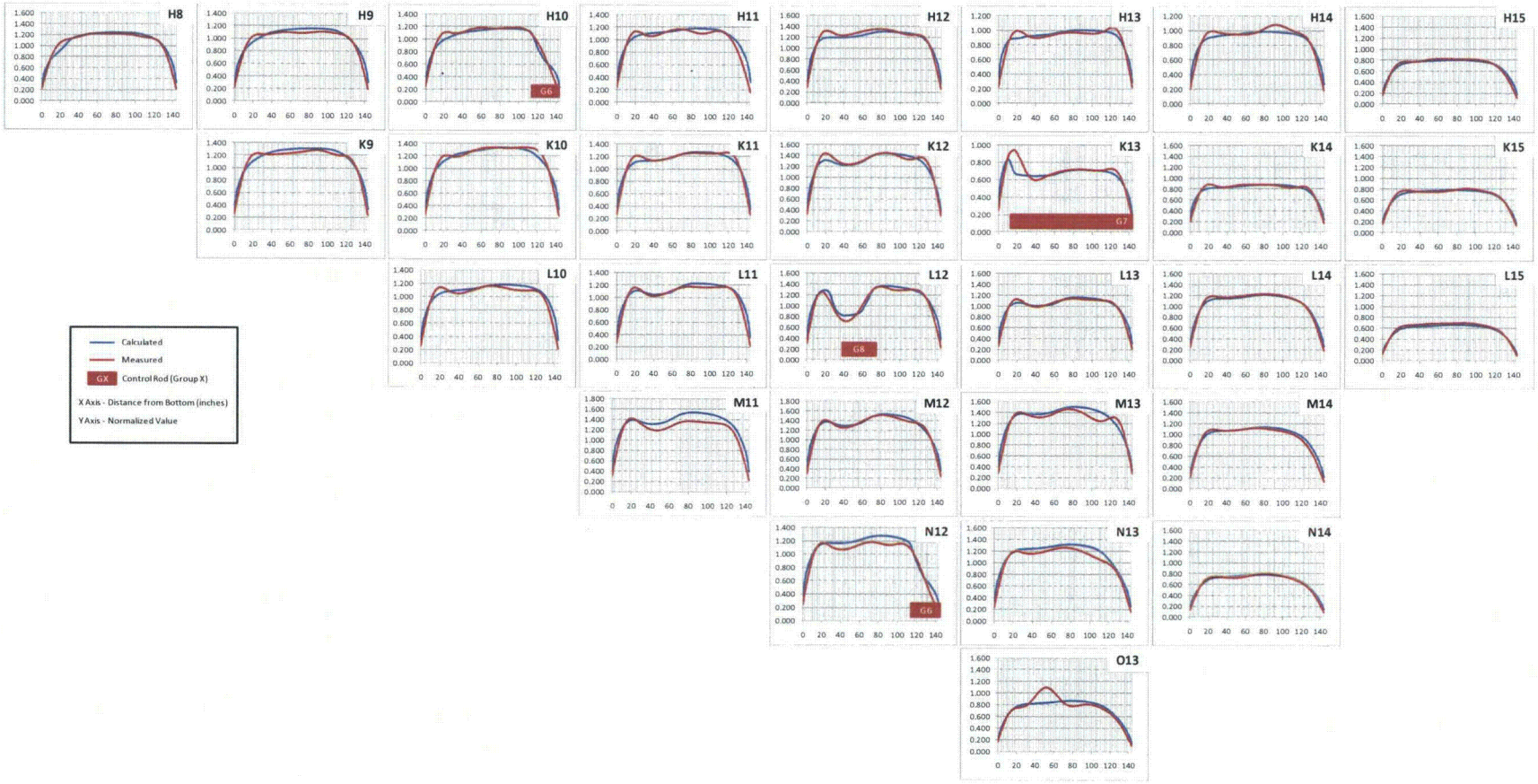

Figure C-138: TMI-1, Cycle 2 Axial Power Distribution Comparison at 3373 MWd/MtU

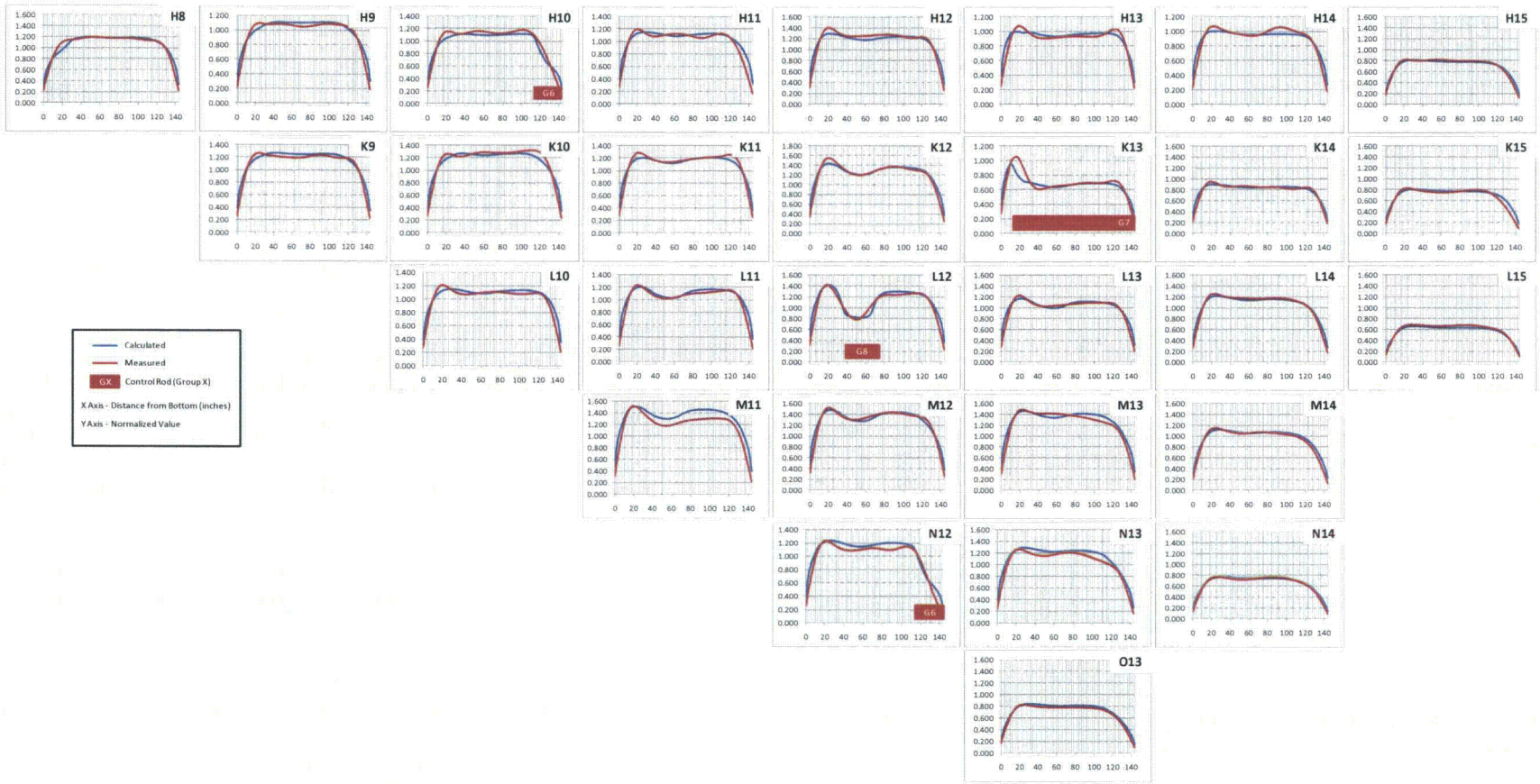

Figure C-139: TMI-1, Cycle 2 Axial Power Distribution Comparison at 3832 MWd/MtU

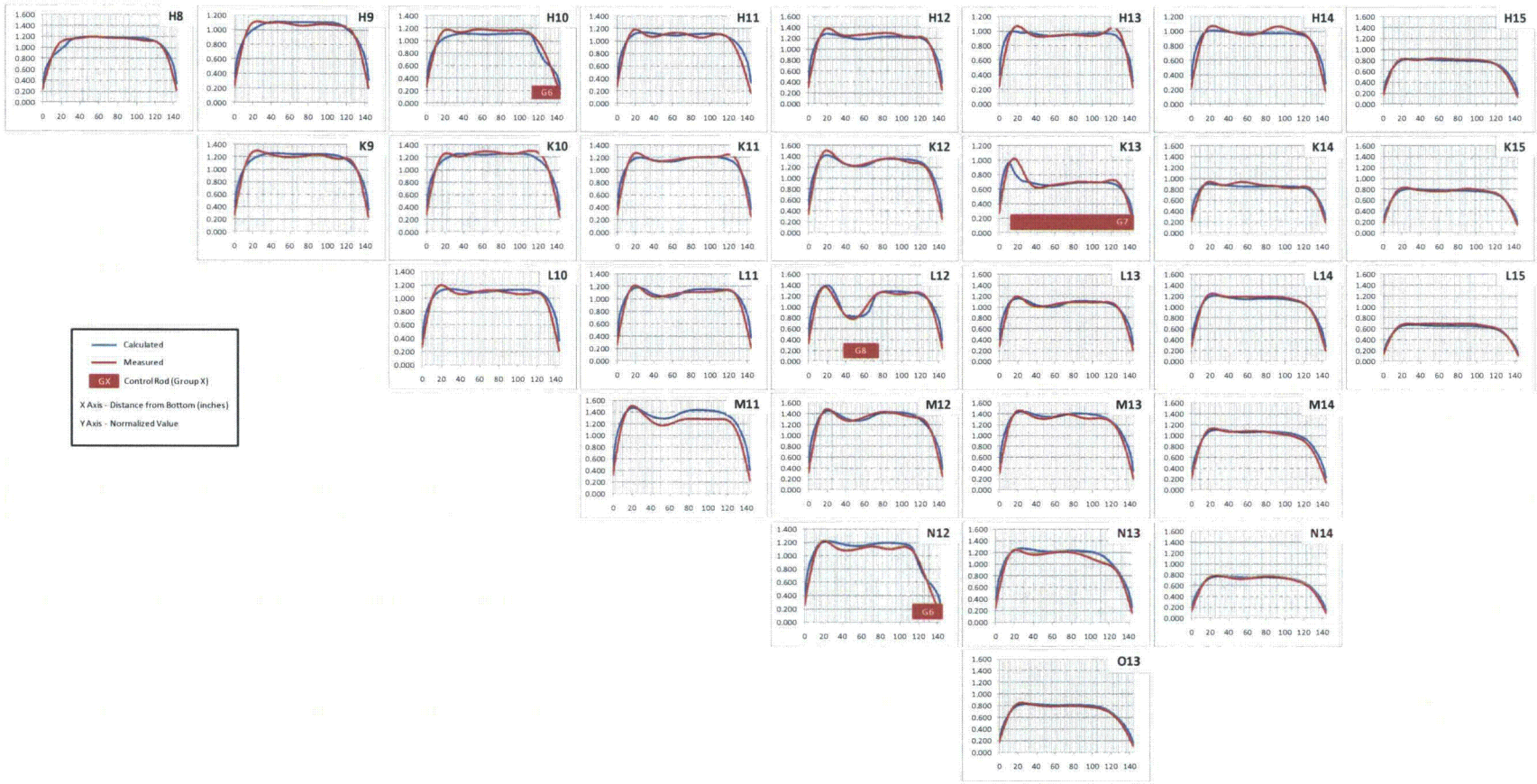

Figure C-140: TMI-1, Cycle 2 Axial Power Distribution Comparison at 4231 MWd/MtU

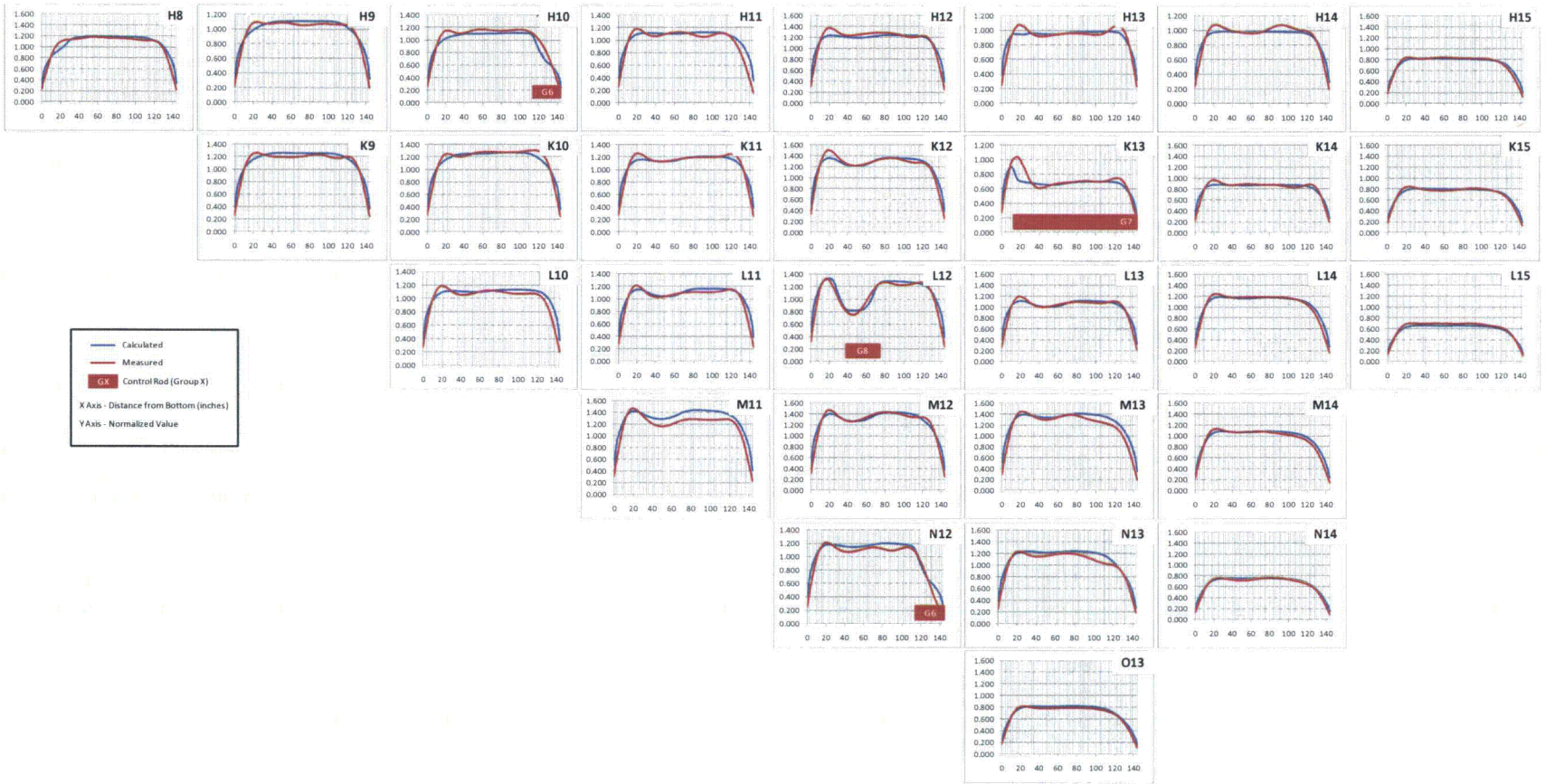

Figure C-141: TMI-1, Cycle 2 Axial Power Distribution Comparison at 4628 MWd/MtU

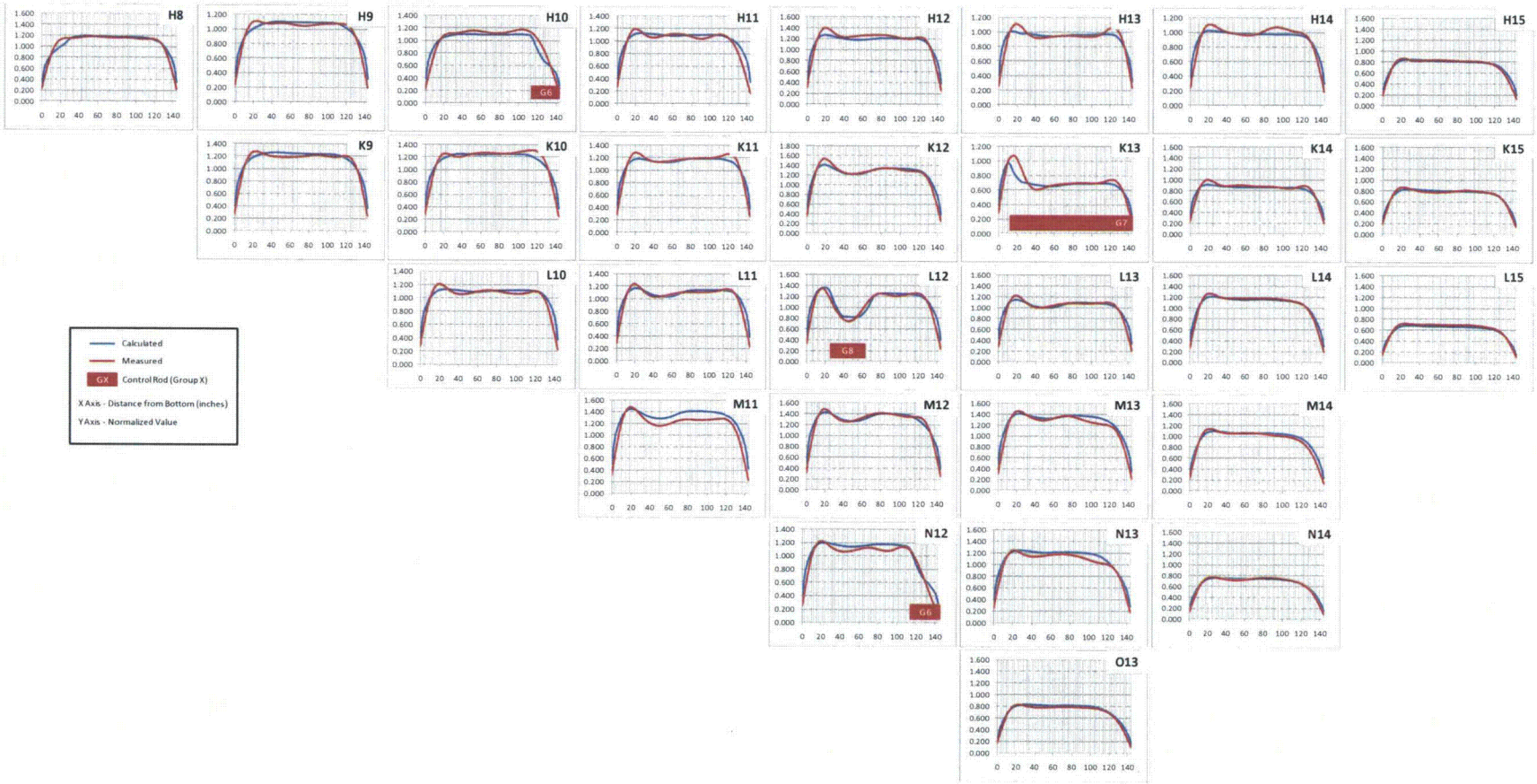

Figure C-142: TMI-1, Cycle 2 Axial Power Distribution Comparison at 5042 MWd/MtU

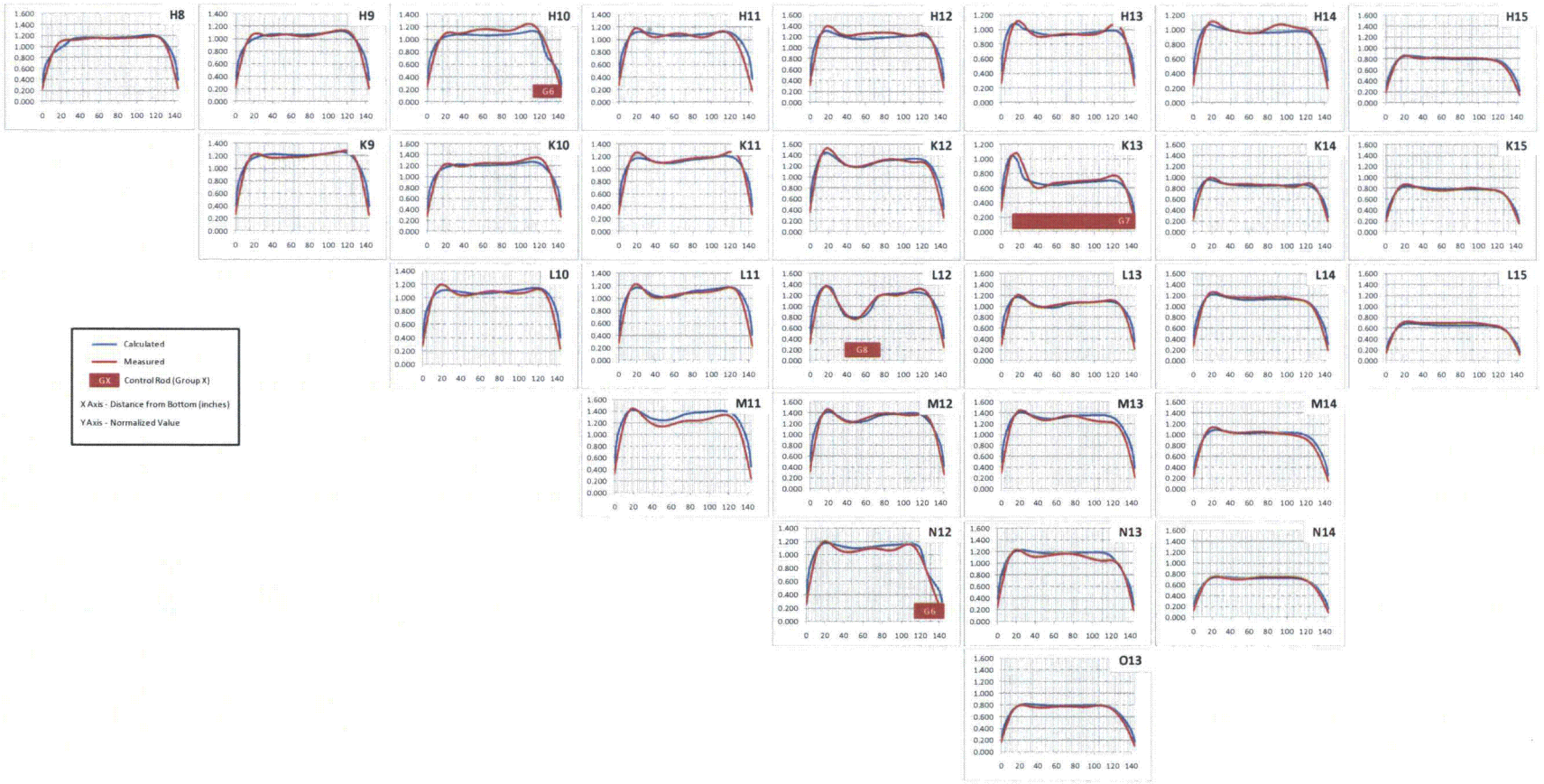

Figure C-143: TMI-1, Cycle 2 Axial Power Distribution Comparison at 5469 MWd/MtU

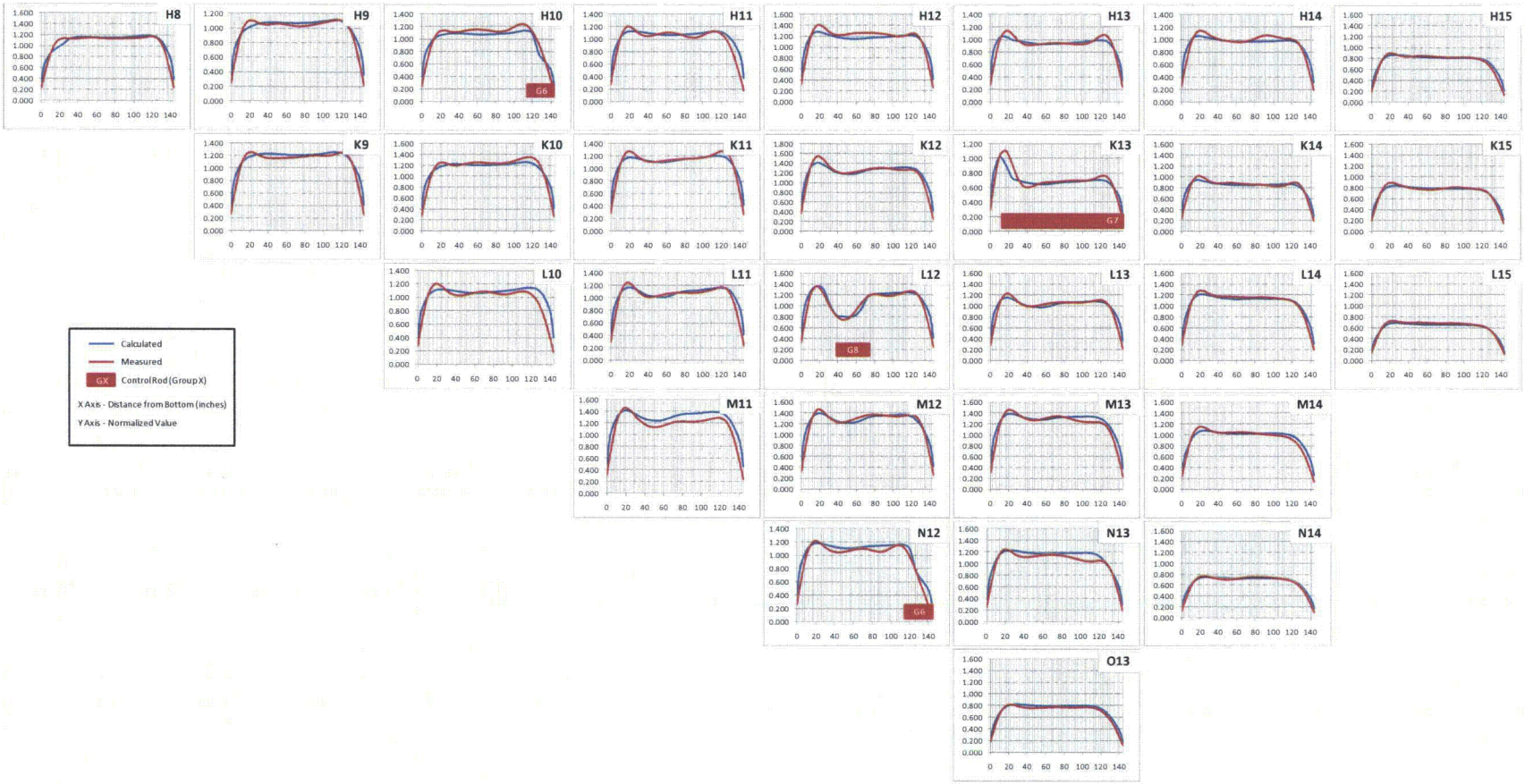

Figure C-144: TMI-1, Cycle 2 Axial Power Distribution Comparison at 5906 MWd/MtU

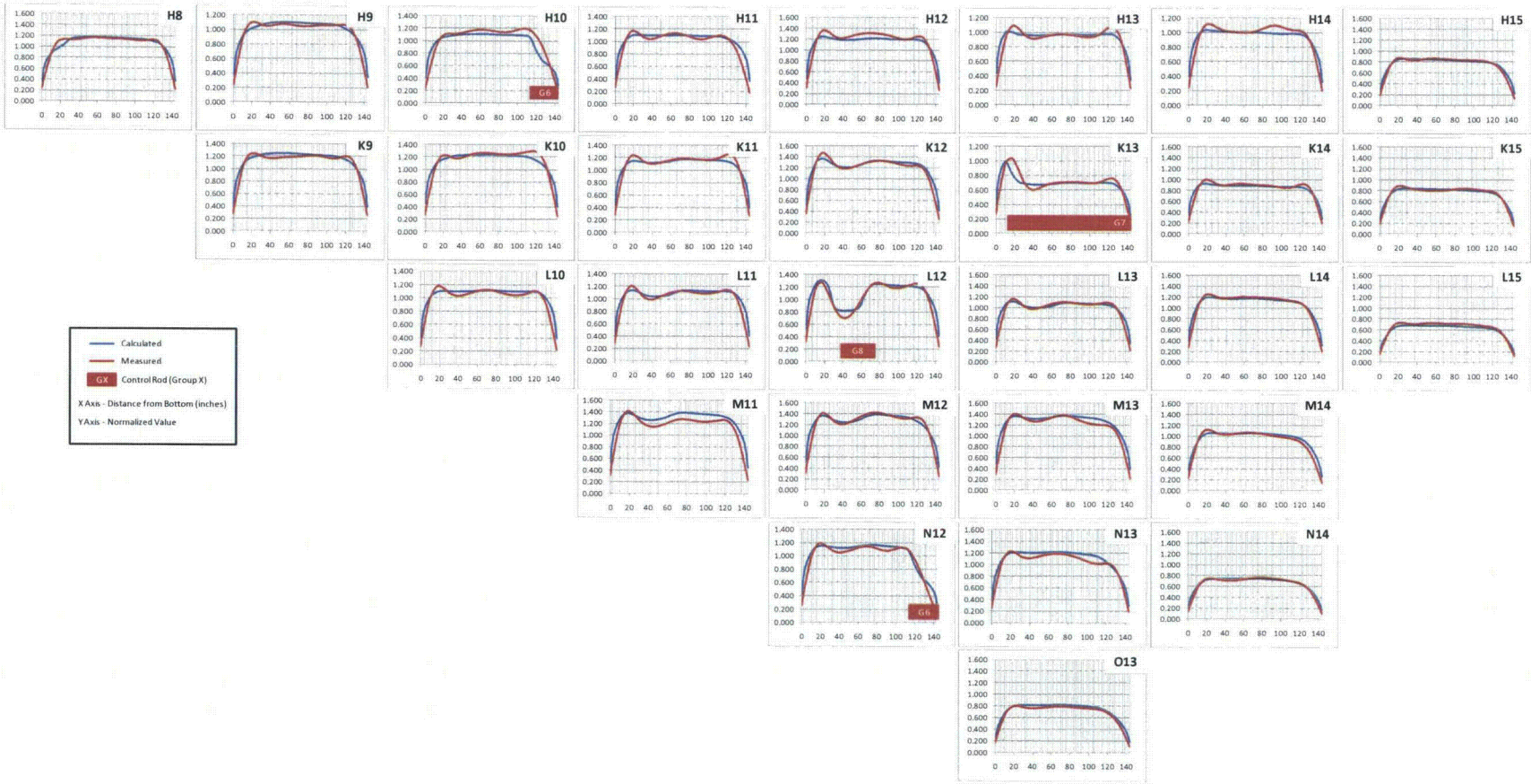

Figure C-145: TMI-1, Cycle 2 Axial Power Distribution Comparison at 6327 MWd/MtU

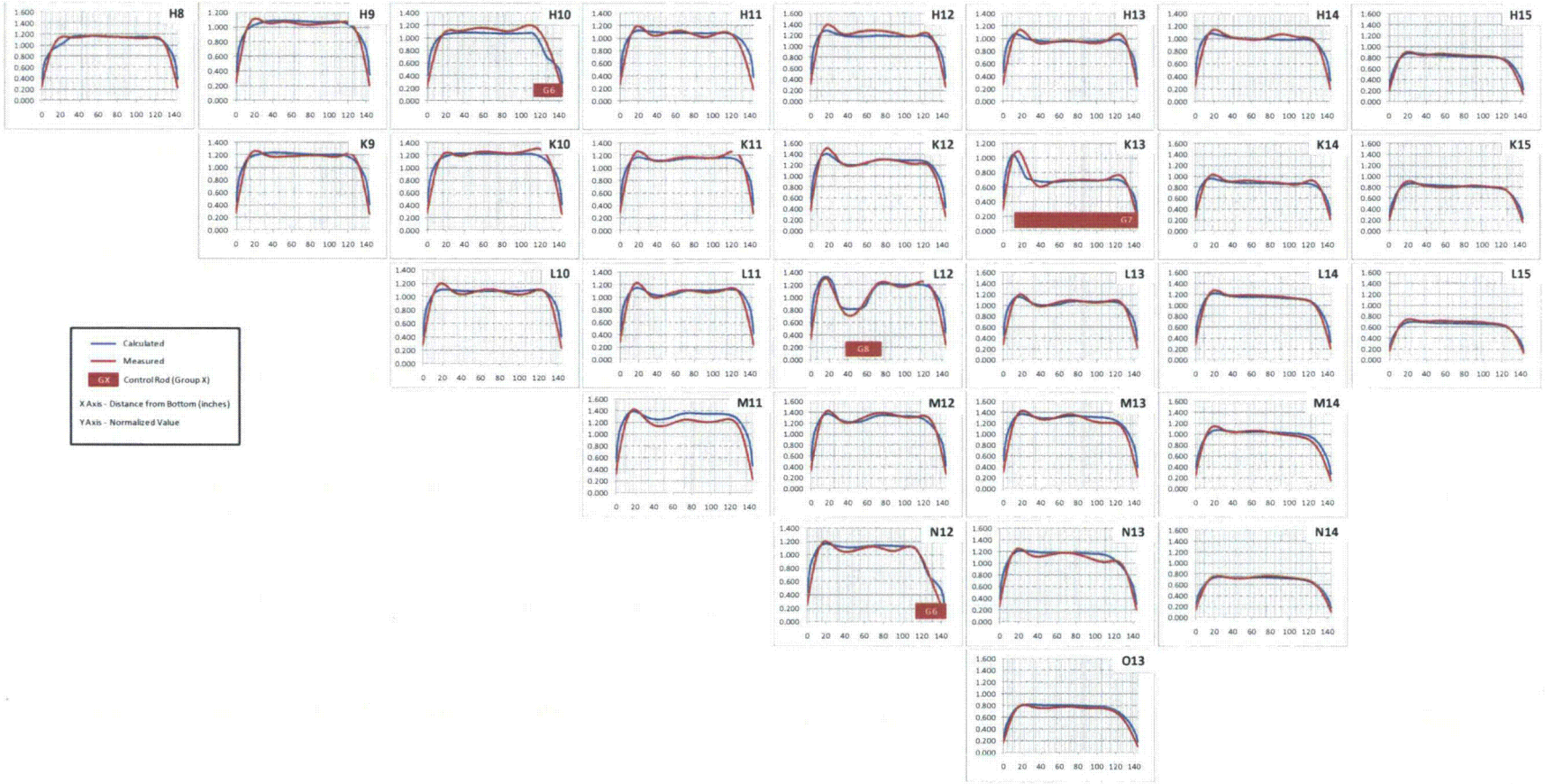

Figure C-146: TMI-1, Cycle 2 Axial Power Distribution Comparison at 6758 MWd/MtU

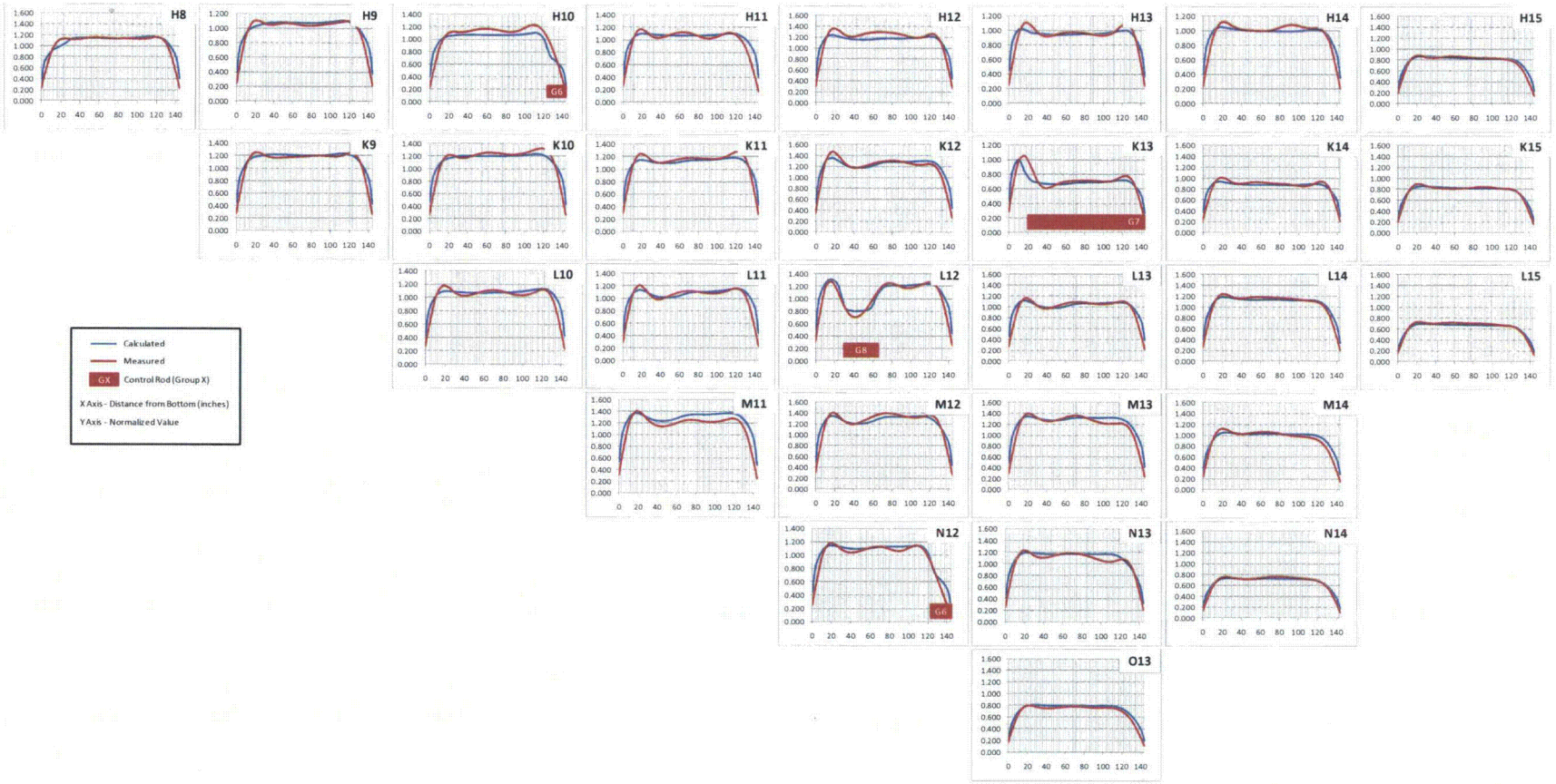

Figure C-147: TMI-1, Cycle 2 Axial Power Distribution Comparison at 7176 MWd/MtU

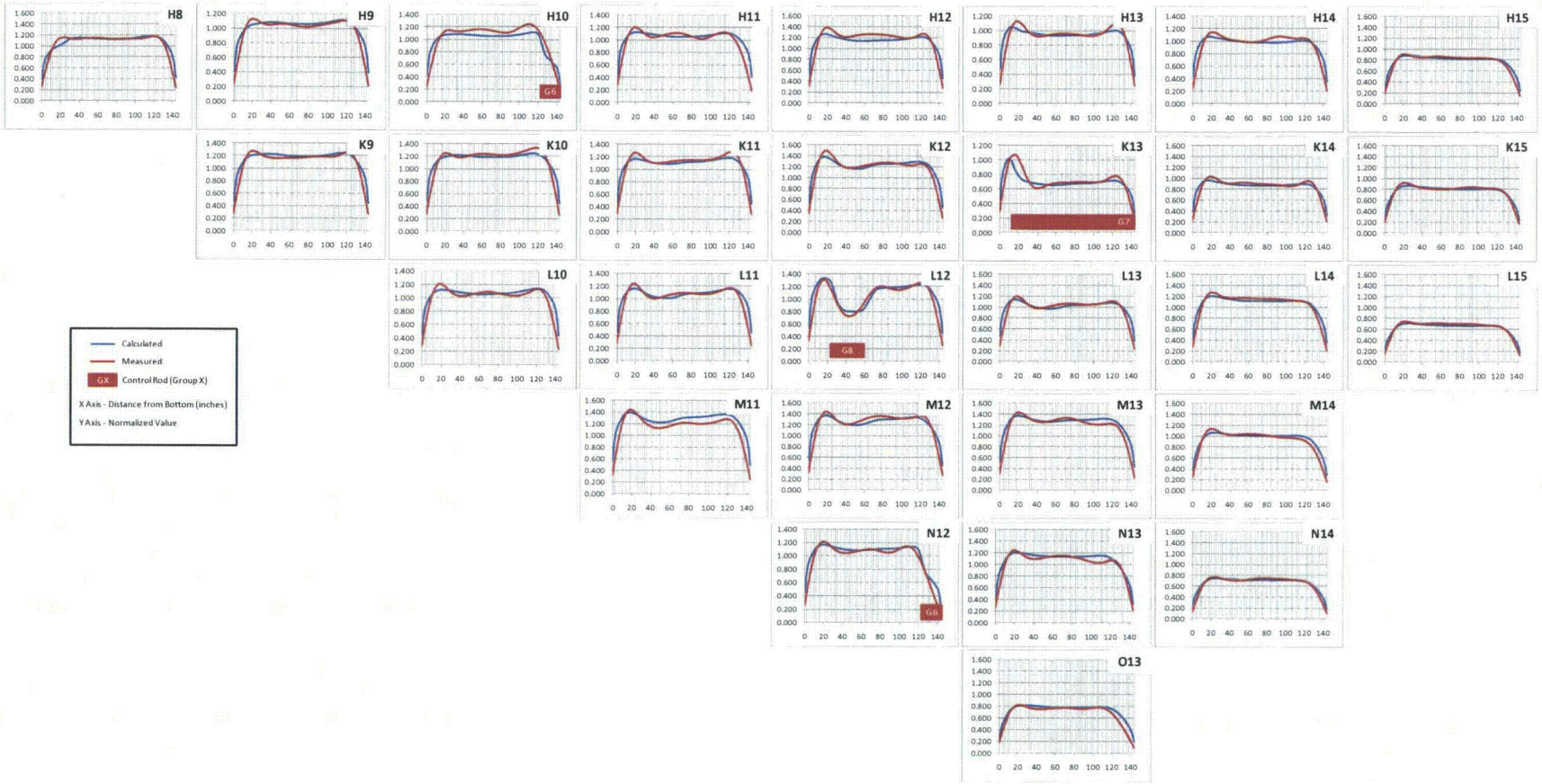

Figure C-148: TMI-1, Cycle 2 Axial Power Distribution Comparison at 7609 MWd/MtU

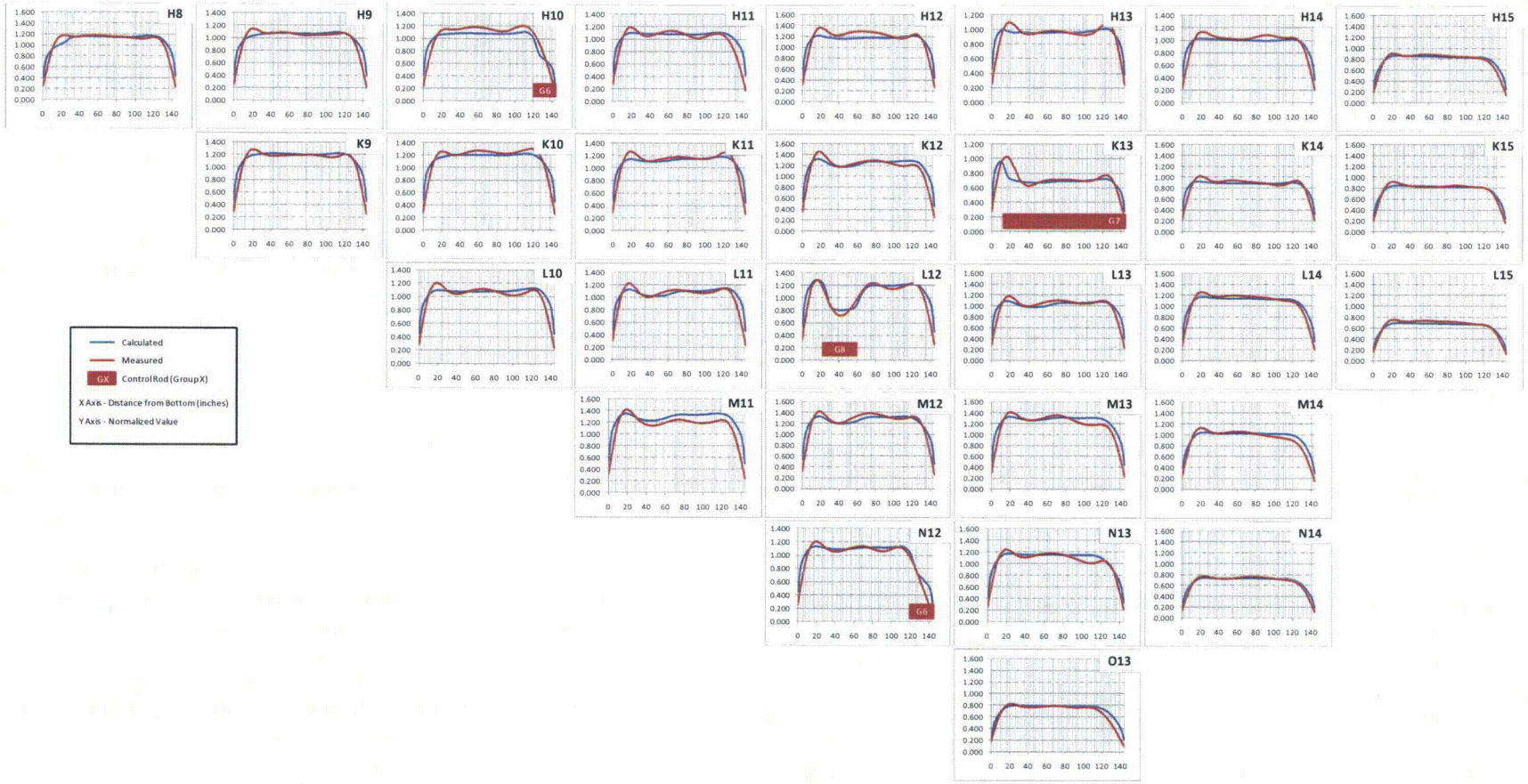

Figure C-149: TMI-1, Cycle 2 Axial Power Distribution Comparison at 8079 MWd/MtU